AFRL-VA-WP-TR-2000-3030

ENHANCEMENTS TO REPAIR ASSESSMENT PROCEDURE AND INTEGRATED DESIGN (RAPID)

ANALYSIS METHODS ENHANCEMENTS

CHUN CHEN
MILES NOMURA
JIN YU

THE BOEING COMPANY
2401 E. WARDLOW ROAD
LONG BEACH, CA 90807-5309

JUNE 2000

FINAL REPORT FOR PERIOD OF 01 NOVEMBER 1998 – 31 MAY 2000

Approved for public release; distribution unlimited.

AIR VEHICLES DIRECTORATE
AIR FORCE RESEARCH LABORATORY
AIR FORCE MATERIEL COMMAND
WRIGHT-PATTERSON AIR FORCE BASE, OH 45433-7542

REPORT DOCUMENTATION PAGE

Form Approved OMB No. 0704-0188

1. REPORT DATE (DD-MM-YYYY)	2. REPORT TYPE	3. DATES COVERED (FROM - TO)
01-06-2000		01-11-1998 to 31-05-2000

4. TITLE AND SUBTITLE
Enhancement to Repair Assessment Procedure and Integrated Design (RAPID) Analysis Methods Enhancements
Unclassified

5a. CONTRACT NUMBER
5b. GRANT NUMBER
5c. PROGRAM ELEMENT NUMBER

6. AUTHOR(S)

5d. PROJECT NUMBER
5e. TASK NUMBER
5f. WORK UNIT NUMBER

7. PERFORMING ORGANIZATION NAME AND ADDRESS
THE BOEING COMPANY
2401 E. WARDLOW ROAD
LONG BEACH, CA90807-5309

8. PERFORMING ORGANIZATION REPORT NUMBER

9. SPONSORING/MONITORING AGENCY NAME AND ADDRESS
,

10. SPONSOR/MONITOR'S ACRONYM(S)
11. SPONSOR/MONITOR'S REPORT NUMBER(S)

12. DISTRIBUTION/AVAILABILITY STATEMENT
APUBLIC RELEASE
,

13. SUPPLEMENTARY NOTES

14. ABSTRACT
This document describes the technical details of the analysis methodology used in the static and damage tolerance analysis modules of the Repair Assessment Procedure and Integrated Design (RAPID) program. In this document, the static strength analysis method for repaired fuselage skin and skin modifications to antenna installation is first described. Next, a description of the damage tolerance method is provided. This document also includes descriptions of the methods developed for the damage tolerance analysis of common repairs including a repair near another repair and repairs at stiffeners. Flowcharts of static and damage tolerance analysis methods are provided.

15. SUBJECT TERMS

16. SECURITY CLASSIFICATION OF:			17. LIMITATION OF ABSTRACT	18. NUMBER OF PAGES	19. NAME OF RESPONSIBLE PERSON
a. REPORT	b. ABSTRACT	c. THIS PAGE	Same as Report (SAR)	319	Cornell, Elizabeth ecornell@dtic.mil em1133
Unclassified	Unclassified	Unclassified			19b. TELEPHONE NUMBER International Area Code Area Code Telephone Number DSN

NOTICE

USING GOVERNMENT DRAWINGS, SPECIFICATIONS, OR OTHER DATA INCLUDED IN THIS DOCUMENT FOR ANY PURPOSE OTHER THAN GOVERNMENT PROCUREMENT DOES NOT IN ANY WAY OBLIGATE THE US GOVERNMENT. THE FACT THAT THE GOVERNMENT FORMULATED OR SUPPLIED THE DRAWINGS, SPECIFICATIONS, OR OTHER DATA DOES NOT LICENSE THE HOLDER OR ANY OTHER PERSON OR CORPORATION; OR CONVEY ANY RIGHTS OR PERMISSION TO MANUFACTURE, USE, OR SELL ANY PATENTED INVENTION THAT MAY RELATE TO THEM.

THIS REPORT IS RELEASABLE TO THE NATIONAL TECHNICAL INFORMATION SERVICE (NTIS). AT NTIS, IT WILL BE AVAILABLE TO THE GENERAL PUBLIC, INCLUDING FOREIGN NATIONS.

THIS TECHNICAL REPORT HAS BEEN REVIEWED AND IS APPROVED FOR PUBLICATION.

MICHAEL T. MYERS, Capt, UASF
Lead Engineer, Aircraft Repair
Analytical Structural Mechanics Branch

DAVID M. AGINS, Maj, USAF
Chief, Analytical Structural Mechanics Branch
Structures Division

JEFFREY S. TURCOTTE, LTC, USAF
Deputy Chief
Structures Division

Do not return copies of this report unless contractual obligations or notice on a specific document requires its return.

REPORT DOCUMENTATION PAGE

Form Approved
OMB No. 074-0188

1. AGENCY USE ONLY (Leave blank)	2. REPORT DATE	3. REPORT TYPE AND DATES COVERED
	JUNE 2000	Final, 11/01/1998 – 05/31/2000

4. TITLE AND SUBTITLE
ENHANCEMENTS TO REPAIR ASSESSMENT PROCEDURE AND INTEGRATED DESIGN (RAPID)

ANALYSIS METHODS ENHANCEMENTS

5. FUNDING NUMBERS
C: F33615–95–D–3217
PE: 69199F
PR: OAFF
TA: 98
WU: 16

6. AUTHOR(S)

Chun Chen, Miles Nomura, and Jin Yu

7. PERFORMING ORGANIZATION NAME(S) AND ADDRESS(ES)

THE BOEING COMPANY
2401 E. WARDLOW ROAD
LONG BEACH, CA 90807-5309

8. PERFORMING ORGANIZATION REPORT NUMBER
CRAD-9902-TR-6440

9. SPONSORING / MONITORING AGENCY NAME(S) AND ADDRESS(ES)

AIR VEHICLES DIRECTORATE
AIR FORCE RESEARCH LABORATORY
AIR FORCE MATERIEL COMMAND
WRIGHT-PATTERSON AIR FORCE BASE, OH 45433-7542
POC: EDWARD SCHOPLER, AFRL/VASM, (937) 656-5755

10. SPONSORING / MONITORING AGENCY REPORT NUMBER
AFRL-VA-WP-TR-2000-3030

11. SUPPLEMENTARY NOTES:

12a. DISTRIBUTION / AVAILABILITY STATEMENT
Approved for public release; distribution unlimited.

12b. DISTRIBUTION CODE

13. ABSTRACT ***(Maximum 200 Words)***

This document describes the technical details of the analysis methodology used in the static and damage tolerance analysis modules of the Repair Assessment Procedure and Integrated Design (RAPID) program. In this document, the static strength analysis method for repaired fuselage skin and skin modifications to antenna installation is first described. Next, a description of the damage tolerance method is provided. This document also includes descriptions of the methods developed for the damage tolerance analysis of common repairs including a repair near another repair and repairs at stiffeners. Flowcharts of static and damage tolerance analysis methods are provided.

14. SUBJECT TERMS
Computer design tool, Design and analysis, Bolted repairs, Damage tolerance, Aircraft repair

15. NUMBER OF PAGES
322

16. PRICE CODE

17. SECURITY CLASSIFICATION OF REPORT	18. SECURITY CLASSIFICATION OF THIS PAGE	19. SECURITY CLASSIFICATION OF ABSTRACT	20. LIMITATION OF ABSTRACT
Unclassified	Unclassified	Unclassified	SAR

NSN 7540-01-280-5500

Standard Form 298 (Rev. 2-89)
Prescribed by ANSI Std. Z39-18
298-102

Table of Contents

Appendices

1. Introduction

This document describes technical details of the analysis methodology used in the static and damage tolerance analysis modules of the Repair Assessment Procedure and Integrated Design (RAPID) program. In this document, the static strength analysis method for repaired fuselage skin and skin modifications to antenna installation is first described. Next, a description of the damage tolerance analysis method is provided. This document also includes descriptions of the methods developed for the damage tolerance analysis of common repairs including a repair near another repair and repairs at stiffeners. Flow charts of static and damage tolerance analysis methods are provided.

RAPID is an analysis tool that performs the static strength and damage tolerance analysis of aircraft fuselage skin repairs and skin modifications to antenna installation. The tool assists the user in assessing mechanically fastened fuselage skin repairs with doublers and skin modifications with a mounting plate for antenna installation. The static analysis determines if the doublers, mounting plate, and fasteners are statically adequate, and the damage tolerance analysis yields the residual strength and the crack growth life to assist users in determination of inspection intervals for maintenance schedule.

With the added 2-D stress analysis capability, RAPID can now directly calculate the load transfers at critical fasteners and stress gradients along the potential crack growth path in a repair or antenna installation.

In the following, static strength and damage tolerance analysis methods for fuselage skin repairs are described. Analysis methods for modified skin to antenna installation are described in Appendix K.

An executable version of this program is available at http://aar400.tc.faa.gov/rapid under the title "RAPID v 3.0 Pre-Beta Release".

2. Static Module

Typical repairs on the aircraft fuselage generally involve removing the damaged skin area and replacing it with repair doublers. The repair doublers are mechanically fastened to the skin around the skin cutout. To assess the static strength of fuselage skin repairs, three independent criteria are used to evaluate the margins of safety of repair doublers and fasteners.

2.1 The Repair Doubler Allowable and Margin of Safety

To assess the strength restored by the repair, the margin of safety of repair doublers is calculated as

$$\text{Margin of Safety} = \frac{P_{du}}{P_d} - 1$$

where P_{du}, the doubler force allowable per inch, is calculated using the equation

$$P_{du} = \sum_{1}^{N} F_{tu}\ t_D$$

in which F_{tu} and t_D are the ultimate tensile strength of the doubler material and the thickness of each repair doubler, respectively, and N is the total number repair doublers.

The skin internal force per inch, P_d, is calculated using the equation

$$P_d = \sum_{1}^{L} \sigma_u t_s$$

where σ_u and t_s are the design ultimate tensile stress of the skin material and the thickness of each skin layer, respectively, and L is the total number skin layers.

2.2 The Fastener Joint Allowable and Margin of Safety

In the vicinity of a skin repair, skin stresses are transferred to the repair doublers through the fasteners via fastener shear and hole bearing. The fastener with the skin and repair doubler(s) represents a fastener joint. This joint as a whole can only transfer a certain amount of load until it fails. The point at which this fastener joint fails is the joint allowable. The calculation of the joint allowable is based upon two loading conditions, fastener shear and hole bearing. Two hole types also have to be considered when determining the joint allowable, straight shank and countersunk.

2.2.1 Fastener Joint Allowable in Straight Shank Holes

Straight shank holes are used for protruding head fasteners and for the layers of the repairs that have a flush head fastener installed but are not countersunk. The joint allowable is the lower of the shear allowable or the hole bearing allowable. An allowable is calculated for each layer of the skin and repair doubler that the fastener goes through.

The single shear allowable for straight shank holes is calculated using the following equation

$$P_{su} = F_{su} \times A_f \times S_{CF1}$$

The double shear allowable for straight shank holes is calculated using the following equation

$$P_{su} = 2 \times F_{su} \times A_f \times S_{CF2}$$

In both equations, F_{su} is the ultimate shear strength of the fastener material, A_f is the cross-sectional area of each fastener, S_{CF1} is the single shear correction factor and S_{CF2} is the double shear correction factor. S_{CF1} and S_{CF2} are used only for solid rivets and can be found in MIL-Handbook 5F Table 8.1.2.1(b).

The hole bearing allowable for the straight shank hole is calculated using the following equation

$$P_{bru} = F_{bru} \times d \times t$$

in which F_{bru} is the ultimate bearing stress of the plate (skin or doubler) material, d is the fastener hole diameter, and t is the thickness of that layer. Currently, the F_{bru} is the case from E/D (edge distance to hole diameter) equal to 2.0.

The joint allowable for a particular fastener installed in a particular material and thickness and in a particular hole condition is the lower of P_{su} or P_{bru}. The specific joint allowable is $P_{joint.}$

2.2.2 Fastener Joint Allowable in Countersunk Holes

The fastener joint allowable for countersunk holes is different from the straight shank holes. The joint allowables for countersunk holes are determined by tests and are tabulated in MIL-Handbook 5F Section 8.

2.2.3 Fastener Joint Margin of Safety

The fastener joint margin of safety is determined using the total fastener joint allowable in the skin layers and repair doubler layers, and this is done for each side of the repair. The total fastener joint allowable is determined using the following equation

$$P_{total} = \sum_{n=1}^{K} \left(P_{joint}\right)_n$$

in which P_{total} is the total fastener joint load, $(P_{joint})_n$ is the fastener joint load for the nth fastener and K is the number fasteners. P_{total} is determined for each skin and repair doubler layer for each side of the repair. If multiple skin layers are present, then the fastener joint allowable for each layer in the skin is added together for the P_{total} for the skin layers. If multiple-repair doubler layers are present then the fastener joint allowable for each repair doubler layer is added together for the P_{total} for the repair doublers.

After P_{total} is determined for the skin layers and repair doubler layers for each side, then the values of the skin layers and repair doubler layers are compared. The smaller of the two is the fastener joint allowable for that side of the repair and is used in determining the margin of safety for the fastener joints.

An applied load is needed to determine a margin of safety. That load is the ultimate applied load to the structure, or if that is not known, then it is based on the tensile ultimate strength of the material F_{tu}. This applied load $P_{applied}$ is calculated using the following equation

$$P_{applied} = \sum_{n=1}^{L} \left(\sigma_u \, l \, t_s\right)_n$$

where σ_u is the design ultimate tensile stress or the tensile ultimate skin strength, t_s is the thickness of each skin layer, l is the length of damage treatment (cutout, blendout, etc.) normal to the fastener load direction, and L is the number of skin layers. The margin of safety is given by the following equation

$$\text{Margin of Safety} = \frac{P_{total}}{P_{applied}} - 1$$

2.2.4 Shear Margin of Safety

The shear margin of safety of the repair is calculated using the following equation

$$\text{Margin of Safety} = \frac{\sum_{i=1}^{\text{number of layers}} (F_{su} * \text{thickness})_{doublers}}{\sum_{k=1}^{\text{number of layers}} (F_{su} * \text{thickness})_{skin}} - 1$$

where F_{SU} is the ultimate shear strength of the skin or doubler material. The equation is used for each side of the repair.

2.3 Margin of Safety

The margins of safety (MS) based on the repair doubler allowable and the fastener joint allowables are calculated to determine the adequacy of the repair.

- MS < 0 Repair is statically inadequate
- MS = 0 Repair is marginally adequate
- MS > 0 Repair is statically adequate

For repairs that are not statically adequate, the repair must be redesigned to ensure the adequacy of the repair.

2.4 The Stiffness Check of the Repair

The stiffness ratio between the repair doublers and the skin layers is calculated using the following equation

$$\text{Stiffness Ratio} = \frac{\sum_{i=1}^{\text{number of layers}} \left(T_{repair} * E_{doubler}\right)}{\sum_{k=1}^{\text{number of layers}} \left(T_{skin} * E_{skin}\right)}$$

The repair is considered adequate if the ratio is between 1.0 and 1.5. The repair is too stiff when the value is greater than 1.5 and not stiff enough when it is less than 1.0.

2.5 The Fastener Bending Check of the Repair

The fastener bending is checked using the following equation

$$Q = \frac{\text{thickness of stack-up layers}}{\text{fastener diameter}}$$

The parameter Q is the fastener bending indicator. For aluminum fasteners, the bending is impertinent when Q is less than 2.0. For steel and titanium fasteners, there is no constraint for typical fuselage repairs.

2.6 The Inter-Rivet Buckling Guideline

To avoid inter-rivet buckling in the repaired skin, the fastener spacing should be four to six times the diameter of the fastener shank diameter.

3. Damage Tolerance Module

The damage tolerance of a repaired skin is the ability of that repaired skin to resist failure due to the presence of cracks for a specified period of unrepaired usage of the aircraft. In essence, for a repaired skin to be damage tolerant, the repair must be designed so that the residual strength never falls below a specified level. An inspection schedule must be determined, based on the residual strength and crack growth life of the repaired skin, to ensure this

3.1 Crack Growth Analysis

Initial crack locations, crack lengths, and the subsequent crack growths need to be assumed to perform the crack growth analysis of a repaired skin. Elements needed for the crack growth analysis include

- Load transfer at critical fastener locations
- Initial crack and subsequent damage assumptions
- Crack growth rate data of the material
- Stress intensity factors of relevant crack configurations
- Stress spectra and/or equivalent stress
- Crack growth life prediction methods

3.1.1 Load Transfers at Critical Fastener Locations

The crack growth life prediction of a repaired skin requires an accurate estimate of skin stresses and load transfers along the critical fastener row. The data needed to make these estimates have been obtained for three basic repairs shown in figure 1 using a two-dimensional finite element analysis. Appendix A describes details of the database development. The effect on load transfers in a basic repair due to the presence of an adjacent basic repair is provided in appendix E. The database development for load transfer in repairs at stiffeners and circular repairs is described in appendices F and G, respectively.

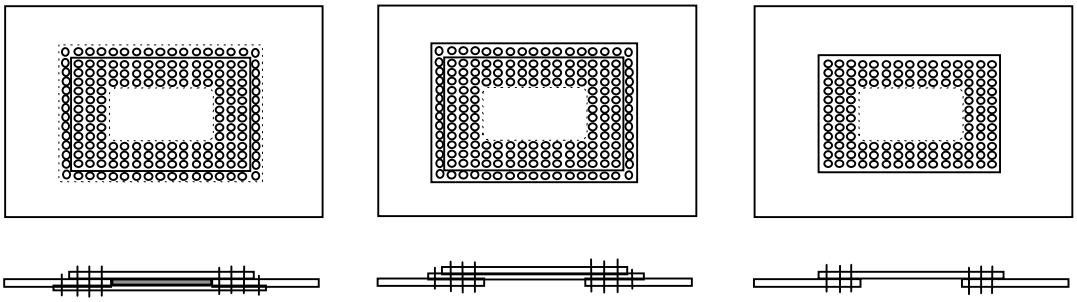

Type I Repair Type II Repair Type III Repair

Figure 1. Three Basic Repairs

3.1.2 Initial Crack and Subsequent Damage Assumptions

Based on the two-dimensional analysis of three basic repairs, the load transfer at the corner fasteners is higher than that at other fasteners along the critical outermost fastener row. It is rational to postulate an initial crack at the corner fastener hole. Furthermore, a crack initiating at the center fastener hole can be critical because the crack may be hidden from visual inspection before it reaches the critical length. In RAPID, initial damage configurations and subsequent damage for repairs are described below.

Scenario 1: Center fastener hole in the outermost fastener row

Initial Crack: Two diametric through cracks of lengths 0.05" and 0.005", respectively, emanating from the center fastener hole together with a 0.005" crack at one side of every other hole

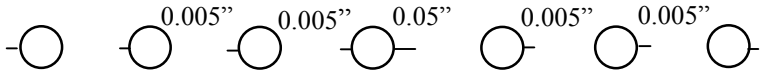

Subsequent Damage: All cracks grow concurrently but independently, interaction between cracks being ignored. The amount of growth δa_1 for the 0.005" crack is added to its original length when the 0.05" crack grows into the adjacent hole. The same process continues in successive growth.

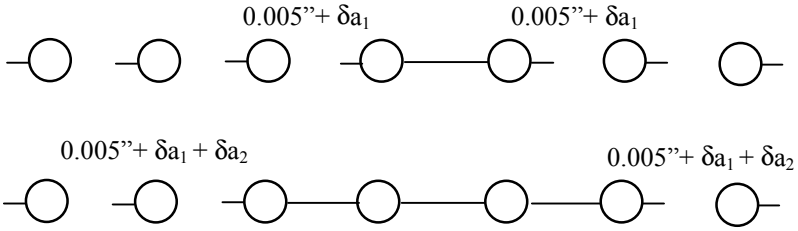

Scenario 2: Corner fastener hole in the outermost fastener row

Initial Crack: Two diametric through cracks of lengths 0.05", pointing toward the adjacent hole, and 0.005", respectively, emanating from the corner fastener hole together with a 0.005" crack at one side of every other hole

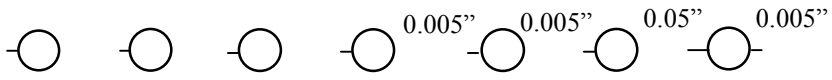

Subsequent Damage: All cracks grow concurrently but independently, without interaction between cracks being considered. The amount of growth δa for the 0.005" crack is added to its original length when the 0.05" crack grows into the adjacent hole. The same process continues in successive growth.

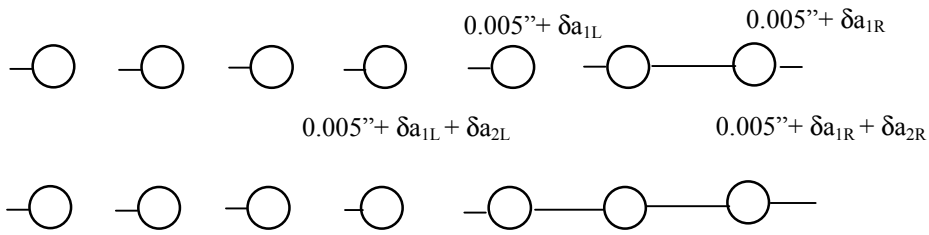

It is noted that successive growths of the 0.005" at corner fastener hole $\delta a_{1R,}$ $\delta a_{2R,}$ etc. are different from the growths at other holes $\delta a_{1L,}$ $\delta a_{2L,}$ etc. because the former does not grow toward an adjacent hole but others do.

Figure 2. Initial Flaws and Subsequent Growths Assumptions

For circular repairs, it is postulated that two initial diametric cracks with 0.05" and 0.005" at the top or bottom fastener exist in the outermost ring. The cracks grow concurrently but independently in the skin.

3.1.3 Crack Growth Rate Data

The crack growth rate baseline data obtained experimentally from constant amplitude coupon tests in the form of da/dN versus ΔK for the material are generally documented in a tabular form. The tabulated data can be used directly in the crack growth calculation using the cycle-by-cycle method. In RAPID, the following da/dN versus ΔK tabular data of thirteen materials are included in the material database.

(1) .....2024-T3 Clad Sheet, -T42 Bare Sheet, L-T RT LA DW
(2) .....2024-T3 Clad Sheet, -T42 Bare Sheet, T-L RT LA DW
(3) .....2024-T351 Plate, -T3511 Extrusion, L-T RT LA DW
(4) ..... 7050-T7452 Forging, L-T T-L LA RT
(5) .....7050-T74511, -T76511 Extrusion, L-T RT LA DW
(6) ..... 7050-T74511 Extrusion, L-T RT STW
(7) ..... 7050-T7651, -T7451 Plate, L-T T-L RT LA DW
(8) ..... 7050-T76511 Extrusion, L-T RT STW
(9) .....7475-T7351 Plate, L-T LA RT
(10) ..... 7475-T7651 Plate, L-T LA RT DW
(11) .....7475-T761 Clad Sheet, L-T RT LA DW
(12) .....7075-T6 Clad Sheet, L-T RT LA
(13) ..... 2014-T6 Sheet, T=0.05 L-T RT LA 10 HZ

where

L-T:.....longitudinal-transverse material orientation
T-L:.....transverse-longitudinal material orientation
RT:.....room temperature test condition
LA: .....laboratory air environmental test condition
DW: .....distilled water environmental test condition
STW: .....sump tank water environmental test condition

RAPID also provides user with direct input of da/dN tabular data or Walker's coefficients. The input format of the da/dN tabular data is described as follows.

```
Line 1 → 1
         3          30      (2024-T3 CLAD SHEET,-T42 BARE SHEET, L-T RT LA DW)
         0.05            0.40        0.80
Line 4 →0.100E-31        0.100E-07   0.300E-07   0.500E-07   0.700E-07   0.800E-07   0.100E-06   0.200E-06
         0.300E-06       0.500E-06   0.800E-06   0.100E-05   0.200E-05   0.500E-05   0.800E-05   0.100E-04
         0.200E-04       0.400E-04   0.800E-04   0.100E-03   0.200E-03   0.500E-03   0.100E-02   0.300E-02
         0.800E-02       0.200E-01   0.500E-01   0.100E+00   0.200E+00   0.100E+01
Line 8 →2.8990           2.9000      2.9010      3.0000      3.2000      3.3000      3.6000      4.7500
         5.5000          6.2000      6.6000      6.8000      8.0000      10.1000     12.2000     13.2500
         16.9000         20.0000     24.2000     25.6000     29.6000     36.0000     41.0000     50.5000
         61.0000         70.0000     78.0000     87.0000     92.0000     93.0000
Line 12→2.3480           2.3490      2.3500      2.3600      2.5000      2.6000      2.8800      3.9000
         4.5000          5.1500      5.7000      6.0000      7.0000      8.7500      9.9000      10.5000
         13.2500         16.0000     19.5000     21.0000     24.5000     29.0000     33.5000     41.5000
         48.0000         51.0000     54.0000     56.5000     57.0000     58.0000
Line 16→1.7490           1.7500      1.7600      1.7700      1.8200      1.8750      2.0500      2.8500
         3.4000          4.0000      4.5000      4.8000      5.6000      7.0000      8.0000      8.4000
         9.9000          11.5000     13.0000     13.5000     15.3000     18.0000     19.8000     20.0000
         20.0010         20.0020     20.0030     20.0040     20.0050     20.0060
```

Line	Acronym	Type	Definition
1	NMAT	Integer	The material number that corresponds with the material number containing the Walker's C, p and q values
2	MRATIO	Integer	The first integer number is the number of different ratio values in line 3; the maximum value is 10
2	MVALUE	Integer	The second integer value is the number of da/dN values in lines 4-7, and ΔK values in lines 8-11, 12-15, and 16-19; the maximum value is 40
2	-	-	Description of the material; optional
3	RATIOV	Real	The different ratio values in ascending order; there are *MRATIO* values
4-7	DADN	Real	The da/dN values; there are *MVALUE* values for this y-axis
8-11, 12-15, 16-19	DELTAK	Real	The ΔK values; there are *MVALUE* values, and *MRATIO* sets for this x-axis

When the crack growth analysis is performed using the simplified method (section 3.1.6.1), the crack growth rate data need to be curve fitted to the Walker's equation:

$$\frac{da}{dN} = C\left[\left(1-R\right)^{q} \, K_{max} \right]^{p}$$

In practice, the coefficients C and p are determined from the R = 0 test data. In this case, the above equation is reduced to

$$\frac{da}{dN} = C\left[K_{max} \right]^{p}$$

Taking the logarithm of both sides of the above equation, the following linear equation is obtained

$$\log\left(\frac{da}{dN} \right) = \log\left(C \right) + p \log\left(K_{max} \right)$$

A least square fit is then used to determine the values of C and p. Data for the positive stress ratio determines the value of q. Let ζ_{ij} represent the ratio of the j-th da/dN data between the $R_I > 0$ and R = 0 conditions, respectively,

$$\zeta_{ij} = \frac{\left(da/dN\right)_{j \; R_i > 0}}{\left(da/dN\right)_{j \; R=0}}$$

Substitution of the Walker's equation into the above equation leads to

$$\zeta_{ij} = (1 - R_i)^{p \, q_{ij}}$$

For each j-th raw datum, the coefficient q_{ij} can be expressed as

$$q_{ij} = \frac{\log \zeta_{ij}}{p \log(1 - R_i)}$$

The coefficient $\bar{q}_i$ for each set of $R_i > 0$ raw data is then determined by taking the average of the sum of q_{ij} for all data points, i.e.,

$$\bar{q}_i = \frac{1}{M} \sum_{j=1}^{M} q_{ij}$$

where M is the number of data points in the R_i raw rate data. The coefficient q in the Walker's equation is obtained by averaging the $\bar{q}$ values, i.e.,

$$q = \frac{1}{N}\sum_{i=1}^{N} \bar{q}_i$$

where N is the number of positive stress ratio sets for the material. In RAPID, the crack growth due to negative stress ratios ($R < 0$) is treated as the same as $R = 0$. The coefficients C, P, and q for the above mentioned thirteen materials have been obtained and stored in the material database. The values can also be input through the edit boxes in the skin material property window.

3.1.4 Stress-Intensity Factors

The stress-intensity factor of a crack, denoted by K, characterizes the stress field near the crack tip. It has been successfully used in crack growth prediction models under cyclic load as well as in fracture toughness measurements. The value of K depends on the crack configuration in the structural geometry and the loads applied in the structure.

Stress-intensity factor solutions for the crack geometries in the crack sequences described in section 3.1.2 are required for damage tolerance analysis. Two types of stress-intensity factor solutions are used in RAPID. The first are basic solutions and the second are solutions derived from the basic solutions using engineering methods.

For a simple crack configuration such as two diametric through cracks of unequal lengths emanating from a circular hole in a wide plate subjected to uniform far field stress, closed-form solutions for stress-intensity factors have been obtained analytically based on the theory of elasticity. Closed-form solutions for more complex crack configuration such as through cracks emanating from linked holes are not available. In such a case, engineering methods are generally used to estimate the solutions.

One engineering method widely used in the aircraft industry is the compounding method. The method is generally used when there are boundaries such as edges, holes, and stiffened attachments in the cracked structures. In this method, the geometry factor due to each boundary is individually calculated. A compounded geometry factor is then obtained by multiplying all individual geometry factors. The stress-intensity factor of the cracked structure with boundaries is estimated as the compounded geometry factor times the stress-intensity factor for the same cracked structure without the boundary effects.

Another method used in engineering practice is the similarity method. For example, the stress-intensity factor under one load condition can be estimated from that under another load condition by a correction factor. In another example, the stress-intensity factor for one crack configuration can be estimated based on that for another crack configuration multiplied by a correction factor.

A third method used is the superposition method. This method is used for the problem of a cracked structure subjected to a combination of several loads.

3.1.4.1 Compounding Method

In the compounding method, the stress-intensity factor of a cracked structure with boundary is estimated by multiplying the stress-intensity factor of the cracked structure without the boundary by a compounded geometry factor

$$K_{\text{with boundary}} = K_{\text{without boundary}}\, \beta_{\text{Compounded}}$$

The compounded geometry factor is the product of a set of geometry factors that account for the boundary effects

$$\beta_{\text{Compounded}} = \prod_{i=1}^{M} \beta_i$$

where $\prod$ represents the mathematical symbol for the product, β_i the geometry factor for the i-th geometry, and M is the total number of boundaries.

As an example, consider a through crack at a hole growing towards an adjacent hole in a wide plate subjected to uniform far field stress as shown in figure 5.

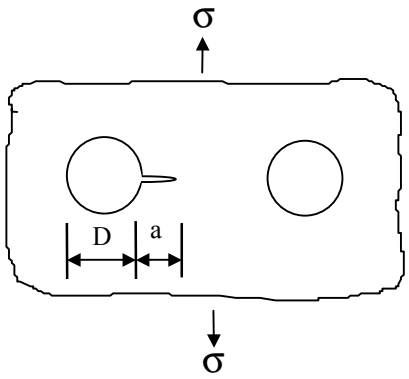

Figure 5. Illustration of the Compounding Method

The stress-intensity factor can be estimated as

$$K = K_0\, \beta_{\text{Compounded}}$$

where K_0 is the stress-intensity factor equal to $\sigma\sqrt{\pi a}$ for a through crack in a wide plate subjected to far field stress, and $\beta_{\text{Compounded}}$ is the compounded geometry factor obtained as the product of geometry factors β_A and β_B for the cracked structures as shown in figure 6(A) and 6(B), respectively.

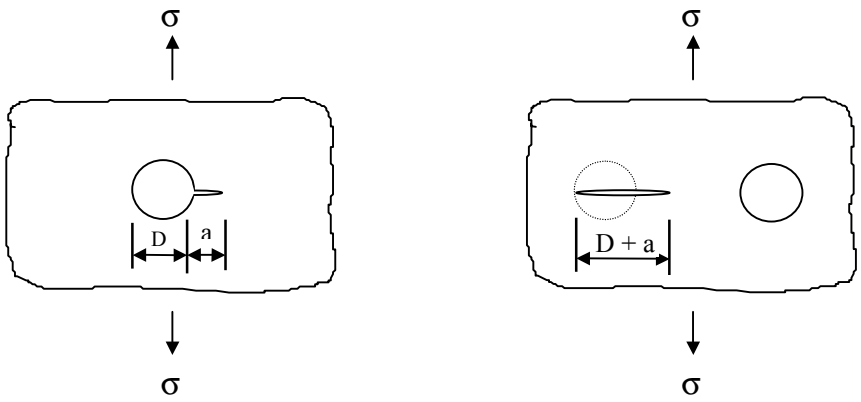

(a) A Crack at a Hole in a Wide Plate Subjected to Far Field Stress

(b) A Crack Approaching an Adjacent Hole

Figure 6. Cracked Structures Considered for Compounding

The compounded geometry factor $\beta_{Compounded}$ can be calculated as

$$\beta_{Compounded} = \beta_A \beta_B$$

In the above equation, the β's are defined as

$$\beta_i = \frac{K_i}{\sigma\sqrt{\pi a^*}} \qquad (i = A, B)$$

where K_A and K_B are the stress-intensity factors for the cracked structures in figure 6(A) and 6(B), respectively. The crack length a^* is the crack length a in case 6(A), and is one half of the crack length D+a in case 6(B).

3.1.4.2 The Similarity Method

The similarity method can be illustrated using an example problem. Suppose one wants to estimate the stress-intensity factors of two unequal-length cracks emanating from opposite sides of a hole in a wide plate subjected to a pair of point loads acting on the hole as shown in figure 7.

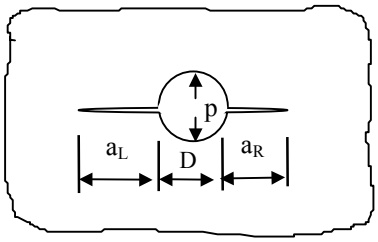

Figure 7. A Plate with Two Cracks at a Hole

To estimate the stress-intensity factors for both cracks, consider the three cases as shown in figure 7.

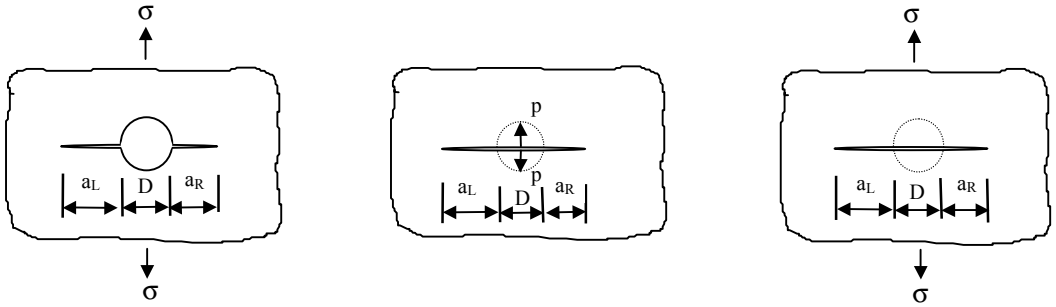

(A) Two Unequal Length Cracks at a Hole in a Wide Plate Under Uniform FarFfield Stress

(B) A Through Crack in a Wide Plate Subjected a Pair of Point Loads on Crack Surfaces

(C) A Through Crack in a Wide Plate Under Uniform Far Field Stress

Figure 8. Cracked Plates for Illustration of the Similarity Method

The stress-intensity factors K_L and K_R for the left and right cracks, respectively, in figure 8 can be estimated using the relation

$$K_i = K_{i,A} \frac{K_{i,B}}{K_{i,C}} \quad \text{..... } (i = L, R)$$

With this relation, the compounded geometry factor can be obtained as

$$\beta_{i,\text{Compounded}} = \beta_{i,A} \frac{\beta_{i,B}}{\beta_{i,C}} \qquad (i = L, R)$$

where β_A, β_B, and β_C are the geometry factors for crack configurations figure 8(a), (b), and (c).

In the above equation, $\beta_{i,\text{Compounded}}$ is the compounded geometry factor for the cracked structure in figure 8. It is defined as

$$\beta_{i,Compounded} = \frac{K_i}{\frac{p}{D}\sqrt{\pi a_i}} \quad (i = L, R)$$

where K_i is the stress-intensity factor for the crack i. The geometry factors $\beta_{i,A}$, $\beta_{i,B}$, and $\beta_{i,C}$ are defined as

$$\beta_{ij} = \frac{K_{ij}}{K_{0,ij}} \qquad (i = L, R \text{ and } j = A, B, C)$$

in which K_{ij} is the stress-intensity factor for the crack i (left or right) in the case j. The referenced stress-intensity factor $K_{0,ij}$ is defined as

$$K_{0,ij} = \sigma^* \sqrt{\pi a^*} \quad (i = L, R \text{ and } j = A, B, C)$$

In the above equation, σ^* is the far field stress for cases A and C, and is the stress p/D per unit thickness of the plate for case B. The crack length a^* is the crack length a_L or a_R for case A, and is one half of the crack length $a_L + D + a_R$ for cases B and C.

3.1.4.3 The Superposition Method

The superposition method is used to obtain the stress-intensity factors in a cracked structure subjected to combined loads. As the term superposition implies, the stress-intensity factor due to combined loads is the sum of contribution from each load condition. The given loading is decomposed into a set of loads for which solutions are available. For instance, the stress-intensity factor for a crack emanating from a hole in a wide plate subjected to the remote gross stress σ_{Gross}, the bearing stress $\sigma_{Bearing}$, and the bypass stress σ_{Bypass} can be determined by superimposing two stress-intensity factors. One is the remote stress equal to one half of the sum of σ_{Gross} and σ_{Bypass}, and the other one half of a pair of bearing stresses $\sigma_{Bearing}$ in the hole. If ξ and ζ denote the ratios of bypass and bearing stresses to the gross stress, respectively, the superposition method can be illustrated in figure 9.

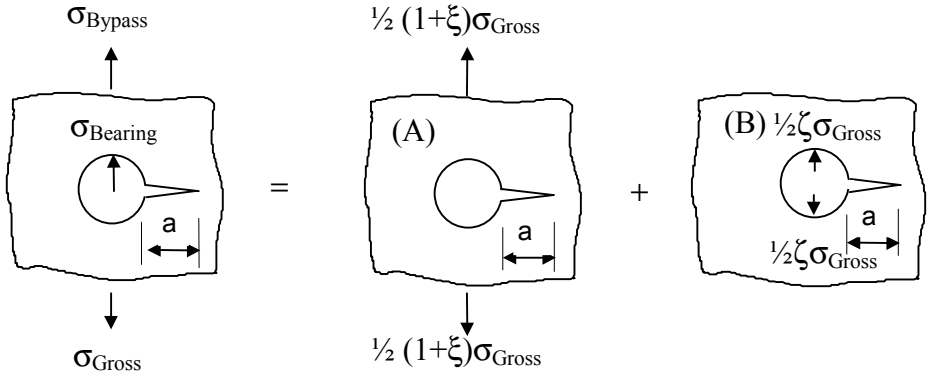

Figure 9. Illustration of the Superposition Method

The stress-intensity factor K is then obtained using the superposition method as

$$K = K_A + K_B$$

$$= \tfrac{1}{2}\left(1+\xi\right)\sigma_{Gross}\sqrt{\pi a}\,\beta_A + \tfrac{1}{2}\zeta\,\sigma_{Gross}\sqrt{\pi a}\,\beta_B$$

$$= \tfrac{1}{2}\left[\left(1+\xi\right)\beta_A + \zeta\beta_B\right]\sigma_{Gross}\sqrt{\pi a}$$

In the above equation, β_A and β_B are the geometry factors for case A and case B, respectively. The geometry factor for the cracked structure subjected to the combined stresses is therefore obtained as

$$\beta = K / K_o$$

$$= \tfrac{1}{2}\left[\,(1+\xi)\,\beta_B + \zeta\,\beta_C\,\right]$$

where K_o is the stress-intensity factor equal to $\sigma_{Gross}\sqrt{\pi a}$.

With these three methods, stress-intensity factors of crack geometries in the crack sequences as described in section 3.1.2 can be obtained. Geometry factors can be printed out when requested by the user. Stress-intensity factor solutions for simple crack configurations and the derived solutions for a crack passing through multiple holes are described in Appendix B.

3.1.5 Stress Spectrum and Equivalent Stress

To predict the crack growth life of a repaired fuselage skin, the stress spectrum at the repair location needs to be prescribed. RAPID generates the stress spectrum from the load spectrum at the fuselage center of gravity. There are two generic load spectra built in RAPID, one for the narrow-body and the other for the wide-body aircraft. In addition, RAPID accepts a stress spectrum that can be provided by the user.

The stress spectrum, either generated by RAPID or provided by the user, can be used in the cycle-by-cycle crack growth analysis. A one cycle equivalent stress representing a flight cycle can be calculated from the stress spectrum and used in the simplified crack growth analysis. The user can provide RAPID with the equivalent stress as well. The analysis process is described in figure 10.

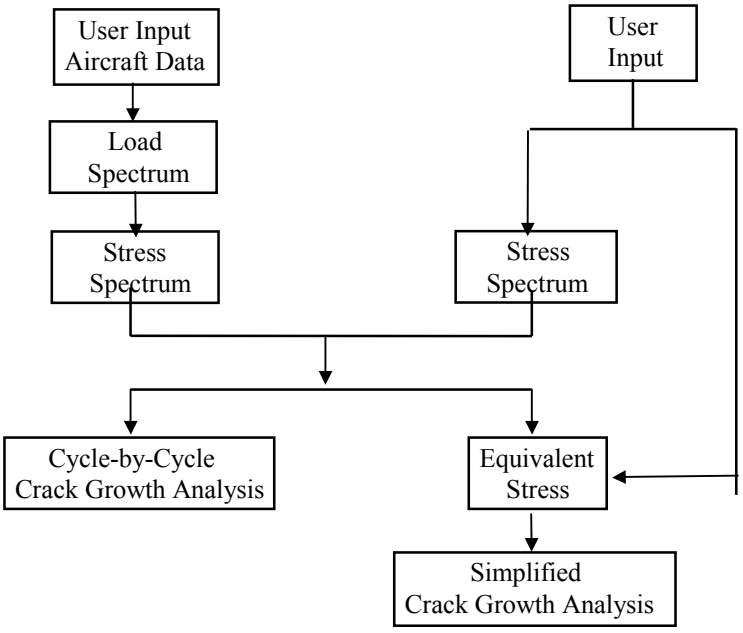

Figure 10. RAPID Analysis Process

Load spectrum development and the stress spectrum generation methods have been developed for RAPID. Appendix C provides the details. For the calculation of one cycle equivalent stress, the method is described in appendix D.

3.1.6 Crack Growth Analysis Methods

Two methods have been implemented in RAPID for the crack growth analysis, the simplified method [1] and the cycle-by-cycle method. In the cycle-by-cycle method, the retardation effect due to occasional stress overloads is accounted using the Generalized Willenborg Model [2,3,4]. In RAPID, the crack growth analysis is performed up to 300,000 flight cycles.

3.1.6.1 The Simplified Method

In the simplified crack growth analysis method, the number of flights for a crack growing from the size a_i to the size a_j ($a_j > a_i$) can be calculated by the equation

$$N_{ij} = \frac{1}{C} (S G_{ij})^{-p}$$

where C and p are the coefficients in the Walker's equation (see section 3.1.3), S is the equivalent stress, and G_{ij} is the geometry term. The quantity G_{ij} represents the cumulative geometry effect and is calculated by the equation

$$G_{ij}^{-p} = \int_{a_i}^{a_j} \left[\beta(a)\sqrt{\pi a} \right]^{-p} da$$

where $\beta(a)$ is the geometry factor. The integration is carried out numerically using the Gaussian quadrature method [5]. In this method, the integral can be approximated by the following equation

$$G_{ij}^{-p} = \frac{a_j - a_i}{2} \sum_{k=1}^{K} w_k \, g(a_k)$$

where

$$g(a_k) = [\beta(a_k)\sqrt{\pi a_k}]^{-p}$$

and

$$a_k = \frac{(a_j - a_i)\, t_k + (a_j + a_i)}{2}$$

In the above equations, the variables w_k and t_k are the k-th weighting coefficient and root of the K-th order Legendre polynomial $P_K(t) = 0$. Values of w and t for the case of k = 4 are given below.

k	W_k	t_k
1	0.347855	-0.861136
2	0.652145	-0.339981
3	0.652145	0.339981
4	0.347855	0.861136

For a crack emanating from a fastener hole, the crack growth calculation is straightforward. For a through crack passing through multiple fastener holes, an iteration scheme is employed in crack growth calculation. In this scheme, the cracks are assumed to grow, at any stage, an increment of Δa_p for the primary crack and Δa_s for the secondary crack. The number of flights is then calculated independently for each crack. The increment Δa_s is then adjusted accordingly, depending on whether the number of flights for the secondary crack is greater or smaller than that for the primary crack. The iterations continue until the difference in the number of flights is within a specified tolerance level.

3.1.6.2 The Cycle-by-Cycle Method

The cycle-by-cycle crack growth analysis method is illustrated by the example shown in figure11. The analysis procedure is described in the flow chart shown in figure 12.

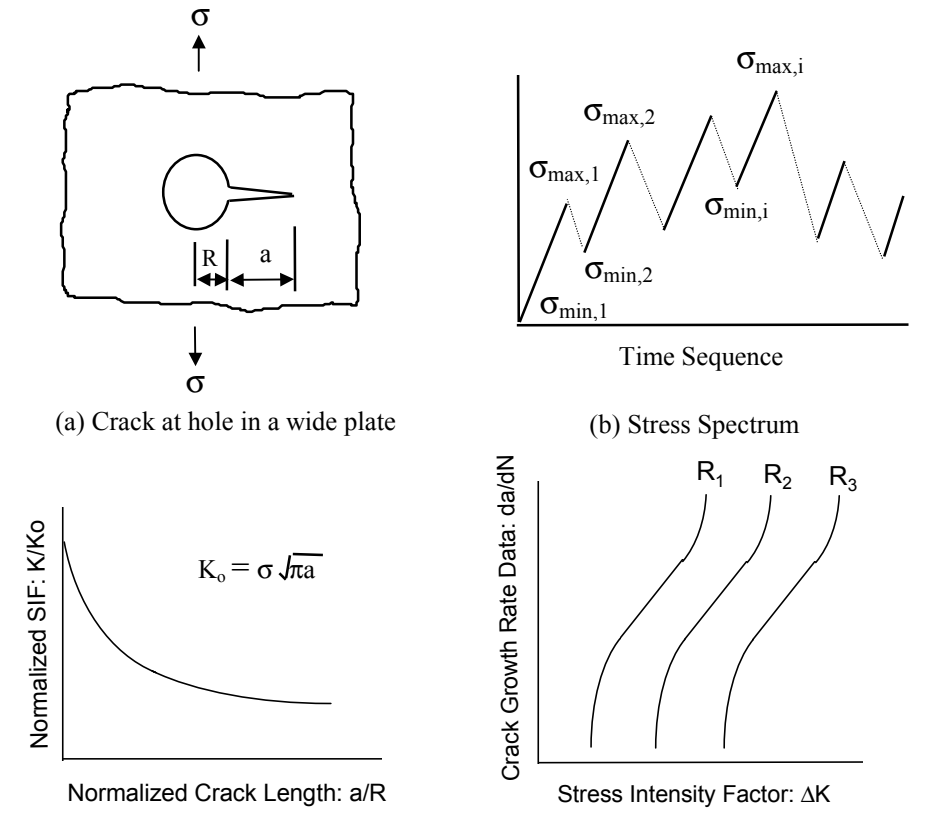

(a) Crack at hole in a wide plate

(b) Stress Spectrum

(c) Normalized Stress-Intensity Factor

(d) Fatigue Crack Growth Rate Data

Figure 11. Description of Crack Growth Analysis

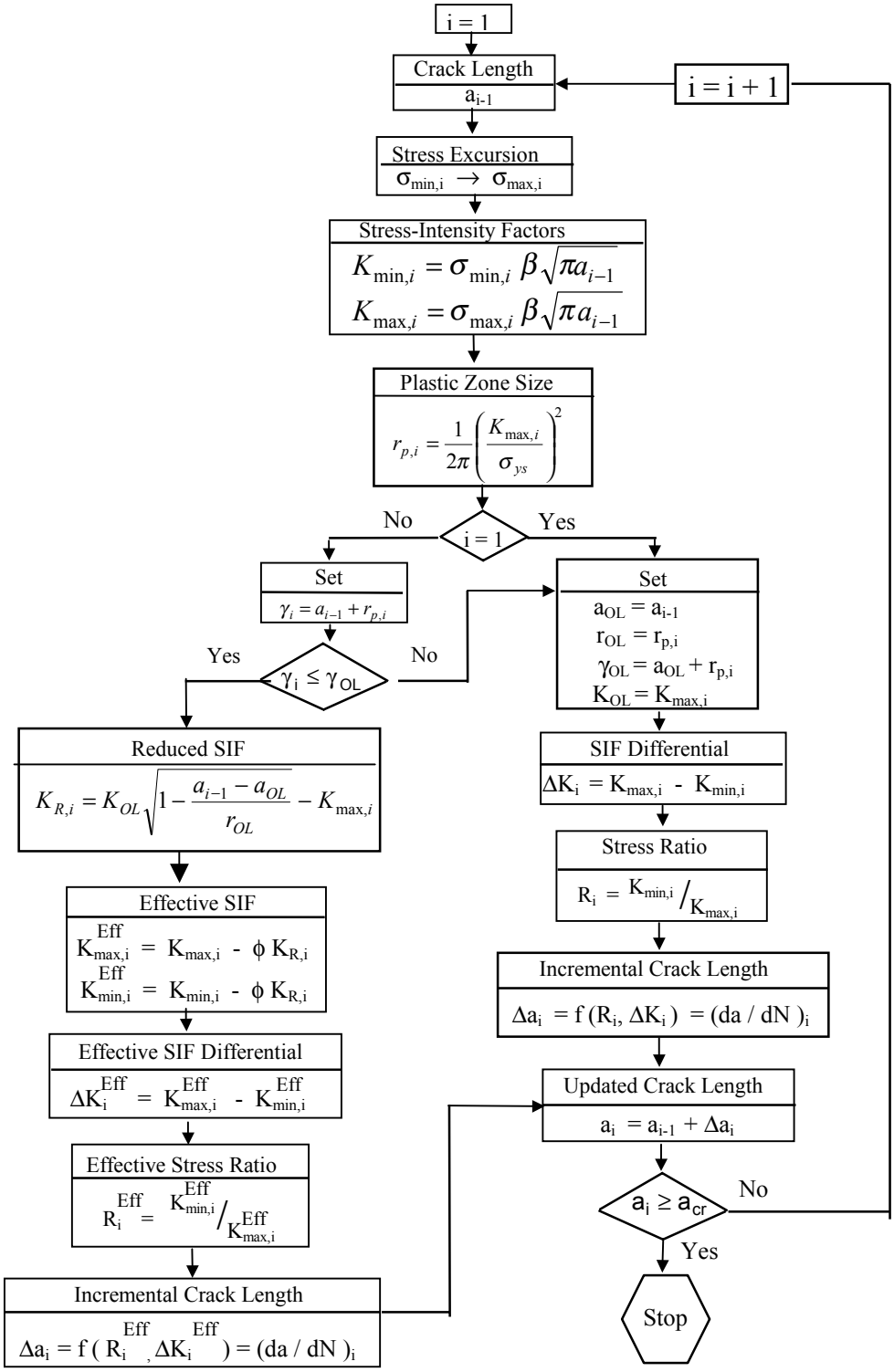

Figure 12. Flow Chart of the Cycle-by-Cycle Crack Growth Analysis

Let a_0 be the initial crack length. The crack growth analysis starts with an initial crack of length a_0 at i = 1. For the first cycle stress excursion, the stress-intensity factors and the plastic zone size are calculated. With the stress ratio R and the change of the stress-intensity factor ΔK, the incremental crack length is obtained from the da/dN data. The crack is incremented to the length a_1.

At each sequential i-th cycle, the crack growth starts with a length equal to a_{i-1}. The stress-intensity factors and the plastic zone size are calculated using the i-th stress excursion. A test is then made to determine if the growth of the progressing crack is retarded. A positive answer leads the analysis to use the Generalized Willenborg retardation model in the calculation of incremental crack length. Otherwise, the retardation effect is bypassed in the calculation. The crack then propagates the length a_i.

The process continues until the crack grows to the critical crack length determined from the residual strength of the structure at the limit stress.

In RAPID, the compression-tension stress cycle is treated as a zero-tension stress cycle and the compression-compression stress cycle is ignored in the crack growth calculation. Furthermore, the parameter ϕ introduced in the generalized Willenborg retardation model is calculated by the equation

$$\phi = \frac{1 - \dfrac{\Delta K_{Threshold}}{\Delta K_i}}{S^{OL} - 1}$$

where $\Delta K_{Threshold}$ is the threshold stress-intensity factor level associated with zero fatigue crack growth rates, and S^{OL} is the overload (shut-off) ratio required to cause crack arrest for the given material. A value of 2.3 is used in RAPID.

3.2 Residual Strength Evaluation

The residual strength of the repaired skin is the load carrying capacity of that skin, should cracks exist after repair. The knowledge of residual strength of a repaired skin is required in order to determine the critical crack length at the limit stress. The limit stress in the circumferential direction, for the longitudinal crack, is calculated using the equation

$$\sigma_{Limit,Circumferential} = 1.1\,\frac{(p + 1.0)R}{t}$$

where p is the pressure differential, R and t are the radius and thickness of the fuselage shell at the location where the damage tolerance analysis is performed. The pressure 1.0 psi added to the pressure differential is to account for the aerodynamic pressure terms per FAR 25.571.

The limit stress in the longitudinal direction, for the circumferential crack, is determined using the equation

$$\sigma_{Limit,Longitudinal} = (p + 1.1)\,\frac{R}{2t} + 2.5\,\sigma_{1G}\,/\,\gamma$$

where p is the pressure differential, γ is the payload reduction factor, R and t are the radius and thickness of the fuselage shell, and σ_{1G} is the one-G stress at the location where the damage tolerance analysis is performed. The pressure 1.1 psi in the above equation is added to account for a 1.0 psi in the aerodynamic pressure terms per FAR 25.571 and a 0.1 psi regulator tolerance per FAR 23.574.

The residual strength of the repaired skin is calculated using the equation based on the fracture toughness approach

$$\sigma_{Residual} = \frac{K_C}{\beta\sqrt{\pi a}}$$

where K_C is the toughness of the skin material, β is the geometry factor, and a denotes the crack length. For small crack lengths, the residual strength is determined using the Fedderson's method. In this method, a tangent line from the yield stress σ_y of the material to the residual strength curve obtained using the fracture toughness method is numerically obtained as illustrated below in figure 13.

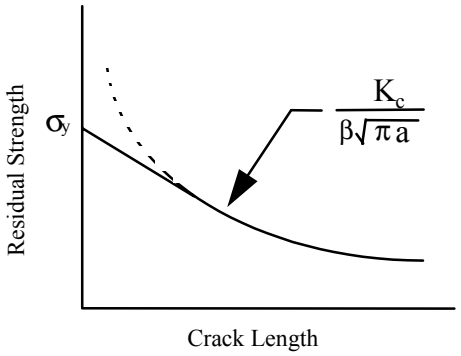

Figure 13. Residual Strength Curve

3.3 Inspection Threshold and Intervals

With the crack growth life of the modified skin provided by RAPID, the user determines the inspection threshold and the inspection interval at the detectable crack length for the desired inspection method.

4. Common Repairs

The common repairs considered in RAPID are proximate repairs and repairs at stiffeners. The circular repairs are actually basic repairs but were not addressed in the early development until later time, and thus are included in this section.

4.1 Proximate Repairs

To predict the crack growth life of a repair near a neighboring repair, the fastener load transfers need to be determined. Because of the mutual influence between the two nearby repairs, the fastener load transfers are affected and so are the crack growth lives. To account for the proximity effect on the fastener load transfers between two repairs, a database of load transfers at the critical fastener location in the subject repair has been developed. An engineering approach has also been developed to estimate the crack growth life of the repair. Appendix E provides the details.

4.2 Repairs at Stiffeners

In repairs at a stiffener, it is a common practice to make use of existing fastener holes for the repair doubler installation. These fastener holes are normally in a fastener row where the frame or the longeron is attached to the fuselage skin. A repair installed at the frame and longeron will affect the fastener load transfers. In addition, a crack growing toward the stiffener will also be influenced. Appendix F provides the fastener load transfer database and the geometry factors of stiffened sheets used in RAPID.

4.3 Circular Repairs

Circular repairs are basic fuselage skin repairs. Generally, a circular repair consists of a circular skin cutout replaced with a circular repair doubler. The doubler is mechanically fastened with fasteners arranged in a circular pattern. To perform the damage tolerance evaluation of circular repairs, the critical fastener location first needs be determined. Appendix G provides the study of fastener load transfers in circular repairs.

5. RAPID-FEM Program and Repair at Door Cutout

5.1 RAPID-FEM program

RAPID-FEM program is a two-dimensional finite element analysis program tailored for multiple-layered sheet structures. The program, developed by Cornell University, was initially used to analyze the repairs at a fuselage door opening utilizing an idealized two-dimensional model. It can also conduct analysis on any skin repairs or antenna installations. Validations and descriptions of the program are provided in Appendix H. The report by Cornell University is also provided in Appendix I.

5.2 Repair at Door Cutout

Fatigue cracks usually initiate at the corner of a fuselage door cutout. A notch is introduced to remove the sharp crack tip before the doublers are applied. Complicate geometry and loads impose difficulty in repair design as well as analysis. An engineering approach is hereby proposed to facilitate the assessment process. This approach bases on the assumption that a three dimensional effects on the stresses at a cutout corner is bounded and can be quantified. If sufficient numbers of various cutout configurations are examined, an upper bound of the effects can be established in terms of a single-value correction factor. This number can then be used to set the upper bound of a 3-D result utilizing the simplified 2-D analysis. Appendix J presents the approach and the findings on the repairs of three case studies.

6. Analysis Procedure Flow Charts

The RAPID analysis program consists of a static module and a damage tolerance analysis module. The static module performs the static strength analysis of the repaired fuselage skin. Margins of safety are calculated based on three independent criteria. RAPID calculates the load carrying capacity lost due to the damage treatment and the margin of safety based on the joint allowable which includes the fastener shear and hole bearing allowables. It calculates the margin of safety based on the ultimate tensile strengths of the doubler and the design ultimate tensile strength of the skin. The margin of safety for shear is also calculated based on the shear allowables of the skin and doubler. In addition, the stiffness ratio between the repair doublers and the skin layers and the bending of the fastener going through the stack-up layers are also calculated (sections 2.4 and 2.5). The program then checks adequacy of the repair. RAPID either recommends redesign due to inadequate static design or deems the repair to be statically adequate. The analysis procedure is described in the flow chart in figure 15.

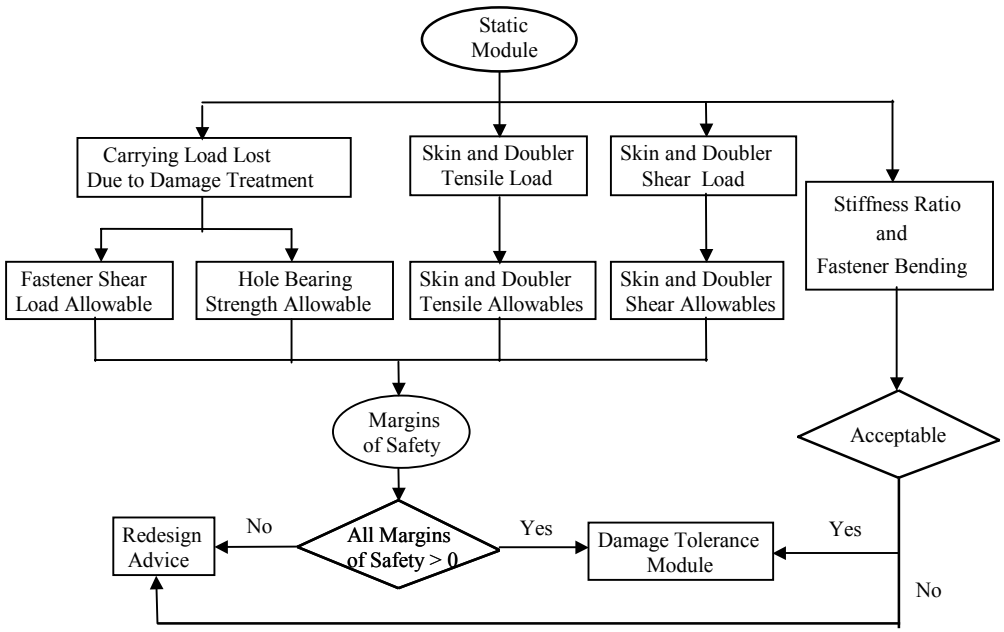

Figure 15. Flow Chart of the Static Module

The damage tolerance module performs the crack growth and the residual strength analysis of the repaired skin. The analysis is performed for crack(s) initiating at the center and the corner fastener holes. Three initial crack configurations are considered for basic repairs. The gross, bearing, and bypass factors are calculated by interpolating the data from the database. Stress-intensity factors are then calculated from the compounded geometry factors interpolated from the database. The residual strength is calculated and the crack growth analysis is performed using either the simplified or the cycle-by-cycle method. The residual strength is then checked against the limit stress to determine whether the crack advances. Based on the damage tolerance analysis results, the inspection threshold and inspection intervals are then determined. The analysis procedure is described in figure 16.

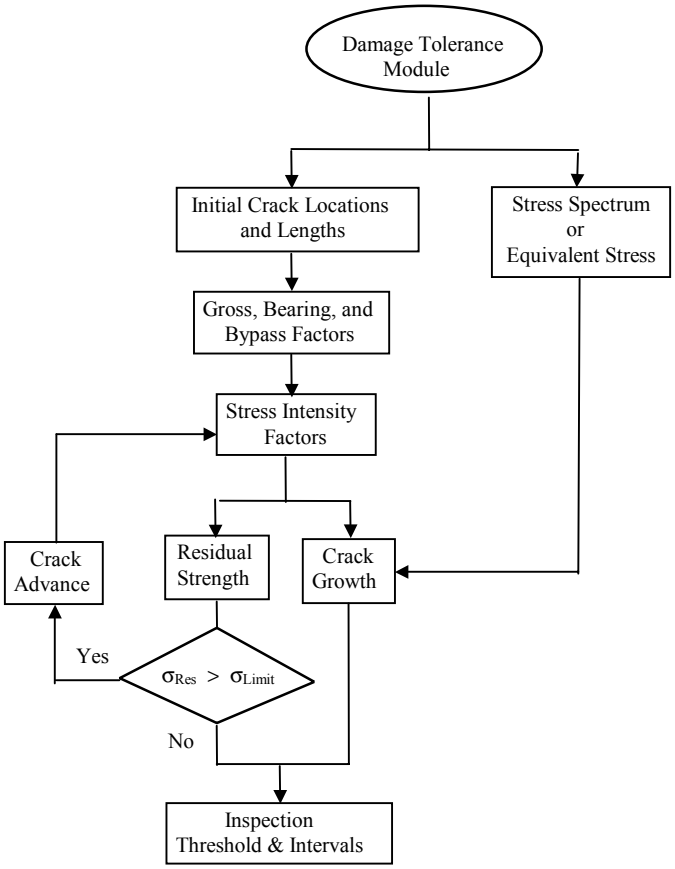

Figure 16. Flow Chart of the Damage Tolerance Module

The analysis procedure is used for crack growth calculation in RAPID. The inspection threshold and inspection intervals are provided in the output for the maintenance schedule of the repair.

7. References

1. T. Swift, "Repairs to Damage Tolerant Aircraft," in Structural Integrity of Aging Airplanes, Editors: S. N. Atluri, S. G. Sampath, P. Tong, and Springer-Verlag, 1991.

2. J. D. Willenborg, R. M. Engle, and H. A. Wood, "A Crack Growth Retardation Model Using an Effective Stress Concept," AFFDL-TM-71-1-FBR, 1971.

3. J. P. Gallagher and T. F. Hughes, "Influence of the Yield Strength on Overload Affected Fatigue-Crack-Growth Behavior of 4340 Steel," AFFDL-TR-74-27, 1974.

4. R. M. Engle and J. L. Rudd, "Analysis of Crack Propagation Under Variable-Amplitude Loading Using the Willenborg Retardation Model," AIAA Paper No. 74-369, 1974.

5. Handbook of Mathematical Functions with Formulas, Graphs, and Mathematical Tables, Edited by Milton Abramowitz and Lrene A. Stegun, Dover Publications, Inc., New York, 1972.

Appendix A - Fastener Load Transfers Using Two-Dimensional Analysis

A1. Introduction

This appendix describes parametric study and database development of load transfers along the critical fastener row in the three baseline skin repairs. Fastener loads at the critical center and corner fastener locations due to 1000 psi reference far field stress are printed in the output when requested by the user.

A2. Approach

The study was conducted using the two-dimensional analysis of the repaired skin. Generally, the repaired skin consists of a skin cutout which is replaced with repair doubler(s). Figure A1 shows the three baseline repairs.

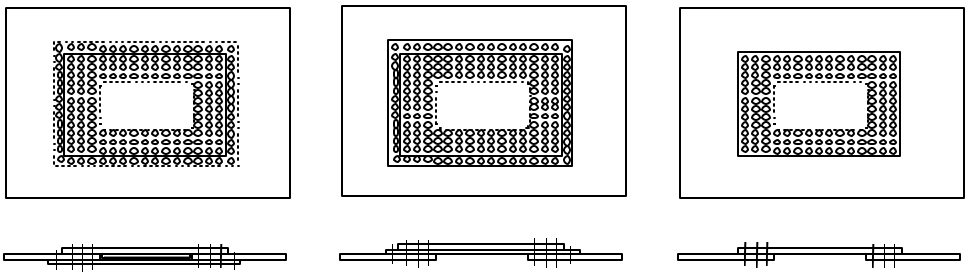

Type I Repair Type II Repair Type III Repair

Figure A1. Baseline Repairs

Parameters considered in the two-dimensional analysis of the baseline repairs include

- Repair size: One frame bay by two longeron bays
- Skin Thickness: 0.032″, 0.040″, 0.050″, 0.063″, 0.071″, 0.080″, and 0.090″
- Doubler Thickness: 0.025″, 0.032″, 0.040″, 0.050″, 0.063″, 0.071″, 0.080″, 0.090″, and 0.100″
- Skin and doubler material: Aluminum 2024-T3 Clad Sheet
- Fastener material: Aluminum
- Fastener diameter, pitch, and edge distance
  - Diameter: 1/8″, 5/32″, 3/16″, and 1/4″
  - Pitch: 5 fastener diameters
  - Edge Distance: 2.5 fastener diameters

- Number of fastener rows 3, 4, and 5

The parametric study was done using the finite element computer code CAP V which is basically the Structural Analysis Program (SAP) developed at University of California at Berkeley.

Due to double symmetry of the geometry as well as the stress applied in the skin, the analysis was performed on one-quarter of the repaired skin as shown below in figure A2 for a Type III repair.

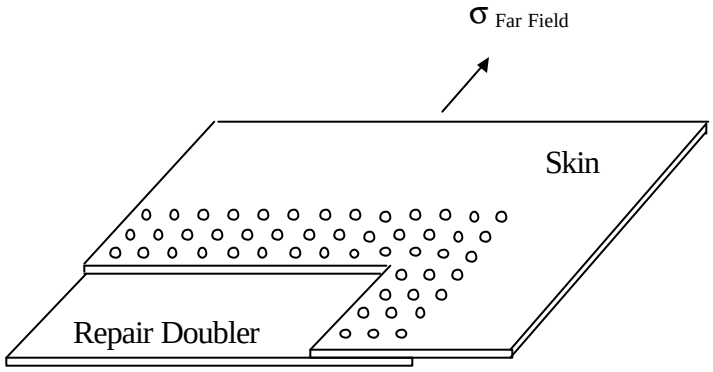

Figure A2. One-Quarter of the Repaired Skin

A typical finite element model representing one-quarter of the repaired skin is shown below in figure A3.

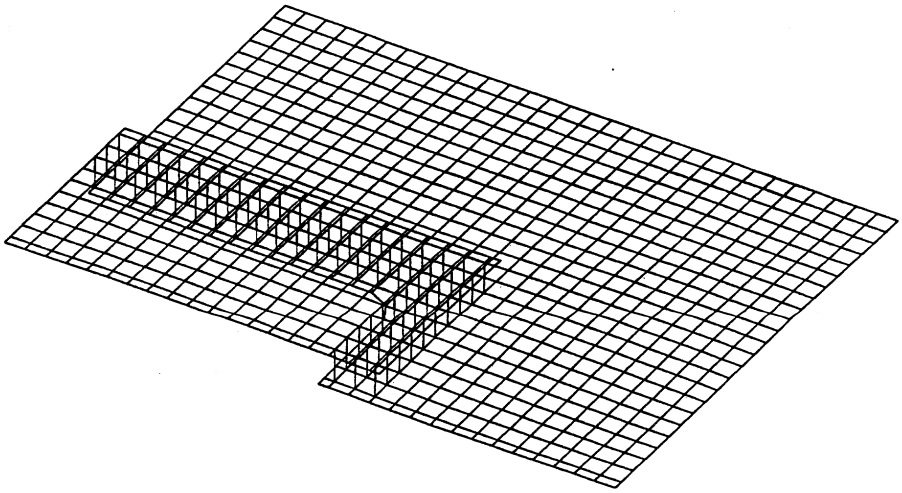

Figure A3. Finite Element Model of 1/4 of the Repaired Skin

In the model, the skin and the repair doubler are modeled using quadrilateral membrane elements. The shear rigidity of fasteners is calculated based on Swift's equation:

$$K = \frac{Ed}{A + B\left(\frac{d}{t_{Skin}} + \frac{d}{t_{Doubler}}\right)}$$

where E is the average of the moduli modules of skin and doubler materials, d is the fastener hole diameter, t_{Skin} and $t_{Doubler}$ are the thickness of the skin and doubler, and A and B are empirical constants taking the values of 5.0 and 0.8 for aluminum rivets, respectively. The calculated value is input directly to the CAP V program. In the analysis, the repaired skin is subjected to a reference far field stress of 1000 psi.

To perform the damage tolerance analysis of skin repairs, the stress field near fastener holes in the skin needs to be known. Let the skin stress prior to the load transfer be referred as the gross stress, the bearing stress as the average hole bearing stress in the skin exerted by the fastener load, and the bypass stress as the skin stress after the load transfer. These skin stresses are shown below in figure A4.

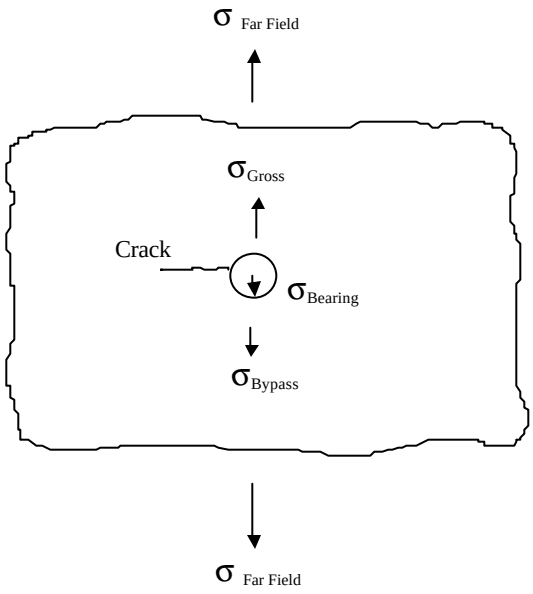

Figure A4. Skin Stresses before and after load transfer

Analysis results are presented in terms of bearing factors, bypass factors, and stress scale factors in the database. The bearing and bypass factors are the ratios of the bearing and bypass stresses in the skin divided by the gross stress. The stress scale factor is the ratio between the gross stress and the reference applied far field stress. These factors are calculated as follows.

Bearing Factor (BRF) = $\sigma_{Bearing}/\sigma_{Gross}$

Bypass Factor (BPF) = $\sigma_{Bypass}/\sigma_{Gross}$

Stress Scale Factor (SSF) = $\sigma_{Far\ Field}/\sigma_{Gross}$

Analysis results in terms of (A) bearing factors, (B) bypass factors, and (C) stress scale factors along the critical fastener row are presented in a graphical form for each of the three repair configurations shown in figure A1. In each graph, the first fastener column refers to the center fastener, and the last fastener column refers to the corner fastener.

A2.1 Fastener Loads for Type III Repairs

Parameters used in the analysis of Type III repairs are shown below. The analysis was performed for the cases of 3, 4, and 5 fastener rows.

Assembly Number	Thickness (in)		Fastener Hole Diameter (in)			
	Skin	Doubler				
1	0.032	0.040	1/8	—	—	—
2	0.040	0.050	1/8	5/32	—	—
3	0.050	0.063	1/8	5/32	3/16	—
4	0.063	0.071	1/8	5/32	3/16	1/4
5	0.071	0.080	1/8	5/32	3/16	1/4
6	0.080	0.090	1/8	5/32	3/16	1/4
7	0.090	0.100	1/8	5/32	3/16	1/4

Analysis results for Type III baseline repair configurations are presented in figures A1a through A8c. For repair configurations other than the baseline configurations, e.g., a repair doubler with thickness two or more gauges higher than the skin thickness or a repair with other fastener materials, correction factors are applied to the above results. These correction factors are obtained as the ratios of the bearing factors, bypass factors, and stress scale factors between the subject repair and the baseline repair using the one-dimensional analysis procedure in RAPID.

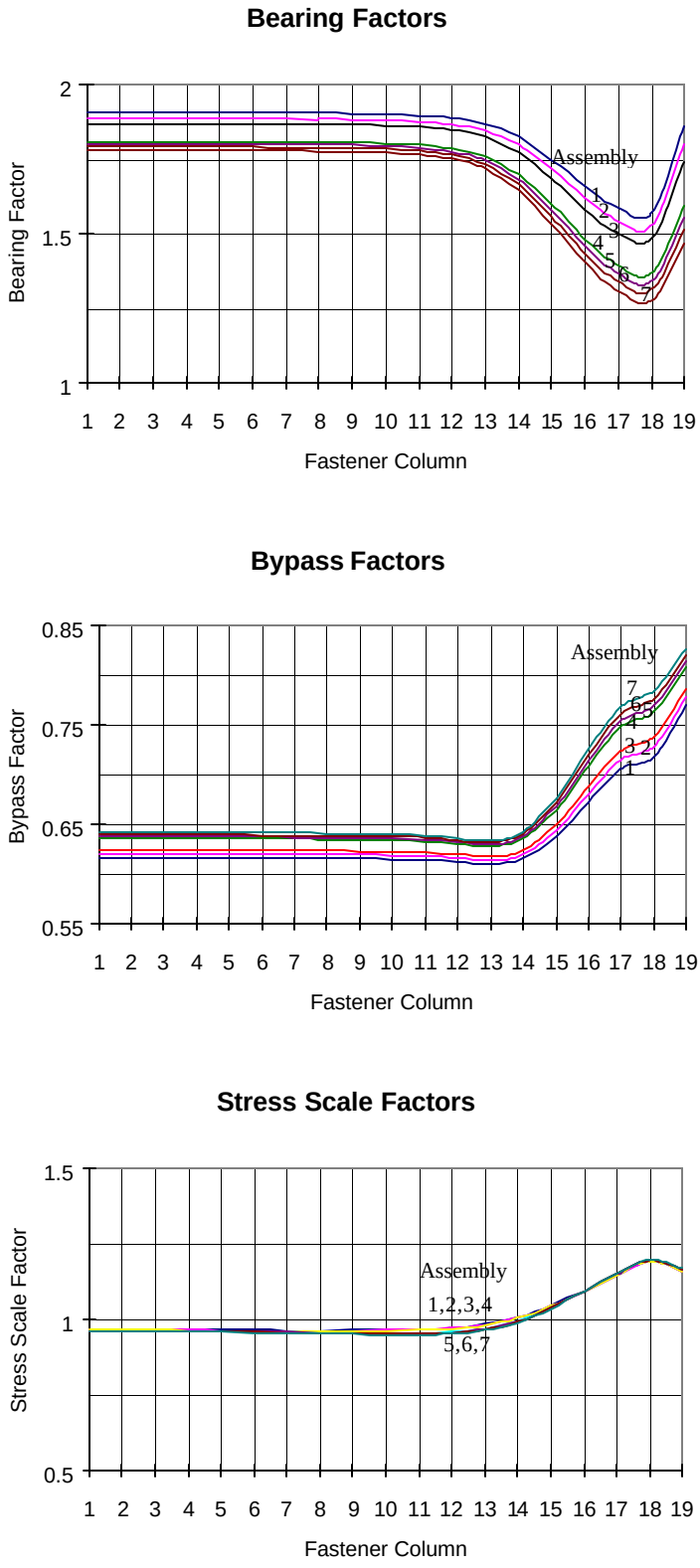

Figure A5a. Fastener Diameter 1/8 in, Three Fastener Rows

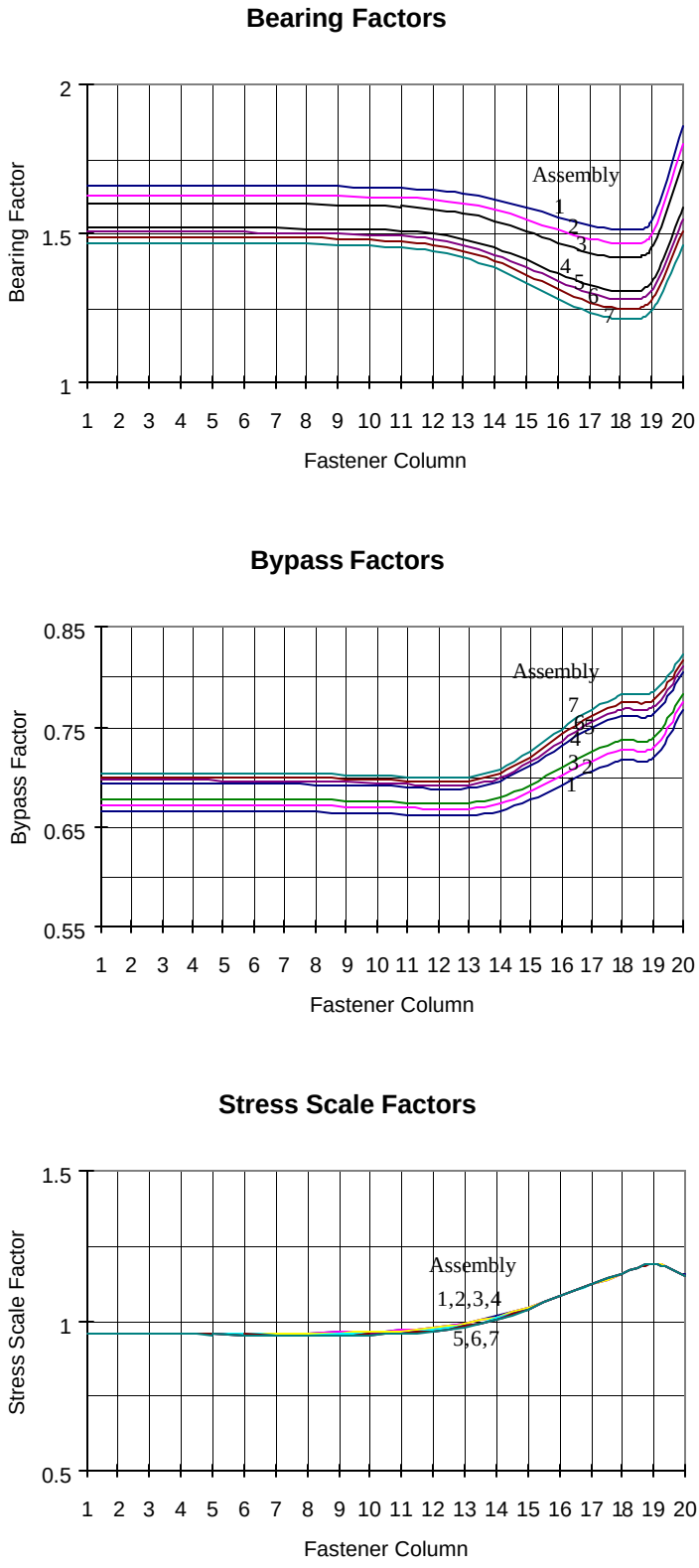

Figure A5b. Fastener Diameter 1/8 in, Four Fastener Rows

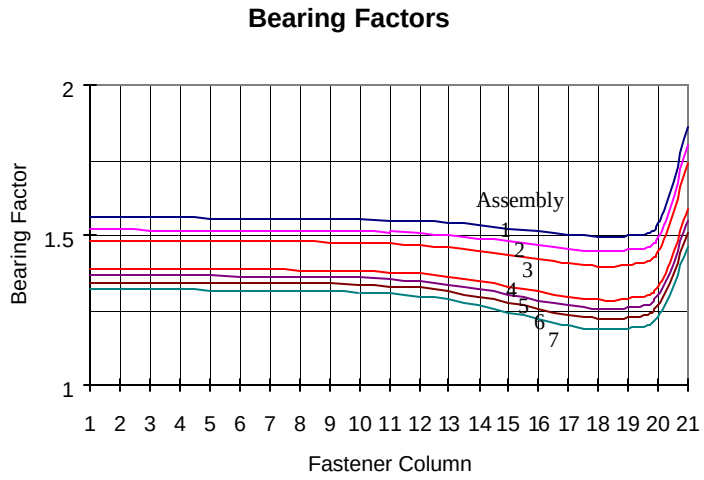

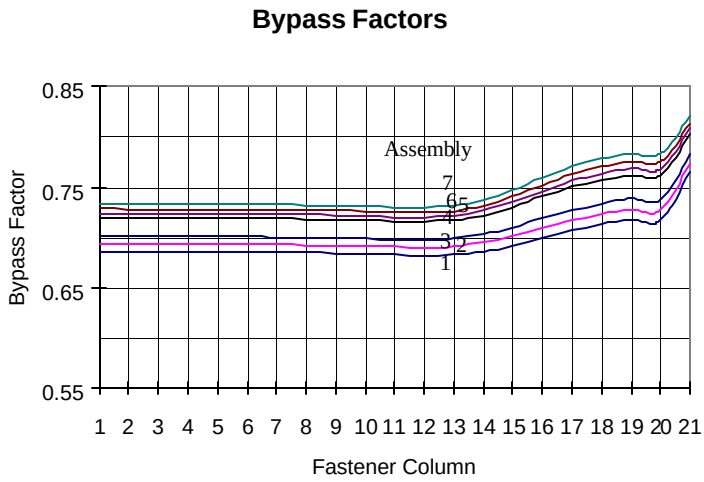

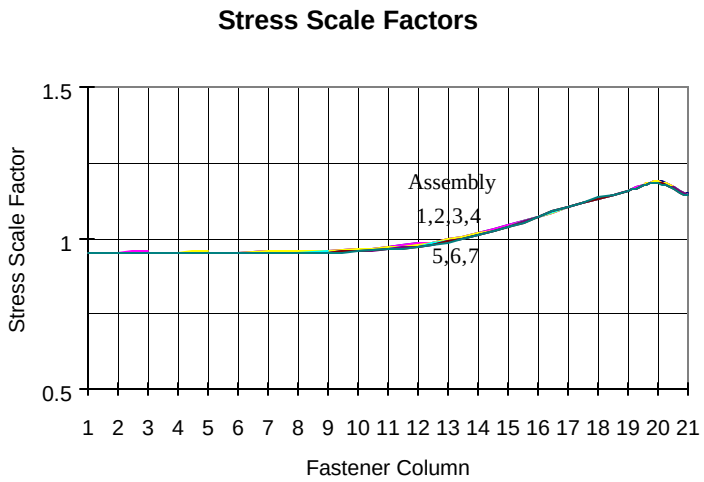

Figure A5c. Fastener Diameter 1/8 in, Five Fastener Rows

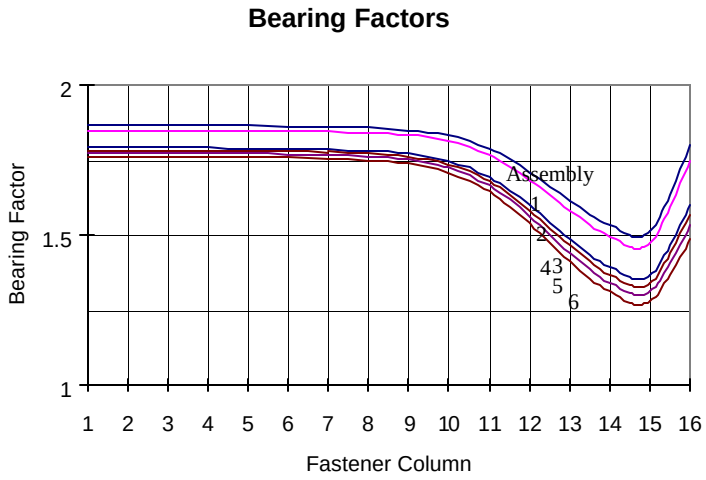

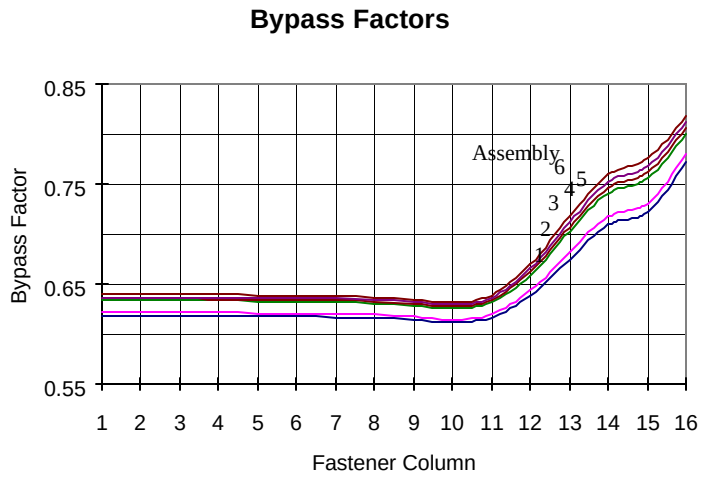

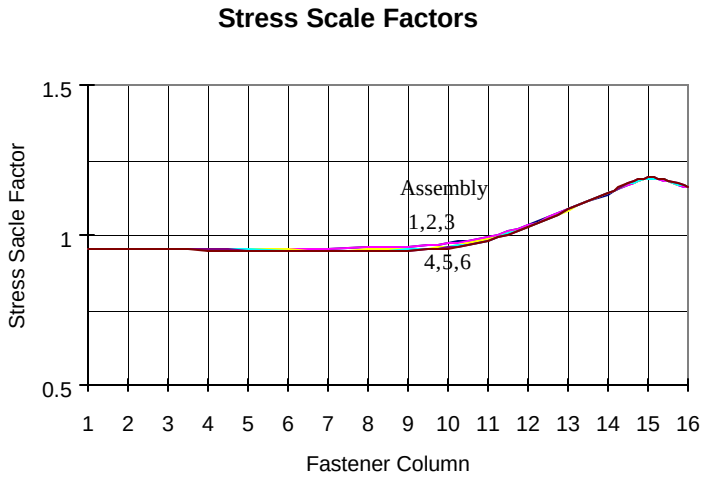

Figure A6a. Fastener Diameter 5/32 in, Three Fastener Rows

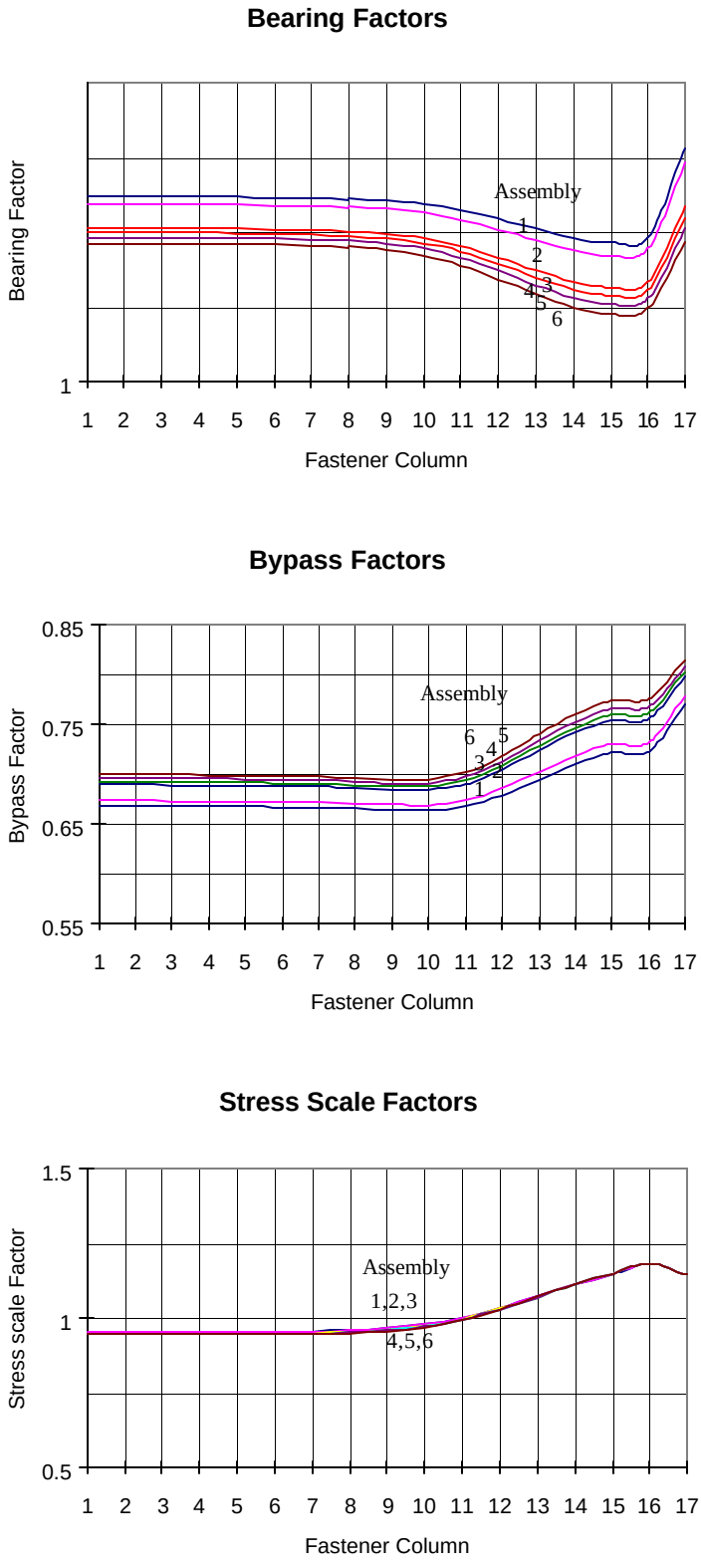

Figure A6a. Fastener Diameter 5/32 in, Four Fastener Rows

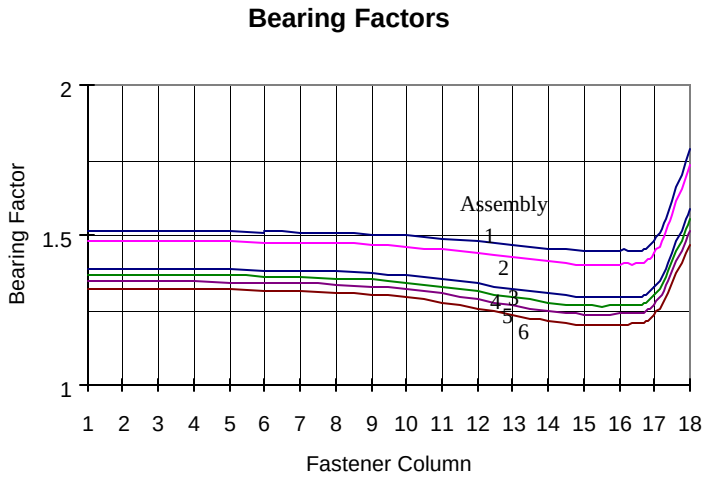

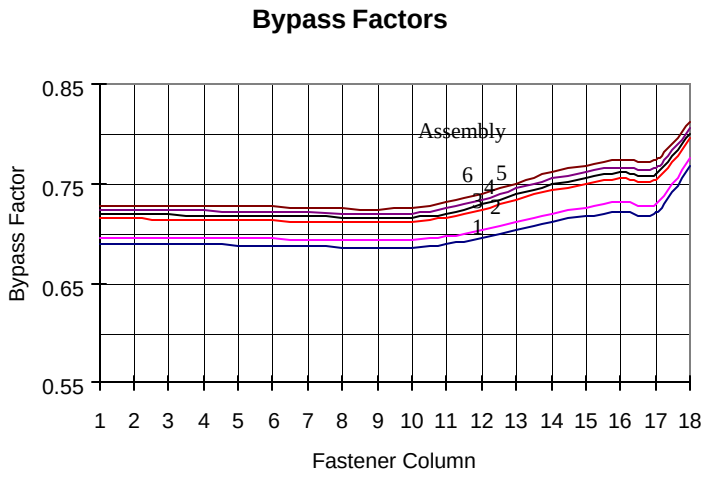

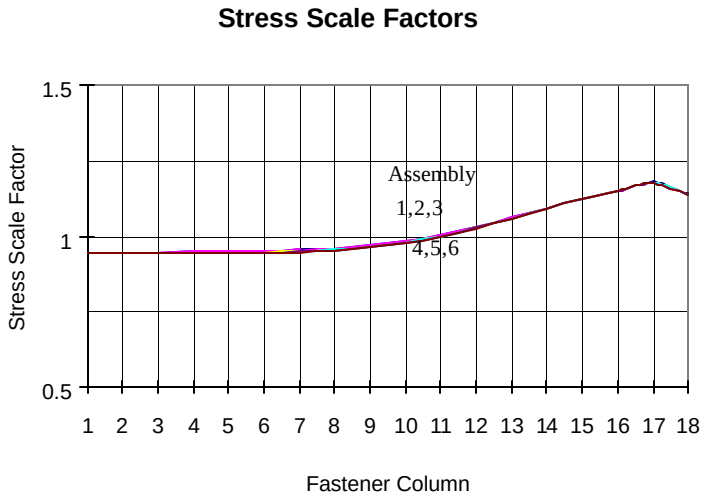

Figure A6c. Fastener Diameter 5/32 in, Five Fastener Rows

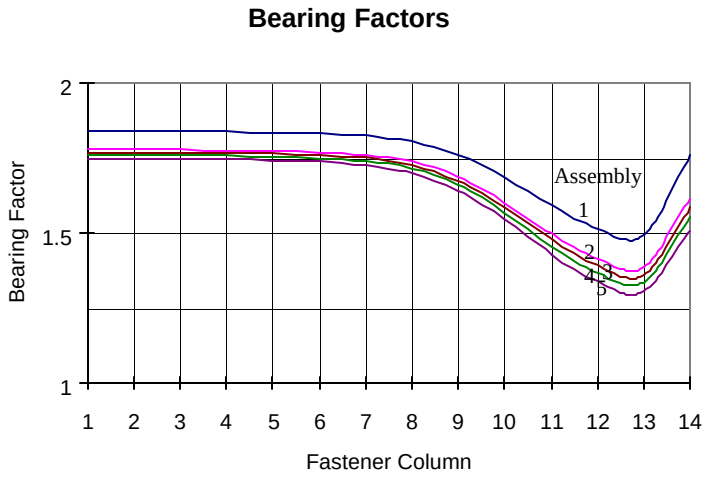

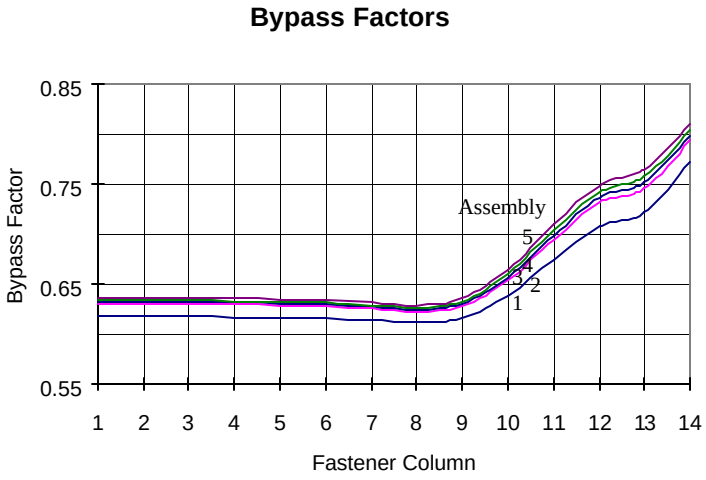

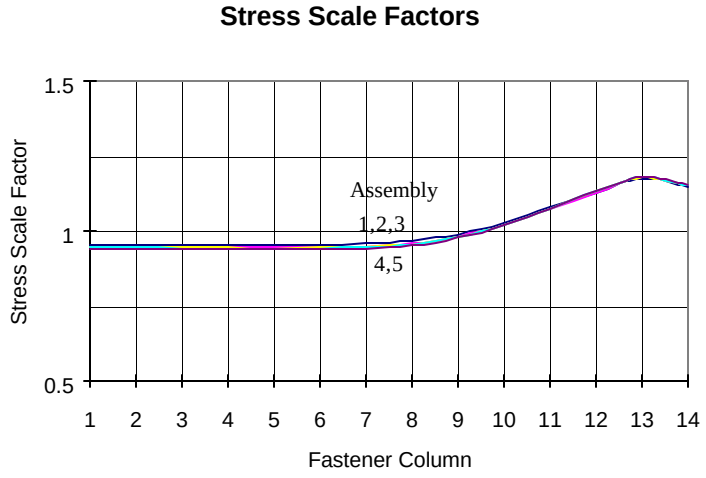

Figure A7a. Fastener Diameter 3/16 in, Three Fastener Rows

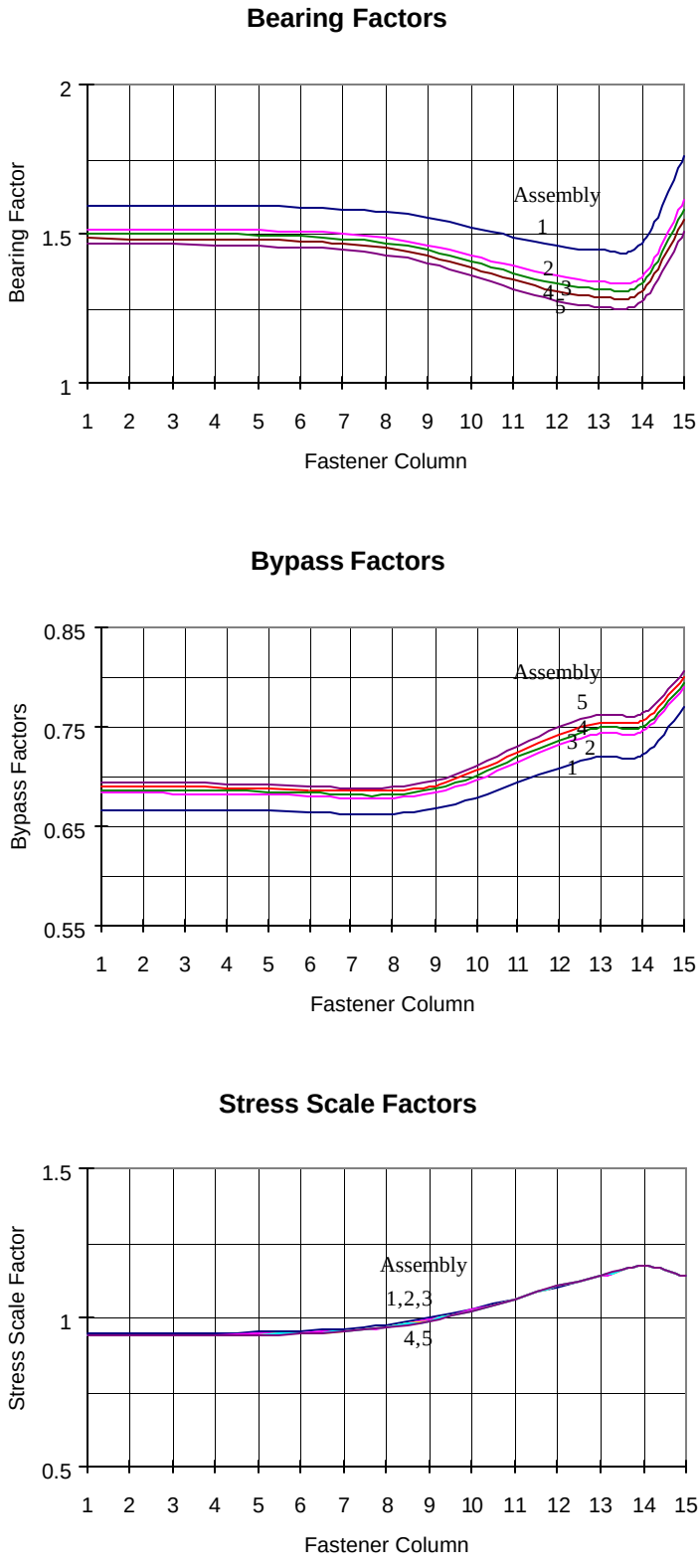

Figure A7b. Fastener Diameter 3/16 in, Four Fastener Rows

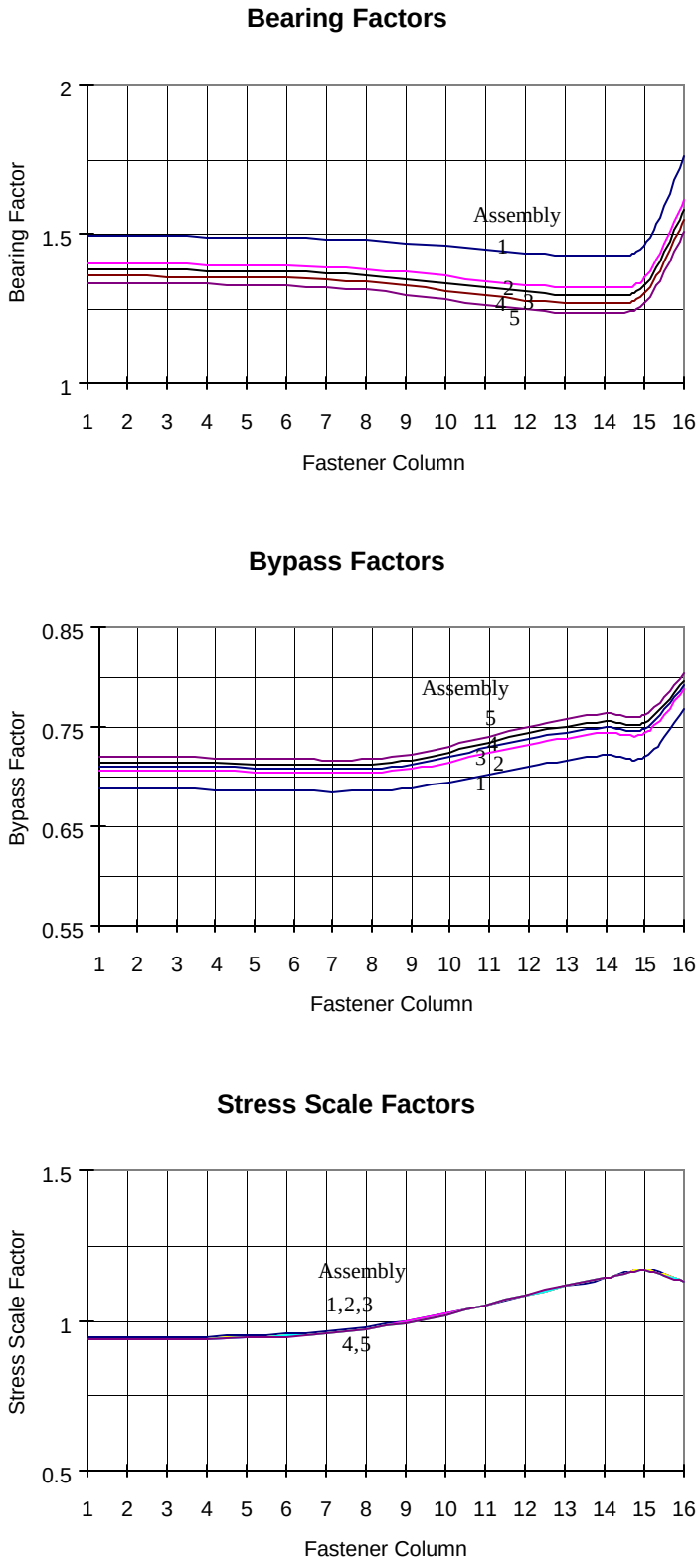

Figure A7c. Fastener Diameter 3/16 in, Five Fastener Rows

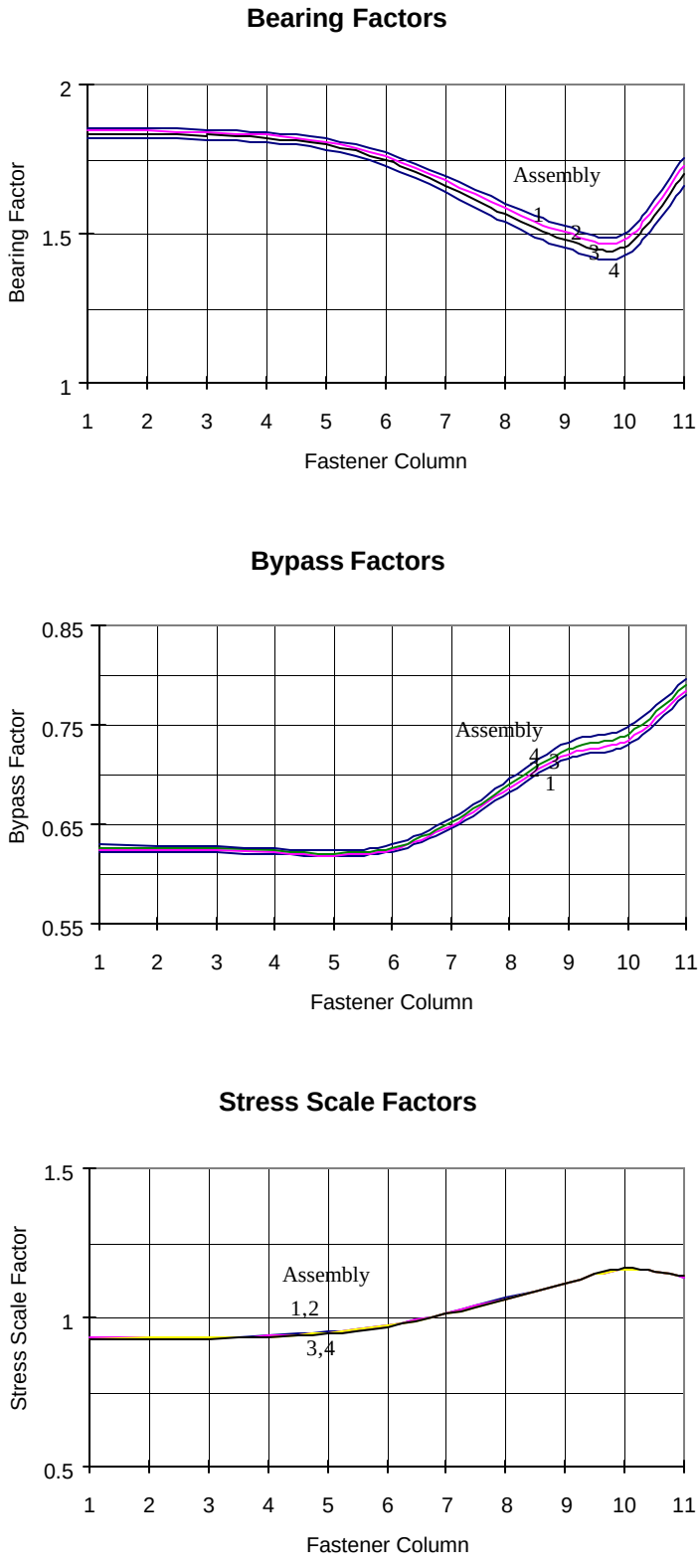

Figure A8a. Fastener Diameter 1/4 in, Three Fastener Rows

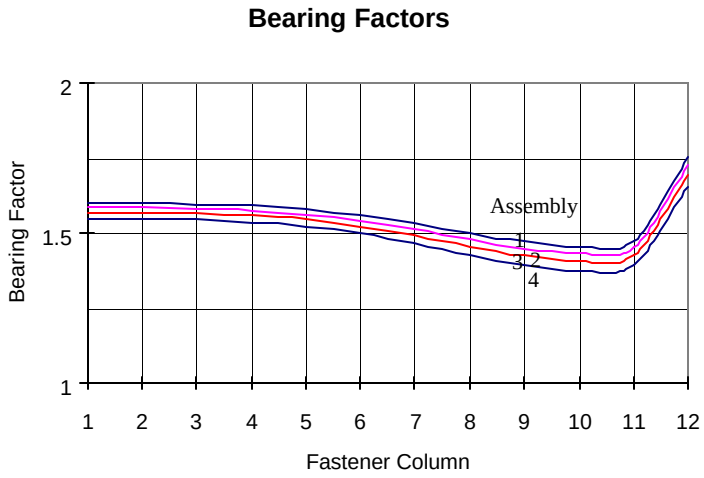

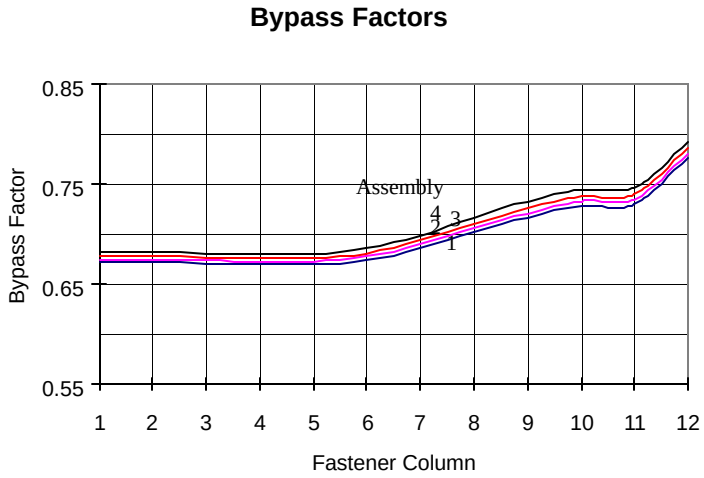

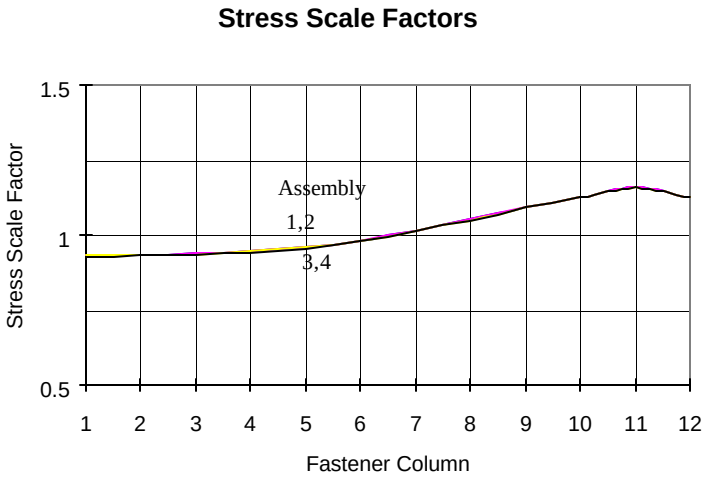

Figure A8b. Fastener Diameter 1/4 in, Four Fastener Rows

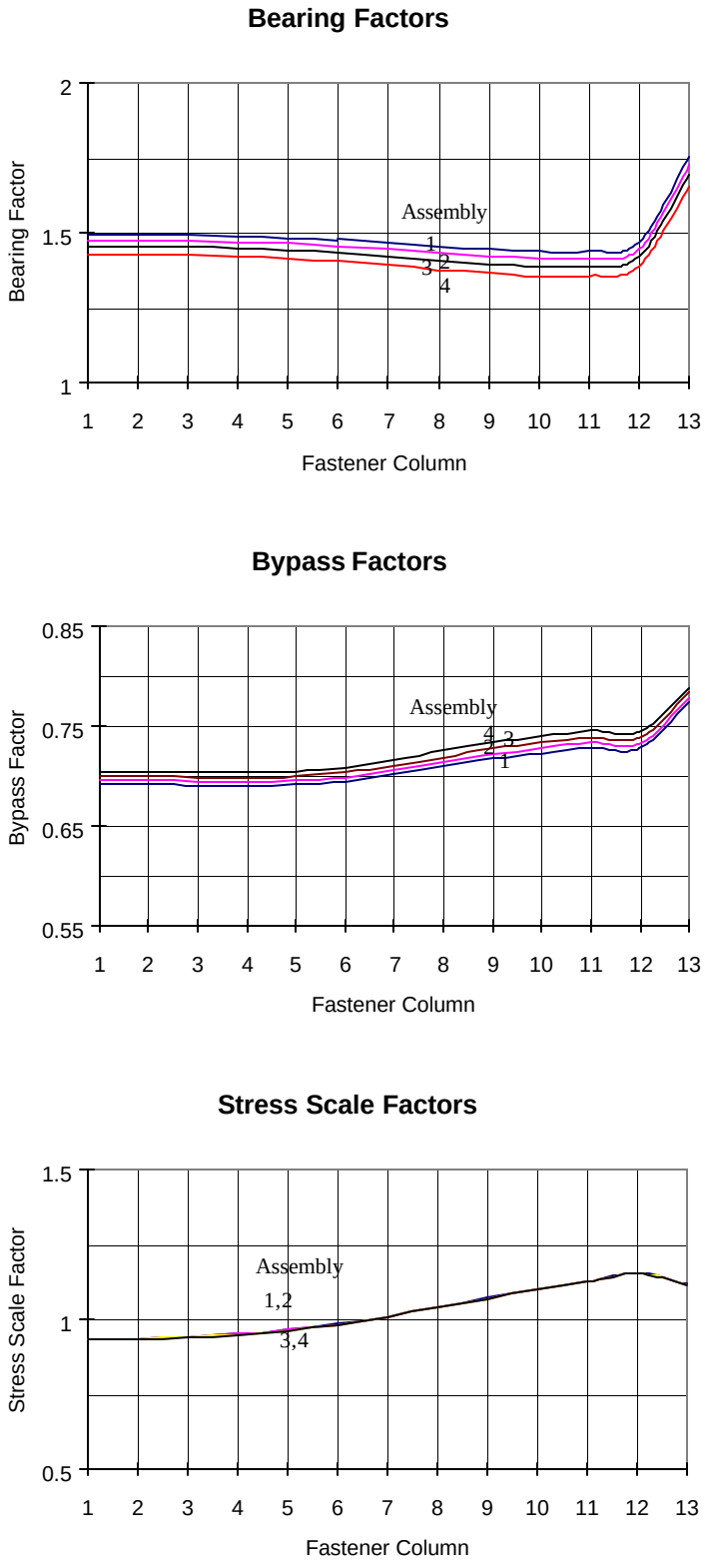

Figure A8c. Fastener Diameter 1/4 in, Five Fastener Rows

A2.2 Fastener Loads for Type II Repairs

Parameters used in the analysis of Type II repairs are shown below in the table. For each skin thickness, only one outer doubler thickness was considered because the change of outer doubler thickness only negligibly affects the load transfers. The analysis was performed for the cases of 3, 4, and 5 fastener rows.

Assembly No.	Thickness (in)			Fastener Hole Diameter (in)			
	Skin	$Doubler_{Inner}$	$Doubler_{Outer}$				
1	0.050	0.025	0.071	1/8	5/32	3/16	
2		0.032					
3		0.040					
4	0.063	0.025	0.080	1/8	5/32	3/16	1/4
5		0.032					
6		0.040					
7		0.050					
8	0.071	0.025	0.090	1/8	5/32	3/16	1/4
9		0.032					
10		0.040					
11		0.050					

Analysis results for Type II baseline repair configurations with 3 fastener rows are presented in figures A9a through A11d.

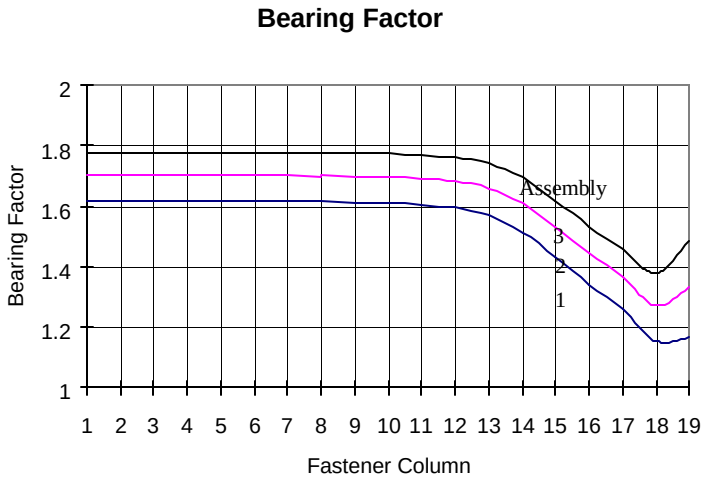

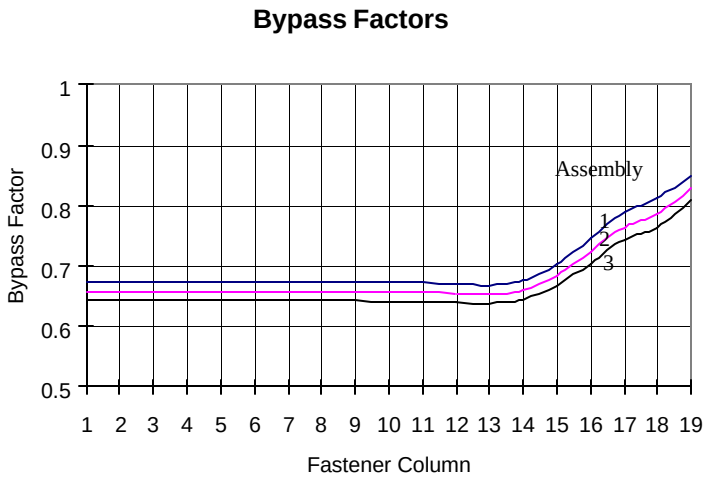

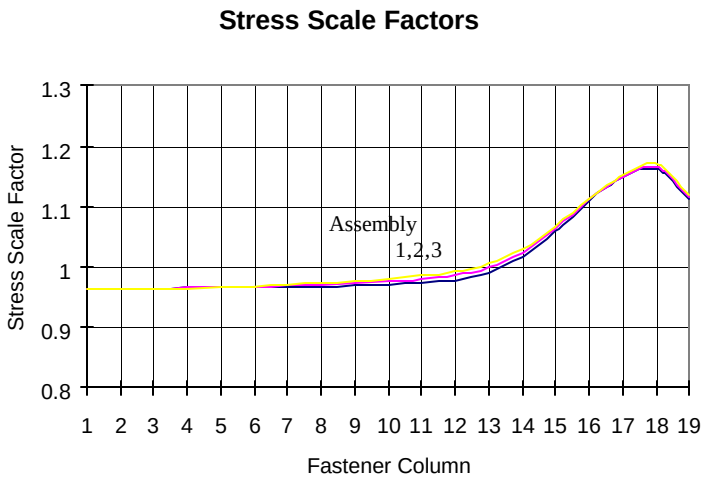

Figure A9a. Skin Thickness 0.050 in, Fastener Hole Diameter 1/8 in

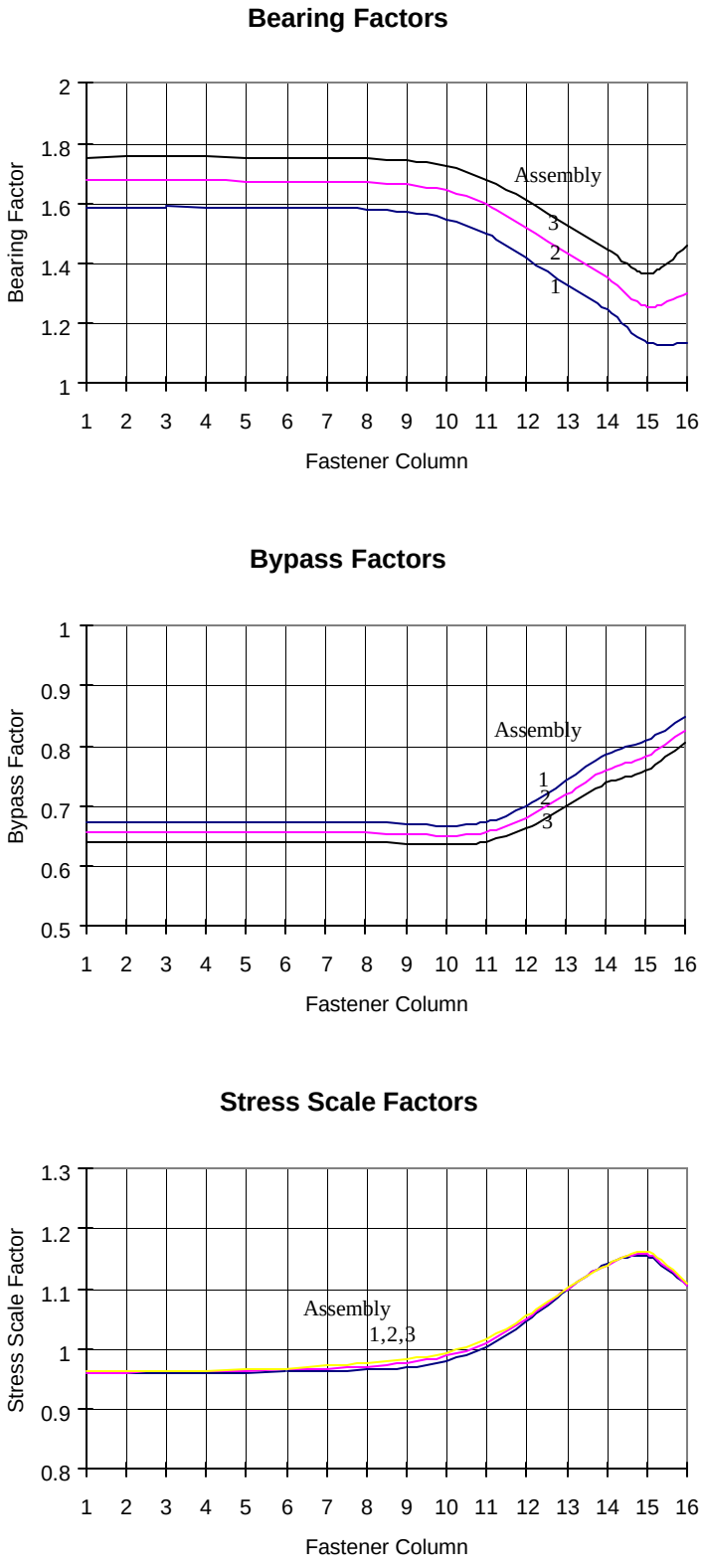

Figure A9b. Skin Thickness 0.050 in, Fastener Hole Diameter 5/32 in

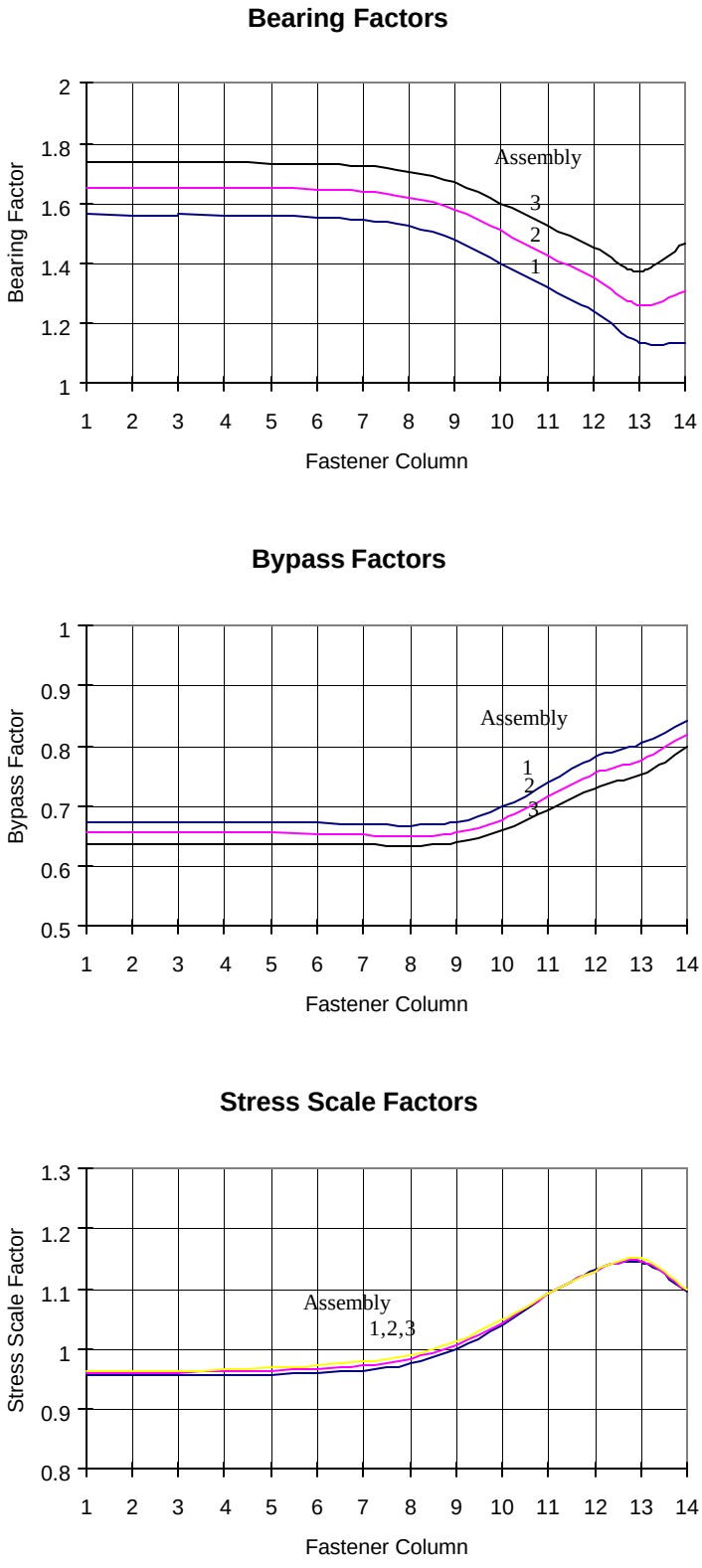

Figure A9c. Skin Thickness 0.050 in, Fastener Hole Diameter 1/4 in

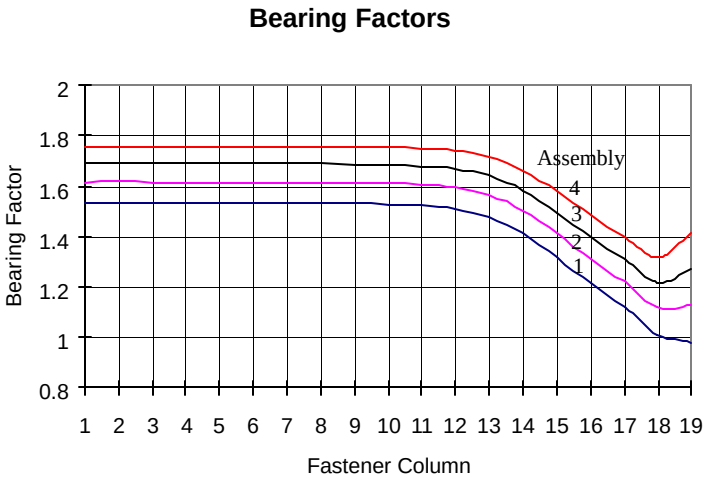

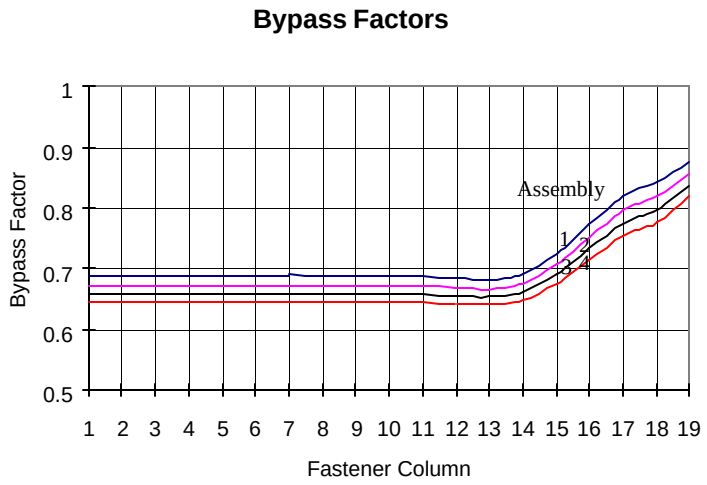

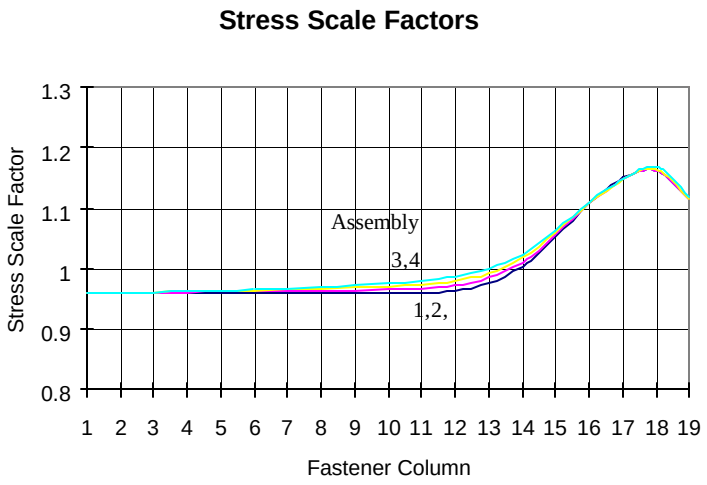

Figure A10a. Skin Thickness 0.063 in, Fastener Hole Diameter 1/8 in

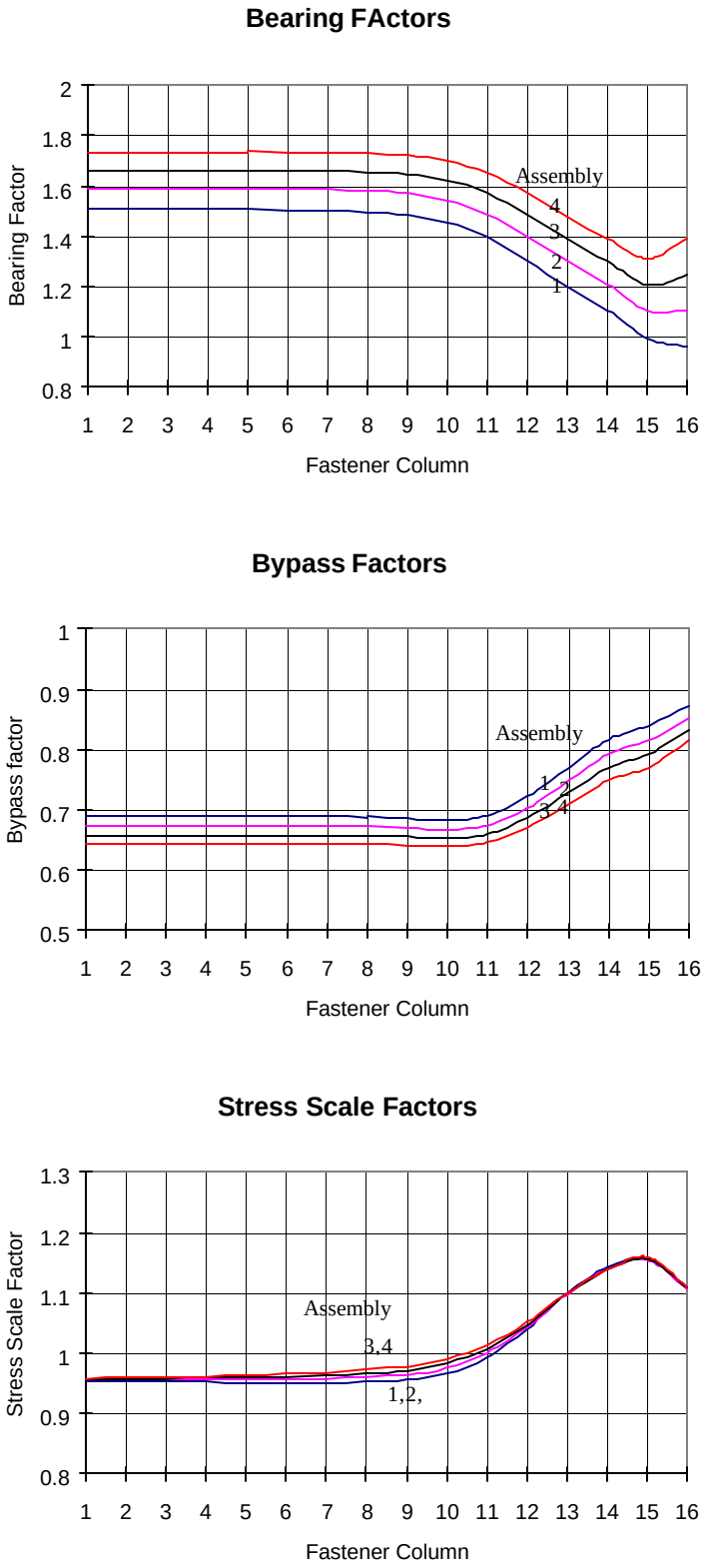

Figure A10b. Skin Thickness 0.063 in, Fastener Hole Diameter 5/32 in

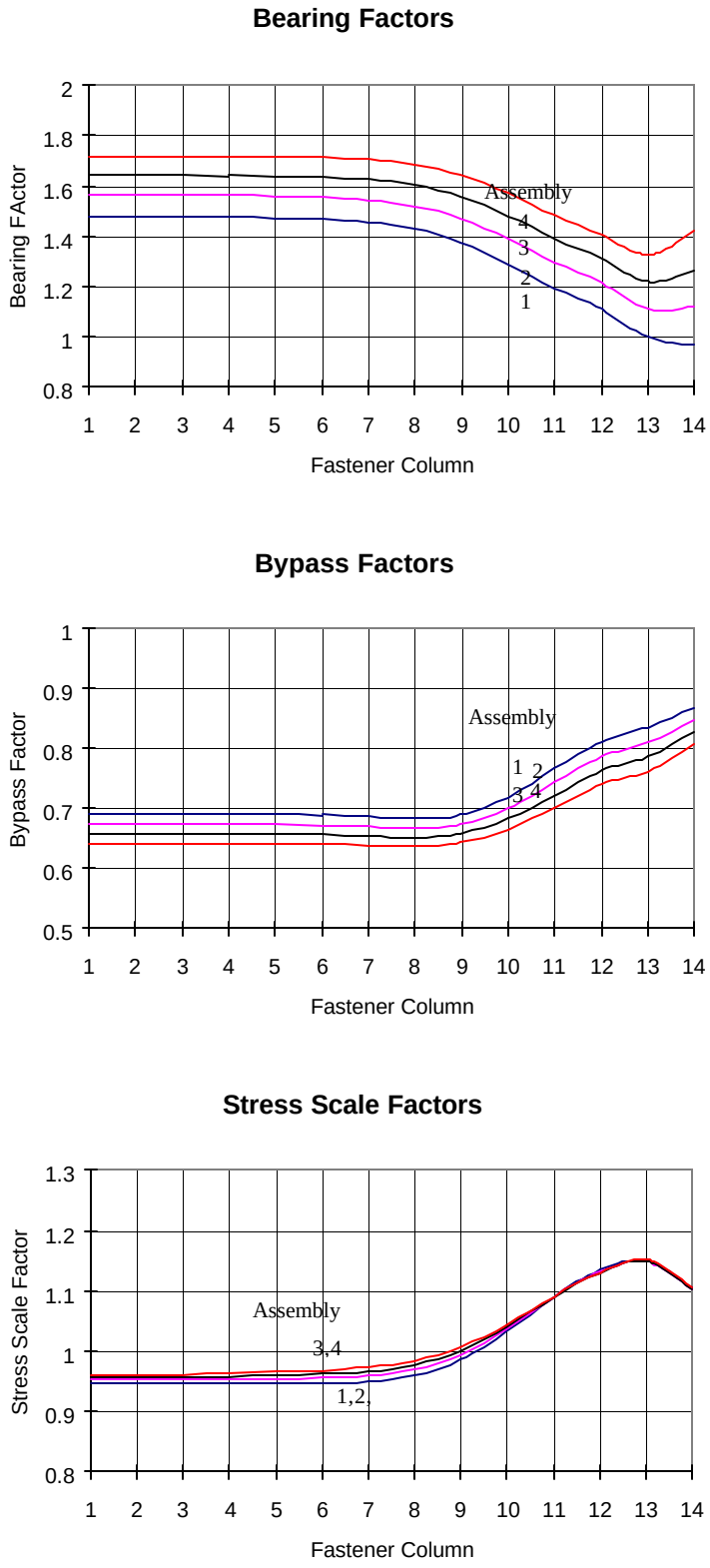

Figure A10c. Skin Thickness 0.063 in, Fastener Hole Diameter 3/16 in

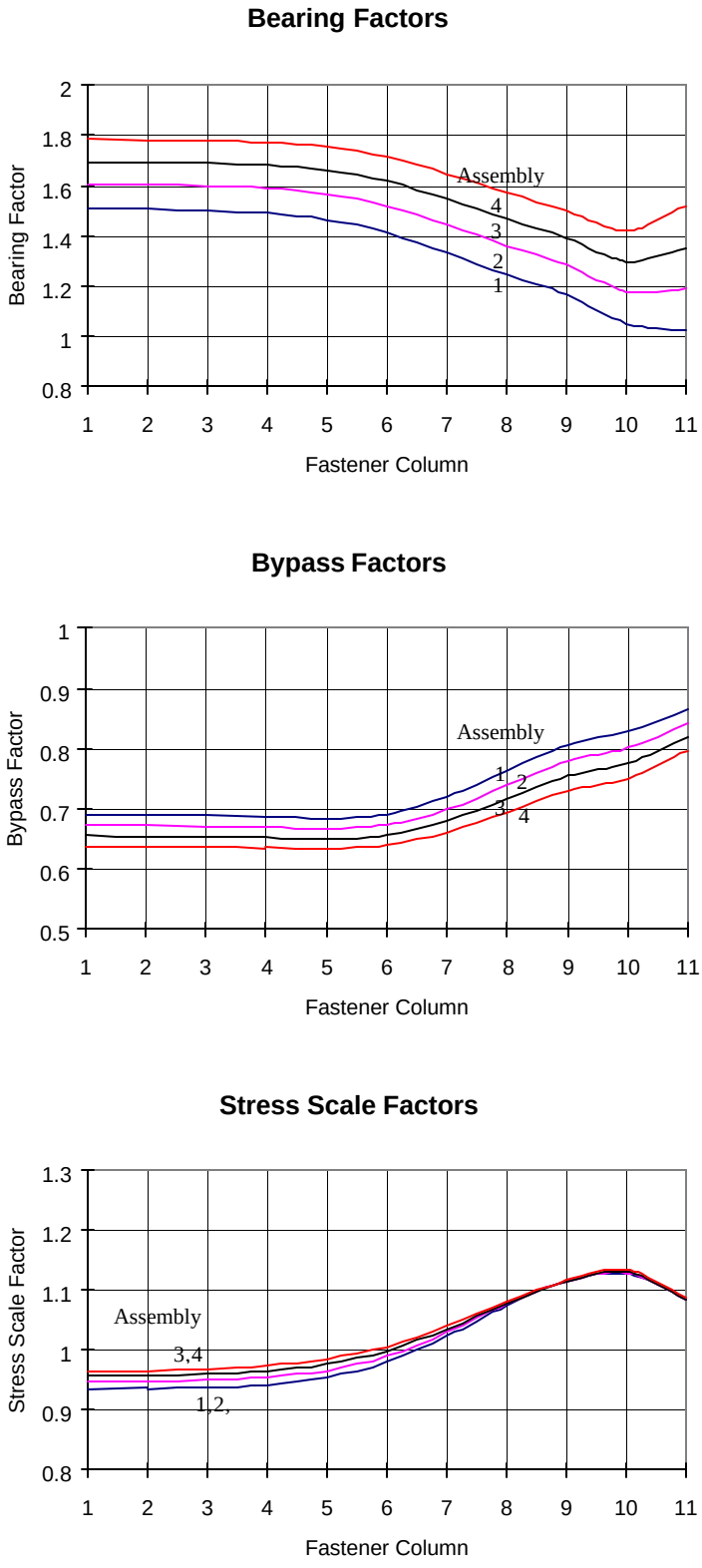

Figure A10d. Skin Thickness 0.063 in, Fastener Hole Diameter 1/4 in

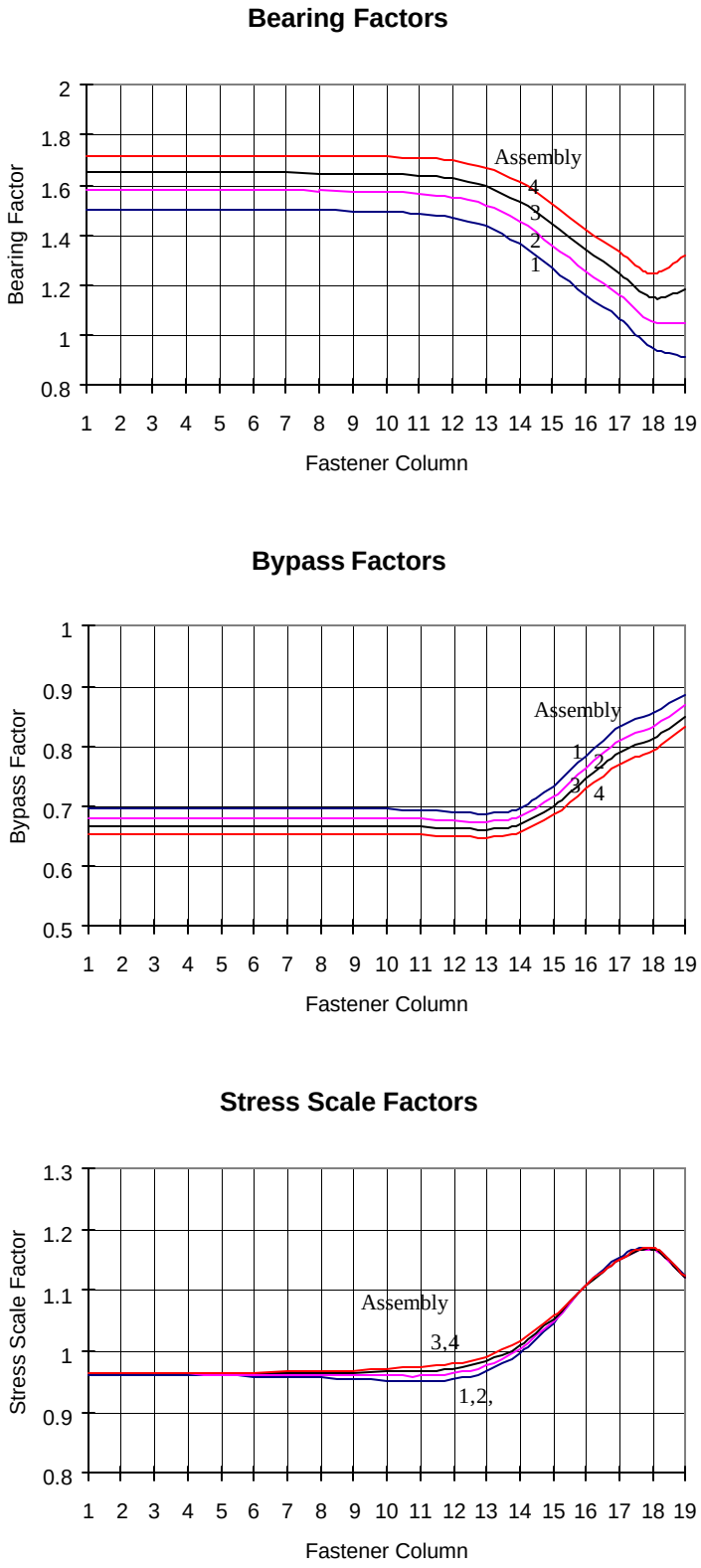

Figure A11a. Skin Thickness 0.071 in, Fastener Hole Diameter 1/8 in

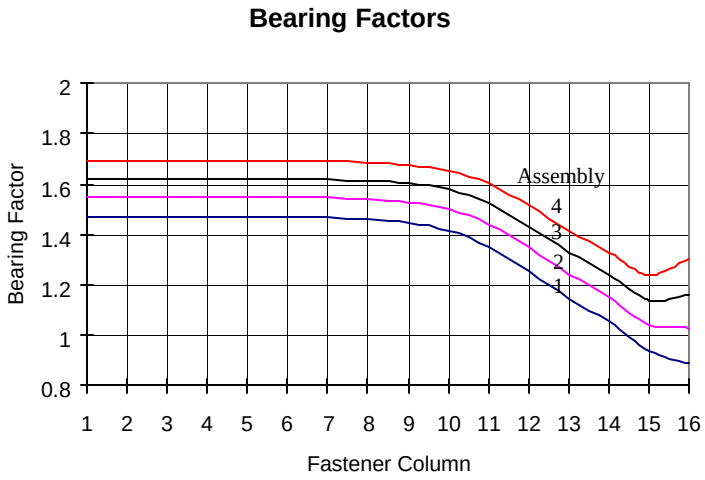

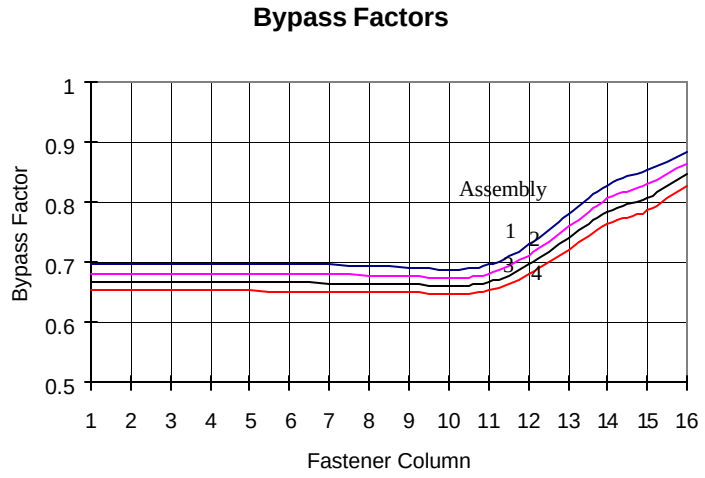

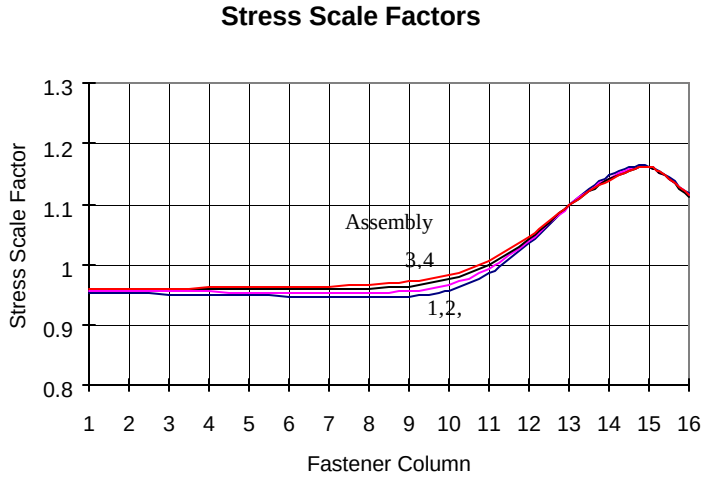

Figure A11b. Skin Thickness 0.071 in, Fastener Hole Diameter 5/32 in

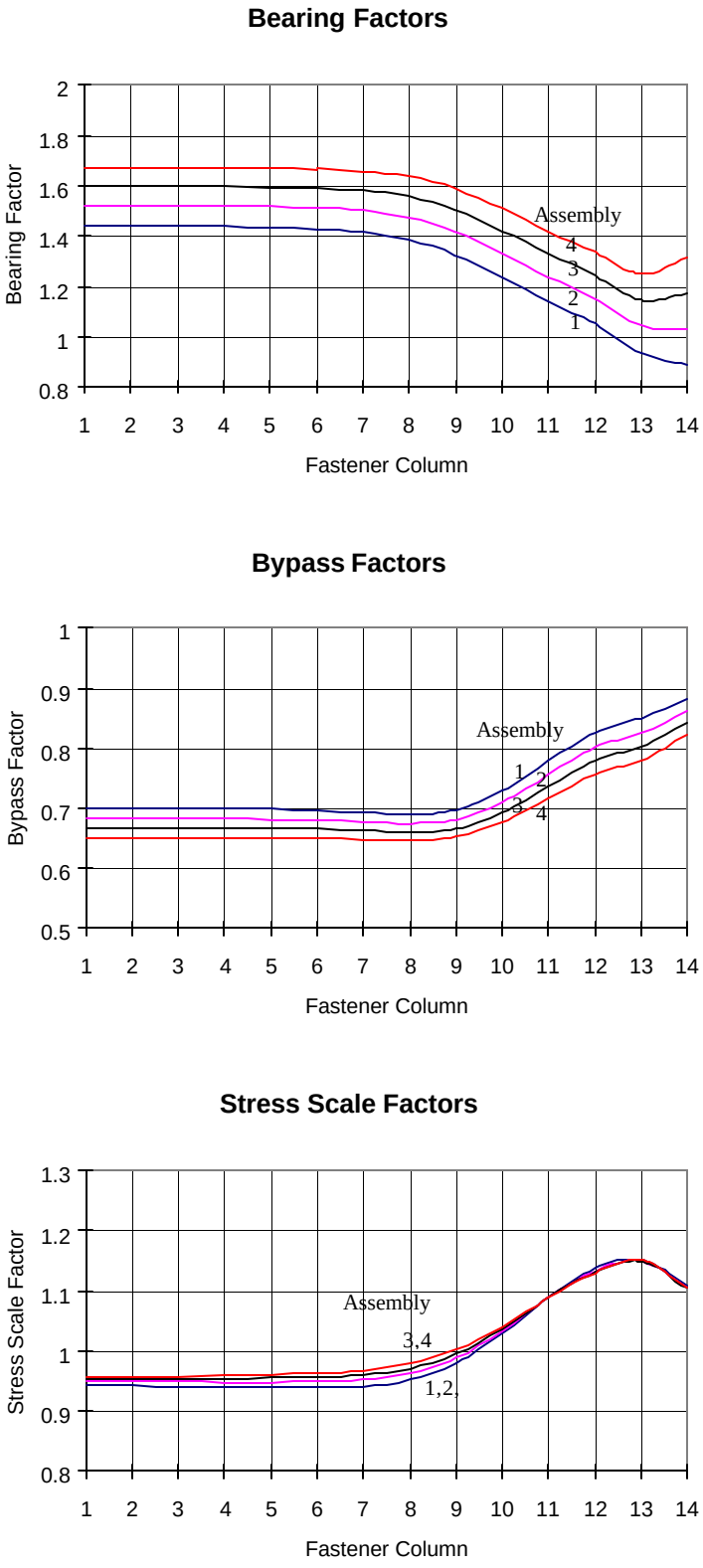

Figure A11c. Skin Thickness 0.071 in, Fastener Hole Diameter 3/16 in

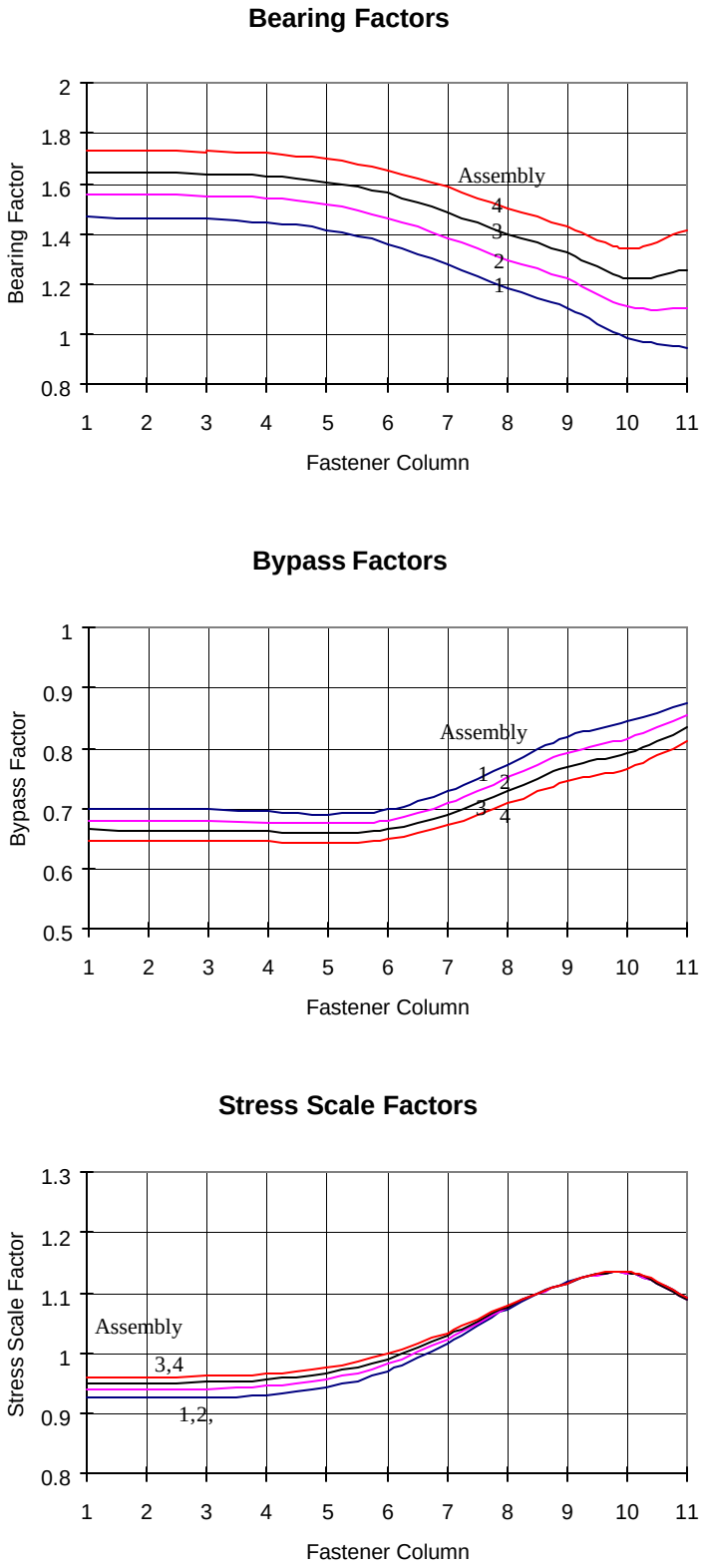

Figure A11d. Skin Thickness 0.071 in, Fastener Hole Diameter 1/4 in

Analysis results presented in figures A9a through A11d are for Type II baseline repair configurations with 3 fastener rows. For repairs with 4 or 5 fastener rows, first interpolate the correction factors for each stress factor at the intermediate fastener locations based on the values at the center and corner fasteners in the table shown below.

Location	Stress Factor	No. of Fastener Rows	
		4	5
Center	BRF	0.85	0.78
	BPF	1.08	1.12
	SSF	1.00	1.00
Corner	BRF	1.00	1.00
	BPF	1.00	1.00
	SSF	1.00	1.00

The bearing factors (BRF), bypass factors (BPF), and the stress scale factors (SSF) are then obtained by multiplying the results for the case of 3 fastener rows by the interpolated correction factors.

For a skin thickness other than the baseline thickness, first inter/extrapolate the stress factors for the subject skin thickness for the case of 3 fastener rows. When the number of fastener rows is not 3, the process described earlier is then used. For steel or titanium fasteners, correction factors are applied to the stress factors for the aluminum fasteners. These correction factors are obtained as the ratios of the stress factors between the subject fasteners and the aluminum fasteners using the one-dimensional analysis procedure in RAPID.

A2.3 Fastener Loads for Type I Repairs

Parameters used in the analysis of Type I repairs are shown below in the table. An outer doubler thickness of 0.05″ was first used in the analysis. Additional analyses were also performed for outer doubler thickness equal to 0.063″, 0.071″, and 0.080″. The analysis was performed for the cases of 3, 4, and 5 fastener rows.

Assembly No.	Thickness (in)			Fastener Hole Diameter (in)			
	Skin	$Doubler_{Inner}$	$Doubler_{Outer}$				
1	0.050	0.025	0.050	1/8	5/32	3/16	—
2		0.032					
3		0.040					
4	0.063	0.025		1/8	5/32	3/16	1/4
5		0.032					
6		0.040					
7		0.050					
8	0.071	0.025		1/8	5/32	3/16	1/4
9		0.032					
10		0.040					
11		0.050					

Analysis results for Type I baseline repair configurations with 3 fastener rows are presented in figures A12a through A14d.

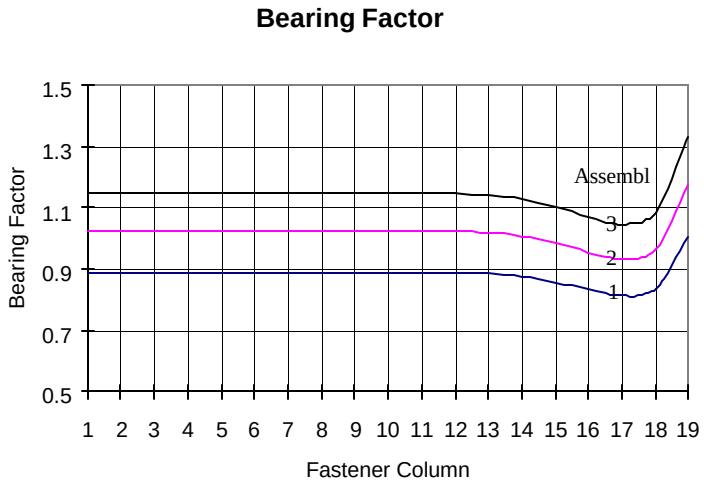

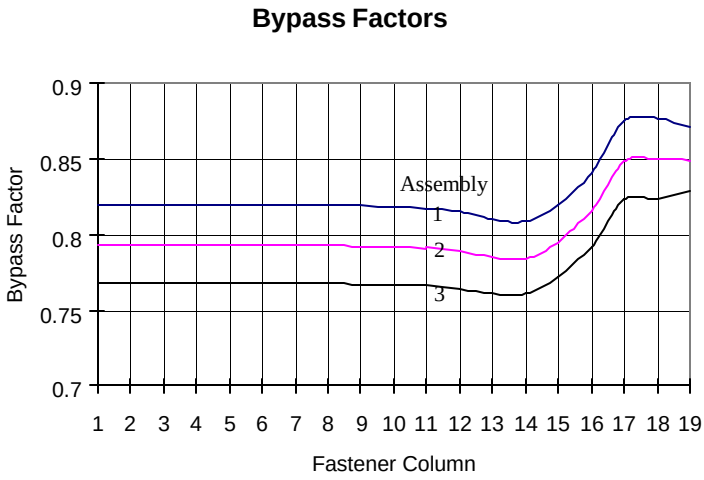

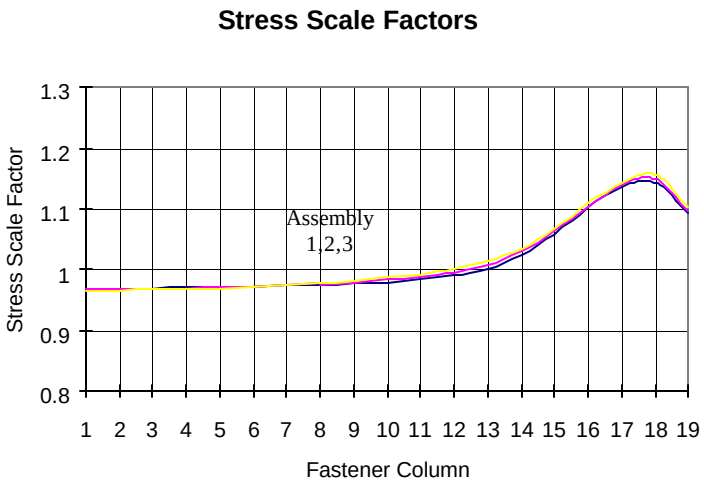

Figure A12a. Skin Thickness 0.050 in, Fastener Hole Diameter 1/8 in

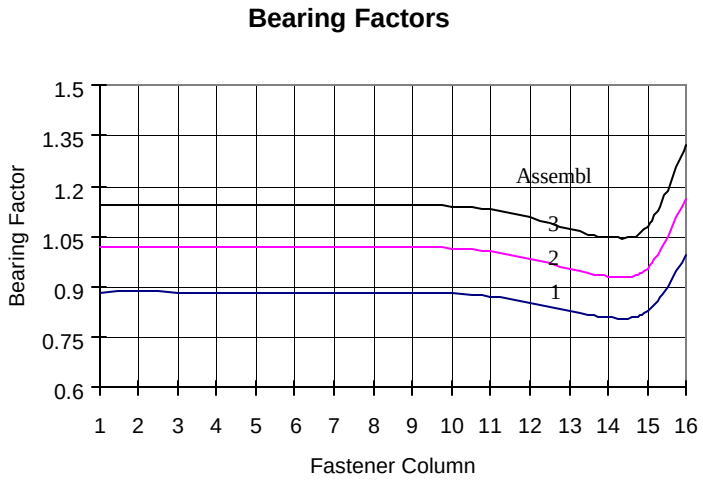

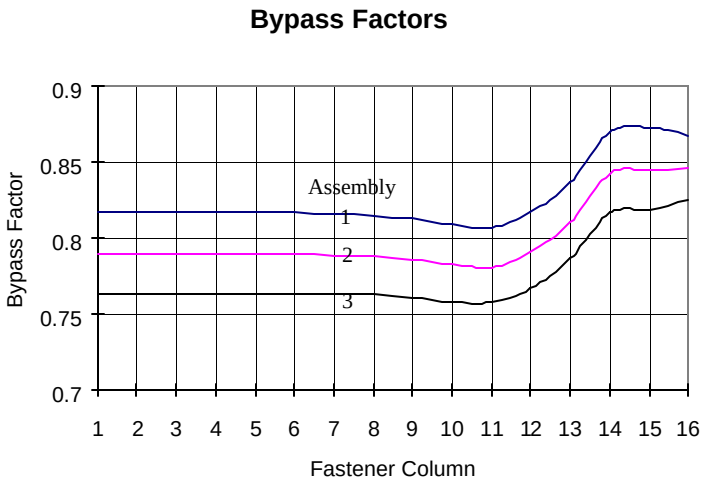

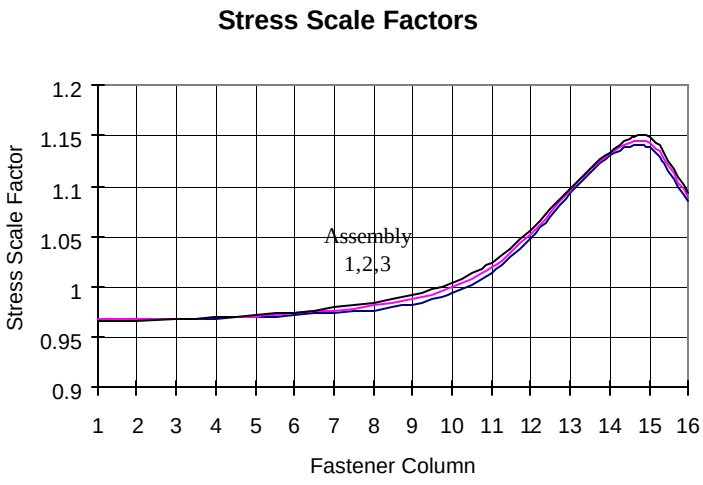

Figure A12b. Skin Thickness 0.050 in, Fastener Hole Diameter 5/32 in

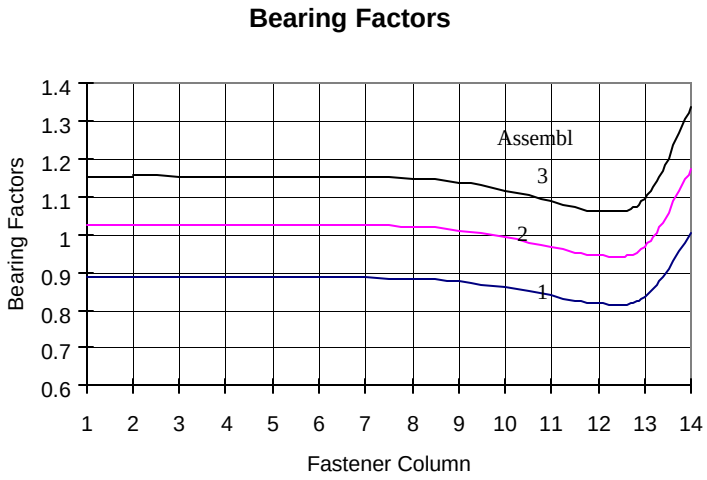

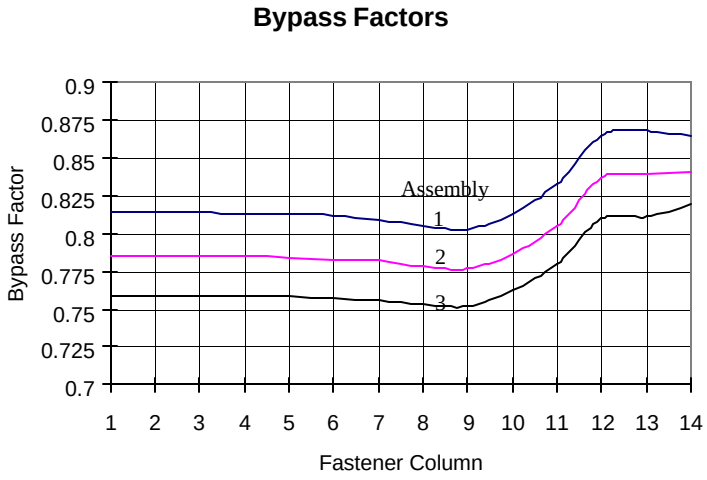

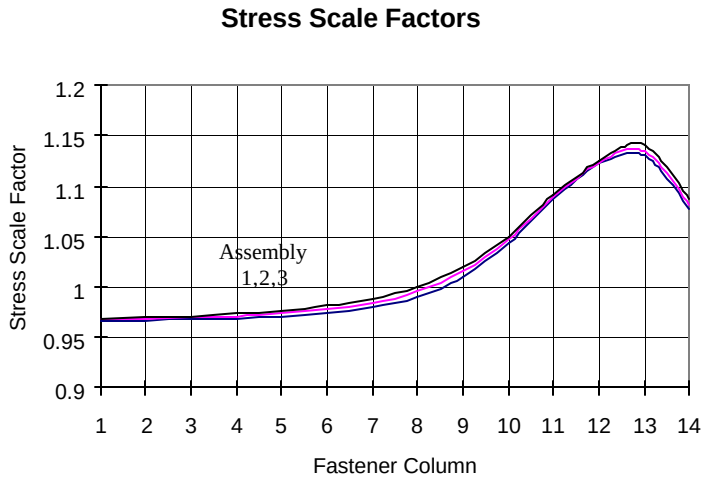

Figure A12c. Skin Thickness 0.050 in, Fastener Hole Diameter 3/16 in

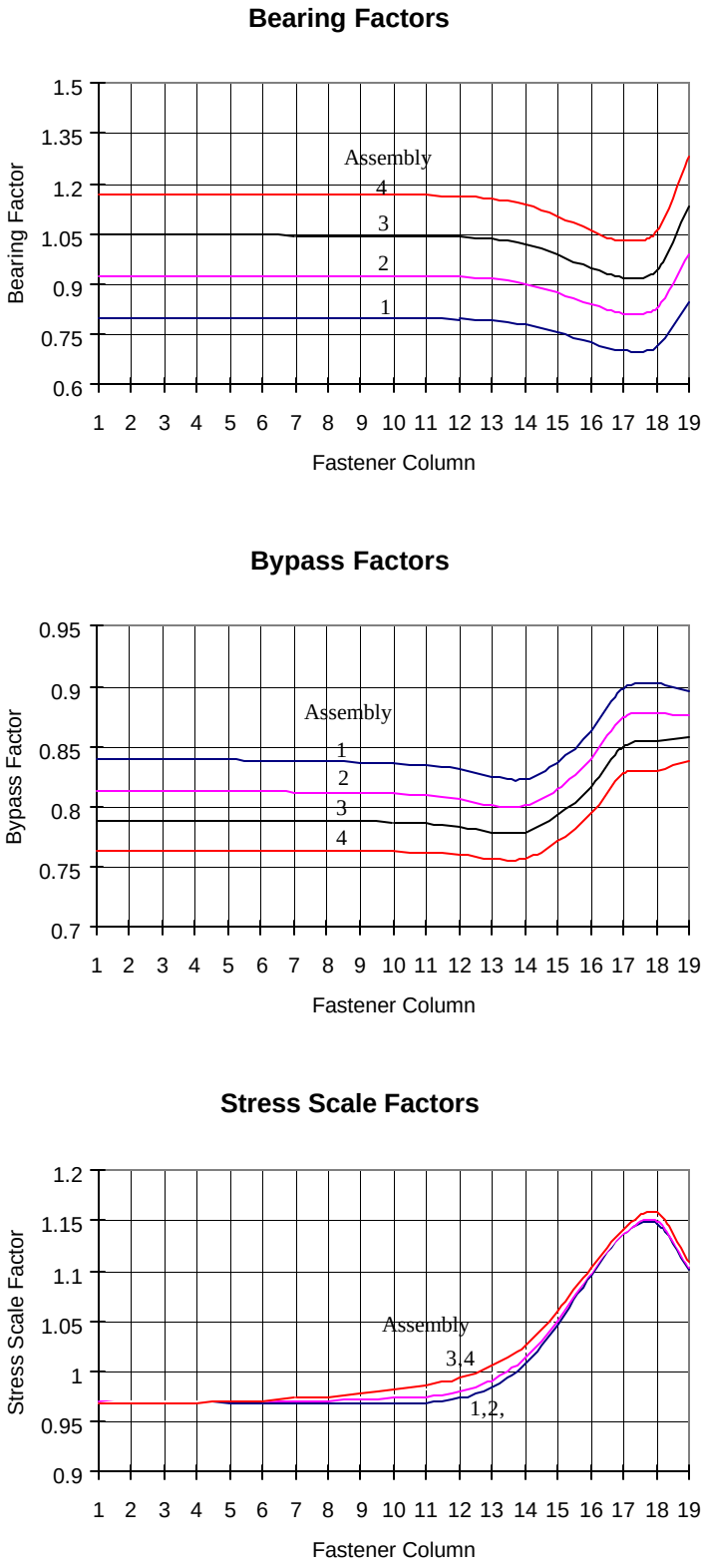

Figure A13a. Skin Thickness 0.063 in, Fastener Hole Diameter 1/8 in

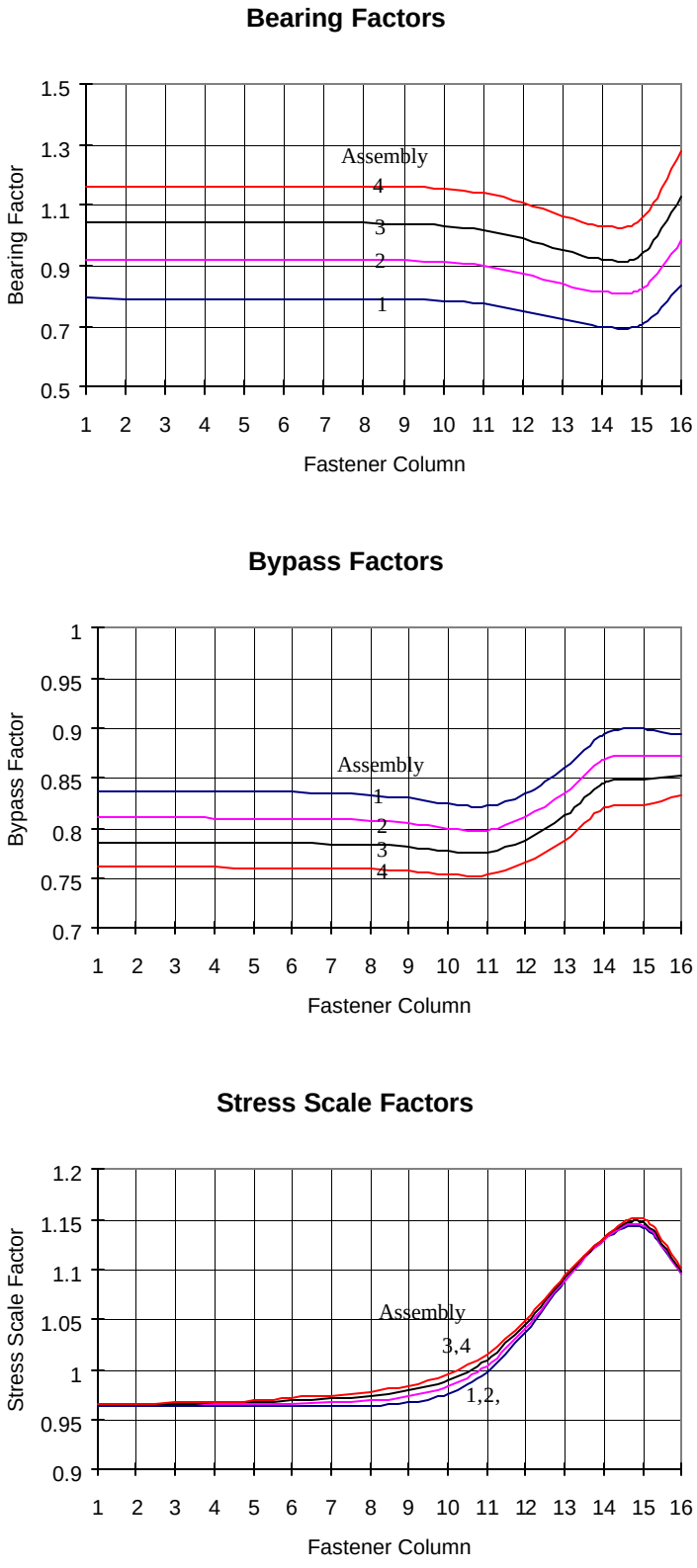

Figure A13b. Skin Thickness 0.063 in, Fastener Hole Diameter 5/32 in

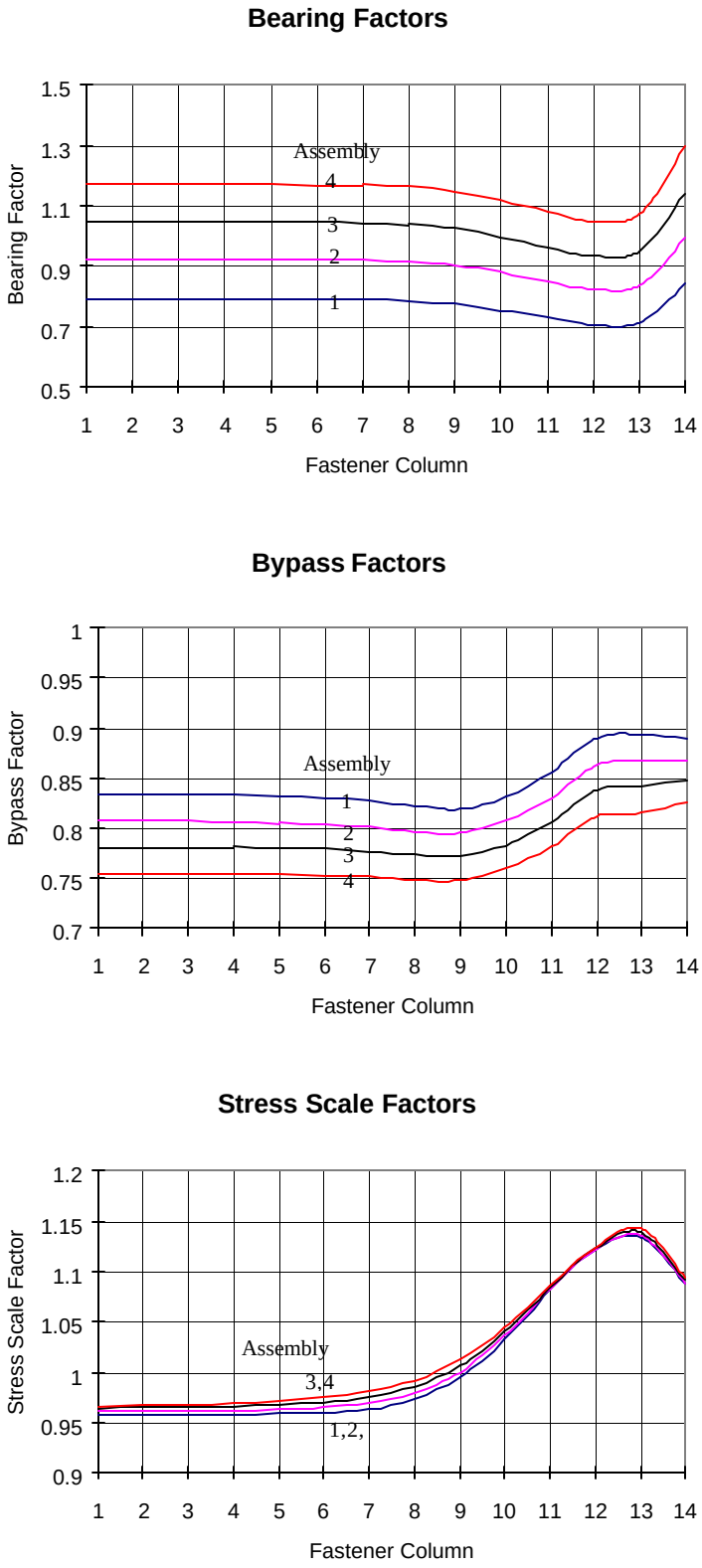

Figure A13c. Skin Thickness 0.063 in, Fastener Hole Diameter 3/16 in

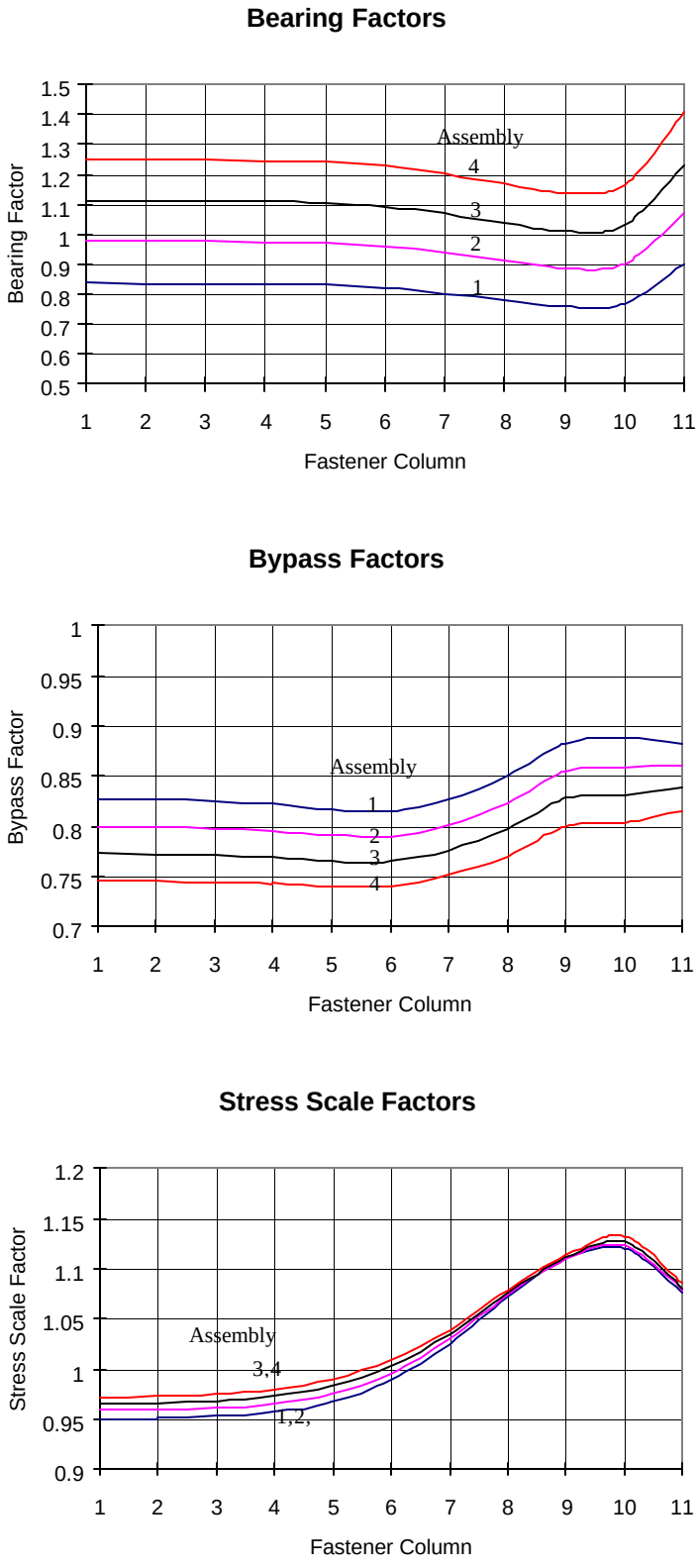

Figure A13d. Skin Thickness 0.063 in, Fastener Hole Diameter 1/4 in

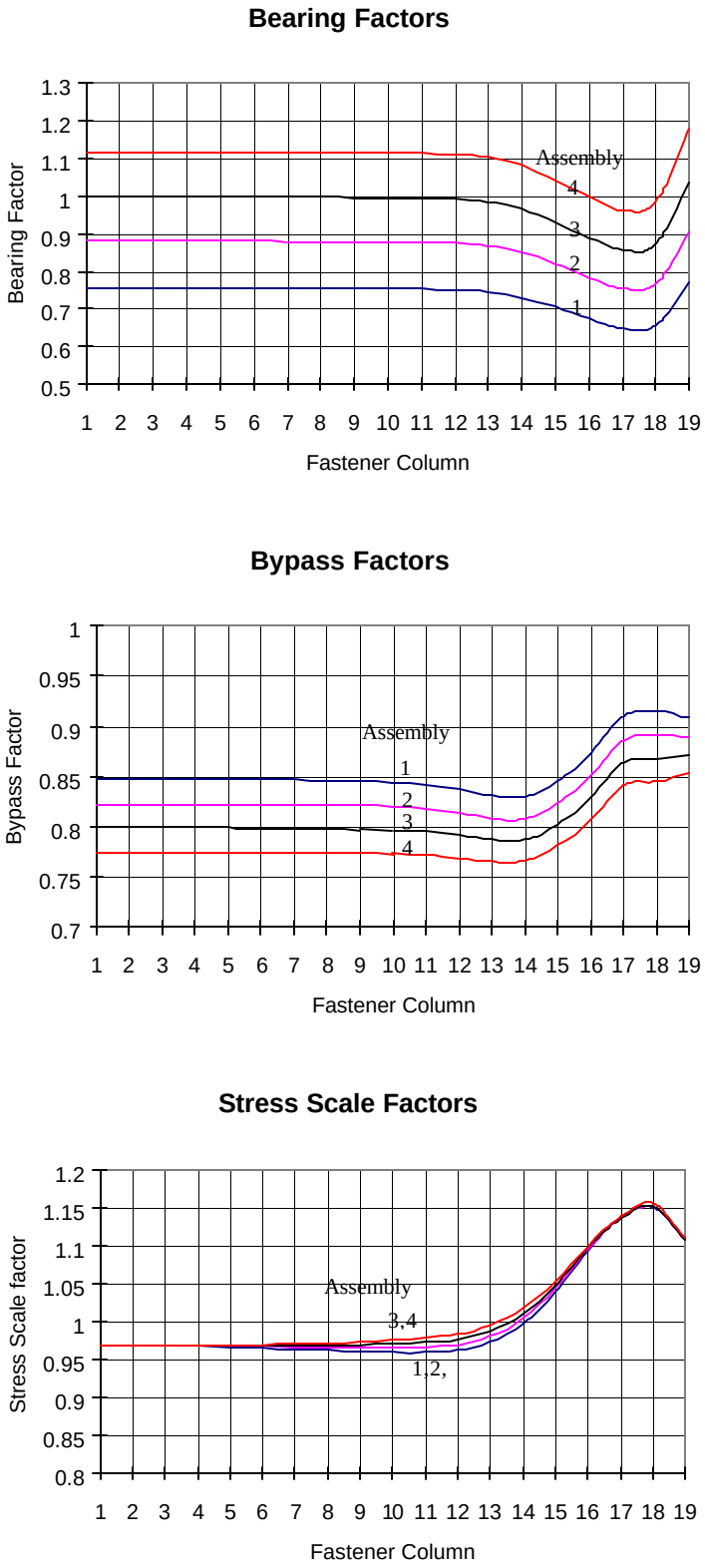

Figure A14a. Skin Thickness 0.071 in, Fastener Hole Diameter 1/8 in

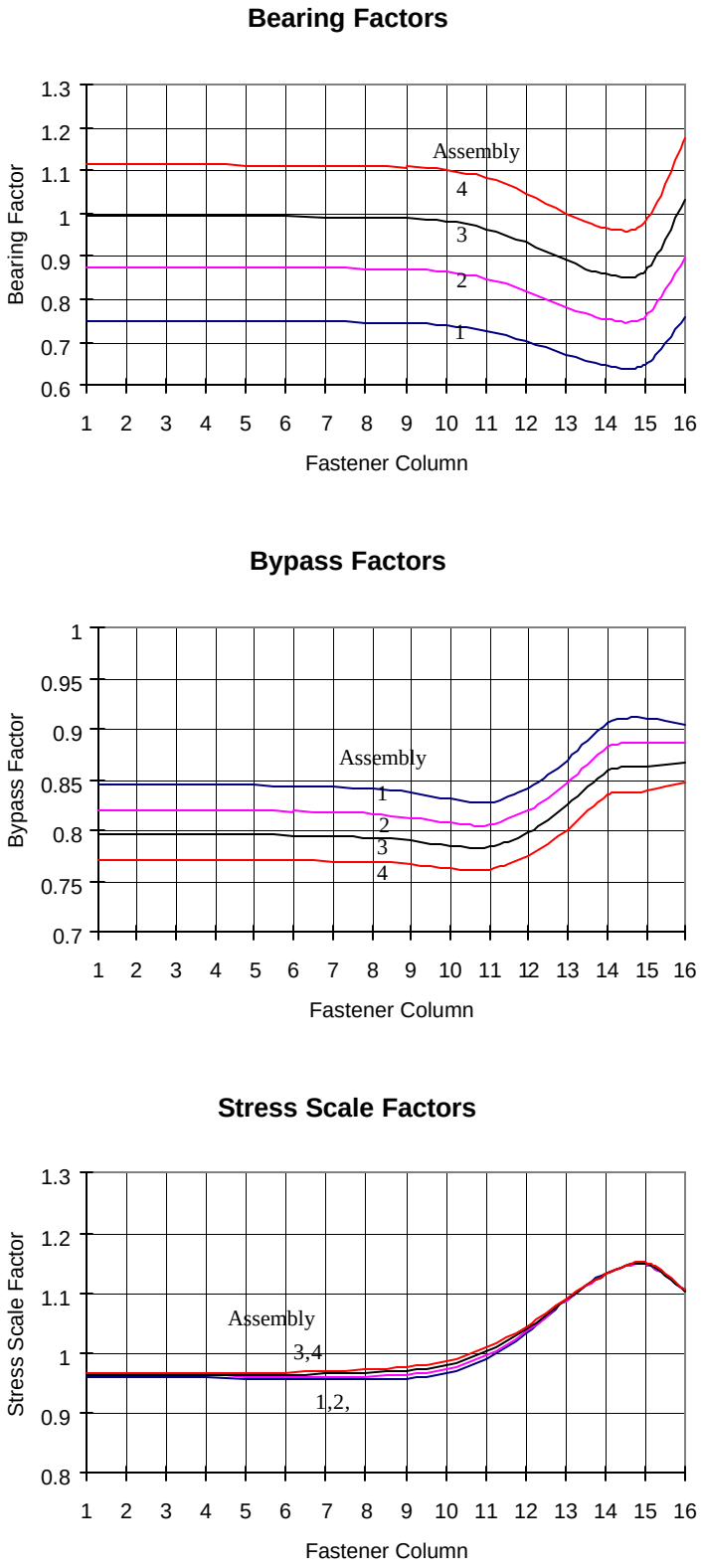

Figure A14b. Skin Thickness 0.071 in, Fastener Hole Diameter 5/32 in

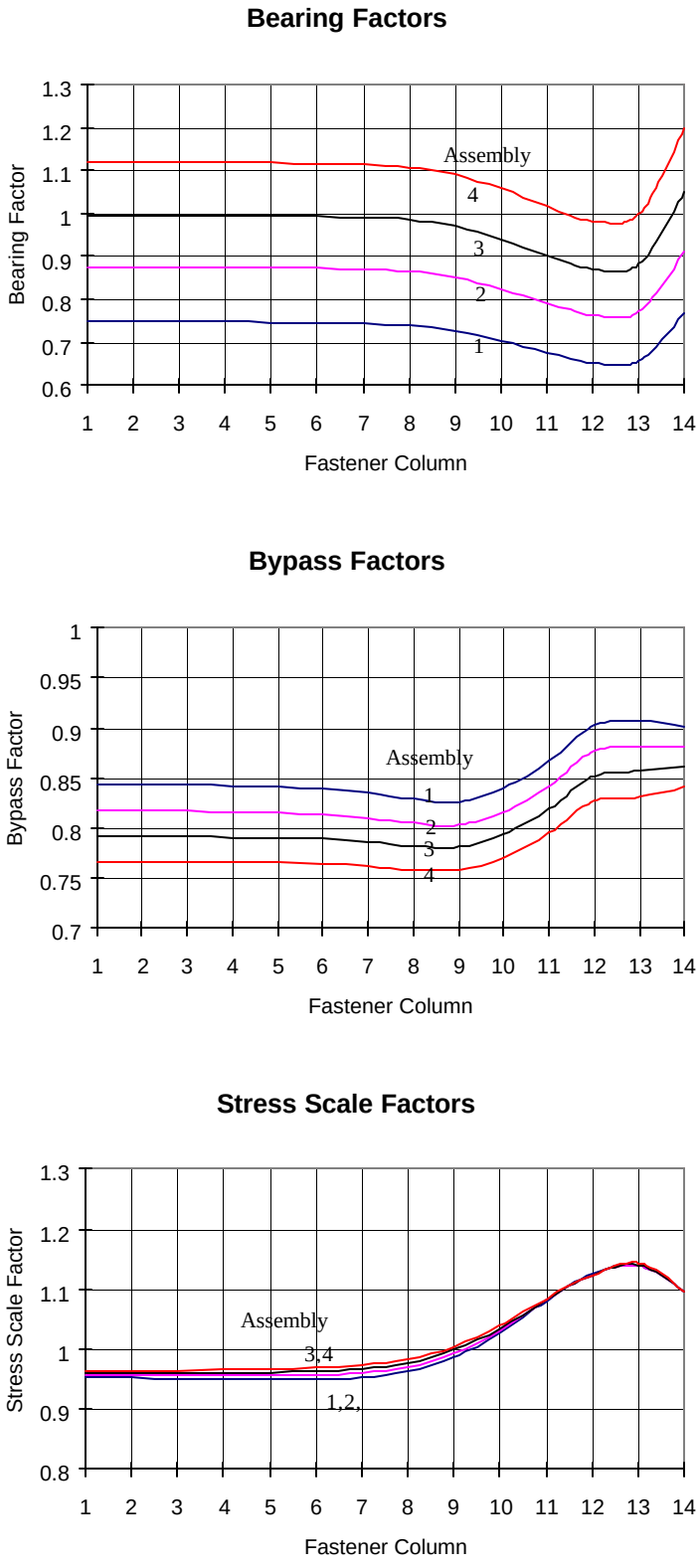

Figure A14c. Skin Thickness 0.071 in, Fastener Hole Diameter 3/16 in

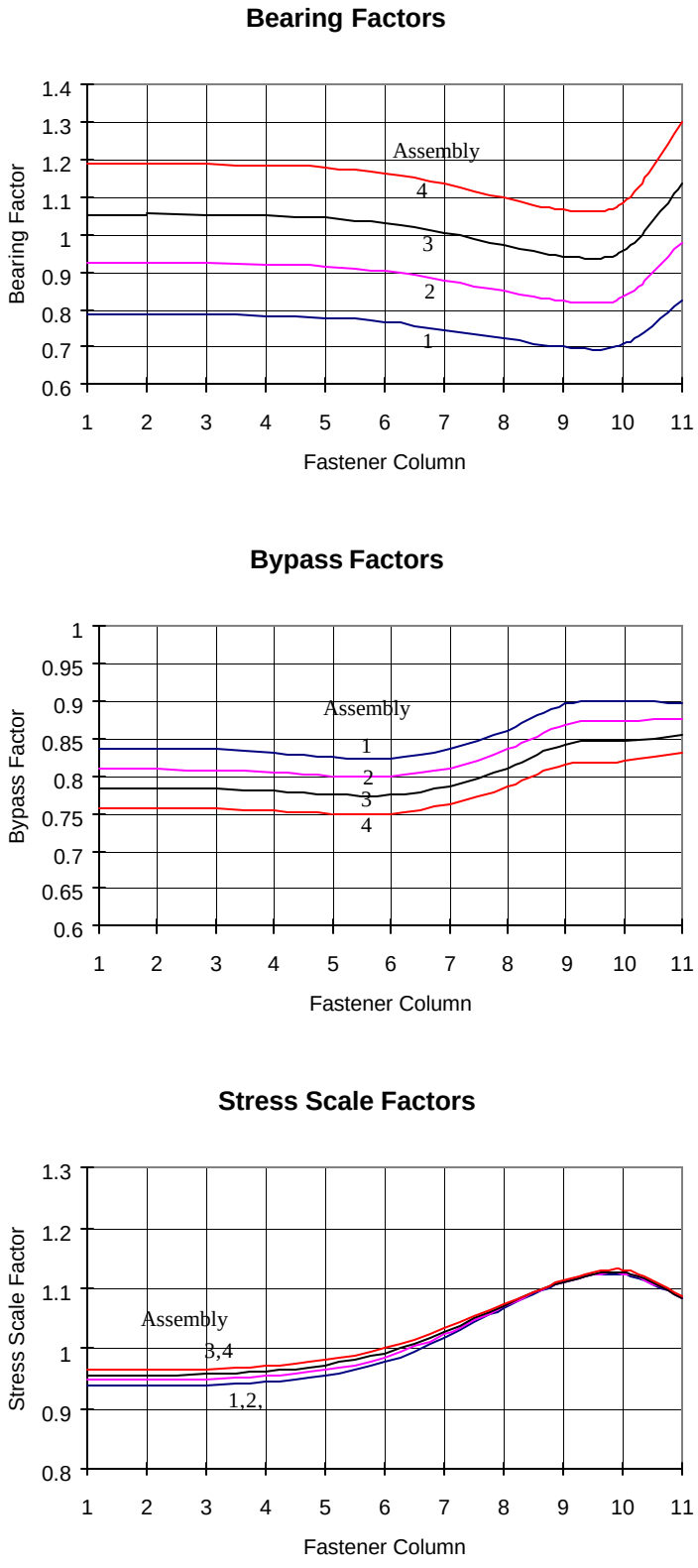

Figure A14d. Skin Thickness 0.071 in, Fastener Hole Diameter 1/4 in

Analysis results presented in figures A12a through A14d are for Type I baseline repair configurations with 3 fastener rows. For repairs with 4 or 5 fastener rows, first interpolate the correction factors for each stress factor at the intermediate fastener locations based on the values at the center and corner fasteners in the table shown below.

Location	Stress Factor	No. of Fastener Rows	
		4	5
Center	BRF	0.85	0.78
	BPF	1.09	1.13
	SSF	1.00	1.00
Corner	BRF	1.00	1.00
	BPF	1.00	1.00
	SSF	1.00	1.00

The bearing factors (BRF), bypass factors (BPF), and the stress scale factors (SSF) are then obtained by multiplying the results for the case of 3 fastener rows by the interpolated correction factors.

For baseline repairs with the outer doubler thickness equal to 0.063″, 0.071″, and 0.080″, first interpolate the correction factors for each stress factor at the intermediate fastener locations based on the values at the center and corner fasteners in the table shown below.

Location	Stress Factor	Outer Doubler Thickness		
		0.063”	0.071”	0.080”
Center	BRF	0.96	0.94	0.92
	BPF	1.01	1.02	1.03
	SSF	1.00	1.00	1.00
Corner	BRF	1.00	1.00	1.00
	BPF	1.00	1.00	1.00
	SSF	1.00	1.00	1.00

The bearing factors (BRF), bypass factors (BPF), and the stress scale factors (SSF) are then obtained by multiplying the results for outer doubler thickness equal to 0.05″ by the interpolated correction factors.

For a skin thickness other than the baseline thickness, first inter/extrapolate the stress factors for the subject skin thickness for the case of 3 fastener rows. When the number of fastener rows is not 3, the process described earlier is then used. For steel or titanium fasteners, correction factors are applied to the stress factors for the aluminum fasteners. These correction factors are obtained as the ratios of the stress factors between the subject fasteners and the aluminum fasteners using the one-dimensional analysis procedure in RAPID.

A3. Size Effect on Crack Growth Life

A standard repair size equal to one-frame bay by two-longeron bay is used in the analysis for baseline Type I, II, and III repairs. For repairs other than the standard size, scale factors for fastener loads were obtained at the center and corner fasteners as shown in figure A15. The scale factor is the ratio of fastener loads between the size of the subject repair and standard size of the baseline repair.

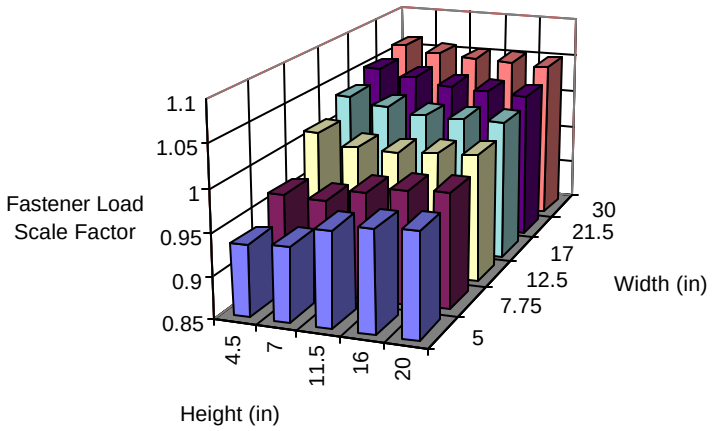

(a) Center Fastener

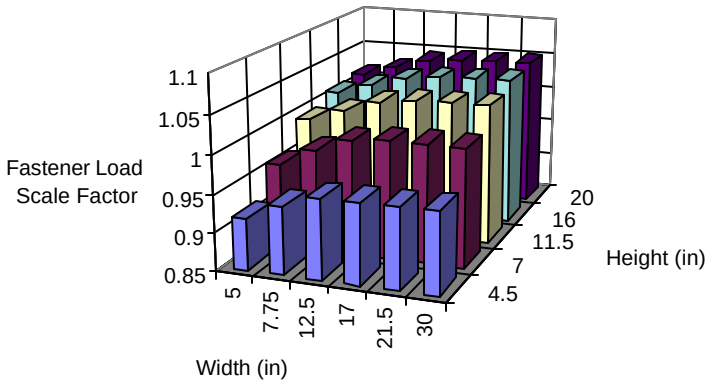

(b) Corner Fastener

Figure A15.

These fastener load scale factors are used to determine the life correction factor for the subject repair as shown in figure A16. In the figure, F is the fastener load in the subject repair and F_o is that in the baseline repair.

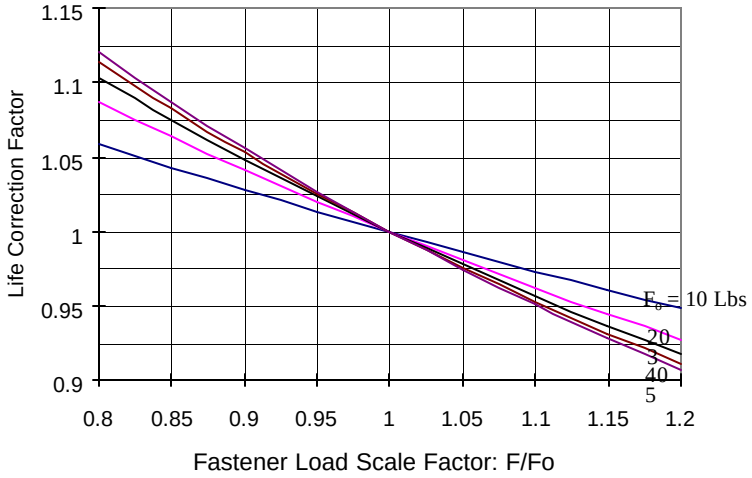

Figure A16.

The crack growth life of a repair with nonstandard size is then estimated by multiplying the life correction factor by the crack growth life of the same type of repair with standard size.

Appendix B – Stress Intensity Factor Solutions

B1. Introduction

This appendix presents stress-intensity factor solutions for the damage tolerance analysis of the repaired skin. There are two types of solutions in RAPID: the basic solutions for simple crack configurations and the derived solutions for cracks at linked holes. The basic solutions are known solutions in the open literature. The derived solutions are approximate solutions obtained from basic solutions using the methods described in section 3.1.4.

Geometry factors (Beta factors) as a function of crack length can be printed in the output when requested by the user. The geometry or the beta factors are the normalized stress intensity factors as described in this Appendix.

B2. Basic Stress-Intensity Factor Solutions

Stress-intensity factor solutions for three basic crack configurations are incorporated in the database. These solutions are presented below.

B2.1 A Through Crack Emanating From a Circular Hole in a Wide Plate

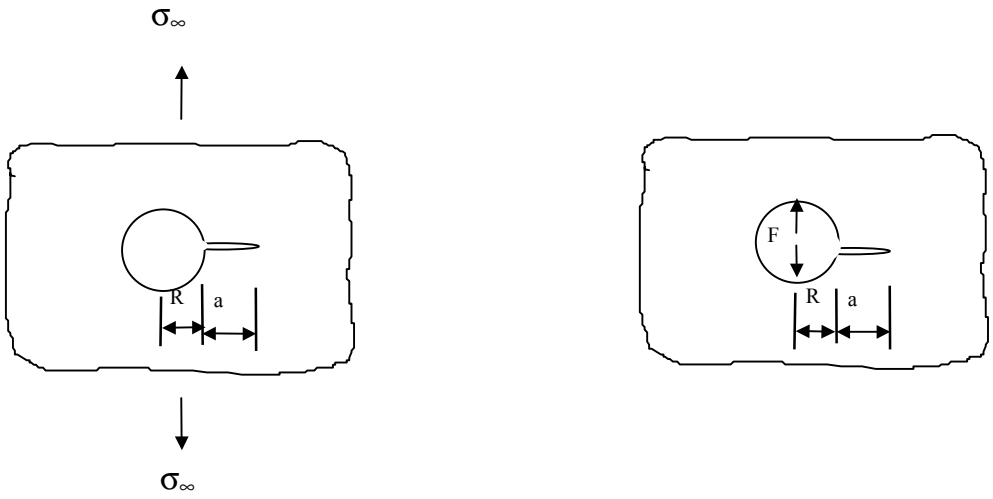

(a) Far Field Stress (b) A Pair of Point Loads

Figure B1. A Through Crack Emanating From a Circular Hole in a Wide Plate

For a through crack emanating from a hole in a wide plate, the solution was first solved by Bowie [1] and improved later by Tweed and Rooke [2]. It was also solved by Shivakumar and Forman [3]. Normalized stress-intensity factors obtained from Reference 3 are shown in figure B2. The referenced stress-intensity factor K_0 is defined as $\sigma_\infty\sqrt{\pi a}$ or $(F/2R)\sqrt{\pi a}$ for the plate subjected to the far field stress or the point load, respectively, and a is the crack length between the crack tip and edge of the hole, and R is the radius of the hole.

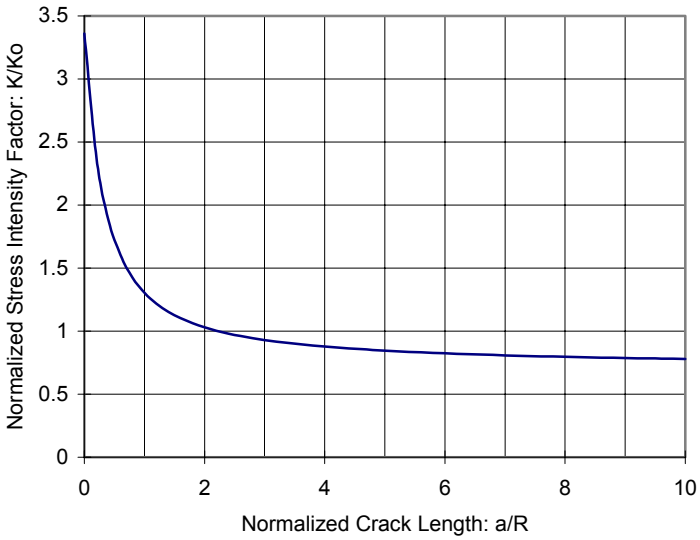

(a) Uniform Far Field Stress: $K_o = \sigma_\infty \sqrt{\pi a}$

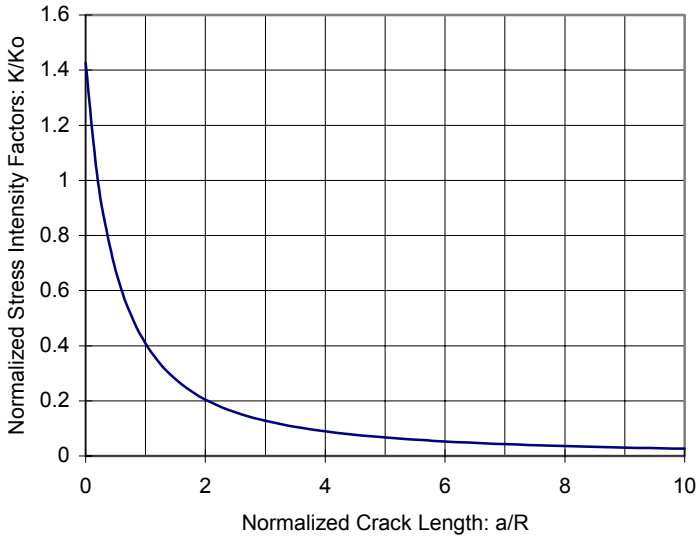

(b) A Pair of Point Loads: $K_o = \frac{F}{2Rt}\sqrt{\pi a}$

Figure B2. Normalized Stress-Intensity Factors for a Crack Emanating From a Hole

B2.2 Two Diametric Through Cracks of Unequal Lengths Emanating From a Circular Hole in a Wide Plate

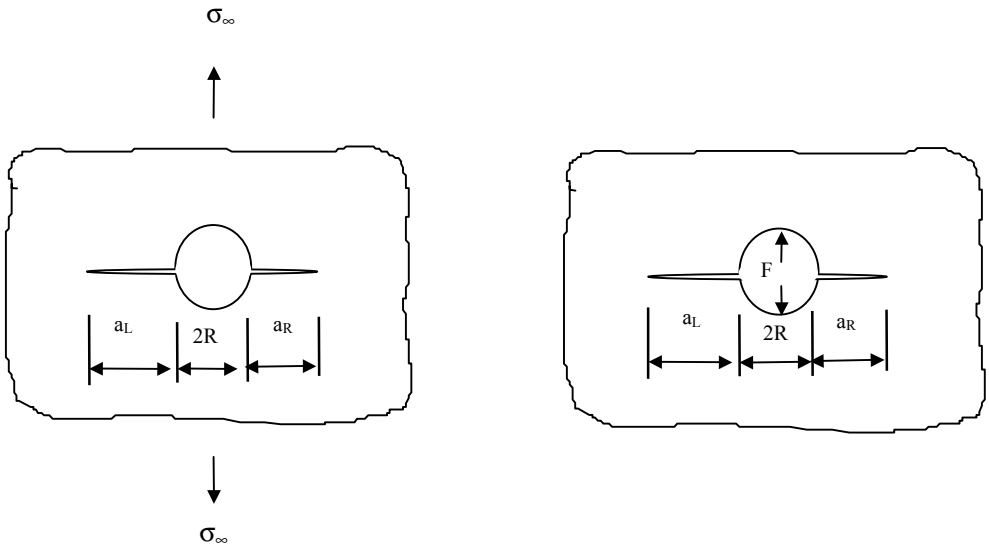

(a) Far Field Stress (b) A Pair of Point Loads

Figure B3. Two Diametric Through Cracks of Unequal-Lengths Emanating From a Circular Hole in a Wide Plate

The problem of stress-intensity factor solutions for two unequal length through cracks emanating diametrically from a hole in a wide plate was solved analytically by Tweed and Rooke [4]. By using a superposition principle, it was shown that the stress-intensity factors were related to the solution of a pair of simultaneous singular integral equations that were solved by Gaussian quadrature techniques. The solutions were recompiled for both the uniform far field tension and a pair of point loads, respectively, and presented in figure B4. The force F is the point force per unit plate thickness. The referenced stress-intensity factor K_0 is defined as $\sigma_\infty\sqrt{\pi a}$ or $(F/2R)\sqrt{\pi a}$ for the plate subjected to the far field stress or the point loads, respectively. The terms a_L and a_R are the left and right crack lengths between the crack tip and edge of the hole, respectively, and R is the radius of the hole.

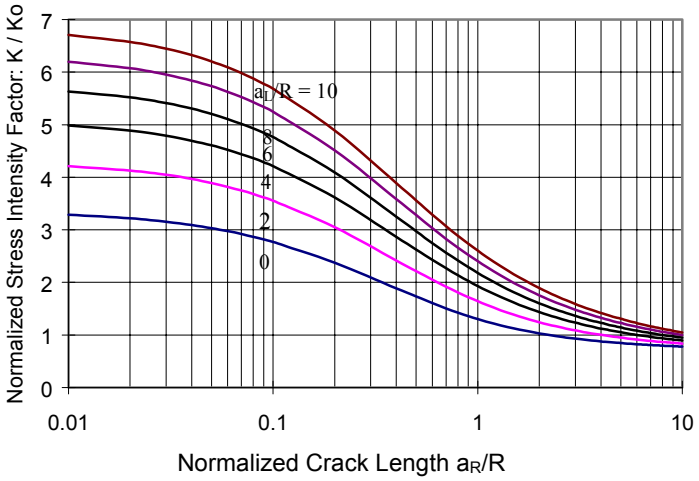

(a) Uniform Far Field Stress: $K_o = \sigma_\infty \sqrt{\pi a}$

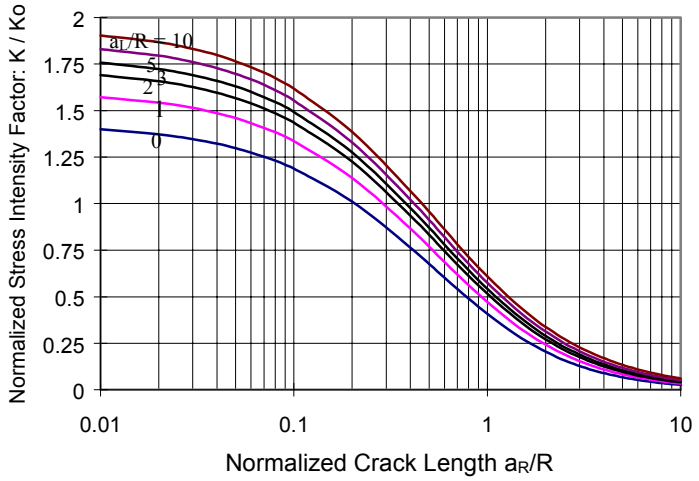

(b) A Pair of Point Loads: $K_o = \frac{F}{2Rt}\sqrt{\pi a}$

Figure B4. Normalized Stress-Intensity Factors for Two Unequal Length Cracks Emanating From a Hole

B2.3 A Through Crack Approaching a Circular Hole in a Wide Plate

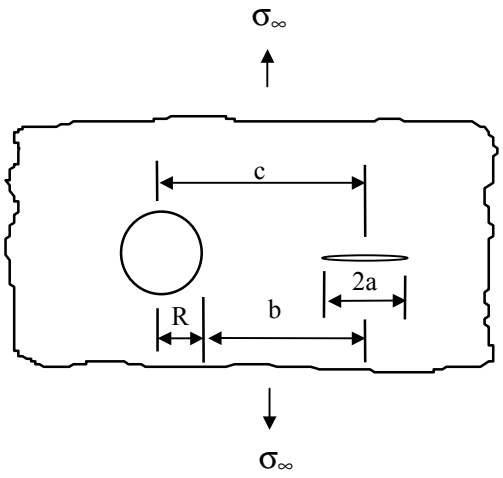

Figure B6. A Through Crack Approaching a Circular Hole in a Wide Plate

The stress-intensity factor solutions solutions for the far field stress were obtained by Isida using the Laurent's expansions in the complex stress potentials method [5] and are shown in figure B7. The referenced stress-intensity factor K_0 is defined as $\sigma_\infty\sqrt{\pi a}$.

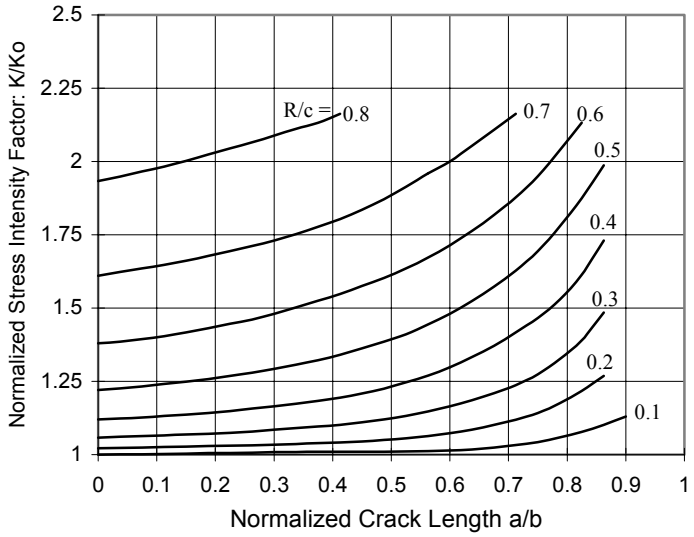

Figure B7. Normalized Stress-Intensity Factors for a Crack Approaching a Hole

B3. Derived Stress-Intensity Factor Solutions

The derived stress-intensity factor solutions for linked holes are approximate solutions obtained from basic solutions using the method described in section 3.1.4. This method is illustrated below for two cracks emanating from two linked holes as shown in figure B8.

B3.1 Two Unequal-Length Through Cracks Emanating From Two Linked Holes in a Wide Plate.

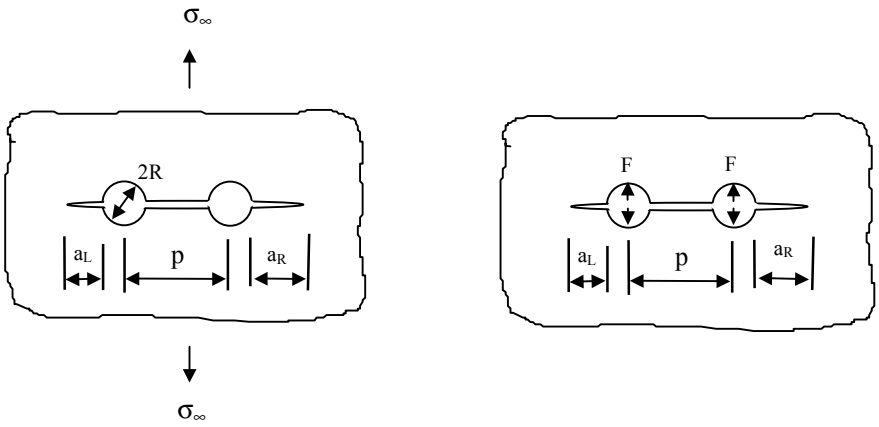

(a) Far Field Stress (b) A Pair of Point Loads

Figure B8. Two Unequal-Length Through Cracks Emanating From Two Linked Holes in a Wide Plate

For the stress-intensity factor of the left crack in case (a), consider the following three crack configurations.

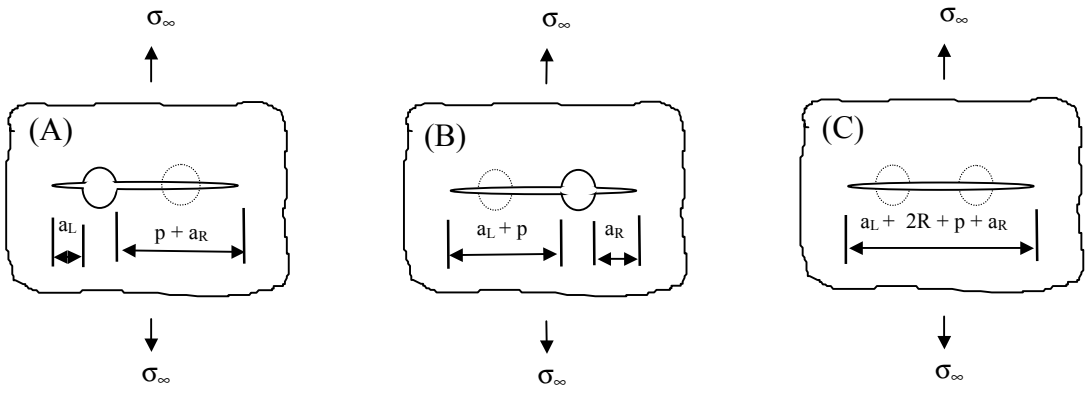

Figure B9. Three Crack Configurations for Use in the Similarity Method

Using the similarity method, the stress-intensity factor for the left crack can be obtained as

$$K_{Left} = K_A \frac{K_B}{K_C}$$

or

$$\sigma_\infty \sqrt{\pi a_L}\, \beta_{Left} = \sigma_\infty \sqrt{\pi a_L}\, \beta_{L,A} \frac{\sigma_\infty \sqrt{\pi (a_L + p)}\, \beta_{L,B}}{\sigma_\infty \sqrt{\pi \left[\tfrac{1}{2} (a_L + 2R + p + a_R) \right]}\, \beta_{L,C}}$$

where $\beta_{L,i}$ (for i = A, B, and C) are the geometry factors.

Let $\beta_L(a_L,a_R+p)$ and $\beta_L(a_L+p,a_R)$ denote $\beta_{L,B}$ and $\beta_{L,C}$, respectively. Since $\beta_{L,D} = 1$, the normalized stress-intensity factor of the left crack in case (a) of figure B8 can be estimated as

$$\beta_L = \beta_L (a_L, a_R + p) \beta_L (a_L + p, a_R) \times Q$$

where Q is given by

$$Q = \sqrt{\frac{a_L + p}{\tfrac{1}{2} (a_L + 2R + p + a_R)}}$$

In the above equation, $\beta_L(\kappa,\lambda)$ is the normalized stress-intensity factor of the left crack in the basic crack configuration as described in section B1.2. The quantities κ and λ are the lengths of the left and right cracks, respectively.

Similarly, for a pair of point loads in the hole, the normalized stress-intensity factor of the left crack can be estimated as

$$\beta_L = \left[\beta_{L_{PointLoad}} (a_L, a_R + p) \beta_{L_{FarField}} (a_L + p, a_R) + \beta_{L_{PointLoad}} (a_L + p, a_R) \beta_{L_{FarField}} (a_L, a_R + p) \right] \times Q$$

As an example, normalized stress-intensity factors for the left crack tip are shown in figure B10. In this example, the pitch between the holes is six times the diameter of the hole. The force F is the point load per unit plate thickness.

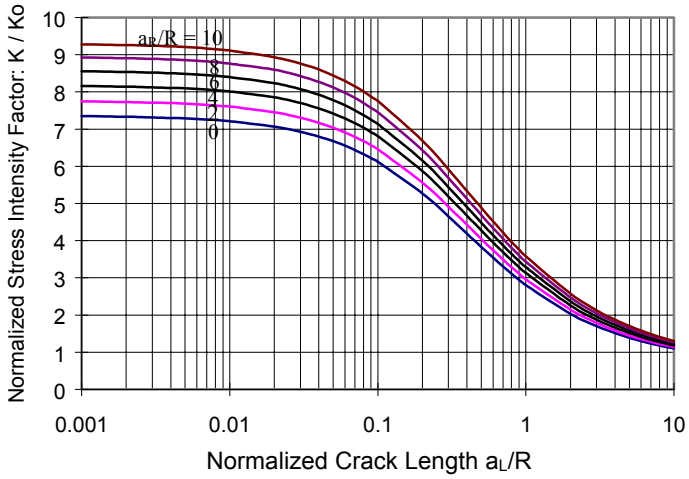

(a) Far Field Stress

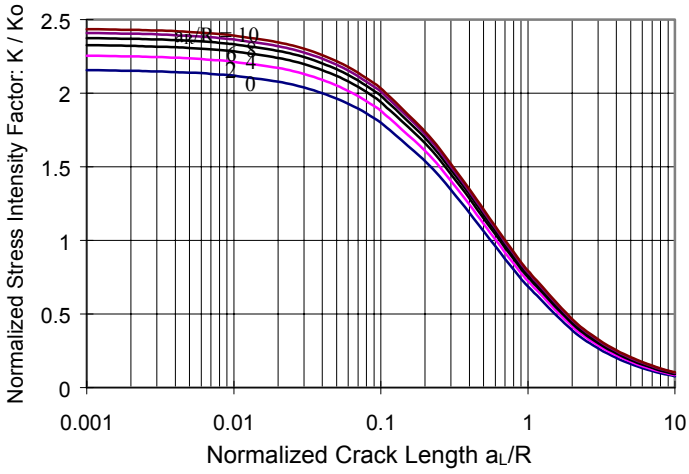

(b) A Pair of Point Loads

Figure B10. Stress-Intensity Factors of the Left Crack in a Two Linked Holes

B3.2 Two Unequal-Length Through Cracks Emanating From a Series of Linked Holes in a Wide Plate

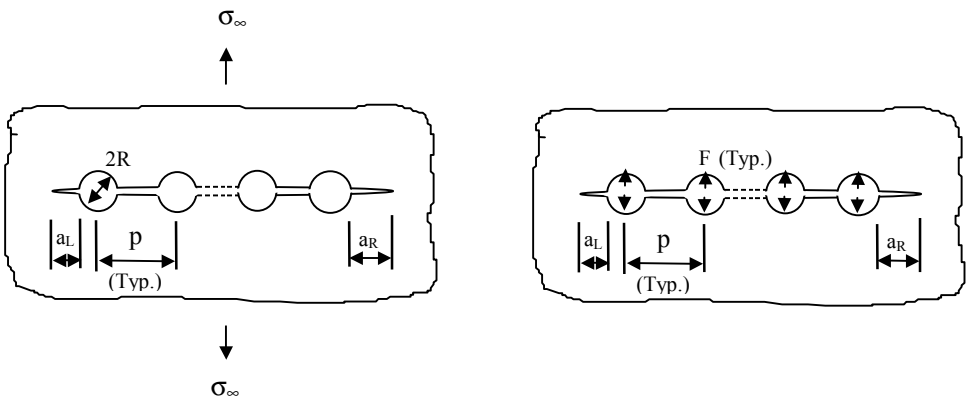

(a) Far field stress (b) A Pair of Point Loads

Figure B11. Two Unequal-Length Cracks Emanating From a Series of Linked Hole in a Wide Plate

The solutions presented in section B2.1 for the case of two linked holes can be extended to a series of linked holes. Let N be the total number of linked holes. The normalized stress-intensity factor of the left crack tip can be estimated, for the far field stress as

$$\beta_L = \left\{ \prod_{i=1}^{N} \beta_{L,i}\left[a_L + (i-1)p, a_R + (N-i)p\right] \right\} \times Q$$

where Q is obtained as

$$Q = \sqrt{\frac{\prod_{k=1}^{N-1} (a_L + kp)}{\{½\left[a_L + 2R + (N-1)p + a_R\right]\}^{N-1}}}$$

Similarly, the solution for a pair of point loads in the hole can be obtained as

$$\beta_L = \left\{ \sum_{i=1}^{N} \left\{ \beta_{L,i_\infty}\left[a_L + (i-1)p, a_R + (N-i)p\right] \times H \right\} \right\} \times Q$$

where H is given by

$$H = \frac{\prod_{j=1}^{N} \beta_{L,j_\infty}\left[a_L + (j-1)p, a_R + (N-j)p\right]}{\beta_{L,i_\infty}\left[a_L + (i-1)p, a_R + (N-i)p\right]}$$

As an example, the normalized stress-intensity factors of the left crack in four linked holes are shown in figure B12. The pitch between two holes is six times the diameter of the hole.

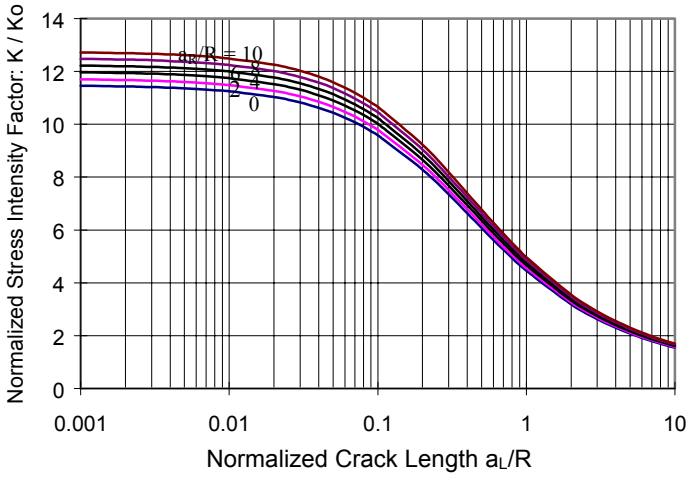

(a) Far Field Stress

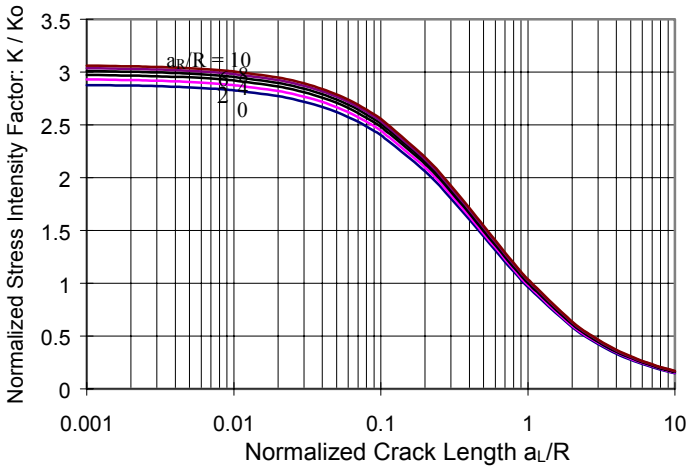

(b) A Pair of Point Loads

Figure B12. Stress-Intensity Factors of the Left Crack in a Four Linked Holes

References

1. Bowie, O. L., "Analysis of an Infinite Plate Containing Radial Cracks Orginating at the Boundaries in an Internal Circular Hole," Journal of Mathematics and Physics, Vol. 35, 1956.

2. Tweed, J. and Rooke, D. P., "The Distribution of Stress Near the Tip of a Radial Crack at the Edge of a Circular Hole," International Journal of Engineering and Science, Vol. 11, 1974.

3. Shivakumar, V. and Forman, R.G., "Green's Function for a Crack Emanating from a Circular Hole in an Infinite Sheet," International Journal of Fracture, Vol. 16, No. 4, 1980.

4. Tweed J. and Rooke, D. P., "The Elastic Problem for an Infinite Solid Containing a Circular Hole with a Pair of Radial Edge Cracks of Different Lengths," International Journal of Engineering Science, Vol. 14, 1976.

5. Isida, M. " On the Determination of Stress-Intensity Factors for Some Common Structural Problems," Engineering Fracture Mechanics, Vol. 2, 1970.

Appendix C—Generic Load/Stress Spectra Development

C1. Introduction

This Appendix describes the procedures used to develop the generic load spectra that are considered to be representative load history for large commercial transport aircraft in service today. The generic spectrum is one of several types of load sequences that are provided for the RAPID users and is recommend to be used for the damage tolerance assessment of the general fuselage skin repair. The steps taken to generate generic stress sequences for the RAPID program are outlined below and shown in figure C1:

a. Obtain dimensions and characteristics of various airplanes, such as the overall length of the airplane, the wing span, the wing area and sweep angle, the operation empty weight (OEW), and the maximum payload.

b. Obtain airplane usage data such as the flight distances, the cruise altitude, the cruise speed, takeoff speed, landing speed, the fuel consumption, and the cabin pressure schedule.

c. Review airplane performances and construct a typical flight profile based on the average usage of the airplane.

d. Obtain statistical data of the aircraft load distribution at the center of gravity for ground operations, flight maneuvers, and airplane gust responses.

e. Create load sequences for the appropriate load environments for each operating stage.

f. Assemble the load sequences from each stage to form a complete flight load sequence. This process is repeated as many times as required to create a block of load sequences.

g. Convert the load sequence to a stress sequence based on the airplane characteristics and the location of the repair.

Two generic load sequences have been created for RAPID, one for narrow-body jets and one for wide-body jets. Each spectrum consists of 6000 unique flights of load sequences in terms of incremental load factors (Δg) at the airplane center of gravity and the differential cabin pressure associated with the flight altitude. The number of flights in the spectrum is one tenth of one design life of a typical narrow-body jet; one design life equals to 60,000 flights.

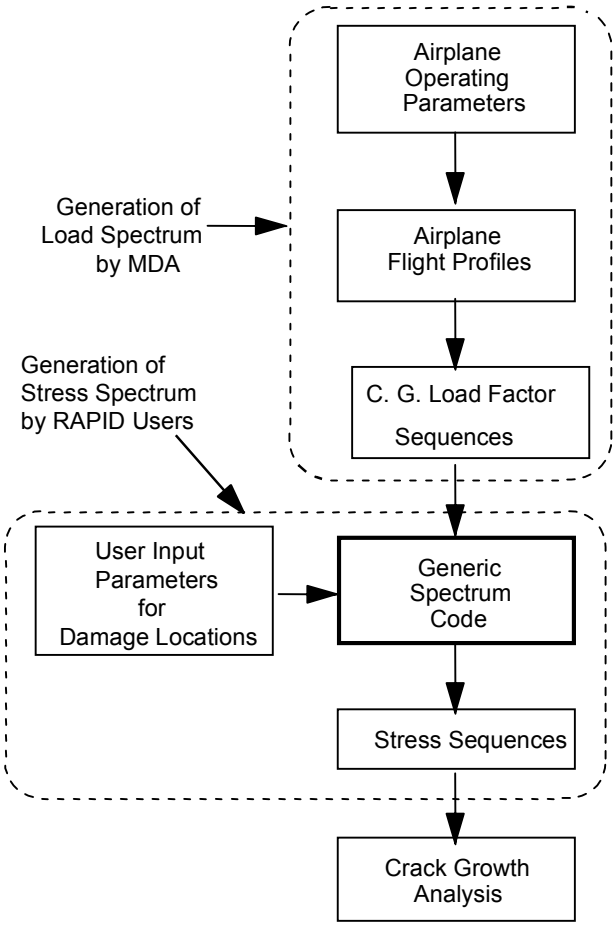

Figure C1. Flow Chart of Generic Stress Sequence Generation

C2. Input Parameter Required

The parameters listed below are required to be input by the RAPID users in order to convert the load sequences into stress sequences for the repair locations. The required parameters are:

a. Airplane type—either wide-body or narrow-body jet
b. Material type
c. Radius of the fuselage
d. Zone number for the repair location as shown in figure C2
e. Length of the zone
f. Distance between the repaired location and the reference point, figure C2
g. Distance between the repair location and the cabin floor
h. Direction of the damage, either longitudinal or transverse

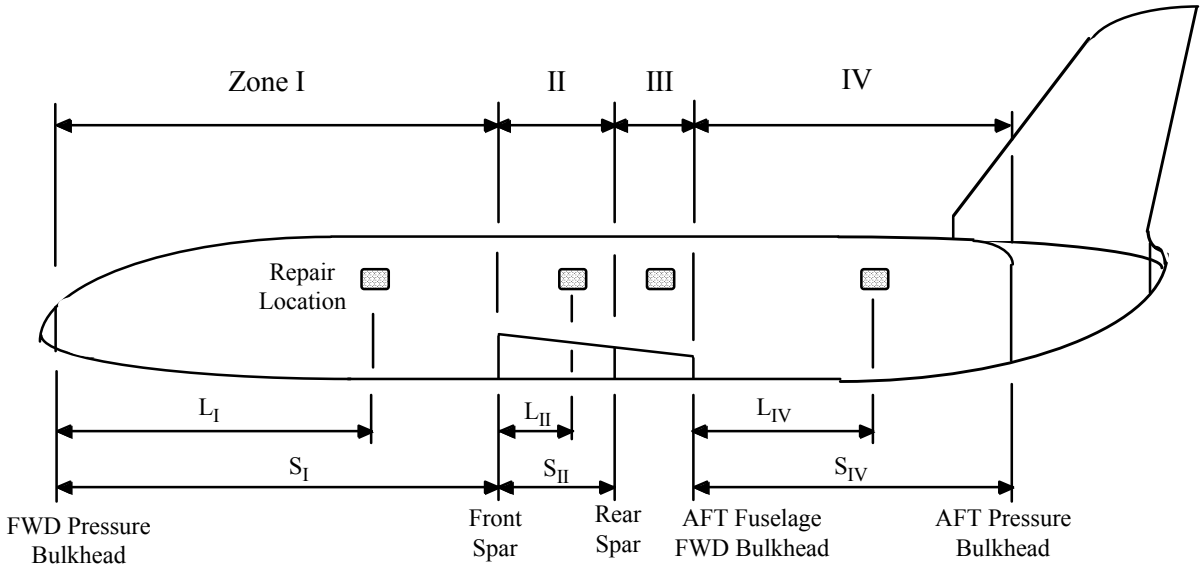

Figure C2. ID Number of Repair Zones

C3. Flight Profile

A typical flight profile of commercial jets can be divided into stages of operation. The time line of the operation stages is shown in figure C3 and the stages used in the RAPID program and the load environments are shown in the table C1.

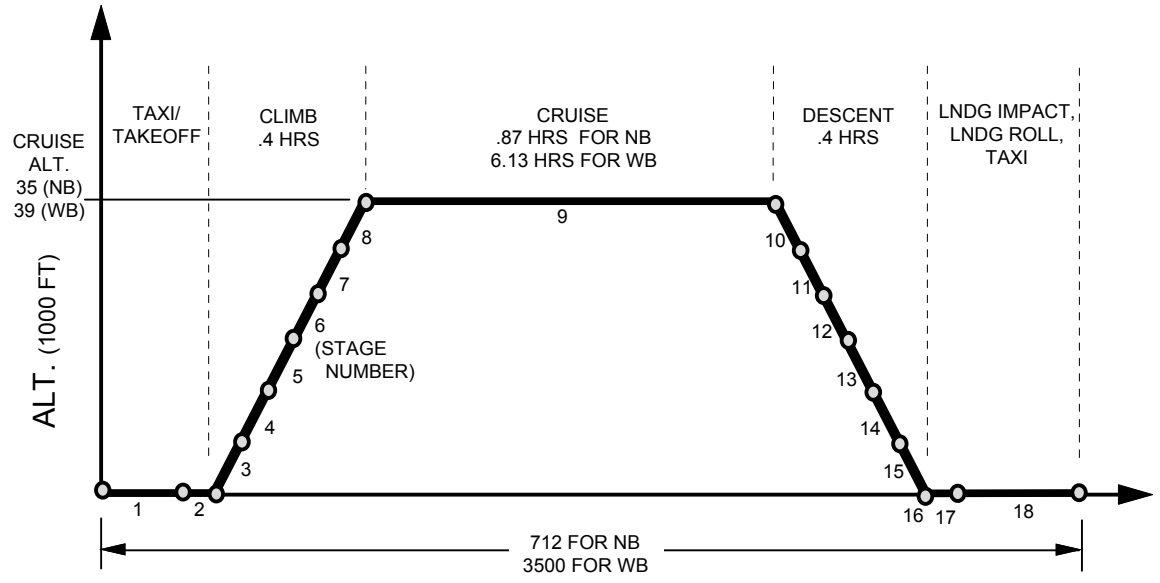

Figure C3. Typical Flight Profile

Table C1.

Stage No	Stage	Load Environment
1	Preflight Taxi	Ground
2	Takeoff Run	Ground
3-8	Climb	Gust and Maneuver
9	Cruise	Gust and Maneuver
10-15	Descent	Gust and Maneuver
16	Landing	Landing Impact
17	Landing Roll	Ground
18	Postflight Taxi	Ground

C3.1 Parameters and Assumptions for Typical Flight Profile

The operation parameters for each stage are estimated based on average airplane usages obtained from published airline reports and magazines [1 and 2], from the manufacturers and assumptions based on engineering experiences. The following basic data and assumptions are used to construct flight profiles.

Average Operation Data Obtained From Publications:

a. Flight distance
b. Operation empty weight (OEW)
c. Maximum payload
d. Payload factor
e. Cruise altitude
f. Fuel consumption rate
g. Reserve fuel weight
h. Takeoff speed
i. Landing speed
j. Cruise speed
k. Wing area

Airplane Characteristics Obtained From Manufacturers:

a. Lift curve slopes
b. Cabin pressure schedule
c. Mean aerodynamic wing cord

Assumptions That Are Used for the Flight Profile:

a. The duration for climb and descent is 0.40 hours each

b. The airplane mach speed increases linearly in proportion to the altitude from the time of takeoff to the beginning of cruise. Similarly, it decreases linearly from cruise to landing during descent.

c. The fuel consumption rate is constant throughout the flight.

C3.2 Formation of Flight Profile

The following steps are coded into a FORTRAN program to create typical flight profiles:

a. Compute average speed for the climbing stages which is linearly interpolated based on the mach speed at takeoff and that at cruise as a function of airplane altitude.

b. Compute average speed for the descending stages which is linearly interpolated based on the mach speed at cruise and that at landing as a function of airplane altitude.

c. Compute the flight distances during the climb and descent stages based on the average speed at each stage.

d. Compute the flight distance during the cruise based on the total flight distance subtracting the distances for climb and descent.

e. Compute the time required for cruise based on the cruise distance and the cruise speed.

f. Compute total flight time based on the time for cruise, climb, and descent.

g. Compute total fuel consumption based on the flight duration and fuel consumption rate.

h. Compute takeoff gross weight which is the sum of fuel consumed, reserved fuel, and airplane OEW.

i. Compute the average payload based on maximum payload multiplied by an average payload factor.

j. Compute the gross weight for each stage based on the takeoff gross weight and fuel consumed up to that stage, i.e., GW= TOW - (Duration)*(Fuel Consumption).

C3.3 Typical Flight Operation Parameters

The following table shows the parameters used to create flight operating profiles for typical narrow-body and wide-body jets respectively. The derivation of these data is discussed in section C3.1 of this appendix.

Table C2. Operation Parameter Profile for Narrow-Body and Wide-Body Jets

Airplane Parameters	Units	Narrow-body Jet	Wide-body Jet
Average Flight Distance	st. miles	712	3500
Operation Empty Weight	lb.	78,500	300,000
Maximum Payload	lb.	44,000	135,000
Typical Payload Factor	none	0.70	0.70
Cruise Altitude	ft.	35,000	39,000
Fuel Consumption Rate	lb./hr	5,600	15,500
Reserve Fuel	lb.	8,500	23,000
Takeoff Speed	mach	.224	.224
Landing Speed	mach	.201	.201
Cruise Speed	mach	.760	.800
Climb Duration	hrs.	.400	.400
Descent Duration	hrs.	.400	.400

Typical flight profile generated from above operation parameters is shown in tables C3 and C4 for narrow-body and wide-body commercial jets respectively.

Table C3. Typical Flight Profile for Narrow-Body Jet

Segment Number	Altitude (1000 Ft.)	Speed Mach No.	Speed Knots	Speed KEAS	Duration (Hours)	Distance (St. Miles)	Gross Wt. (Lbs.)	Fuel Wt. (Lbs.)
1	0	0.0	0.0	0.0	0.0	0.0	0.0	0.0
2	0	0.0	0.0	0.0	0.0	0.0	126690.28	17852.58
3	0-1	0.23166	152.95025	151.83942	0.01143	2.01370	126658.06	17820.37
4	1-5	0.26994	176.68454	169.02179	0.04571	9.30471	126497.01	17659.31
5	5-10	0.33886	218.26106	195.02500	0.05714	14.36781	126207.10	17369.41
6	10-20	0.45371	284.19435	225.47833	0.11429	37.41622	125723.93	16886.24
7	20-30	0.60686	365.29014	244.66520	0.11429	48.09306	125079.71	16242.01
8	30-35	0.72171	420.72739	245.87810	0.05714	27.69588	124596.54	15758.84
9	35	0.76000	438.13194	244.16673	0.86695	437.57307	121991.99	13154.29
10	35-30	0.72007	419.76968	245.31840	0.05714	27.63284	119387.44	10549.74
11	30-20	0.60029	361.33455	242.01581	0.11429	47.57227	118904.27	10066.57
12	20-10	0.44057	257.96202	218.94684	0.11429	36.33237	118260.04	9422.34
13	10-5	0.32079	206.62108	184.62422	0.05714	13.60157	117776.87	8939.17
14	5-1	0.24891	162.92080	155.85498	0.04571	8.57987	117486.97	8649.27
15	1-0	0.20899	137.98157	136.97946	0.01143	1.81663	117325.91	8488.21
16	0	0.0	0.0	0.0	0.0	0.0	117325.91	8488.21
17	0	0.0	0.0	0.0	0.0	0.0	117325.91	8488.21
18	0	0.0	0.0	0.0	0.0	0.0	117325.91	8488.21

Table C4. Typical Flight Profile for Wide-Body Jet

Segment Number	Altitude (1000 Ft.)	Speed Mach No.	Speed Knots	Speed KEAS	Duration (Hours)	Distance (St. Miles)	Gross Wt. (Lbs.)	Fuel Wt. (Lbs.)
1	0	0.0	0.0	0.0	0.0	0.0	0.0	0.0
2	0	0.0	0.0	0.0	0.0	0.0	520303.67	131091.07
3	0-1	0.23138	152.77031	151.66079	0.01026	1.80504	520223.95	131011.35
4	1-5	0.26831	175.61428	167.99795	0.04103	8.29980	519825.33	130612.73
5	5-10	0.33477	215.62799	192.67226	0.05128	12.73864	519107.83	129895.22
6	10-20	0.44554	279.07323	221.41526	0.10256	32.97358	517911.98	128699.38
7	20-30	0.59323	357.08791	239.17148	0.10256	42.19131	516317.52	127104.92
8	30-39	0.73354	423.83110	238.48645	0.09231	45.06955	514802.78	125590.18
9	39	0.80000	458.79201	233.57639	6.13247	3241.18270	466417.64	77205.03
10	39-30	0.73088	422.29774	237.62364	0.09231	44.90649	418032.49	28819.89
11	30-20	0.58497	352.11807	235.84277	0.10256	41.60410	416517.75	27305.15
12	20-10	0.43138	270.20765	214.38135	0.10256	31.92607	414923.29	25710.69
13	10-5	0.31619	203.66242	181.98054	0.05128	12.03175	413727.45	24514.85
14	5-1	0.24708	161.71820	154.70453	0.04103	7.64305	413009.94	23797.34
15	1-0	0.20868	137.77939	136.77874	0.01026	1.62792	412611.32	23398.72
16	0	0.0	0.0	0.0	0.0	0.0	412611.32	23398.72
17	0	0.0	0.0	0.0	0.0	0.0	412611.32	23398.72
18	0	0.0	0.0	0.0	0.0	0.0	412611.32	23398.72

C4. Load Spectrum for Airplane Center-of-Gravity

This section describes the creation of load sequences for the airplane accelerations at its center of gravity.

C4.1 Load Environments

The load environments which may contribute to the crack growth of repairs on the fuselage skin include the following:

a. Inflight maneuver operations during cruise, climb and descent

b. Ground operations such as preflight taxi, postflight taxi, takeoff run, landing roll, and landing impact

c. Gust loads due to air turbulence

d. Cabin pressure

The frequency distribution of the accelerations that the airplane may experience at the center of gravity can be expressed in tabulated forms such as the load exceedance tables or in equations, such as in the airplane gust responses. The details of the acceleration exceedances for each load environment are described in the following sections.

C4.1.1 Maneuver

The distributions of airplane acceleration during climb, descent, and cruise maneuver operations are shown in table C5 for 1,000 hours of operation. They are derived from references 3 and 4 which are based on the distribution of c. g. acceleration measurements of more than 3600 hours of normal airline operations. The calculation of the c. g. acceleration distribution for cruise and climb/descent are shown in tables C6 and C7 and plotted in figures C4 and C5 respectively. The derivation of the exceedance distribution, using table C6 as an example, is outlined as follows :

a. Obtain the occurrence of airplane c.g. acceleration and corresponding flight hours from references 3 and 4 for applicable airplanes. See columns 1 through 5 in table C6.

b. Sum up the occurrence and flight hours for various airplanes. Add occurrences in columns 2 through 5 to obtain total occurrences as shown in column 6.

c. Obtain exceedance distribution by summing up the occurrences. See column 7.

d. Normalize the exceedance distribution to 1,000 flight hours from 3696.5 hours. See column 8.

Table C5. Maneuver Load Exceedances per 1,000 Flight Hours

Incremental C.G. Accel. (Δg)	Climb/Descent	Cruise
1.0	0.000	0.000
0.9	0.616	0.000
0.8	1.232	0.000
0.7	3.695	0.271
0.6	11.08	0.812
0.5	49.26	5.411
0.4	207.5	16.77
0.3	941.5	68.98
0.2	4385.	417.2
0.1	23157	4357
-0.1	16671.0	4343
-0.2	1696.0	291.6
-0.3	233.4	31.65
-0.4	39.41	5.952
-0.5	5.54	0.541
-0.6	0.0	0.271
-0.7	0.0	0.000

Table C6. Incremental C. G. Load Exceedances for Cruise

ΔG	Airplane Types (1) A-1	A-2	B-1	Airplane Operation (2)	Total Occurrence	Exceedances	Normalized Exceedances
-0.9 to -1.0					0	0	**0.00**
-0.8 to –0.9					0	0	**0.00**
-0.7 to –0.8					0	0	**0.00**
-0.6 to –0.7		1			1	1	**0.27**
-0.5 to –0.6		1			1	2	**0.54**
-0.4 to –0.5	4	14		2	20	22	**5.95**
-0.3 to –0.4	43	34	15	3	95	117	**31.65**
-0.2 to –0.3	236	455	197	73	961	1078	**291.63**
-0.1 to –0.2	5273	5126	3221	1357	14977	16055	**4343.30**
0.1 to 0.2	5253	4642	3334	1336	14565	16107	**4357.37**
0.2 to 0.3	352	477	362	96	1287	1542	**417.15**
0.3 to 0.4	81	59	40	13	193	255	**68.98**
0.4 to 0.5	16	10	12	4	42	62	**16.77**
0.5 to 0.6	5	7	3	2	17	20	**5.41**
0.6 to 0.7	1	1			2	3	**0.81**
0.7 to 0.8		1			1	1	**0.27**
0.8 to 0.9					0	0	**0.00**
0.9 to 1.					0	0	**0.00**
Flight Hours	**704.4**	**887.9**	**1167.7**	**936.5**	**3696.5**	3696.5	**1000.00**

Notes: (1) Reference : NASA TN D-4330, Table IV , Page 19
(2) Reference : NASA TN D-1801, Table II, Page 4

Table C7. Incremental C. G. Load Exceedances for Climb/Descent

	Climb			Descent			Climb	Descent			
	Airplane Types (1)						Airplane		Total		Normalized
ΔG	A-1	A-2	B-1	A-1	A-2	B-1	Operations (2)		Occur.	Exceedances	Exceedances
-0.9 to -1.0									**0**	0	**0.0**
-0.8 to –0.9									**0**	0	**0.0**
-0.7 to –0.8									**0**	0	**0.0**
-0.6 to –0.7									**0**	0	**0.0**
-0.5 to –0.6	3	2	2	1	1				**9**	9	**5.54**
-0.4 to –0.5	26	11	8	3	2	1	2	2	**55**	64	**39.41**
-0.3 to –0.4	100	66	52	15	35	19	21	7	**315**	379	**233.4**
-0.2 to –0.3	575	401	282	318	361	188	148	103	**2376**	2755	**1696**
-0.1 to –0.2	4301	2671	2666	4823	3767	2874	1288	1928	**24318**	27073	**16671**
0.1 to 0.2	4645	3276	3319	6004	5186	3944	1477	2633	**30484**	37605	**23157**
0.2 to 0.3	965	698	689	923	882	699	311	425	**5592**	7121	**4385**
0.3 to 0.4	212	179	182	163	200	145	55	56	**1192**	1529	**941.5**
0.4 to 0.5	73	44	34	35	39	20	5	7	**257**	337	**207.5**
0.5 to 0.6	17	14	6	6	13	6			**62**	80	**49.26**
0.6 to 0.7	3	2	2	2	2	1			**12**	18	**11.08**
0.7 to 0.8	1	1			1	1			**4**	6	**3.695**
0.8 to 0.9	0	1							**1**	2	**1.232**
0.9 to 1.	1								**1**	1	**0.616**
Flight Hours	**160.1**	**187.3**	**218**	**243.2**	**281**	**266**	**113.15**	**155.2**	**1624**	**1624**	**1000.00**

Notes: (1) Reference : NASA TN D-4330, Table IV , Page 19
(2) Reference : NASA TN D-1801, Table II, Page 4

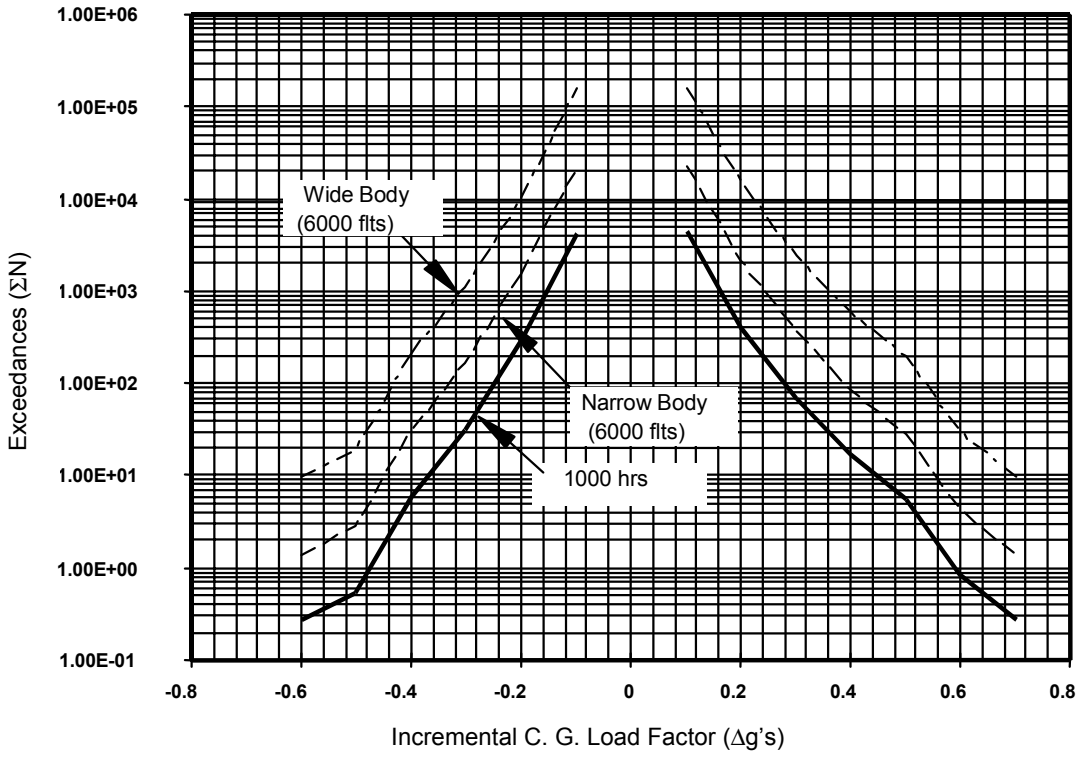

Figure C4. Incremental C. G. Exceedances for Cruise

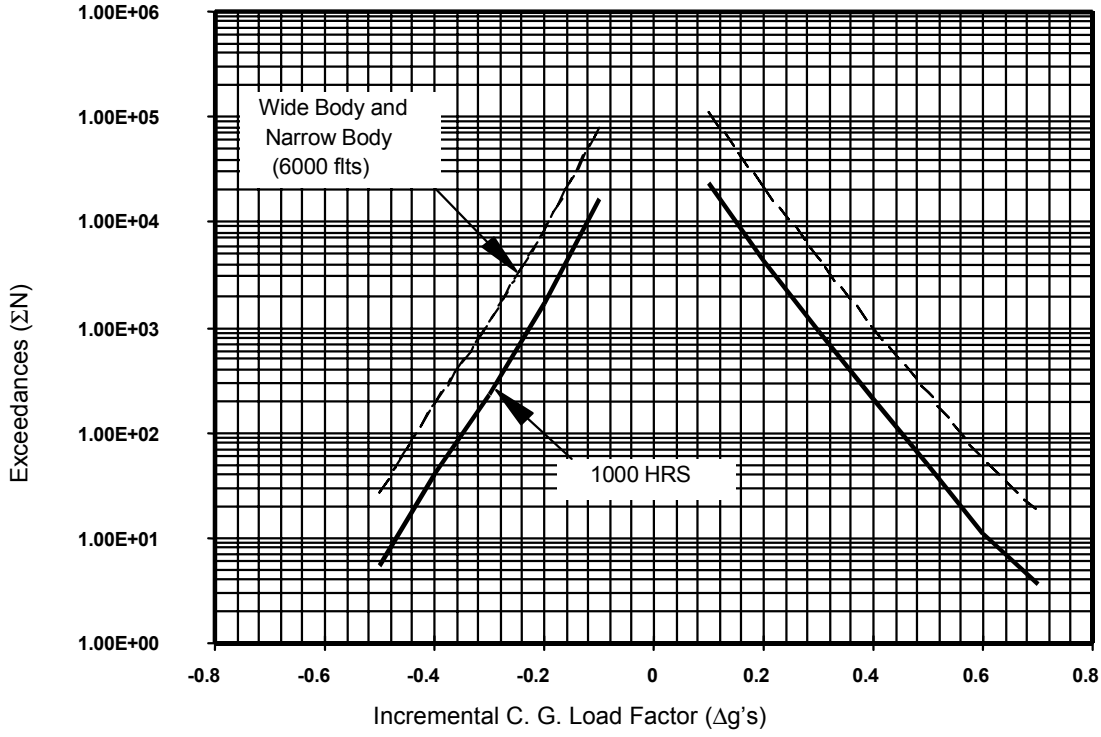

Figure C5. Incremental C. G. Exceedances for Climb/Descent

C4.1.2 Taxi

The distributions of airplane acceleration during ground operations are shown in the tables C8 through C11 for 1,000 flight operations. They are derived from reference 5 which are based on the c. g. acceleration measurements on more than 3000 flights of normal airline operations. The calculations of the distributions of c. g. acceleration for ground operations are shown in table C12 through 15 and plotted in figure C6 through C9 respectively. All load excursions are considered to be fully reversible. The derivation of the exceedance distribution, using table C12 as an example, is outlined as follows :

a. Obtain the occurrence of airplane c.g. acceleration and corresponding flight hours from reference 5. See columns 1 through 6 in table C12.

b. Sum up the occurrence and number of flights for various airplanes. Add occurrences in columns 2 through 6 to obtain total occurrences as shown in column 7.

c. Obtain exceedance distribution by summing up the occurrences. See column 8.

d. Normalize the exceedance distribution to 1,000 flights from 3611 flights. See column 9.

e. Obtain the exceedance distribution based on the average of positive and negative accelerations. See column 10.

Table C8. C. G. Exceedances per 1,000 Preflight Taxi Operations

Incremental C.G. Acceleration (±Δg)	Exceedance
0.1	11420.2
0.2	322.9
0.3	25.1
0.4	2.77
0.5	0.55
0.6	0.14
0.7	0.00

Table C9. C. G. Exceedances per 1,000 Postflight Taxi Operations

Incremental C.G. Acceleration (±Δg)	Exceedance
0.1	9008.2
0.2	239.5
0.3	18.8
0.4	2.39
0.5	0.30
0.6	0.00

Table C10. C. G. Exceedances per 1,000 Takeoff Operations

Incremental C.G. Acceleration (±Δg)	Exceedance
0.1	9842.2
0.2	1116.9
0.3	85.2
0.4	12.5
0.5	1.99
0.6	0.00

Table C11. C. G. Exceedances per 1,000 Landing Rolls

Incremental C.G. Acceleration (±Δg)	Exceedance
0.1	21629.7
0.2	4293.6
0.3	430.1
0.4	60.8
0.5	13.1
0.6	3.30
0.7	1.72
0.8	0.00

Table C12. Incremental C. G. Load Exceedances for Preflight Taxi per 1000 Flights

	Airplane Operations					Total		Normalized	
ΔG	**EIC**	**KID**	**EIIC**	**IIIIA**	**SXIIIA**	**Occurrence**	**Exceedances**	**Exceedances**	
-0.7 to –0.8						**0**	0	**0.00**	
-0.6 to –0.7						**0**	0	**0.00**	
-0.5 to –0.6						**0**	0	**0.00**	
-0.4 to –0.5					7	**7**	7	**1.94**	
-0.3 to –0.4	2		3	1	34	**40**	47	**13.02**	
-0.2 to –0.3	203	37	83	49	542	**914**	961	**266.13**	
-0.1 to -0.2	--	--	9180	--	--	**39091 (*)**	40052	**11091.60**	
0 to -0.1									**Average**
0 to 0.1									**Normalized Exceedances**
0.1 to 0.2	--	--	9641	--	--	**41054 (*)**	42425	**11748.78**	**11420.19**
0.2 to 0.3	274	48	324	85	506	**1237**	1371	**379.67**	**322.90**
0.3 to 0.4	11		51	3	56	**121**	134	**37.11**	**25.06**
0.4 to 0.5			2	1	6	**9**	13	**3.60**	**2.77**
0.5 to 0.6					3	**3**	4	**1.11**	**0.55**
0.6 to 0.7					1	**1**	1	**0.28**	**0.14**
0.7 to 0.8						**0**	0	**0.00**	**0.00**
Number of Flights	645	751	848	662	705	**3611**			

Reference : NASA TN D-6124, Table IV (a) through (g)

(*) Occurrence is factored from the occurrence of EIIC using the formula below due to lack of data for other operations

$\mathbf{OCC_{total}=OCC_{EIIC}*(FLT_{total}/FLT_{EIIC})}$

OCC : Occurrence at the load level

FLT : Number of Flights

Table C13. Incremental C. G. Load Exceedances for Takeoff Run per 1000 Flights

	Airplane Operations					Total		Normalized	
ΔG	**EIC**	**KID**	**EIIC**	**IIIIA**	**SXIIIA**	**Occurrence**	**Exceedances**	**Exceedances**	
-0.7 to -0.8						**0**	0	0.00	
-0.6 to –0.7						**0**	0	0.00	
-0.5 to –0.6	5		1		1	**7**	7	1.99	
-0.4 to –0.5	18	4	2	3	18	**45**	52	14.76	
-0.3 to –0.4	96	19	16	54	51	**236**	288	81.75	
-0.2 to –0.3	1095	411	256	664	1018	**3444**	3732	1059.32	
-0.1 to -0.2	--	--	7694	--	--	**32385 (*)**	36117	10251.68	
0 to -0.1									**Average Normalized Exceedances**
0 to 0.1									
0.1 to 0.2	--	--	6912	--	--	**29093 (*)**	33231	9432.63	**9842.2**
0.2 to 0.3	1393	456	313	732	932	**3826**	4138	1174.57	**1116.9**
0.3 to 0.4	110	30	23	29	84	**276**	312	88.56	**85.2**
0.4 to 0.5	16		1	3	9	**29**	36	10.22	**12.5**
0.5 to 0.6	7					**7**	7	1.99	**1.99**
0.6 to 0.7						**0**	0	0.00	**0.00**
0.7 to 0.8						**0**	0	0.00	**0.00**
Number of Flights	561	750	837	670	705	**3523**			

Reference : NASA TN D-6124, Table IV (a) through (g)

(*) Occurrence is factored from the occurrence of EIIC using the formula below due to lack of data for other operations

$\mathbf{OCC_{total}=OCC_{EIIC}*(FLT_{total}/FLT_{EIIC})}$

OCC : Occurrence at the load level

FLT : Number of Flights

Table C14. Incremental C. G. Load Exceedances for Postflight Taxi per 1000 Flights

	Airplane Operations					Total		Normalized	
ΔG	**EIC**	**KID**	**EIIC**	**IIIIA**	**SXIIIA**	**Occurrence**	**Exceedances**	**Exceedances**	
-0.7 to -0.8						**0**	0.0	0.00	
-0.6 to -0.7						**0**	0.0	0.00	
-0.5 to -0.6						**0**	0.0	0.00	
-0.4 to -0.5					7	**7**	7.0	2.09	
-0.3 to -0.4	4	1	3		20	**28**	35.0	10.46	
-0.2 to -0.3	90	99	97	38	346	**670**	705.0	210.64	
-0.1 to -0.2	--	--	7125	--	--	**28356 (*)**	29061.0	8682.69	
0 to -0.1									**Average Normalized Exceedances**
0 to 0.1									
0.1 to 0.2	--	--	7624	--	--	**30342 (*)**	31239.89	9333.70	**9008.2**
0.2 to 0.3	91	108	238	39	331	**807**	898.00	268.30	**239.5**
0.3 to 0.4	6	14	28	3	31	**82**	91.00	27.19	**18.8**
0.4 to 0.5			2		5	**7**	9.00	2.69	**2.39**
0.5 to 0.6					2	**2**	2.00	0.60	**0.30**
0.6 to 0.7						**0**	0.00	0.00	**0.00**
0.7 to 0.8						**0**	0.00	0.00	**0.00**
Number of Flights	558	724	841	519	705	**3347**			

Reference : NASA TN D-6124, Table IV (a) through (g)

(*) Occurrence is factored from the occurrence of EIIC using the formula below due to lack of data for other operations

$\mathbf{OCC_{total}=OCC_{EIIC}*(FLT_{total}/FLT_{EIIC})}$

OCC : Occurrence at the load level

FLT : Number of Flights

Table C15. Incremental C. G. Load Exceedances for Landing Roll per 1000 Flights

	Airplane Operations					Total		Normalized	
ΔG	**EIC**	**KID**	**EIIC**	**IIIIA**	**SXIIIA**	**Occurrence**	**Exceedances**	**Excd**	
-0.7 to -0.8			9			**9**	9.0	2.58	
-0.6 to -0.7			5			**5**	14.0	4.02	
-0.5 to -0.6	3	2	16	4	1	**26**	40.0	11.48	
-0.4 to -0.5	24	13	42	38	7	**124**	164.0	47.07	
-0.3 to -0.4	423	232	199	254	111	**1219**	1383.0	396.96	
-0.2 to -0.3	3942	4262	1586	2022	2475	**14287**	15670.0	4497.70	
-0.1 to -0.2	--	--	14619	--	--	**63507 (*)**	79177.0	22725.88	
0 to -0.1									**Average**
0 to 0.1									**Normz. Excd**
0.1 to 0.2	--	--	13188	--	--	**57291 (*)**	71538.51	20533.44	**21629.7**
0.2 to 0.3	3717	3624	1787	1524	1982	**12634**	14248.00	4089.55	**4293.6**
0.3 to 0.4	304	298	375	230	147	**1354**	1614.00	463.26	**430.1**
0.4 to 0.5	28	43	73	59	6	**209**	260.00	74.63	**60.85**
0.5 to 0.6	6	6	19	8	3	**42**	51.00	14.64	**13.06**
0.6 to 0.7			6			**6**	9.00	2.58	**3.30**
0.7 to 0.8			3			**3**	3.00	0.86	**1.72**
Number of Flights	558	752	802	667	705	**3484**			

Reference : NASA TN D-6124, Table IV (a) through (g)

(*) Occurrence is factored from the occurrence of EIIC using the formula below due to lack of data for other operations

$OCC_{total}=OCC_{EIIC}*(FLT_{total}/FLT_{EIIC})$

OCC : Occurrence at the load level

FLT : Number of Flights

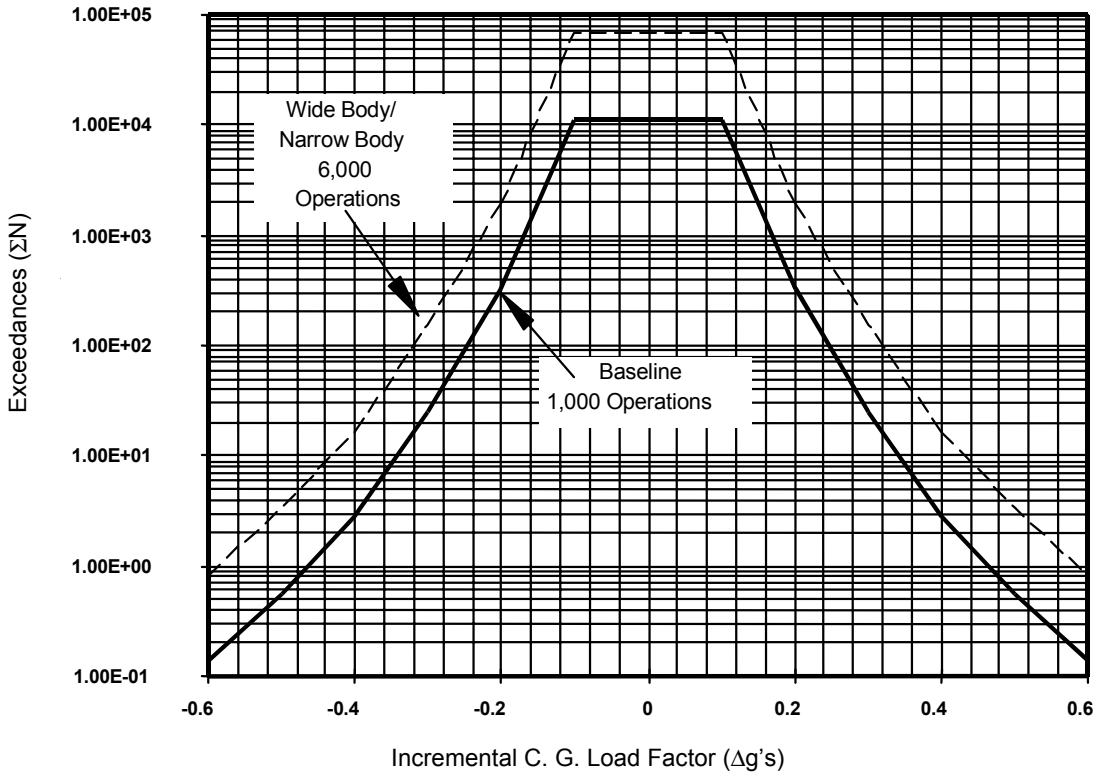

Figure C6. Incremental C. G. Exceedances for Preflight Taxi

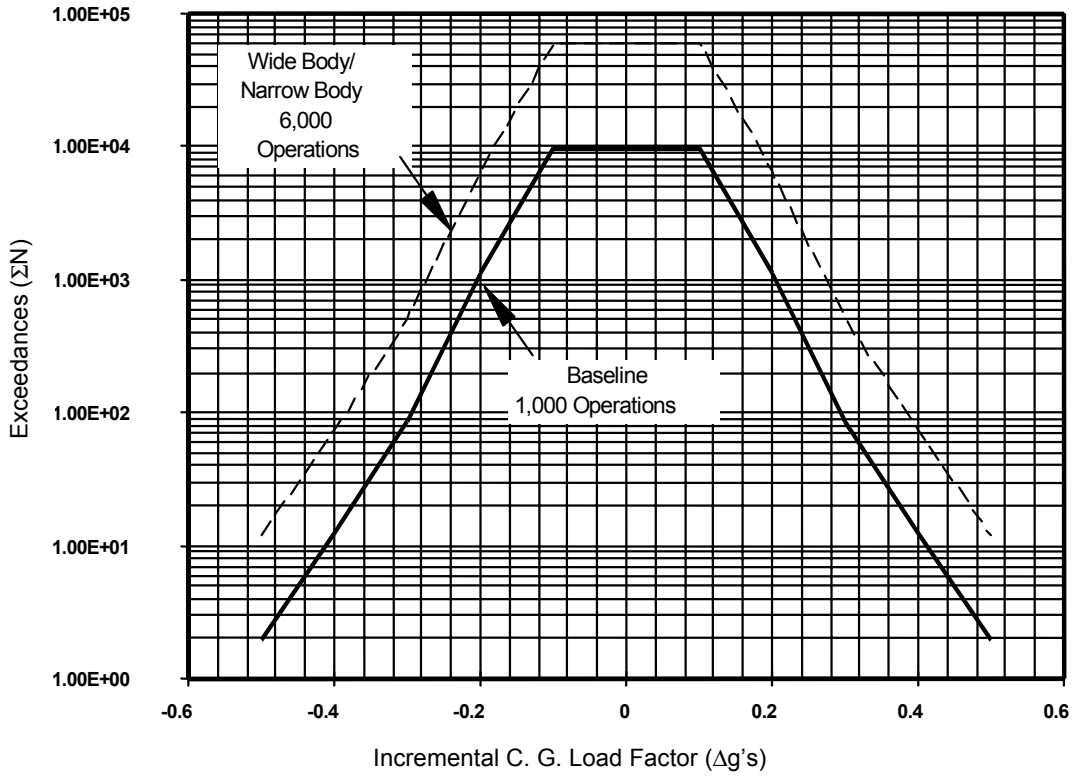

Figure C7. Incremental C. G. Exceedances for Takeoff Runs

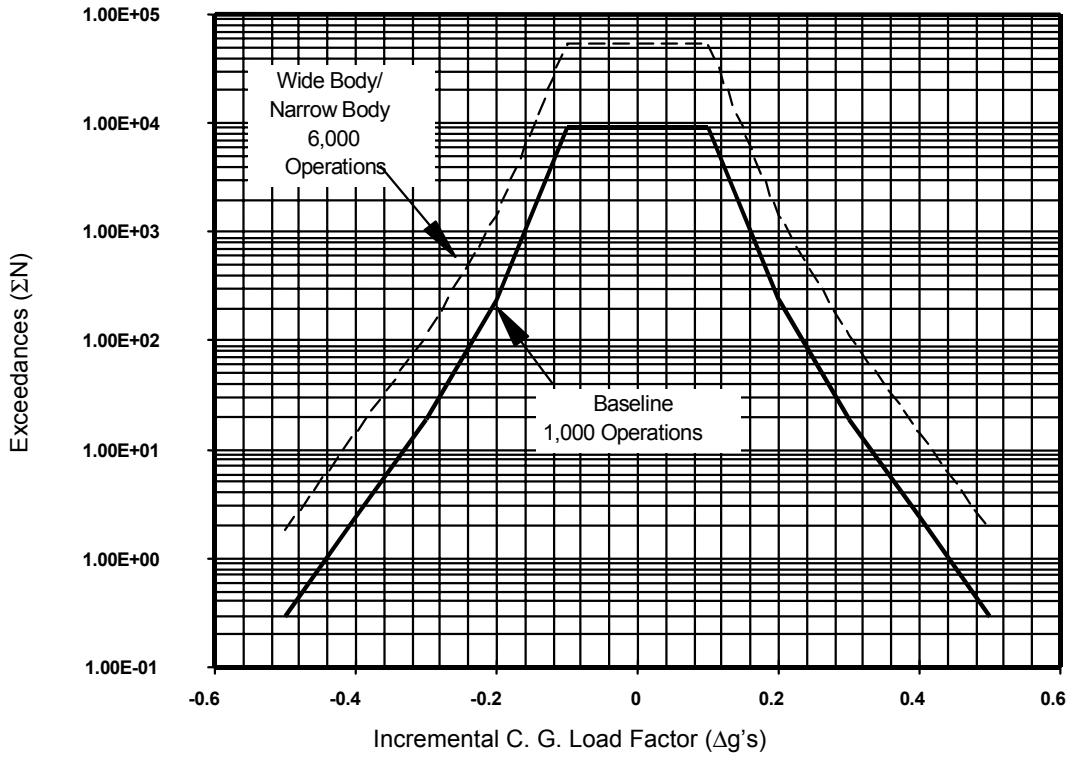

Figure C8. Incremental C. G. Exceedances for Postflight Taxi

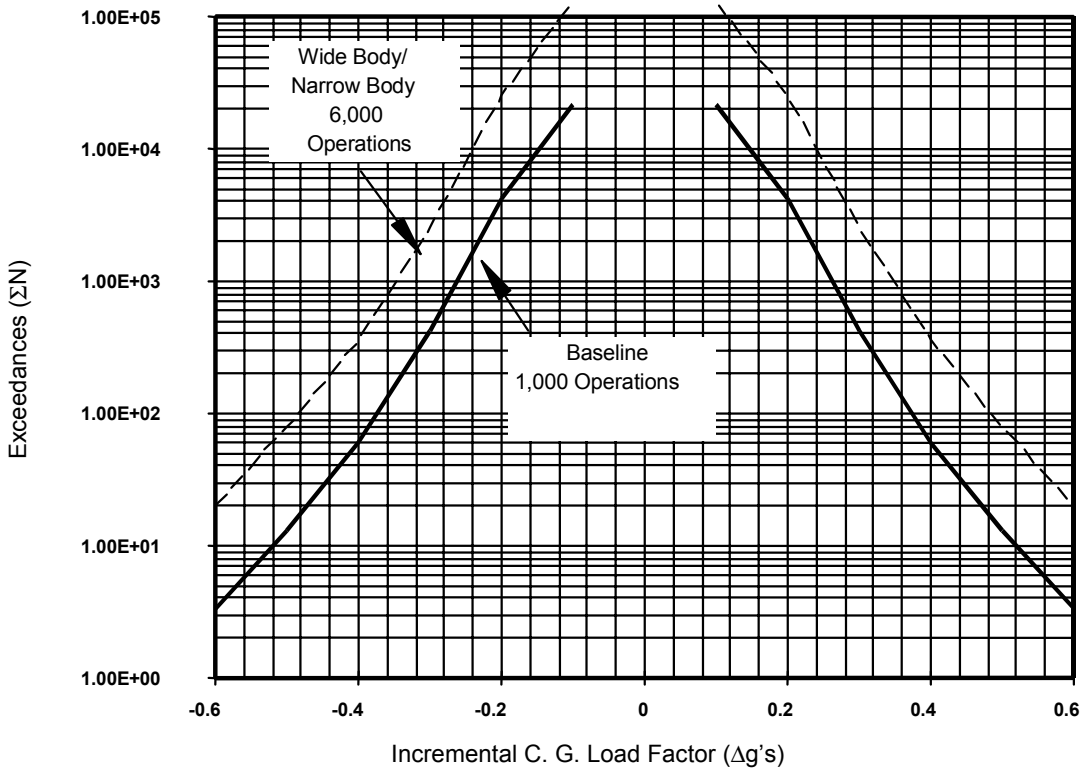

Figure C9. Incremental C. G. Exceedances for landing Roll

C4.1.3 Landing Impact

The distributions of airplane accelerations during landing impacts are derived from reference 5 and are based on a survey of 29 airplanes from 19 airlines for a total of 16913 landings. The frequency distributions during landing impact are shown in the table C16 for 10,000 flight operations. The calculation of the distribution of c. g. acceleration is shown in table C17 and plotted in figure C10. All load excursions are considered to be fully reversible. The derivation of the exceedance distribution, using table C19as an example, is outlined as follows :

a. Obtain the occurrence of airplane c.g. acceleration and corresponding number of flights from reference 5. See column 1 through 20 in table C10.

b. Sum up the occurrences and number of flights for various airplanes. Add occurrences in columns 2 through 20 to obtain total occurrences as shown in column 21.

c. Obtain exceedance distribution by summing up the occurrences. See column 22.

d. Normalize the exceedance distribution to 10,000 flights from 16913 flights. See column 23.

Table C16. Incremental C. G. Load Exceedances for Landing Impact, 10,000 Landings

Incremental C.G. Acceleration (±Δg)	Exceedance
0.0	10,000.0
0.1	9,742.8
0.2	7,468.8
0.3	4,120.5
0.4	1,899.1
0.5	774.0
0.6	295.6
0.7	131.3
0.8	56.8
0.9	23.7
1.0	9.5
1.1	5.9
1.2	3.5
1.3	1.2
1.4	0.59
1.5	0.59
1.6	0.59
1.7	0.59
1.8	0.59
1.9	0.00

Table C17. Incremental C. G. Load Exceedances for Landing Impact, per 10,000 Landings

	Airplane Operations																					
ΔG	**EIA**	**AIA F**	**EIC**	**AIC F**	**KID**	**GII A/B**	**CII B**	**EII C**	**HII C**	**LII C**	**IIII A**	**AVI ILA**	**GVI IIB**	**AIX A**	**UIX A**	**XIX A**	**SXII IA**	**IXI VA**	**JXI VB**	**Occur. for 16913 Landings**	**Excd. for 16913 Landings**	**Excd. for 10,000 Landings**
0 to 0.1	36	25	13	43	5	29	35	35	13	11	26	10	62	40	5	36	6	0	5	**435**	**16913**	**10000.0**
0.1 to 0.2	189	168	179	179	87	236	273	195	150	176	304	218	407	363	113	275	218	28	88	**3846**	**16478**	**9742.8**
0.2 to 0.3	242	245	219	141	203	300	430	213	216	360	456	484	367	427	330	291	438	151	150	**5663**	**12632**	**7468.8**
0.3 to 0.4	162	121	110	114	135	172	398	138	178	231	244	367	185	169	242	144	263	202	182	**3757**	**6969**	**4120.5**
0.4 to 0.5	103	55	38	38	91	126	219	55	101	174	115	216	66	59	65	42	86	109	145	**1903**	**3212**	**1899.1**
0.5 to 0.6	44	26	11	25	44	44	93	28	36	64	40	116	22	21	37	21	23	43	71	**809**	**1309**	**774.0**
0.6 to 0.7	22	4	3	11	8	11	32	14	12	12	12	45	7	8	8	7	5	15	42	**278**	**500**	**295.6**
0.7 to 0.8	6	4		1	2	3	24	7	8	3	4	28	4	2	6	0	4	6	14	**126**	**222**	**131.3**
0.8 to 0.9	2			2	2	1	5	2	8	4	3	13	2	0	1	1		2	8	**56**	**96**	**56.8**
0.9 to 1.0	3			1	4	1	2				1	5		1	3				3	**24**	**40**	**23.7**
1.0 to 1.1				0	0	1	0				1	1			0				3	**6**	**16**	**9.5**
1.1 to 1.2				1	1		0				0	1			0				1	**4**	**10**	**5.9**
1.2 to 1.3							0				1				1				2	**4**	**6**	**3.5**
1.3 to 1.4							0												1	**1**	**2**	**1.2**
1.4 to 1.5							0													**0**	**1**	**.59**
1.5 to 1.6							0													**0**	**1**	**.59**
1.6 to 1.7							0													**0**	**1**	**.59**
1.7 to 1.8							0													**0**	**1**	**.59**
1.8 to 1.9							1													**1**	**1**	**.59**
Total	809	648	573	556	582	924	1512	687	722	1035	1207	1504	1122	1090	811	817	1043	556	715	**16913**		

Reference : NASA TN D-6124, Page 14, Table III - Frequency distribution of landing Impact

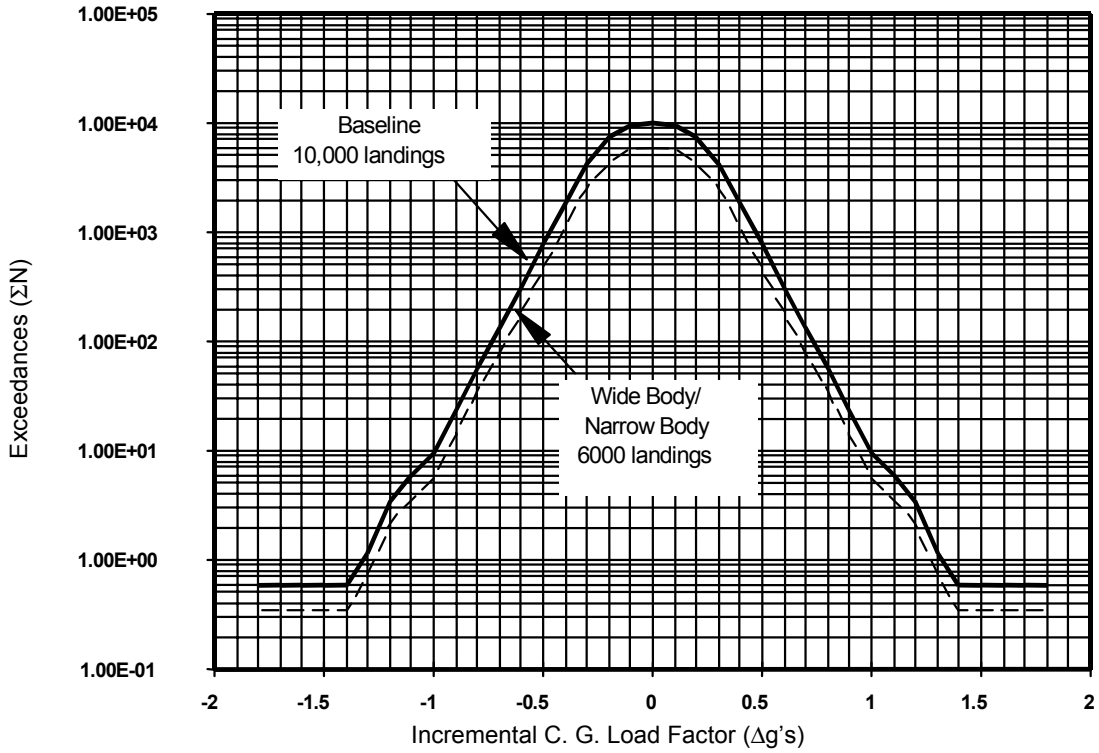

Figure C10. Incremental C. G. Exceedances for landing Impact

C4.1.4 Gust

The airplane responses due to both vertical and lateral gusts have been investigated. The most severe load occurs once per 6000 flights due to lateral gust and is less than 0.15g which is a negligible contribution to the crack growth. Therefore, only the vertical gusts are considered in the RAPID spectrum. The load exceedances due to gust, based on the continuous gust PSD approach, can be expressed in the equation below:

$$\Sigma(\Delta g) = \left(10.0 P_1 e^{-\Delta g / b_1 \bar{A}} + 7.5 P_2 e^{-\Delta g / b_2 \bar{A}} \right) T$$

where

Δg = the incremental load factor responses

P's, b's = the proportion of time spent in turbulence and the turbulence intensity, respectively. These values are defined in reference 6. The tabular form is shown on table C18.

T = the flight distances in statute miles.

10.0, 7.5 = the average number of gust cycles per second for storm and non-storm turbulence [6].

$\bar{A}$ = the ratio of RMS of Δg to RMS of gust velocity, and can be calculated as follows [6]

$$\bar{A} = \left(V_e mS / 498W\right) K_{\sigma u}$$

where

V_e = Equivalent airspeed, knots

m = Lift curve slope, per radian

S = Wing area, ft^2

W = Airplane gross weight, lbs

$K_{\sigma u}$ = Gust alleviation factor as specified in reference 6, the tabular form is shown on table C19

$$k_{\sigma u} = \left[4u_g \Big/ \left(4u_g + 2\pi/m\right) \right] \sqrt{I\left[\left(4u_g + \left(2\pi/m\right)\right),\ \left(L/c\right)\right] / \pi}$$

u_g = Mass parameter equals to $2W / \rho \bar{c} mgS$

ρ = Air density, $slug/ft^3$

$\bar{c}$ = Mean aerodynamic wing chord, ft

L = Scale of turbulence, ft

g = gravitational acceleration, ft/sec^2

Table C18. P's and b's Values

Altitude ft x 10^{-3}	P1	P2	b1	b2	L
0 - 1	1.0	0.0100	2.70	5.40	500
1.0 - 2.5	0.70	0.0075	2.70	5.91	750
2.5 - 5.0	0.48	0.0050	2.70	6.79	930
5.0 - 10	0.25	0.00210	2.70	7.30	1000
10 - 20	0.09	0.00055	2.27	7.30	1000
20 - 30	0.04	0.00023	1.84	6.93	1000
30 - 40	0.017	0.00020	1.46	4.89	1000
40 - 50	0.007	0.00025	1.35	3.58	1000
50 - 60	0.0031	0.00016	1.30	2.33	1000
60 - 70	0.0014	0.00012	0.81	1.24	1000

Table C19. Gust Alleviation Factor

$x = L / \bar{c}$ and $y = 4u_g + (2\pi / m)$

values are (Anti log $\sqrt{I(y,x) / \pi}$)

x\y	10	20	30	40	50	70	100	150	300	500	1000
6	2.954	3.800	4.220	4.460	4.680	5.012	5.346	5.624	6.026	6.096	6.166
10	2.690	3.590	4.075	4.360	4.630	5.065	5.520	6.026	6.457	6.684	6.839
14	2.515	3.310	3.800	4.140	4.360	4.900	5.500	6.050	6.746	6.919	7.145
18	2.295	3.020	3.510	3.800	4.150	4.670	5.370	6.030	6.903	7.228	7.413
22	2.162	2.820	3.315	3.635	3.980	4.460	5.140	5.890	6.919	7.328	7.586
30	1.972	2.514	2.950	3.275	3.550	4.070	4.670	5.630	6.839	7.345	7.727
40	1.820	2.190	2.632	2.884	3.160	3.630	4.260	5.140	6.607	7.245	7.763
60	1.622	1.884	2.190	2.510	2.755	3.160	3.720	4.520	5.950	6.887	7.586
80	1.514	1.719	1.998	2.290	2.483	2.850	3.350	4.070	5.370	6.457	7.379
100	1.413	1.597	1.820	2.020	2.240	2.630	3.020	3.645	4.900	5.950	7.079
120	1.349	1.480	1.680	1.862	2.090	2.400	2.755	3.390	4.560	5.630	6.808
140	1.289	1.413	1.604	1.740	1.950	2.240	2.632	3.125	4.260	5.250	6.562
160	1.259	1.350	1.513	1.700	1.862	2.090	2.514	2.920	4.070	5.010	6.309
180	1.231	1.303	1.446	1.640	1.780	1.995	2.345	2.758	3.800	4.740	6.030
240	1.162	1.202	1.319	1.480	1.620	1.800	2.090	2.458	3.315	4.160	5.310

C4.1.5 Differential Cabin Pressure

The differential cabin pressure, ΔP, is defined as the difference between the cabin pressure, P_{cabin}, and the atmospheric pressure, P_{atm}, thus $\Delta P = P_{cabin} - P_{atm}$. The cabin pressure is generally expressed as cabin pressure altitude, H_{cabin}, and is limited to 8000 feet under normal operating conditions set forth in FAR 25.841. The atmospheric pressure for any altitude is obtained from the Standard Atmosphere table published by ICAO, International Civil Aviation Organization, [7]. For the generic load spectrum development, it is assumed that H_{cabin} is a function of the airplane altitude, H_{plane}, which varies from 0 at takeoff to a maximum cruise altitude in a parabolic function as shown below:

$$H_{cabin} = C_p \times (H_{plane})^n$$

where

H_{cabin} = Cabin pressure altitude in feet

H_{plane} : = Airplane altitude in feet

n = Cabin pressurization factor, n=1.6 produces good agreement with the MD-80's pressure schedule [8].

C_p = Constant which produces a maximum differential pressure of 7.78 psi for narrow body and 9.00 psi for wide body aircraft, respectively

The equation for the cabin pressure altitude is illustrated in figure 11.

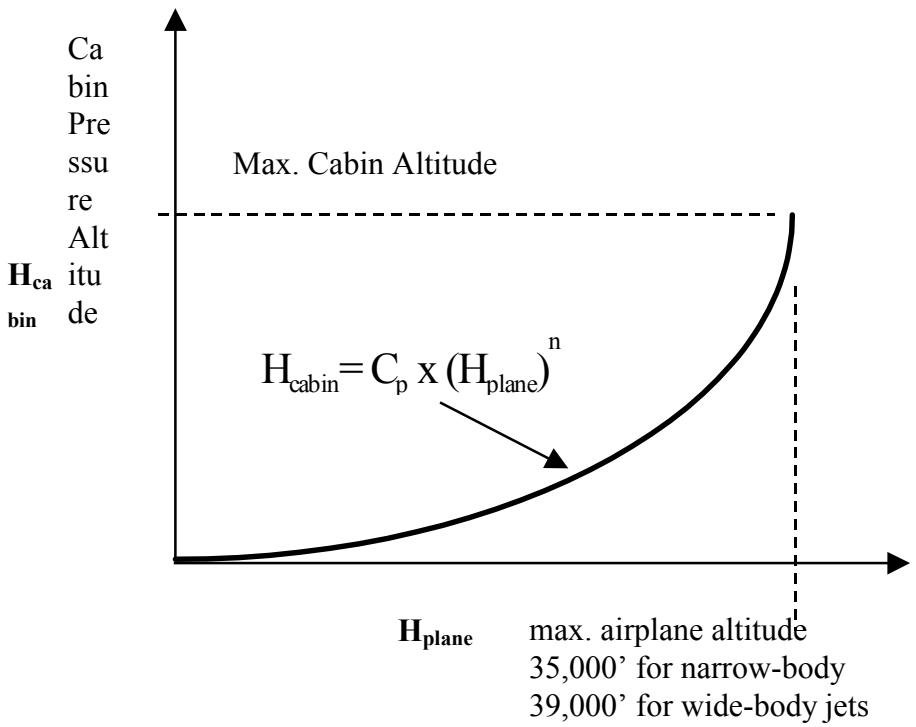

Figure 11. Illustration of the Equation for Cabin Pressure Altitude

The cabin pressure altitude and the differential pressure for the narrow-body and wide-body jets are shown in table C20 at an interval of 2000 feet. The differential cabin pressure for the load spectrum is linearly interpolated from the table as a function of average airplane altitude for each operation stage.

Table C20. Differential Cabin Pressure

Airplane Altitude H_{plane} (Feet)	Atmospheric Pressure P_{atm} (In Hg)	Wide-Body Jet ΔP (Psi)	Narrow-Body Jet ΔP (Psi)
0	29.92	0.00	0.00
2000	27.82	1.01	0.99
4000	25.84	1.92	1.89
6000	23.98	2.77	2.69
8000	22.22	3.54	3.43
10000	20.58	4.24	4.08
12000	19.03	4.89	4.67
14000	17.58	5.47	5.20
16000	16.22	6.00	5.66
18000	14.94	6.48	6.08
20000	13.75	6.91	6.44
22000	12.64	7.29	6.75
24000	11.60	7.63	7.01
26000	10.63	7.93	7.24
28000	9.73	8.19	7.42
30000	8.89	8.41	7.56
32000	8.11	8.60	7.67
34000	7.38	8.75	7.75
35000	7.04	8.82	7.78
36000	6.71	8.88	
38000	6.10	8.97	
39000	5.81	9.00	

Figure C12 shows the cabin pressure schedule plot for narrow and wide body aircraft.

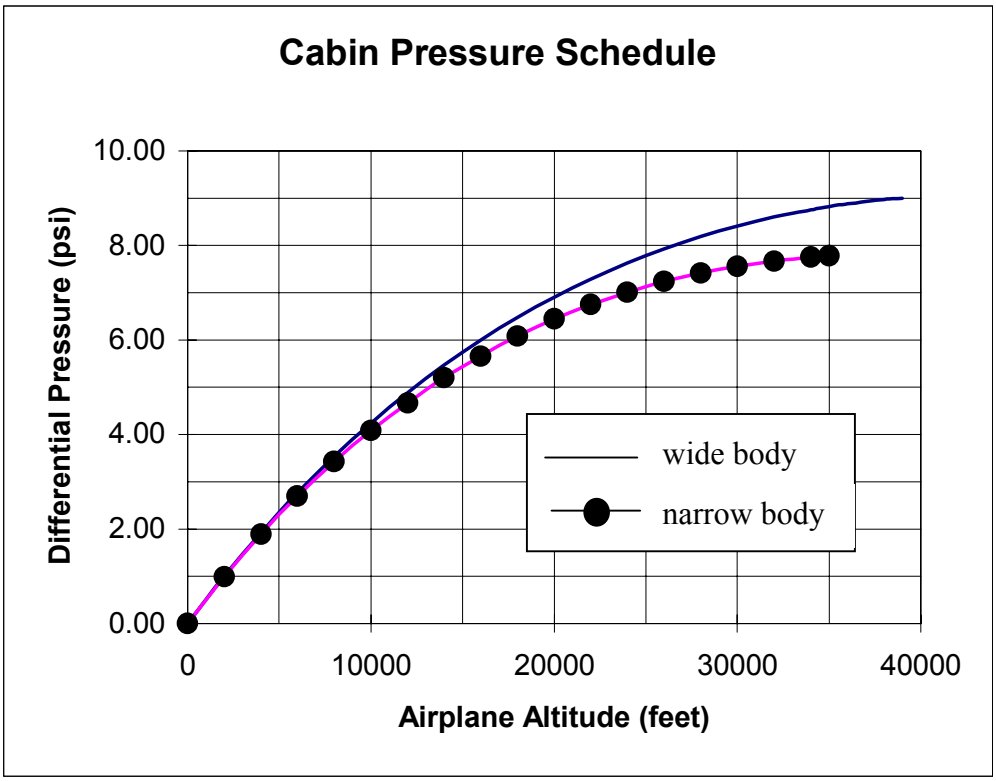

Figure C12. Differential Cabin Pressure

C4.2 Creation of Load Sequences

The load spectra are created according to the typical airplane operation profile described in tables C3 and C4 for narrow-body jets and wide-body jets respectively. Each spectrum consists of 6,000 unique flights. The procedures of load spectrum generation are documented in the FORTRAN computer code "GENRLOAD" and are briefly described below:

a. Create load exceedance tables

The exceedance tables are calculated at 0.1g increments starting at 0.05g for 6,000 flights for each load environment as shown below:

1. For pretaxi, the exceedances in table C8 are factored to 6,000 flights from 1,000 flights.

2. For takeoff runs, the exceedances in table C10 are factored to 6,000 flights from 1,000 flights.

3. For climb and descent, the exceedances in table C5 for climb/descent are factored to 2,400 hours, 4/10 hours for each flight multiplied by 6,000 flights, respectively.

4. For cruise, the exceedances in table C5 for cruise are factored according to the duration of said operation multiplied by 6,000 flights.

5. For landing impact, the exceedances in table C16 are factored down to 6,000 flights from 10,000 flights.

6. For landing roll, the exceedances in table C11 are factored to 6,000 flights from 1,000 flights.

7. For postflight, the exceedances in table C9 are factored to 6,000 flights from 1,000 flights.

8. For gust load in flight conditions, exceedances are calculated based on the equation shown in section C4.1.4 for the distances traveled during the duration discussed in steps (3) and (4) above.

b. Create load occurrence tables

The occurrence tables are calculated at 0.1g increments starting at 0.05g based on the exceedances discussed in step (1) through (8) above. The occurrence tables are also referred as "pool of load cycles".

c. Create load sequence for each flight stage

The load sequence is generated by randomly picking cycles from the appropriate pools for each flight stage. Each cycle can only be picked once and every cycle in the pools is used. The number of cycles for each stage is determined by the duration of the stage and the number of cycles in the pool as follows:

$$N_{pick} = \text{integer}\{N_{pool} \times (T_{stage}/T_{pool})\} + (1)_{nsf}$$

where

N_{pick} = number of cycles to be picked for the stage

N_{pool} = number of cycles in the original pool

T_{stage} = duration of the stage for one flight

T_{pool} = duration of the pool for 6000 flights

$+ (1)_{nsf}$ = additional cycle that is added to the flight every time the accumulation of the fraction portion of $\{N_{pool} \times (T_{stage}/T_{pool})\}$ becomes one cycle. The number of flights that have one additional cycle is determined as follows:

$$nsf = N_{pool} - \text{integer}\{N_{pool} \times (T_{stage}/T_{pool})\} \times 6000$$

In general, the cyclic loads will be symmetrically paired with respect to the 1-g state to form a fully reversed cycle, as shown in figure C13(a) except for the flight maneuvers since there are more positive maneuvers than negative maneuvers in normal flight operations. The load excursions are symmetrically paired first. The remaining positive excursions are then paired with 1-g load to form a half cycle, as shown in figure C13(b). The order of load sequences for airborne stages are as follows: gust, symmetrical maneuvers and unsymmetrical maneuvers. The minimum and maximum load factors and number of cycles for each operation environment are discussed in section C5.

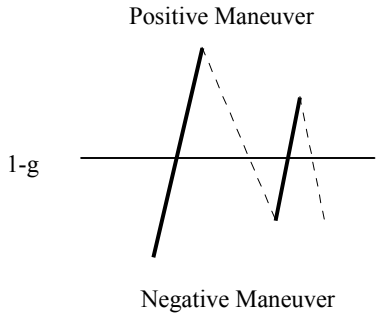

(a) Symmetrical Pairing

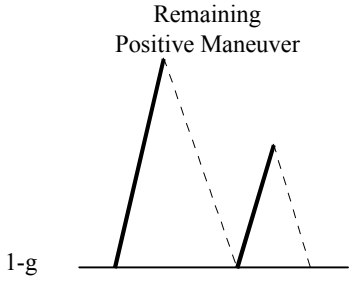

(b) Unsymmetrical Pairing

Figure C13. Range Pairing of Cyclic Loading

C5. Contents of Load Spectrum

The generic load spectra are stored in binary form and can be retrieved using the following FORTRAN code:

```
      READ(iu) NSEG,(CPD(I),I=1,NSEG)
      READ(iu) NFLTS
      DO 110 I=1,NFLTS
          READ(iu) IFLT,IPAIR,(DELTG(J),J=1,IPAIR),
     +                    MCTR,(MNVR0(J),J=1,MCTR),
     +                    (ICSEG(J),J=1,NSEG)
110   CONTINUE
```

where

iu is the FORTRAN unit of the spectrum file

NSEG is the number of stages in the flight profile

CPD is the cabin pressure differentials for each stage of the flight profile; REAL*8

NFLTS is the total number of flights in the spectrum (i.e., 6000)

IFLT is the flight number (i.e., 1 through 6000)

IPAIR is the number of incremental load factors in the flight (max=2000)

DELTG is the array of incremental load factors; REAL*4

MCTR is the number of unsymmetrical maneuver incremental load factors in the flight

MNVR0 is the array of the i^{th} number in the flight which is the unsymmetrical maneuver incremental load factor

ICSEG is the array of the summation count of the number of incremental load factors for each stage of the flight profile

The number of cycles and maximum and minimum load factors in g's are summarized in table 21.

Table C21. Number of Cycles and Maximum and Minimum Load Factors in g's

Description		Wide-Body Jet	Narrow-Body Jet
Preflight Taxi:	Min/Max ±Δg	±0.65	±0.65
	Number of Cycles	68,520	68,520
Takeoff Run:	Min/Max ±Δg	±0.55	±0.55
	Number of Cycles	59,052	59,052
Climb:	Min/Max ±Δg	±0.95	±0.95
	Number of Cycles	1,794,051	1,967,689
Cruise:	Min/Max ±Δg	±0.95	±1.05
	Number of Cycles	6,834,772	923,764
Descent:	Min/Max ±Δg	±0.95	±0.95
	Number of Cycles	843,275	897,518
Landing:	Min/Max ±Δg	±1.25	±1.25
	Number of Cycles	6,000	6,000
Landing Roll:	Min/Max ±Δg	±0.75	±0.75
	Number of Cycles	129,777	129,777
Postflight Taxi:	Min/Max ±Δg	±0.55	±0.55
	Number of Cycles	54,048	54,048
Total Number of Cycles		9,789,495	4,106,368

C6. Formation of Stress Spectrum

The stress spectrum at the repair location, in either the longitudinal or circumferential direction, can be converted from the generic load spectrum discussed in section C5 using the equation shown below:

$$\sigma = \sigma_p + (1+/-\Delta g)\ \sigma_{1g} \qquad \text{(C1)}$$

Where: σ is the stress at the repair location

σ_p is the stress due to cabin pressure at the repair location

$\sigma_p = pr/t$ for longitudinal cracks and

$\sigma_p = pr/2t$ for transverse cracks

σ_{1g} is the 1-g stress due to airplane inertia and aerodynamic loads at the repair location

Δg is the incremental load factors defined in the load spectrum

The estimation of σ_{1g} is discussed in the following sections.

C6.1 Maximum Design 1-G Stress

The 1-g stress (σ_{1g}) at the repair location is to be estimated based on the maximum design 1-g stress (σ_{1gm}) in the longitudinal direction which is assumed to be a function of design limit stress (DLS) and cabin pressure (p). For in-flight conditions, σ_{1gm} can be expressed in the equation below:

$$DLS=(p+1.1) r/2t + DLF* \sigma_{1gm} \quad \text{(C2)}$$

where:

p is the pressure differential

r is the fuselage radius

t is the skin thickness

DLF is the Design Limit Load Factor and $DLF=2.50$ set forth in FAR Section 25.337(b).

The pressure 1.1 psi in the above equation is added to account for a 1.0 psi in the aerodynamic pressure terms per FAR 25.571 and a 0.1 psi regulator tolerance per FAR 23.574.

Based on the material allowable (F_{tu}) and the safety factor (SF) the maximum design limit stress (DLS) can be expressed as follows:

$$DLS=C_{kd} *(F_{tu}/SF) \quad \text{(C3)}$$

Where

C_{kd} is an additional knock down factor applied to the material allowable for assembled structure which is equal to 0.88 based on experimental data

SF =1.50 for the ultimate design load conditions

From equation (1) and (2)

The σ_{1gm} can be expressed as follows:

$$\sigma_{1gm} = \frac{C_{kd} \times \left(F_{tu} / 1.50 \right) - (p + 1.1) r / 2t}{2.50} \quad \text{(C4)}$$

For ground operation conditions, the maximum 1-g stress is assumed to be 1/3 of σ_{1gm} , see section 3 of reference 9.

C6.2 One-G Stress for Repair Location

The maximum 1-g stress (σ_{1gm}) is assumed to occur at the crown area above the wing. By further assuming that the 1-g stress at both ends of the fuselage are equal to 0 and the stress varies linearly between the maximum stress areas and the tip of the fuselage as shown in figure C14(a) and (b) and, the stress varies linearly between the crown area and the cabin floor as shown in figure C14(c), stress areas and the tip of the fuselage the 1-g stress at any repair location can be express as follow:

For flight conditions

for transverse crack in Zone I:

$$\sigma_{1g} = C_2\left(\frac{Z}{r}\right)\left(\frac{L}{S}\right)\sigma_{1gm} \tag{C5}$$

for transverse crack in Zones II and III:

$$\sigma_{1g} = C_2\left(\frac{Z}{r}\right)\sigma_{1gm} \tag{C6}$$

for transverse crack in Zone IV:

$$\sigma_{1g} = C_2\left(\frac{Z}{r}\right)\left(1-\frac{L}{S}\right)\sigma_{1gm} \tag{C7}$$

for longitudinal crack in all zones:

$$\sigma_{1g} = 0 \tag{C8}$$

For ground conditions

for transverse crack in Zones II and IV

$$\sigma_{1g} = C_2\left(\frac{1}{3}\right)\left(\frac{Z}{r}\right)\left(\frac{L}{S}\right)\sigma_{1gm} \tag{C9}$$

for transverse crack in Zones II and III

$$\sigma_{1g} = C_2\left(\frac{1}{3}\right)\left(\frac{Z}{r}\right)\sigma_{1gm} \tag{C10}$$

for transverse crack in Zone I and longitudinal crack in all zones

$$\sigma_{1g} = 0 \tag{C11}$$

where

Z is the distance between the repair location and the cabin floor line, a positive value indicates the repair is above the floor line; a negative value indicates the repair is below the floor line

r is the radius of the fuselage

L is the distance between the repair location and the reference point as shown in figure C2

S is the length of Zone as shown in figure C2

C_2 is the average payload factor, 0.70

C7. Rainflow Count and Truncation

The stress sequences for the repair location will be counted using the rainflow one flight at a time and then truncated at a range of 2000 psi. The rainflow counting method is one of the resequencing processes generally applied to a flight-by-flight stress spectrum prior to the crack growth analysis. The method is illustrated in figure C14. Orienting the graphical display of the stress sequence vertically, it is considered as a stack of roofs. Rain is assumed to flow from each roof. If it runs off the roof, it drops down on the roof below, etc., where it does not continue on a roof that is already wet. The stress range is equal to the rainflow range indicated by AB, CD, etc., in figure C15. The details of standard rainflow counting process are described in ASTM E-1049, reference 10.

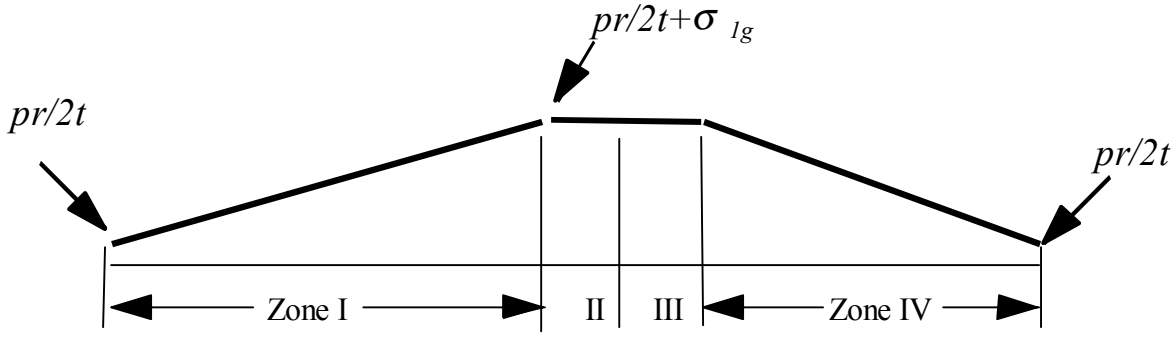

(a) Stress Distribution of Flight Condition S

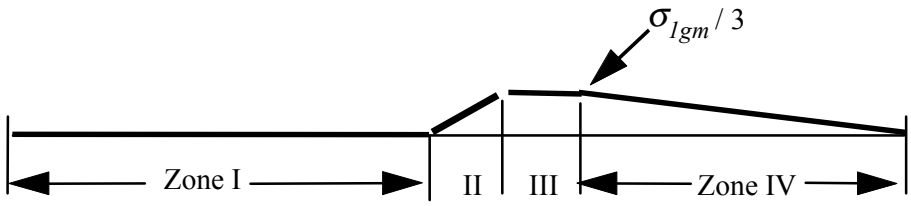

(b) Stress Distribution of Ground Condition

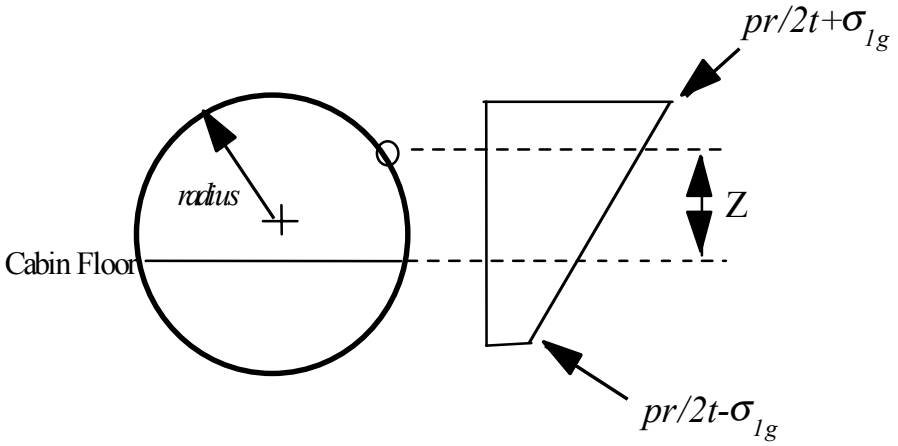

(c)

Figure C14. Stress Distribution Diagram

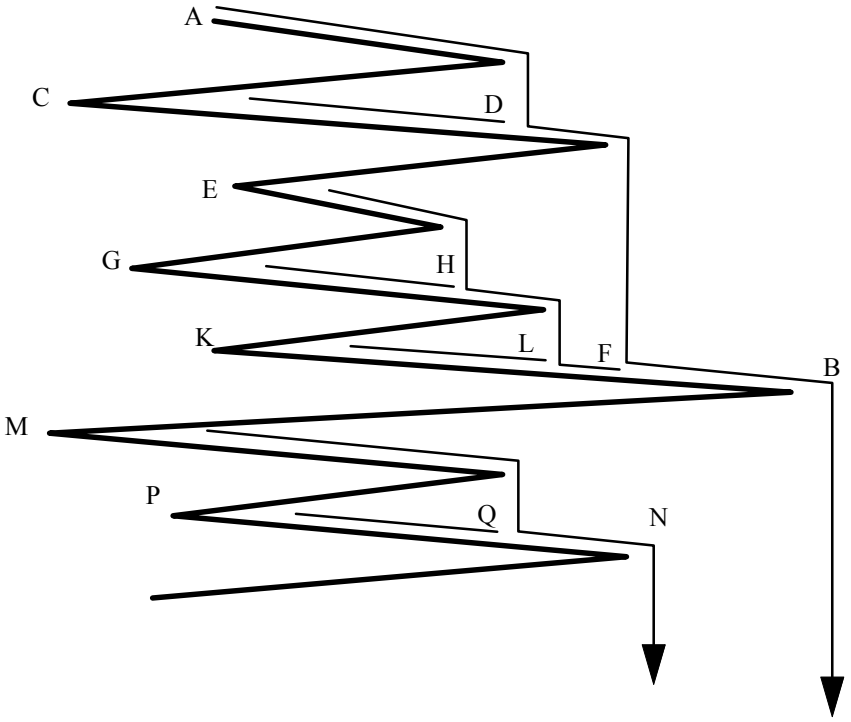

Figure C15. Rainflow Count

The truncation of lower stress levels is important for the efficiency of crack growth calculation. Truncation means that cycles below a certain magnitude are simply omitted. The argument is that low stress excursions do not contribute much to crack growth, especially in view of the retardation effects. Since there are so many cycles of low amplitude, their omission speeds up crack growth calculations. The final stress sequences, after rainflow counting and truncation, are used in the crack growth analysis portion of RAPID program.

C8. References

1. Flight International, "Corporate Aircraft," Various 1995 Issues.

2. Air transport World, "Jet Cost and Statistics," June Through Oct. 995.

3. Paul A. Hunter, "Maneuver Accelerations Experienced During Routine Operations of a Commercial Turbojet Transport Airplane," NASA TND-1801, May 1963.

4. Paul A. Hunter, "An Analysis of VGH Data Collected on One Type of Four-Engine Turbojet Transport Airplane During Commercial Operations," NASA TND-4330, Feb. 1968.

5. Paul A. Hunter, "Summary of Center-of-Gravity Accelerations Experienced by Commercial Transport Airplanes in Landing Impact and Ground Operations," NASA TND-6124, April 1971.

6. Harry Press, Roy Steiner, "An Approach to The Problem of Estimating Severe and Repeated Gust Loads for Missile Operations," NACA report 4332, September 1958.

7. "Aerospace Design Engineer Guide," Page 7-8, AIAA, January, 1987.

8. Environmental Control System Study Guide for the MD-80, ATM 509, July 1992, Allied Signal Aerospace.

9. J. B. de Jonge, et al., "A Standardized Load Sequence for Flight Simulation Tests on Transport Aircraft Wing Structures," LBF-BERICHT FB-106, March 1973.

10. "Standard Practice for Cycle Counting in Fatigue Analysis," ASTM E-1049-85.

Appendix D – One Cycle Equivalent Stress Calculation

D1. Introduction

This appendix describes the derivation of the one-cycle equivalent stress for the stress spectrum either generated by RAPID or provided by the user. The one-cycle equivalent stress is used in the crack growth prediction of the repaired skin using the simplified method. The procedure has been implemented in RAPID and validated through an example repair.

D2. Derivation

In the crack growth analysis using the simplified method, the crack growth life N_{ij} for a crack growing from the size a_i to the size a_j ($a_j > a_i$) under a repeated flight can be calculated using the following equation [1]:

$$N_{ij} = \frac{1}{C}(SG_{ij})^{-p} \tag{D1}$$

In equation 1, C and p are the coefficients in the Walker's crack growth equation,

$$\frac{da}{dN} = C\left\{(1-R)^q K_{Max}\right\}^p \tag{D2}$$

where K_{max} is the stress-intensity factor evaluated at the stress σ_{Max} of the given stress cycle and R is the stress ratio of that cycle.

The parameter S in equation 1 is the one-cycle equivalent stress of the repeated flight, and G_{ij} is the geometry term pertinent to the crack geometry of the repaired skin.

The equivalent stress S can be obtained by the equation:

$$S = \{\sum_{j=1}^{m}\left[\sigma_{Max,j}(1-R_j)^q\right]^p\}^{1/p} \tag{D3}$$

where q is the coefficient in the Walker's crack growth equation, $\sigma_{Max,j}$ and R_j are the maximum stress and the stress ratio, respectively, of the j-th cycle, and m is the total number of cycles in the repeated flight.

The geometry term G_{ij} can be calculated by the equation:

$$G_{ij} = \{\int_{a_i}^{a_j}[\beta(a)\sqrt{\pi a}]^{-p}\,da\}^{-1/p} \tag{D4}$$

where $\beta(a)$ is the geometry factor, and a is the crack length.

Suppose a stress spectrum at the repair location contains M successive flights. Let m_j be the number of stress cycles in the j-th flight. A representative stress spectrum is depicted below in figure D1.

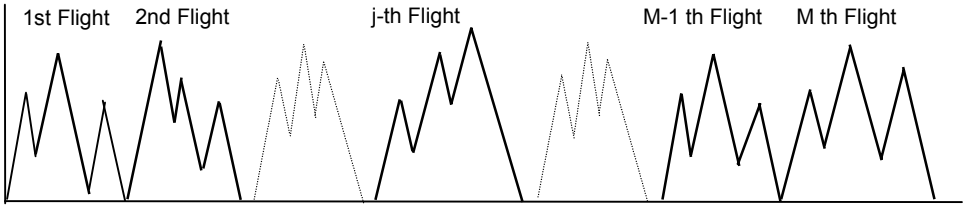

Figure D1. A Representative Stress Spectrum

With the stress spectrum in each flight prescribed, the one-cycle equivalent stress S_j for each j-th flight can be calculated using equation 3, and is schematically shown below in figure D2.

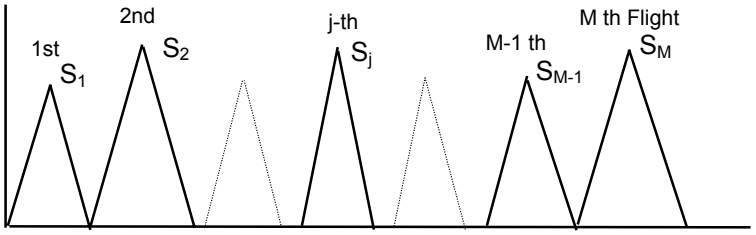

Figure D2. One-Cycle Equivalent Stress

Consider a stress spectrum containing M flights as shown in figure D2. The equivalent stress S_{Eq} of a flight in the spectrum, as shown below in figure D3,

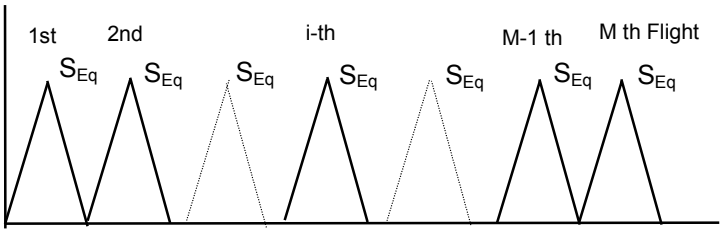

Figure D3. Equivalent Stress of M Flights

can be calculated as

$$S_{Eq} = \left(\frac{\sum_{i=1}^{M} S_k^p}{M} \right)^{1/p} \tag{D5}$$

Substitution of equation 3 into equation 5 gives

$$S_{Eq} = \left(\frac{\sum_{i=1}^{M} \left\{ \sum_{j=1}^{m_i} \left[\sigma_{Max,j} (1 - R_j)^q \right]^p \right\}}{M} \right)^{1/p} \tag{D6}$$

which can be rewritten as

$$S_{Eq} = \left(\frac{\sum_{k=1}^{n} \left[\sigma_{Max,k} (1 - R_k)^q \right]^p}{M} \right)^{1/p} \tag{D7}$$

The variable n in equation 7 is the total number of stress cycles in the stress spectrum.

D3. Implementation and Validation

The calculation of the equivalent stress S_{Eq} for a stress spectrum containing M flights has been implemented in RAPID. The implementation has also been validated through the following examples.

A skin repair with an external doubler mechanically fastened to the skin is shown below in figure D4. The skin and repair doublers are made of the 2024-T3 clad sheet. Two fastener types, NAS1097-E6 and HL326-6 are used. Dimensions of the skin cutout and the repair doublers are given in the figure.

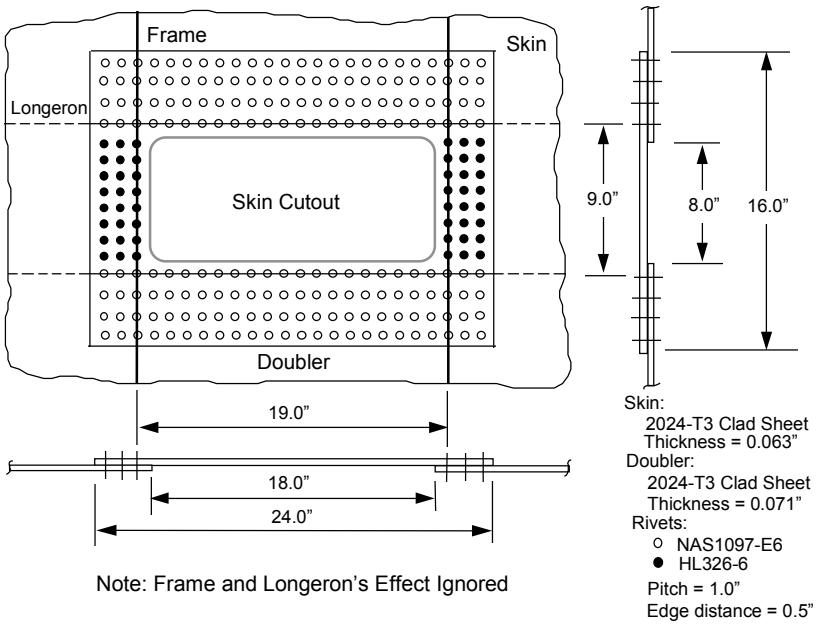

Figure D4. Description of the Example Repair

The radius near the repair is 120.0 inches, and the pressure differential is assumed to be 8.6 psi. To perform the crack growth analysis, initial longitudinal cracks are postulated at the critical center fastener hole in the first fastener row in the skin.

It is assumed that the skin near the repair location is subjected to a stress spectrum of 20,887 stress cycles representing 1/10 of the design life of the aircraft. An overall spectrum summary is provided in the table D1 shown below. A factor of 1.5 in magnitude is used in the analysis.

Table D1 Overall Spectrum Summary

PEAK DISTRIBUTION			RANGE DISTRIBUTION			STRESS RATIO DISTRIBUTION		
Peak Stress		Cycles	Stress Range		Cycles	Stress Ratio		Cycles
Below -5000.		0	Below 0.			Below -2.00		0
-5000.	-4000.	0	0.	1000.	0	-2.00	-1.90	0
-4000.	-3000.	0	1000.	2000.	0	-1.90	-1.80	0
-3000	-2000.	0	2000.	3000.	14585	-1.80	-1.70	0
-2000.	-1000.	0	3000.	4000.	379	-1.70	-1.60	0
-1000.	0.	0	4000.	5000.	13	-1.60	-1.50	0
0.	1000.	0	5000.	6000.	0	-1.50	-1.40	0
1000.	2000.	0	6000.	7000.	2361	-1.40	-1.30	0
2000.	3000.	0	7000.	8000.	3256	-1.30	-1.20	0
3000.	4000.	0	8000.	9000.	270	-1.20	-1.10	0
4000.	5000.	145	9000.	10000.	22	-1.10	-1.00	0
5000.	6000.	7358	10000.	1000.	1	-1.00	-0.90	0
6000.	7000.	1717	11000.	12000.	0	-0.90	-0.80	0
7000.	8000.	802	12000.	13000.	0	-0.80	-0.70	0
8000.	9000.	9697	13000.	14000.	0	-0.70	-0.60	0
9000.	10000.	1085	14000.	15000.	0	-0.60	-0.50	0
10000.	11000.	78	15000.	16000.	0	-0.50	-0.40	0
11000.	12000.	5	16000.	17000.	0	-0.40	-0.30	0
12000.	13000.	0	17000.	18000.	0	-0.30	-0.20	0
13000.	14000.	0	18000.	19000.	0	-0.20	-0.10	0
14000.	15000.	0	19000.	20000.	0	-0.10	0.00	0
15000.	16000.	0	20000.	21000.	0	0.00	0.10	0
16000.	17000.	0	21000.	22000.	0	0.10	0.20	4571
17000.	18000.	0	22000.	23000.	0	0.20	0.30	1340
18000.	19000.	0	23000.	24000.	0	0.30	0.40	17
19000.	20000.	0	24000.	25000.	0	0.40	0.50	126
20000.	21000.	0	25000.	26000.	0	0.50	0.60	2122
21000.	22000.	0	26000.	27000.	0	0.60	0.70	8453
22000.	23000.	0	27000.	28000.	0	0.70	0.80	4258
23000.	24000.	0	28000.	29000.	0	0.80	0.90	0
24000.	25000.	0	29000.	30000.	0	0.90	1.00	0
25000.	26000.	0	30000.	31000.	0	1.00	1.10	0
26000.	27000.	0	31000.	32000.	0	1.10	1.20	0
27000.	28000.	0	32000.	33000.	0	1.20	1.30	0
28000.	29000.	0	33000.	34000.	0	1.30	1.40	0
29000.	30000.	0	34000.	35000.	0	1.40	1.50	0
30000.	31000.	0	35000.	36000.	0	1.50	1.60	0
31000.	32000.	0	36000.	37000.	0	1.60	1.70	0
32000.	33000.	0	37000.	38000.	0	1.70	1.80	0
33000.	34000.	0	38000.	39000.	0	1.80	1.90	0
34000.	35000.	0	39000.	40000.	0	1.90	2.00	0
Above 35000.		0	Above 40000.		0	Above 0.0		0

Total Cycles	=	20887
Total No. of Flights	=	5910
Highest Peak	=	11760.30
Lowest Valley	=	1082.95
Largest Range	=	10283.55

To perform the crack growth analysis, it is assumed that a crack of size equal to 0.05″ initially exists at the critical fastener hole in the skin. The crack grows towards the adjacent hole and enters the hole. When the crack grows into the hole, it is assumed that two equal-length cracks of 0.005″ exist at outer holes. The cracks continue to grow to form linked-up holes. The analysis proceeds until the residual strength of the repaired skin drops to the limit stress of the skin.

The scenarios for (a) a crack growing towards the adjacent hole and (b) continuing damage when the crack growing into the hole are depicted below in figure D5.

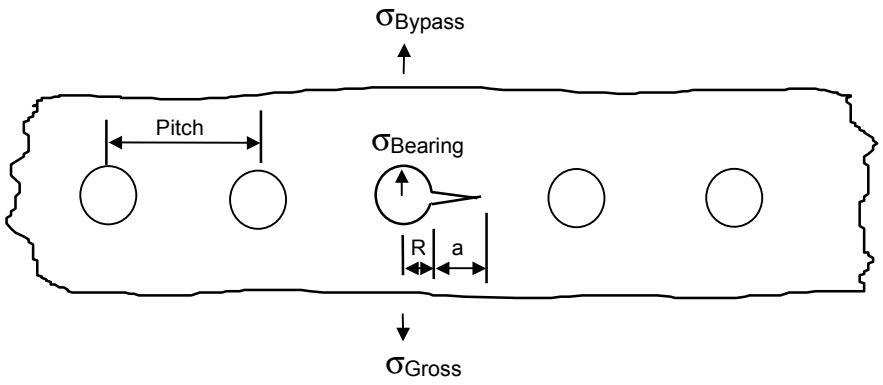

(a) Prior to Entering the Hole

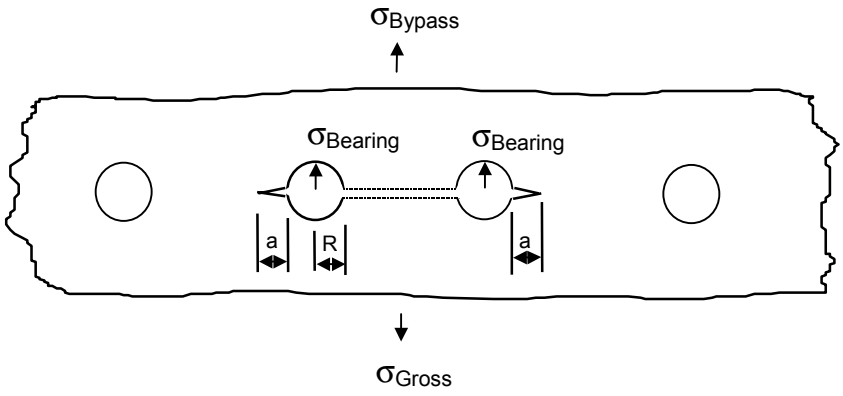

(b) Continuing Damage

Figure D5. Crack Growth Scenario

To perform the crack growth analysis using the simplified method, an equivalent stress S_{eq} equal to 11.915 ksi was calculated using equation 7. With this equivalent stress, RAPID calculates the crack growth. The analysis result was then compared with that obtained using the RAPID cycle-by-cycle method.

Crack growth analysis results obtained from RAPID using the equivalent stress in the simplified method and the cycle-by-cycle method, are plotted in figure D6.

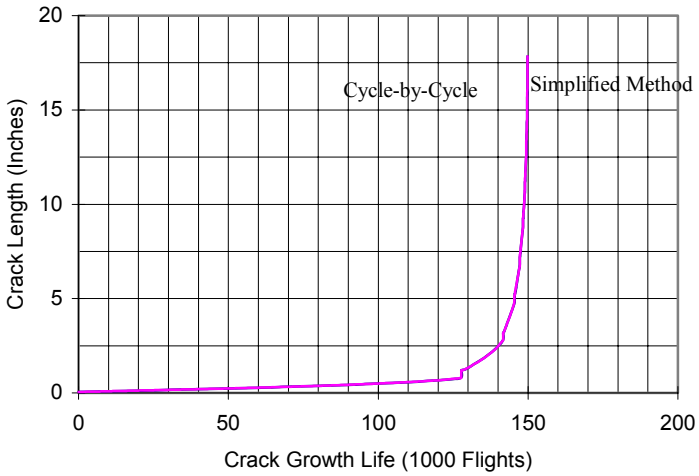

Figure D6. Crack Growth Life of the Example Repair

As shown in figure D6, the crack growth obtained using the equivalent stress in the simplified method is nearly identical to that from the cycle-by-cycle method. In this analysis, the crack growth was calculated based on the zero stress ratio (R = 0.0) in the simplified method. The crack growth da/dN material data used in the cycle-by-cycle method were obtained for various stress R ratios using the Walker's equation. In this manner, the straight-line portion of the da/dN data was used in both analyses. Based on the analysis results shown in figure D6, it demonstrates that the simplified crack growth analysis method based on an equivalent stress converted from the stress spectrum produces the same crack growth life as that using the cycle-by-cycle method

Suppose the actual da/dN data, instead of that from the Walker's equation, were used in the cycle-by-cycle method. The crack growth life obtained is compared with that from the simplified method in figure D7. It shows that the crack growth life obtained from the cycle-by-cycle method (144,757 flights) is about 3.5% shorter than that from the simplified method (149,850 flights).

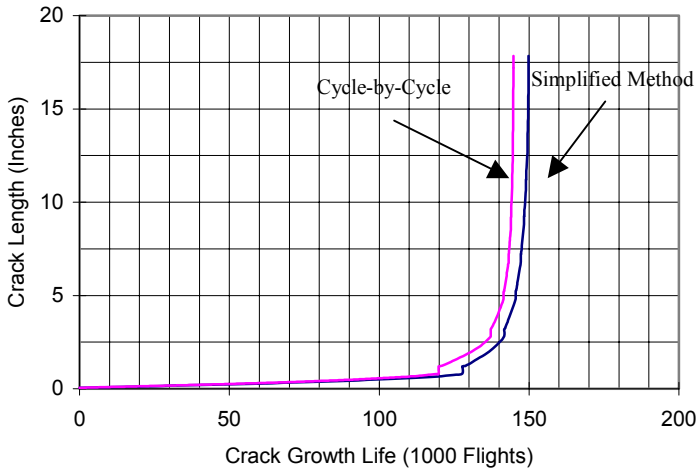

Figure D7. Crack Growth Life of the Example Repair

Reference

1. T. Swift, "Repairs to Damage Tolerant Aircraft," Structural Integrity of Aging Airplanes, Edited by S. N. Atluri, S. G. Sampath, and P. Tong, Springer-Verlag, 1991, pp 433-483.

Appendix E - Proximate Repairs

E1. Introduction

The purpose of the investigation was to evaluate the interaction of two riveted repair patches when they are located in close proximity of each other on a uniaxially loaded flat sheet.

E2. Approach

The study analyzed two rectangular patches situated perpendicular to the load direction. The patches were positioned in parallel formation (side by side), and in-series formation with respect to the load direction, as shown below in figure E1.

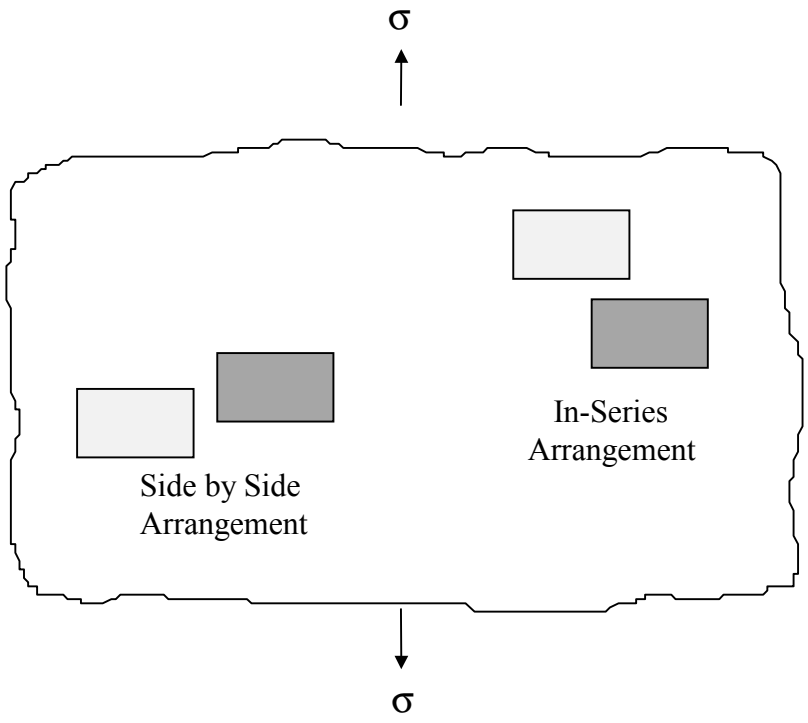

Figure E1. Rectangular Patches Placed Side by Side and In-Series Arrangements Relative to Load

Study parameters included the patch size and patch separation distance in both x and y directions. Two patch sizes, 15″x25″ and 25″x25″ riveted over 10″x15″ and 15″x15″ skin cutouts, were used in various combinations to determine the proximity effects between the patches. The interference between the patches was monitored by evaluating the forces in the patch-to-skin fasteners while moving the proximate patch into different positions around the subject patch.

In the side by side arrangement, figure E2a, the right edge of the subject patch was initially located next to the left edge of the proximate patch and then moved away (in the x direction) with 2″ increments until a total separation of 14″ was reached. The proximate patch was then

moved laterally in the y direction in 2″ increments and the previous x directional positioning sequence was repeated. The y directional relative motion was proceeded until a 24″ lateral shift was attained.

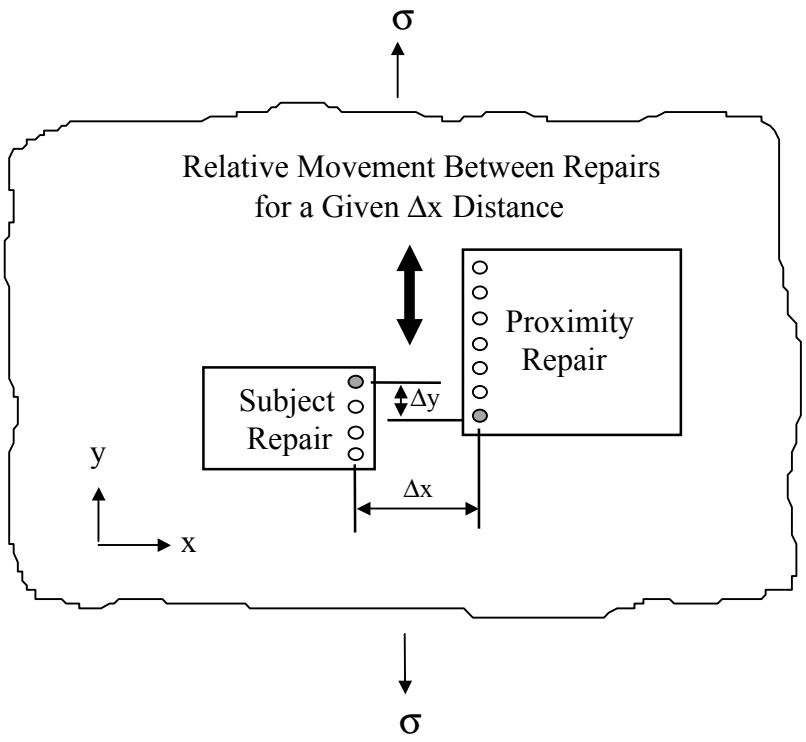

Figure E2A. Side by Side Patch Arrangement in Proximity Interaction Studies

In the in-series arrangement, the bottom edge of the proximate patch was placed next to the top edge of the subject patch and then moved away in the normal direction (y direction) in 2″ increments (figure E2b). The patches were then shifted laterally in the x direction repeating the y directional separation sequence compiling normalized fastener load data into the results matrix. The lateral shift was repeated until the proximate patch had moved 36″ in the y direction from its original position relative to the subject patch.

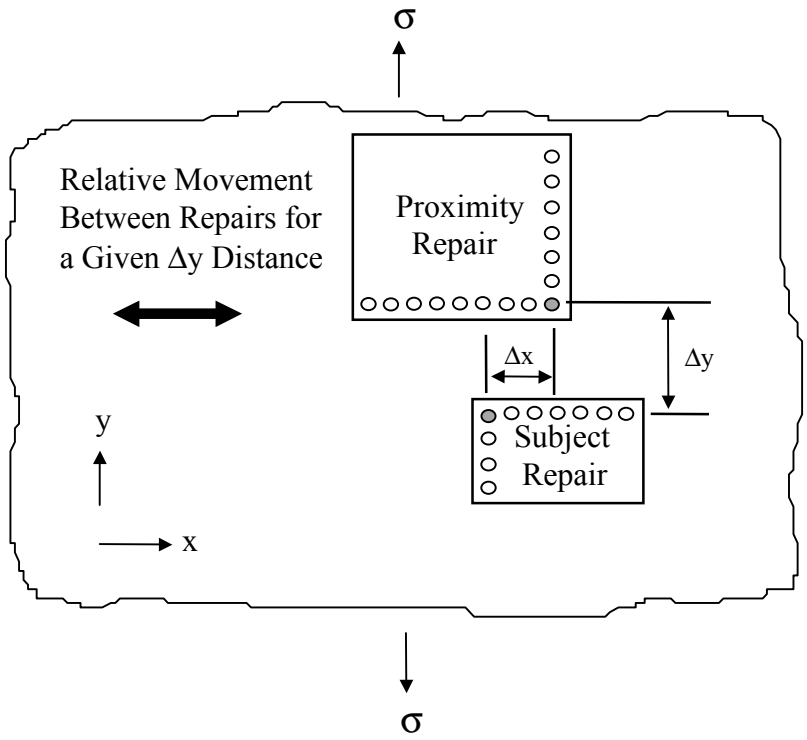

Figure E2B. In-Series Patch Arrangement in Proximity Interaction Studies

The aircraft fuselage skin repair areas were idealized with a large (140″x200″) coarsely meshed flat sheet that had two finely meshed patches located approximately at the center. The damage zone was idealized by removing the skin under the patches except in the rivet zones. The rivets were modeled with beam elements with their stiffnesses calculated as follows:

Shear stiffness of fastener using Swift's equation:

$$K_s = \frac{Ed}{A + B(d/t_1 + d/t_2)}$$

where E (elastic modules) = 10.5×10^6 psi; d = 0.1875″ (3/16″ dia), t_1 = 0.063″, t_2 = 0.071″, and constants A = 5.0 and B = 0.8 for aluminum. Substituting into the above equation results in

$$K_s = 207{,}375 \text{ lbs/in.}$$

The shear stiffness is translated to area factors for shear, K_1 and K_2 using the following beam deflection equation,

$$DEFL = (l^3 / 3 E I)_{bend} + (l / K_1 G A)_{shear}$$

where E I = infinite (no bending allowed), G (shear modulus) = 4.04×10^6 psi, and l = 0.067″.

Solving the above equation for K_1 by substituting unit deflection = 1/207,375:

Area Factor for Shear, $K_1 = 0.125$

A finite element NASTRAN model of one of the cases is shown in figure E3. The model consists of more than 6000 quadrilateral and triangular plate elements to idealize the skin and the patches, and 492 beam elements representing the fastener rivets. The patches were located 0.067″ outside of the skin with the beam elements connecting the corresponding nodes to the skin in three rows around the patch perimeters.

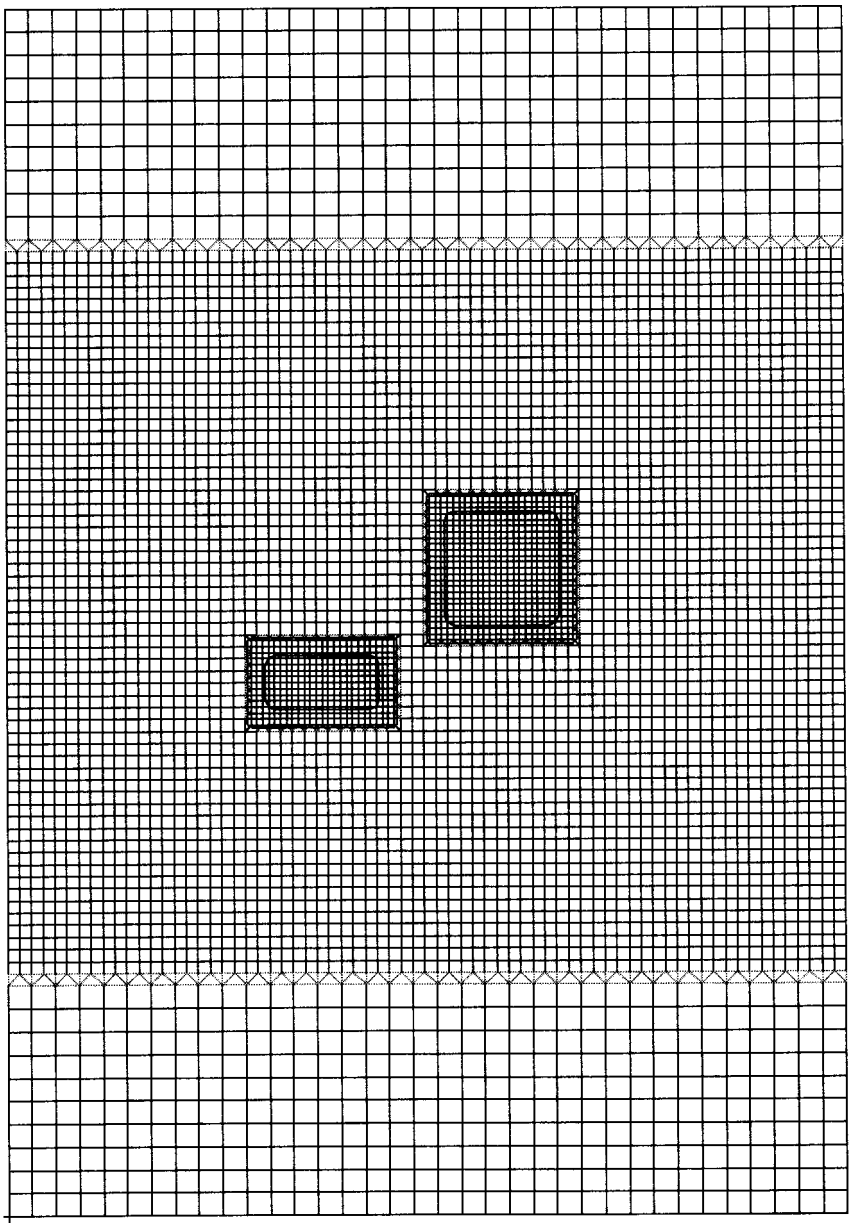

Figure E3. Finite Element NASTRAN Model of Typical Study Case

The repaired sheet containing the patches was subjected to uniform 1000 psi uniaxial far field stress applied in the y direction. Since only shear deformations of the fastener rivets were considered, the skin and the patches were restrained from bending in the out-of-plane direction.

The physical dimensions used in the study simulated those used in commercial aircraft. The skin thickness was selected as 0.063″, and the patch thickness as 0.071″. The rivet size (the diameter) was 0.01875″ (3/16″).

This study included two patch sizes, 25″x15″ and 25″x25″ (outside dimensions). The rivets were placed 1″ apart in three rows around the patch perimeters.

E2. Summary of Results

There were six basic patch arrangements that were included in the study.

- Two side by side small (25″x15″) patches
- A small patch positioned beside a large (25″x25″) patch
- Two side by side large patches
- Two small patches in-series (refer to figure E1 for details)
- A small patch positioned in-series with a large patch
- Two large patches in-series

Each arrangement consisted of approximately 40 relative patch position varying how the proximate patch was situated in relation to the subject patch.

Although a large number of fastener forces were tracked throughout the positioning iterations, only the corner fasteners were identified with highest magnitudes and were included in the result data reduction. Due to the large amount of data accumulated in these analyses, only summaries of results are included in this section.

E2.1 Preliminary Analysis

In the preliminary analysis the following observation were made.

- The fastener loads peaked when the corners of the proximate patch were positioned close to the corners of the subject patch.

- The highest fastener loads occurred when the proximate patch was placed as close to the subject patch as possible.

- The fastener loads approached single patch values quickly in the in-series configuration when the proximate patch was positioned away from the subject patch in the lateral (x) direction.

- The fastener loads approached the single patch values very slowly in the side by side arrangement when the proximate patch was positioned away from the subject patch in the lateral (y) direction. (As seen in figure E1, the normal and lateral distances between the side by side and in-series arrangements are not coincident but in fact are shifted 90 degrees (x and y axes are switched)).

E2.2 Correction Factors

The correction factors for repair patch proximity studies were obtained directly from the increases in the subject patch fastener loads at critical corner locations as the proximate patch was moved with respect to the subject patch. Since the objective of these analyses was to provide input for the automated damage tolerance analysis, the interest lies in the load factor increase and not the decrease. Therefore, only the correction factors exceeding unity are presented.

E2.2.1 Side by Side Patch Arrangement

The correction factors peak at two locations when the proximate patch is moved laterally in the y direction (the x coordinate axis lies horizontally pointing right while the y axis points up) along the subject patch.

The first case occurs when corner no. 3 (p3) of the proximate patch approaches corner no. 1 (s1) of the subject patch (corners 1 though 4 are located counter-clockwise starting with no. 1 at the top right) as shown in figure E4. In the figure, the proximity distance yp3 - ys1 is the relative distance Δy in the y direction between the corner p3 of the proximate patch and s1 of the subject patch. The maximum value is reached when the bottom edge fastener row of the proximate patch is 1 inch above the top edge fastener row of the subject patch in the y direction and horizontally patches lie next to each other.

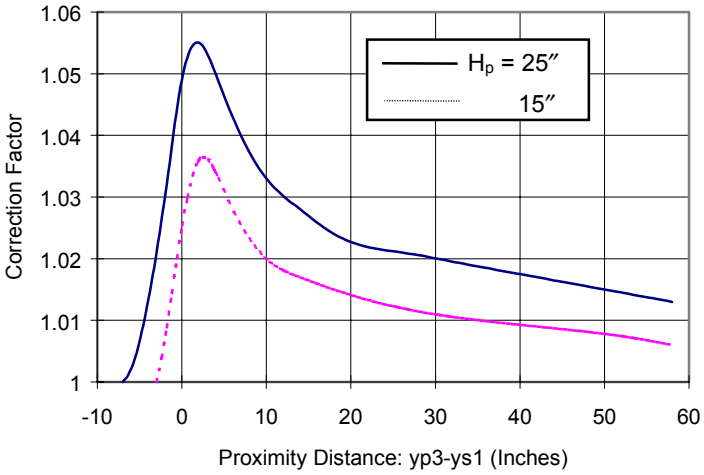

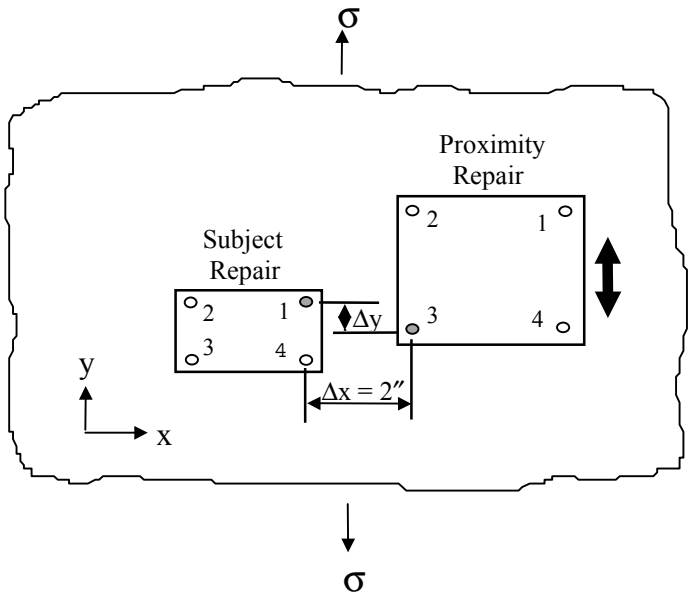

yp3 - ys1 = 0 When p3 Lines Up With s1 in the y Direction

Figure E4. Correction Factor Versus Proximity Distance yp3 - ys1

As the proximate patch is moved further down along the side of the subject patch, the correction factor drops below unity and is therefore not presented until corner no. 2 (p2) of the proximate patch approaches corner no. 4 (s4) of the subject patch. The correction factor peaks at the same values as in the case of the corners no. 3 (p3) of the proximate patch and no. 1 (s1) of the subject patch but in the reverse order due to the y symmetry. This plot is shown in figure E5. In the figure, the proximity distance yp2 - ys4 is the relative distance Δy in the y direction between the corner p2 of the proximate patch and s4 of the subject patch.

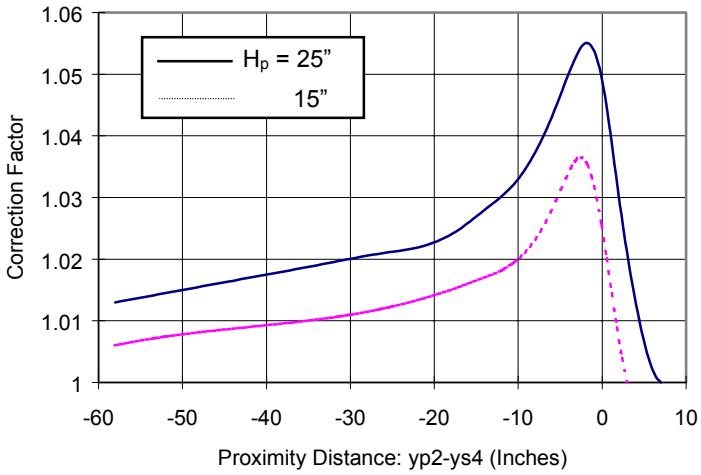

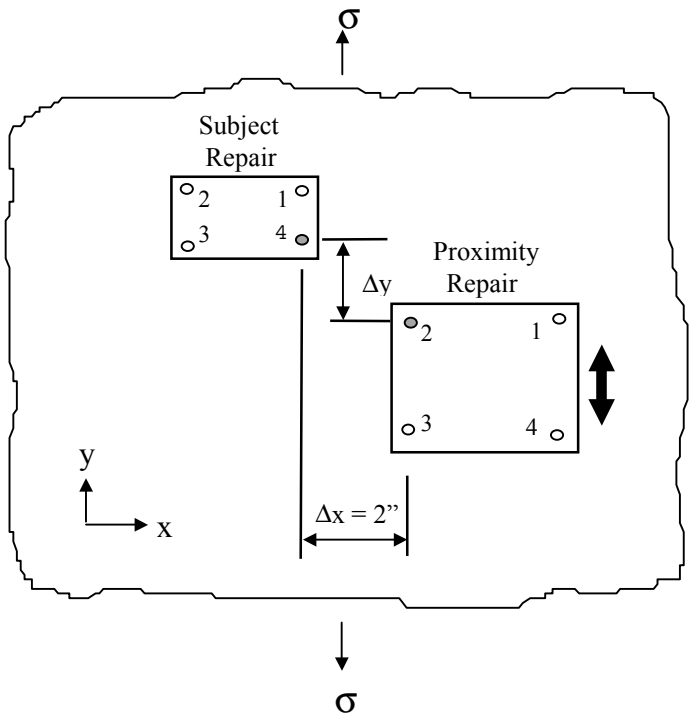

yp2 - ys4 = 0 When p2 Lines Up With s4 in the y Direction

Figure E5. Correction Factor Versus Proximity Distance yp2 - ys4

E2.2.2 In-Series Patch Arrangement

The correction factors peak at four locations when the proximate patch is moved laterally (in the x direction) along the subject patch.

In the first case, corner no. 4 (p4) of the proximate patch approaches corner no. 2 (s2) of the subject patch as shown in figure E6. In the figure, the proximity distance xs2 - xp4 is the relative distance Δx in the x direction between the corner s2 of the subject patch and p4 of the proximate patch. The maximum value is reached when the fastener row of the right edge of the proximate patch is lined up with the fastener row for the left edge of the subject patch.

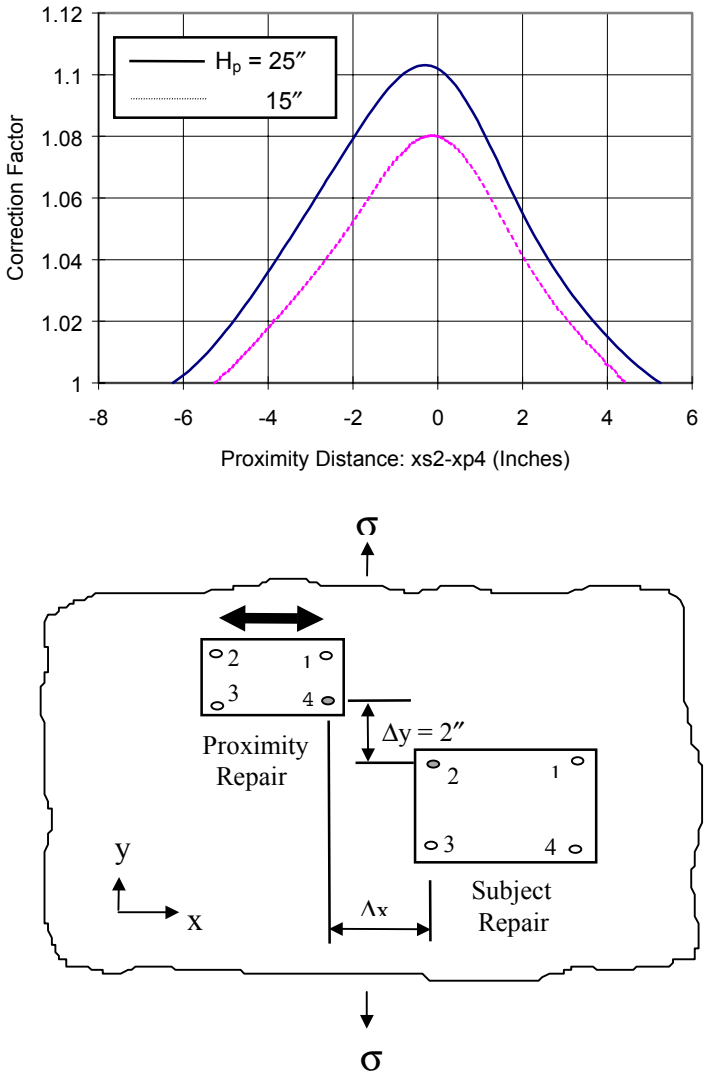

xs2 - xp4 = 0 When s2 Lines Up With p4 in the x Direction

Figure E6. Correction Factor Versus Proximity Distance xs2 - xp4

The next peaks occur when corner no. 3 (p3) of the proximate patch approaches corner no. 2 (s2) of the subject patch (figure E7) or corner no. 4 (p4) of the proximate patch approaches corner no. 1 (s1) of the subject patch (figure E8). The order in which these conditions occur depends on the relative widths of the proximate and the subject patches.

In figure E7, the proximity distance xs2 - xp3 is the relative distance Δx in the x direction between the corner s2 of the subject patch and p3 of the proximate patch.

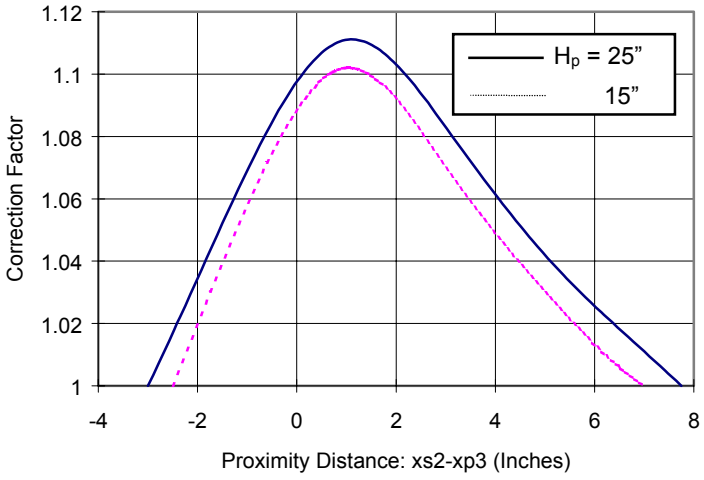

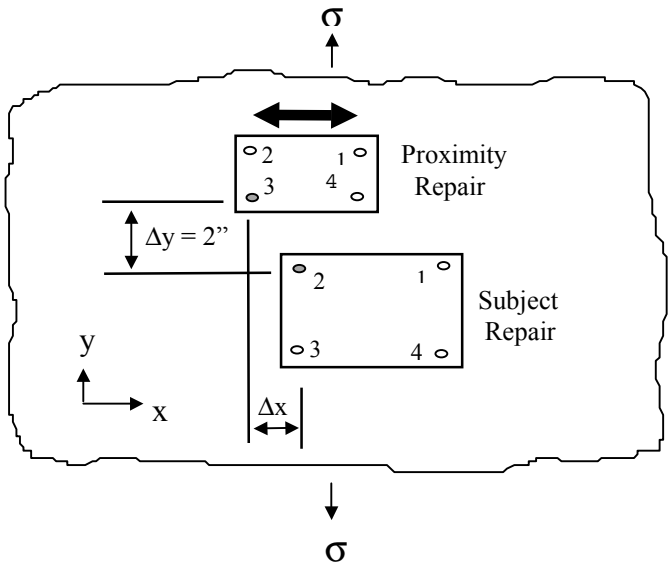

xs2 - xp3 = 0 When s2 Lines Up With p3 in the x Direction

Figure E7. Correction Factor Versus Proximity Distance xs2 - xp3

In figure E8, the proximity distance xs1 - xp4 is the relative distance Δx in the x direction between the corner s1 of the subject patch and p4 of the proximate patch.

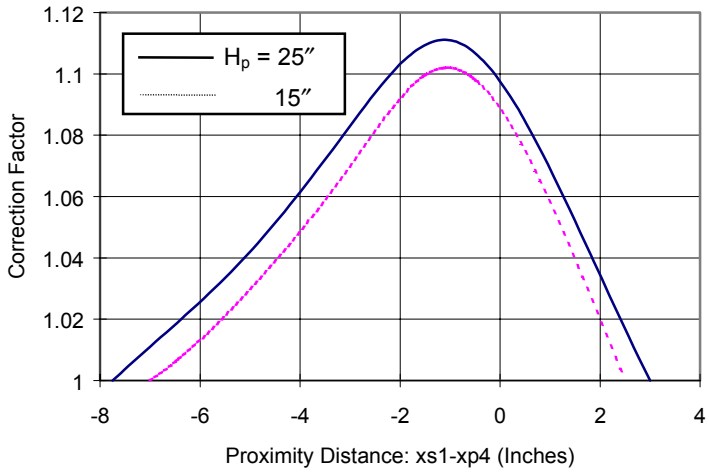

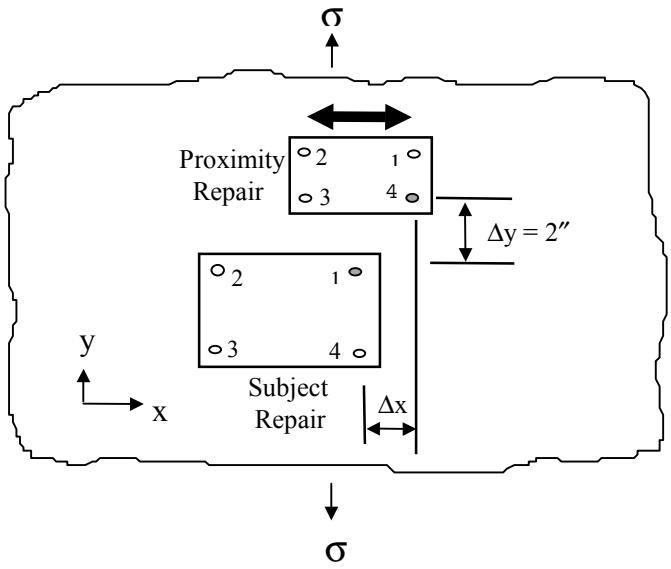

xs1 - xp4 = 0 When s1 Lines Up With p4 in the x Direction

Figure E8. Correction Factor Versus Proximity Distance xs1 - xp4

The fourth peak occurs when corner no. 3 (p3) of the proximate patch approaches corner no. 1 (s1) the subject patch. This case is shown in figure E9. In the figure, the proximity distance xs1 - xp3 is the relative distance Δx in the x direction between the corner s1 of the subject patch and p3 of the proximate patch.

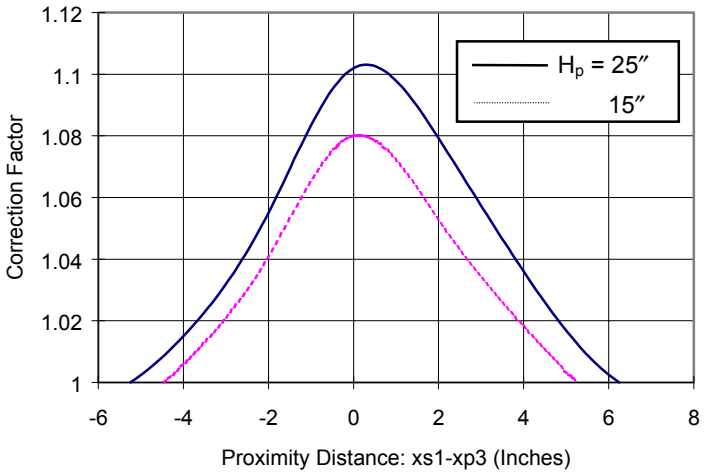

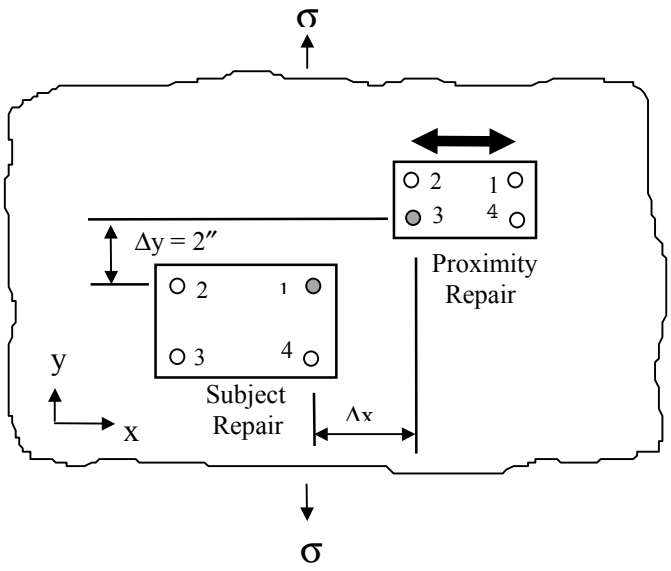

xs1 - xp3 = 0 When s1 Lines Up With p3 in the x Direction

Figure E9. Correction Factor Versus Proximity Distance xs1 - xp3

E2.2.3 Crack Growth Life Prediction

To estimate the crack growth life of a subject repair near a proximate repair, an engineering approach is employed. In this approach, the life of the subject repair alone is first determined. The life is then modified by the life reduction factor to estimate the reduced life due to influence of the proximate repair:

$$\text{Life}_{\text{with proximity effect}} = \text{Life}_{\text{w/o proximity effect}} * \text{LRF}$$

The life reduction factor (LRF) is plotted against the fastener load correction factor $F_{proximity} / F_0$ in figure E10. In the figure, F_0 is the critical corner fastener load of the subject repair alone based on 1000 psi reference applied stress. The fastener load correction factor is the correction factor discussed in section E2.2 (figures E4 through E9).

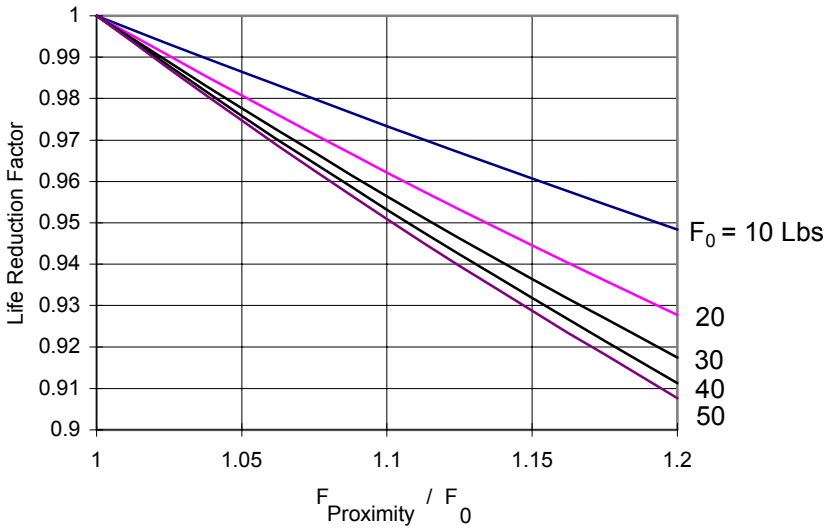

Figure E10. Life Reduction Factor Versus Fastener Load Correction Factor

Appendix F - Repairs at Stiffeners

F1. Introduction

This appendix describes the database development of load transfers along the critical fastener row in a skin repair at stiffeners. The stiffening effect on geometry factors compiled from open literature is also provided for the crack growth of repaired skin.

F2. Approach

A parametric study was conducted for Type III repairs, using the two-dimensional finite element method, to obtain fastener load transfers in skin repairs at a stiffener. Parameters considered in the study included (1) location of the stiffener, (2) cross-sectional area of the stiffener, and (3) skin thickness. Figure F1 shows the four stiffener locations considered in the study.

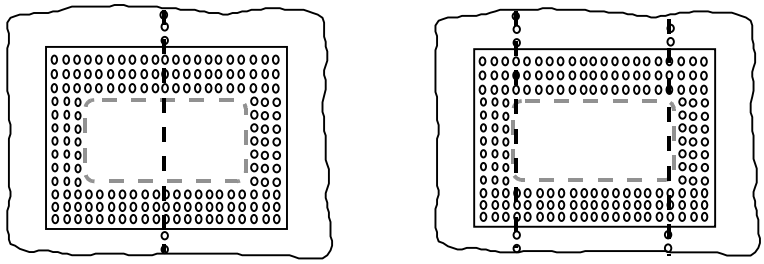

(a) at Center Fastener Column

(b) at Fastener Columns Along the Edge of Skin Cutout

(c) at Fastener Columns Next to Skin Cutout

(d) at Corner Fastener Columns

Figure F1. Stiffener Locations in Parametric Study

The three cross-sectional areas of the stiffener considered in the study were 0.25, 0.50, and 1.0 square inch. Three skin thicknesses, 0.050″, 0.071″, and 0.090″ were used, and the doubler thickness was one gauge more than that of the skin. In this study, the bending rigidity of the stiffener was ignored.

The study was conducted using the two-dimensional finite element method. Due to double symmetry of the geometry as well as the stress applied in the skin, the analysis was performed on one quarter of the repaired skin. A typical finite element model representing one quarter of the repaired skin is shown in figure F2.

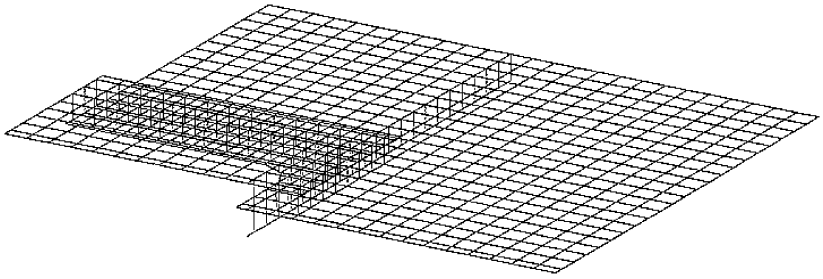

Figure F2. Typical Finite Element Model of a Repair at Stiffener

In the model, the skin and the repair doubler were modeled using the quadrilateral membrane element. The stiffener was modeled using the rod element, and the fastener was modeled using the beam element with the shear rigidity calculated based on the Swift's equation:

$$K = \frac{Ed}{A + B\left(\frac{d}{t_{Skin}} + \frac{d}{t_{Doubler}}\right)}$$

In the above equation, E is the average of the moduli of sheet materials jointed together, d is the fastener hole diameter, t_{Skin} and $t_{Doubler}$ are the thicknesses of the skin and doubler, and A and B are empirical constants taking the values of 5.0 and 0.8 for aluminum rivets, respectively. The calculated value was input directly to the finite element program. In the analysis, the repaired skin is subjected to a reference far field stress of 1000 psi.

To perform the damage tolerance analysis of skin repairs, the stress field near fastener holes in the skin needs to be known. The skin stress prior to the load transfer is referred to as the gross stress, the bearing stress as the average hole bearing stress in the skin exerted by the fastener load, and the bypass stress as the skin stress after the load transfer. These skin stresses are shown below in figure F3.

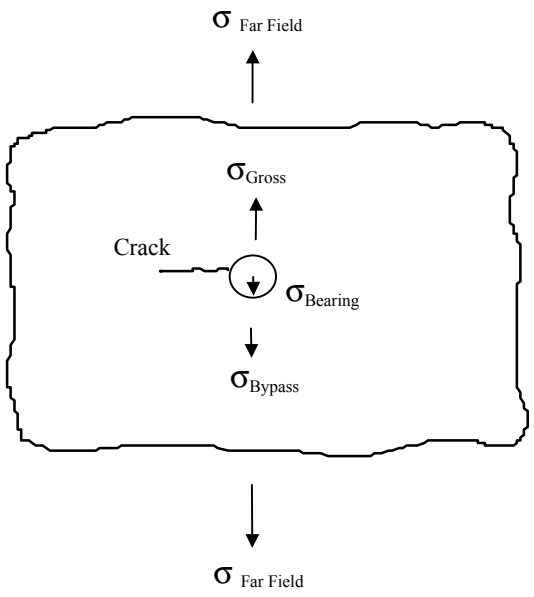

Figure F3. Skin Stresses Near a Fastener Hole

Analysis results are presented in terms of bearing factors, bypass factors, and stress scale factors in the database. The bearing and bypass factors are the ratios of the bearing and bypass stresses in the skin divided by the gross stress, respectively. The stress scale factor is the ratio between the gross stress and the reference applied far field stress. These factors are calculated as follows.

$$\text{Bearing Factor (BRF)} = \sigma_{Bearing}/\sigma_{Gross}$$

$$\text{Bypass Factor (BPF)} = \sigma_{Bypass}/\sigma_{Gross}$$

$$\text{Stress Scale Factor (SSF)} = \sigma_{Gross}/\sigma_{Far\ Field}$$

In the figures F4.1 through F7.3, analysis results in terms of (a) fastener load transfers, (b) bearing factors, (c) bypass factors, and (d) stress scale factors are presented for each stiffener location. The results are plotted for each stiffener area considered together with the case of zero area which means no stiffener.

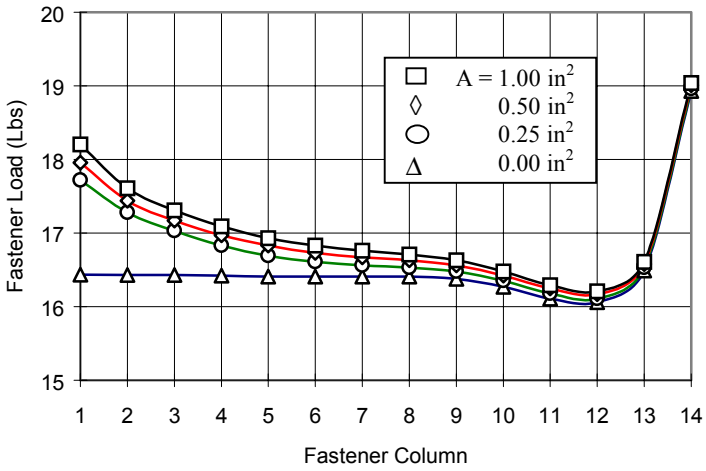

(a) Fastener Load Transfers

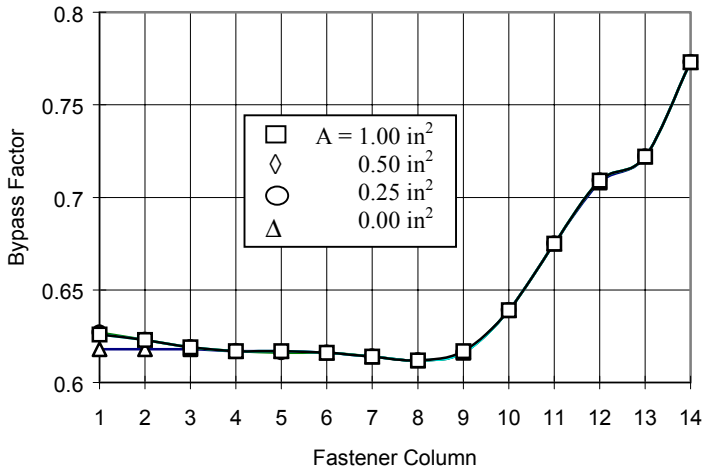

(c) Bypass Factors

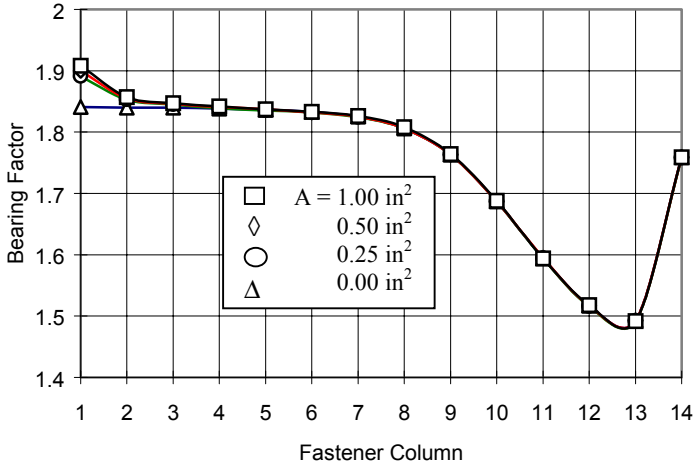

(b) Bearing Factors

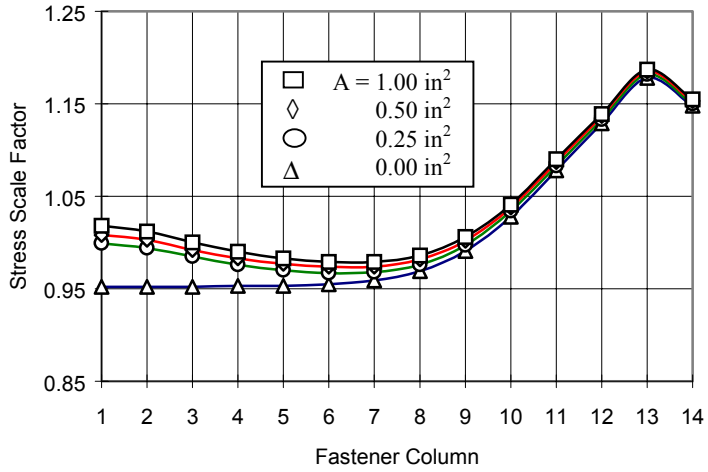

(d) Stress Scale Factors

Figure F4. Fastener Loads for Stiffener Located at the Center Fastener Column, Skin Thickness = 0.050″, Doubler Thickness = 0.063″

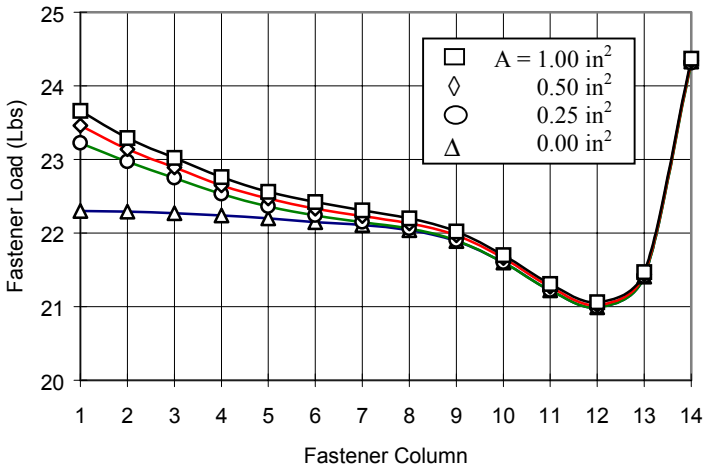

(a) Fastener Load Transfers

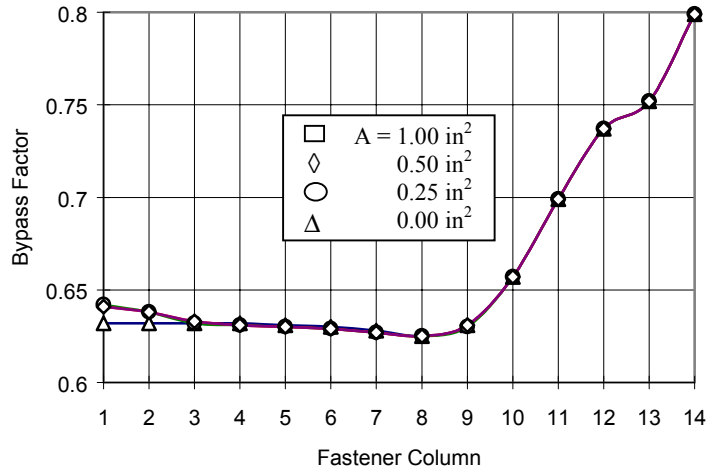

(c) Bypass Factors

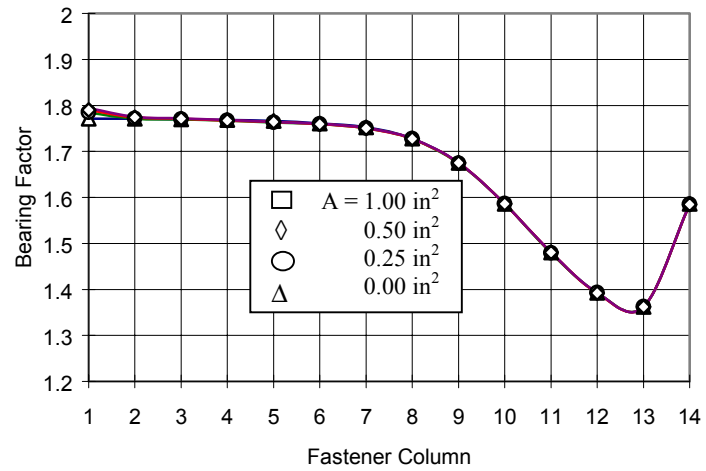

(b) Bearing Factors

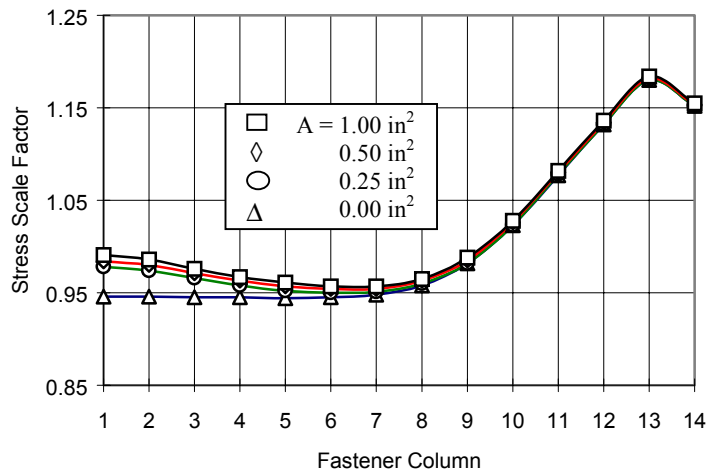

(d) Stress Scale Factors

Figure F5. Fastener Loads for Stiffener Located at the Center Fastener Column, Skin Thickness = 0.071″, Doubler Thickness = 0.080″

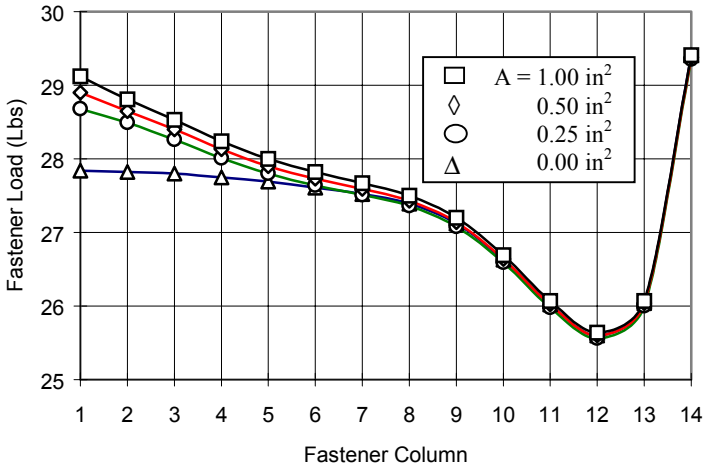

(a) Fastener Load Transfers

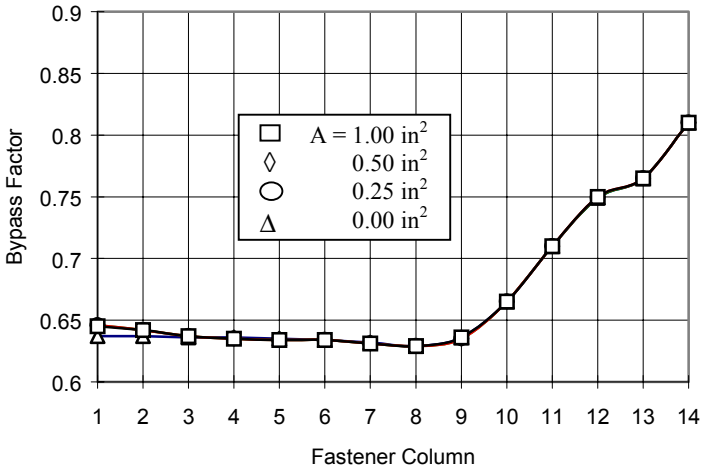

(c) Bypass Factors

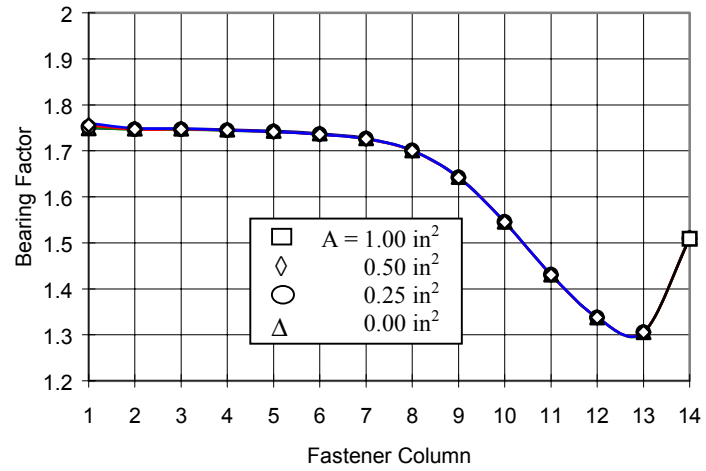

(b) Bearing Factors

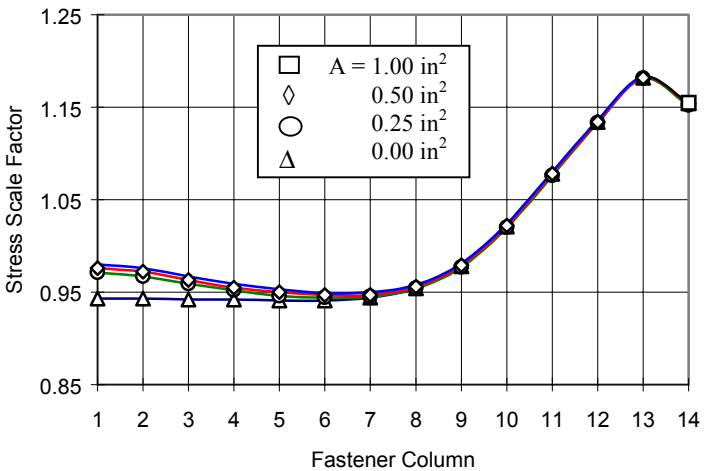

(d) Stress Scale Factors

Figure F6. Fastener Loads for Stiffener Located at the Center Fastener Column, Skin Thickness = 0.090″, Doubler Thickness = 0.100″

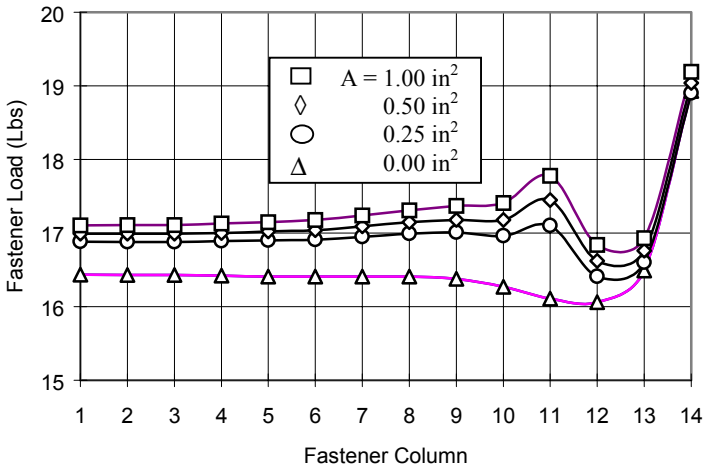

(a) Fastener Load Transfers

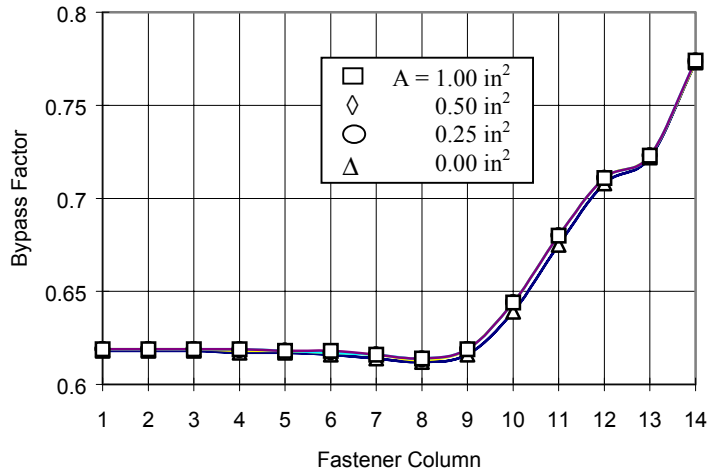

(c) Bypass Factors

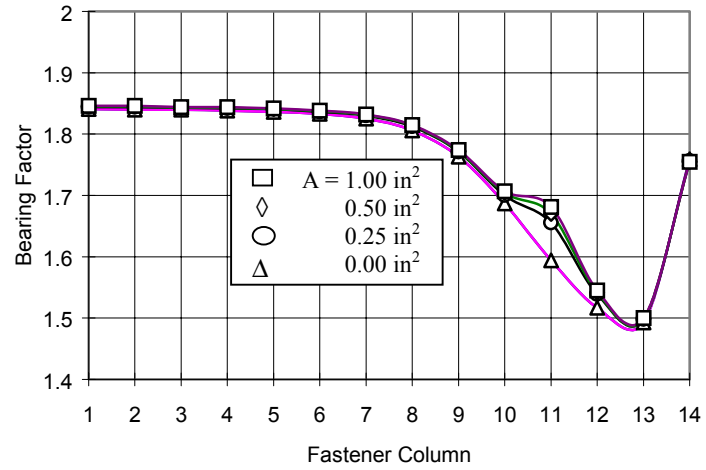

(b) Bearing Factors

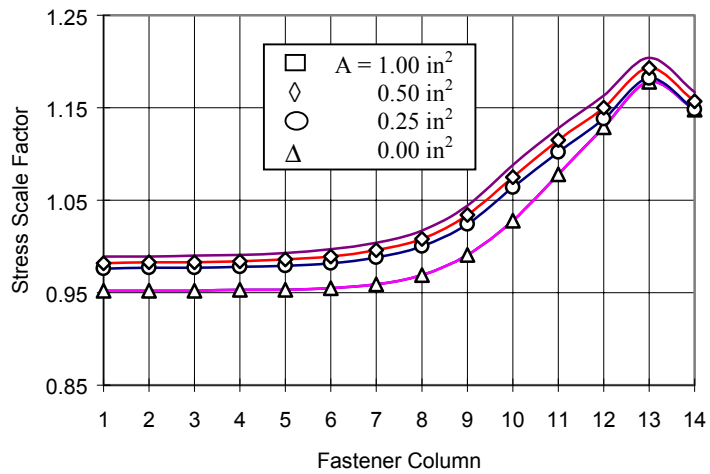

(d) Stress Scale Factors

Figure F7. Stiffener Located at the Fastener Column Alone the Edge of Skin Cutout, Skin Thickness = 0.050″, Doubler Thickness = 0.063″

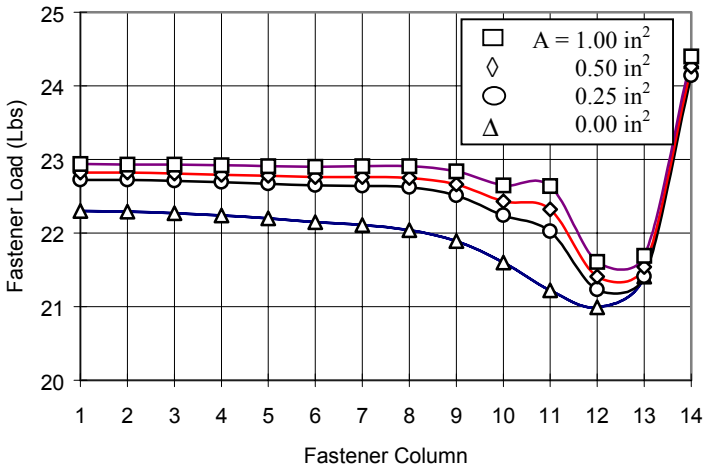

(a) Fastener Load Transfers

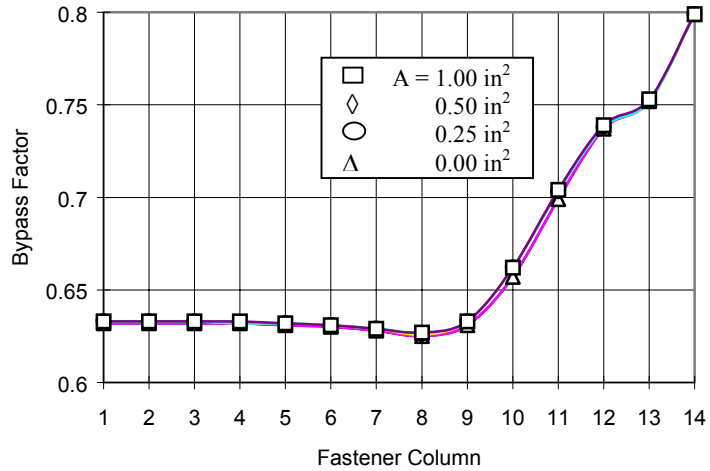

(c) Bypass Factors

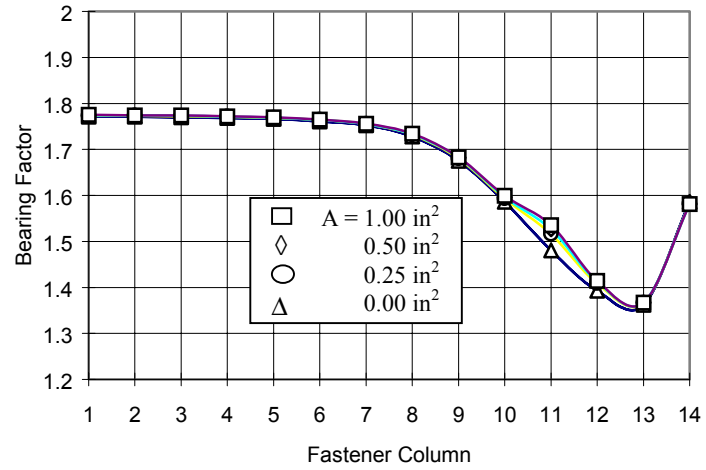

(b) Bearing Factors

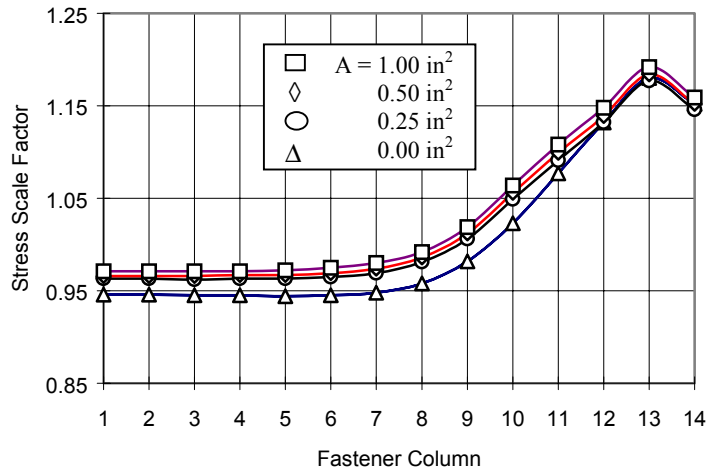

(d) Stress Scale Factors

Figure F8. Stiffener Located at the Fastener Column Alonf the Edge of Skin Cutout, Skin Thickness = 0.071″, Doubler Thickness = 0.080″

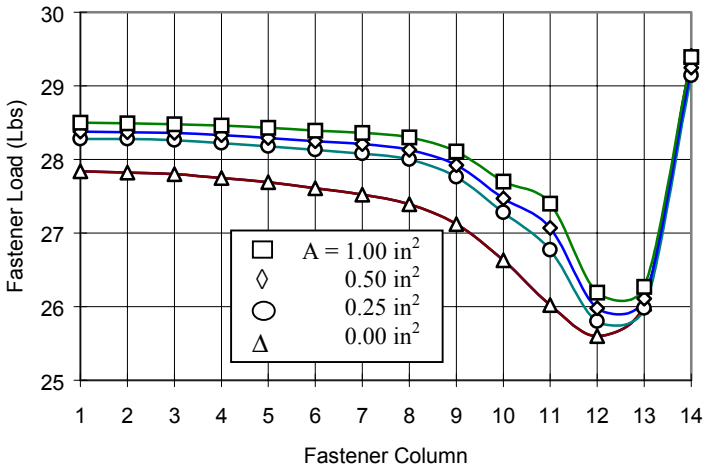

(a) Fastener Load Transfers

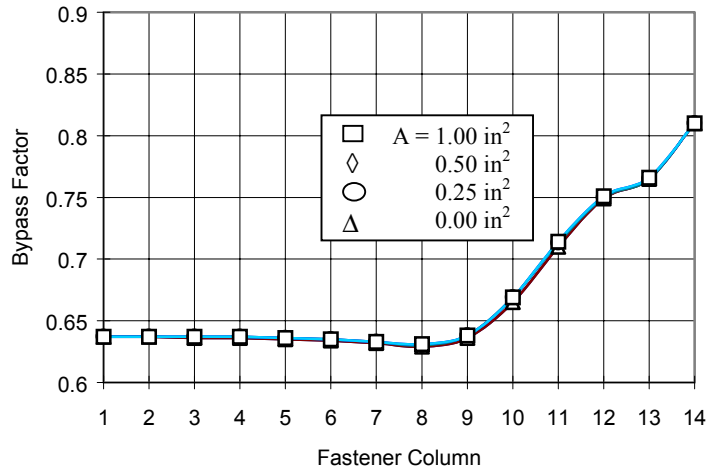

(c) Bypass Factors

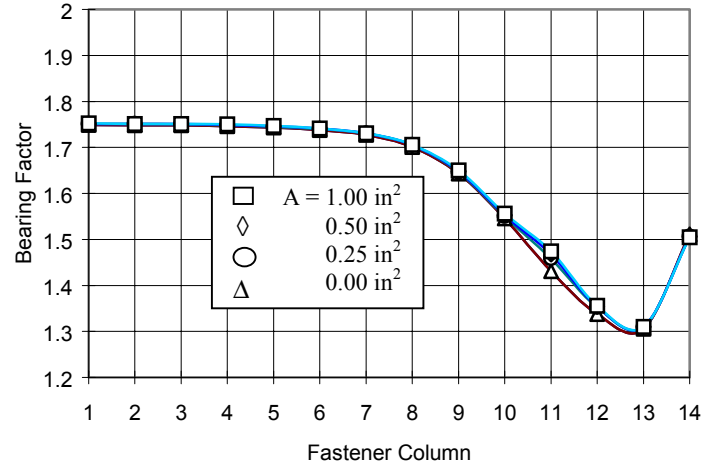

(b) Bearing Factors

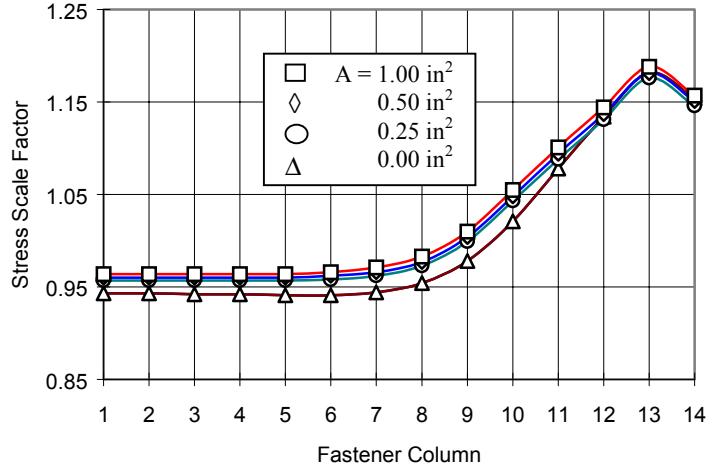

(d) Stress Scale Factors

Figure F9. Stiffener Located at the Fastener Column Alonf the Edge of Skin Cutout, Skin Thickness = 0.090″, Doubler Thickness = 0.100″

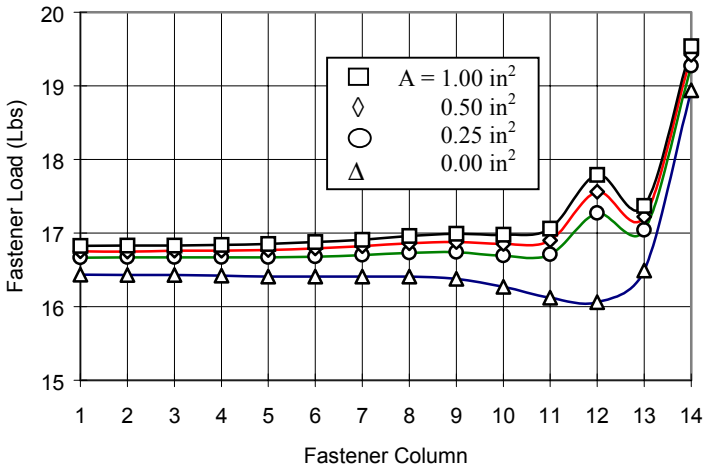

(a) Fastener Load Transfers

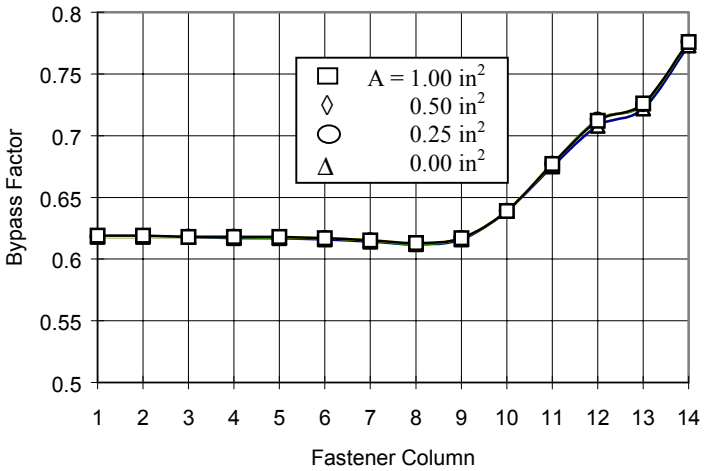

(c) Bypass Factors

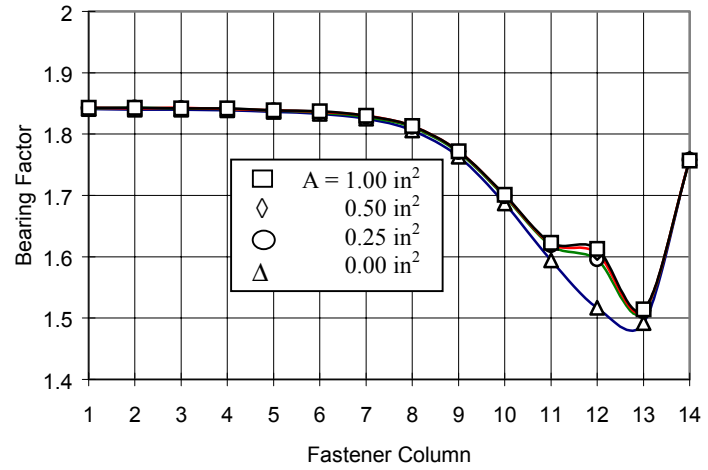

(b) Bearing Factors

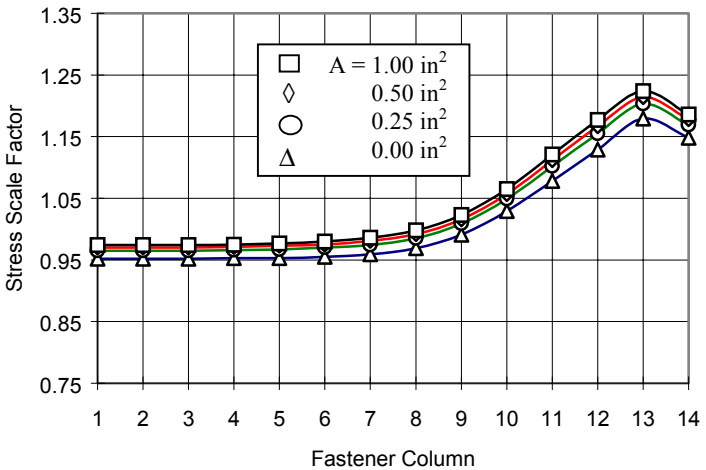

(d) Stress Scale Factors

Figure F10. Stiffener Located at the Fastener Column Next to Skin Cutout, Skin Thickness = 0.050″, Doubler Thickness = 0.063″

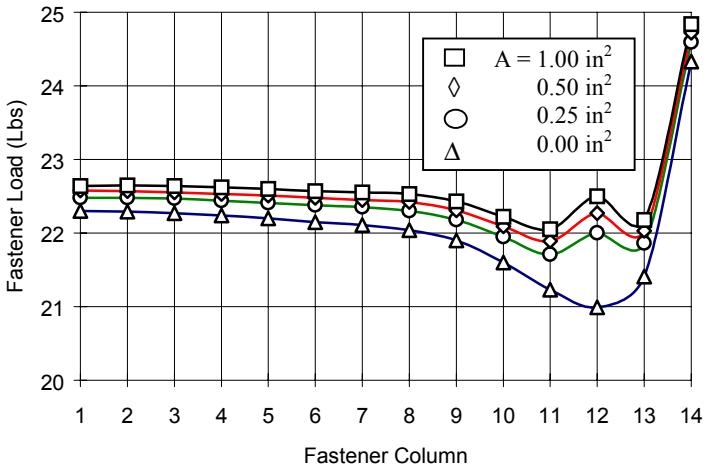

(a) Fastener Load Transfers

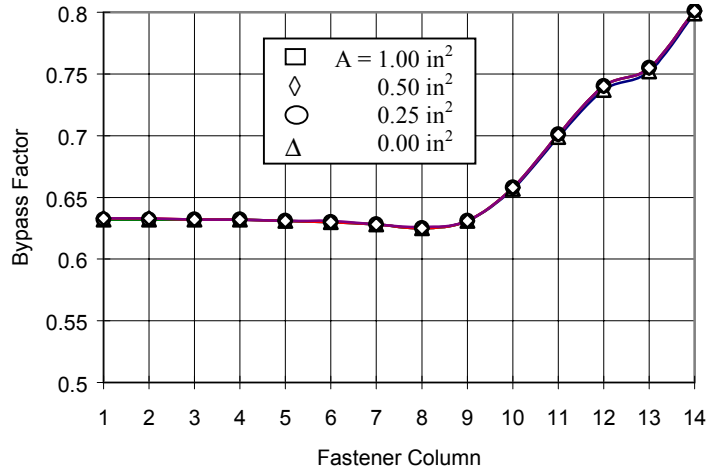

(c) Bypass Factors

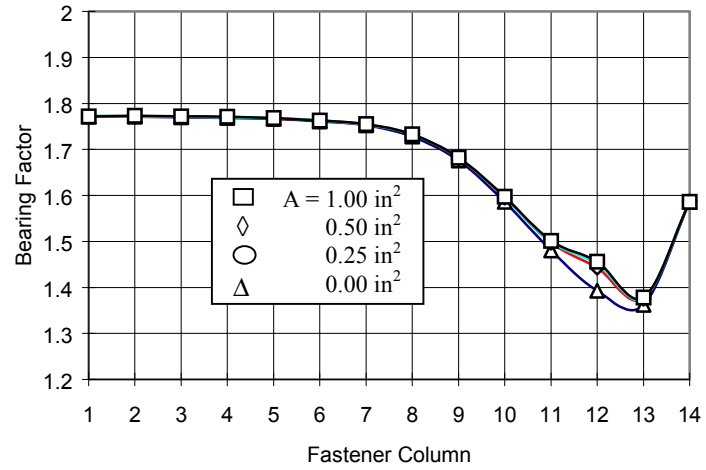

(b) Bearing Factors

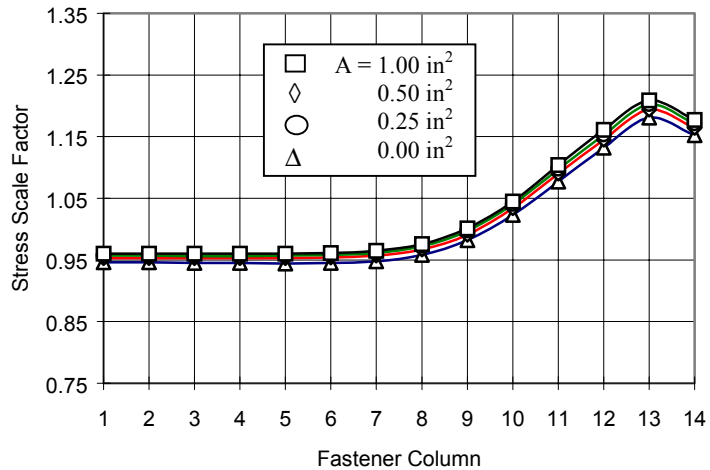

(d) Stress Scale Factors

Figure F11. Stiffener Located at the Fastener Column Next to Skin Cutout, Skin Thickness = 0.071″, Doubler Thickness = 0.080″

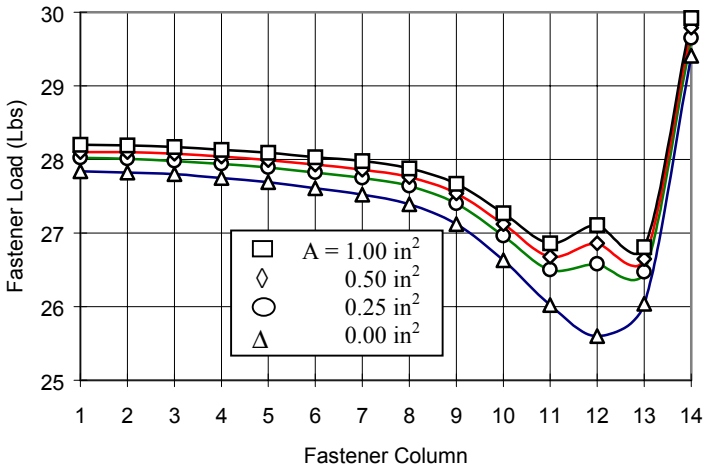

(a) Fastener Load Transfers

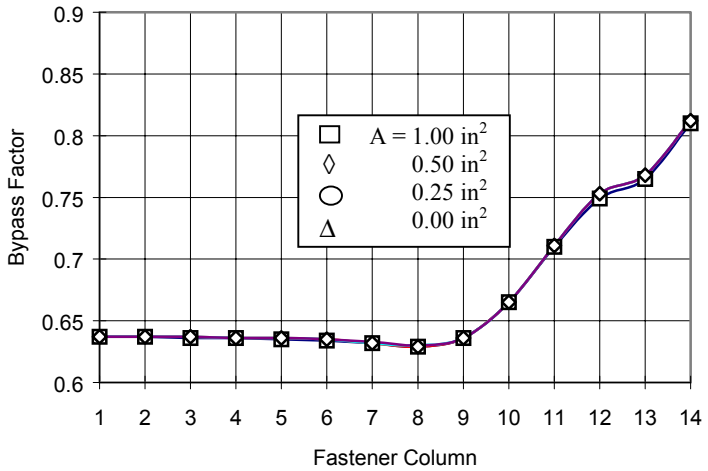

(c) Bypass Factors

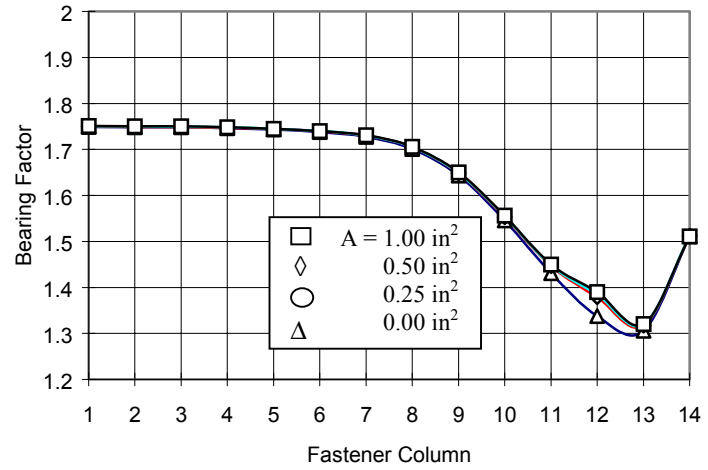

(b) Bearing Factors

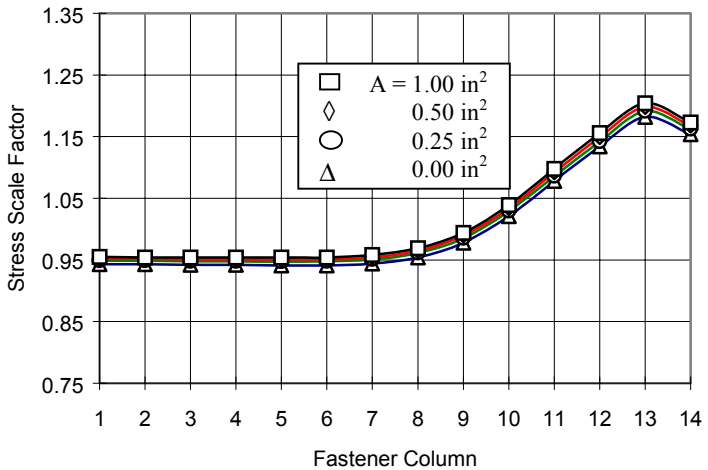

(d) Stress Scale Factors

Figure F12. Stiffener Located at the Fastener Column Next to Skin Cutout, Skin Thickness = 0.090″, Doubler Thickness = 0.100″

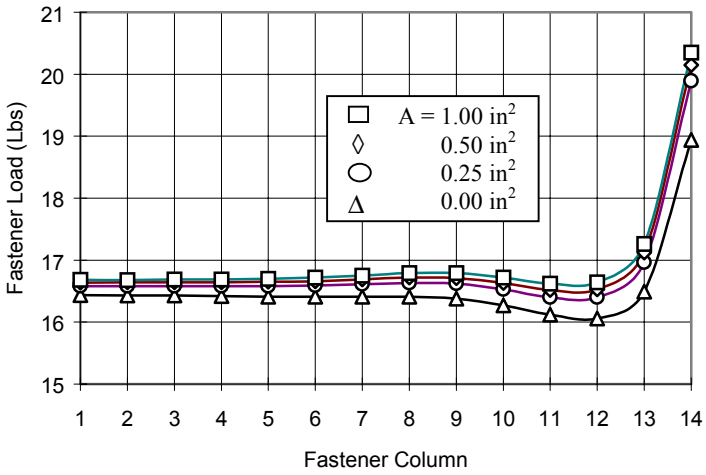

(a) Fastener Load Transfers

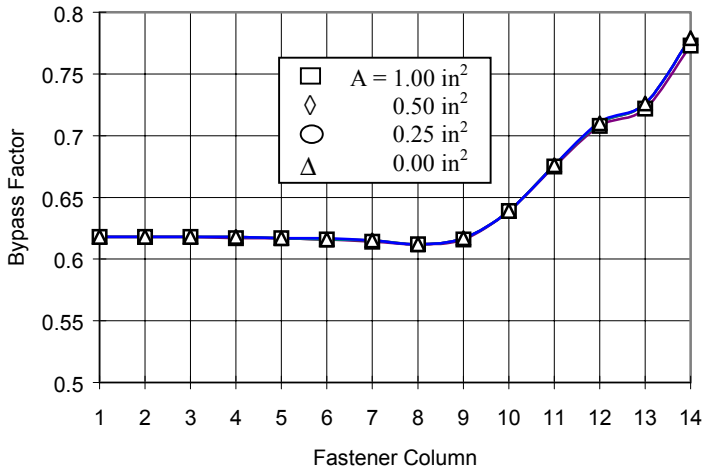

(c) Bypass Factors

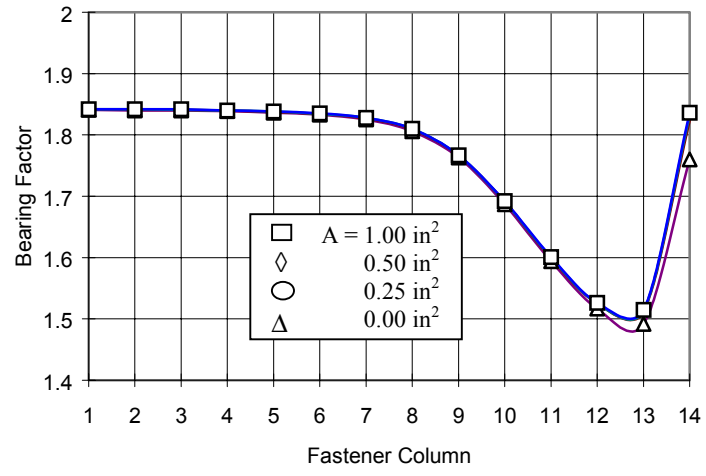

(b) Bearing Factors

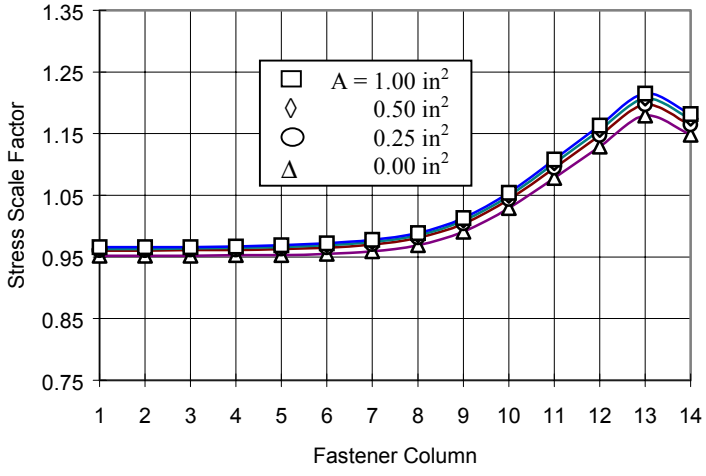

(d) Stress Scale Factors

Figure F13. Stiffener Located at the Corner Fastener Column, Skin Thickness = 0.050″, Doubler Thickness = 0.063″

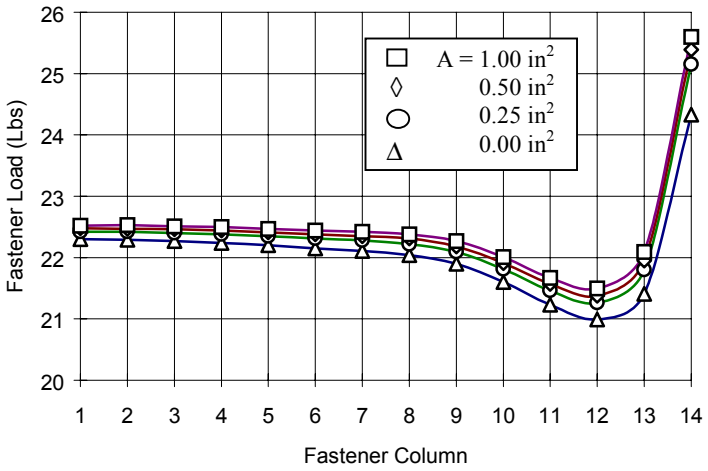

(a) Fastener Load Transfers

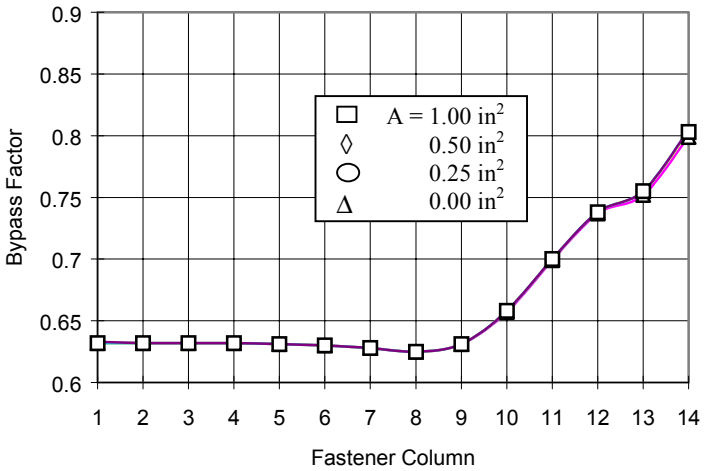

(c) Bypass Factors

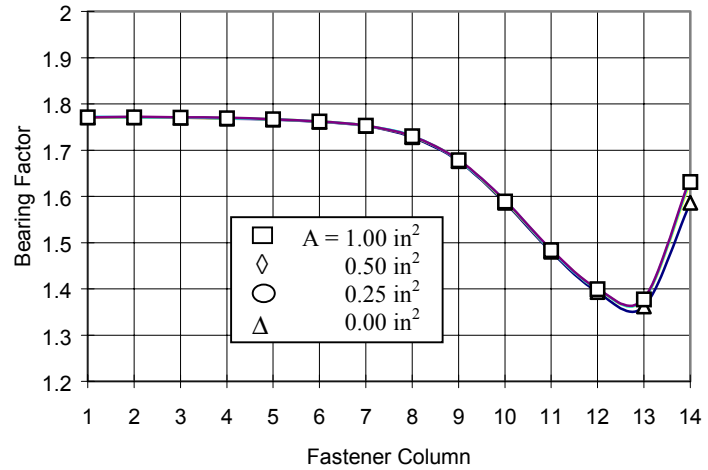

(b) Bearing Factors

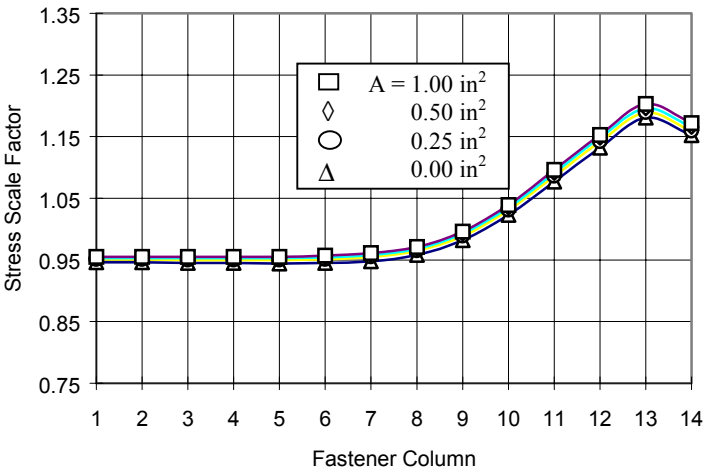

(d) Stress Scale Factors

Figure F14. Stiffener Located at the Corner Fastener Column, Skin Thickness = 0.071″, Doubler Thickness = 0.080″

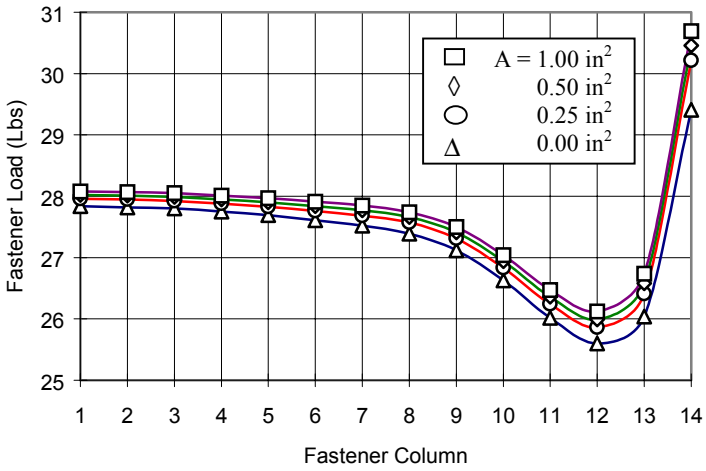

(a) Fastener Load Transfers

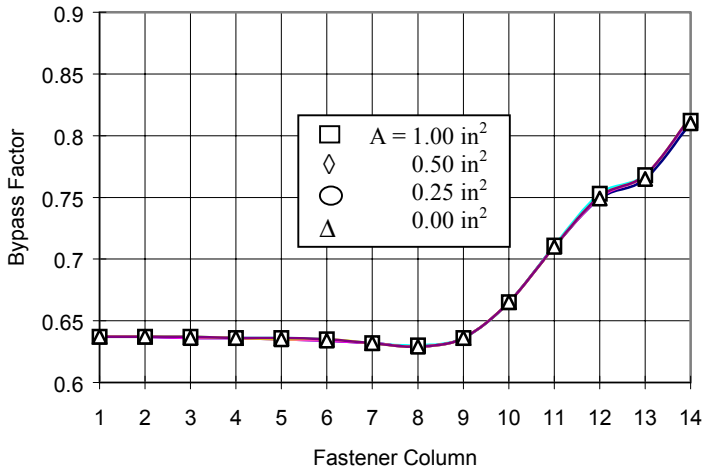

(c) Bypass Factors

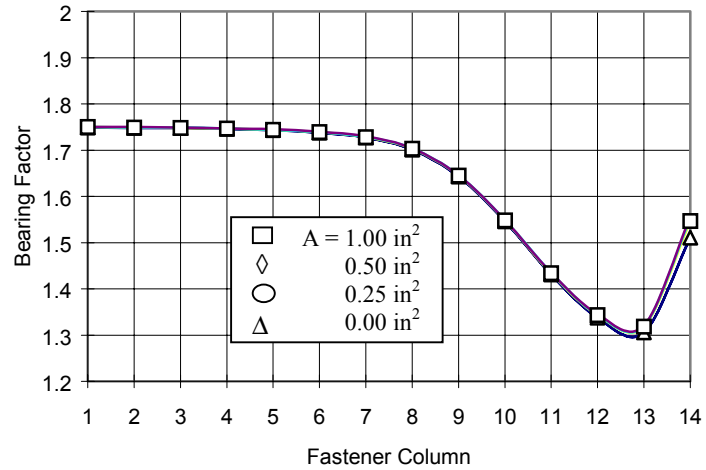

(b) Bearing Factors

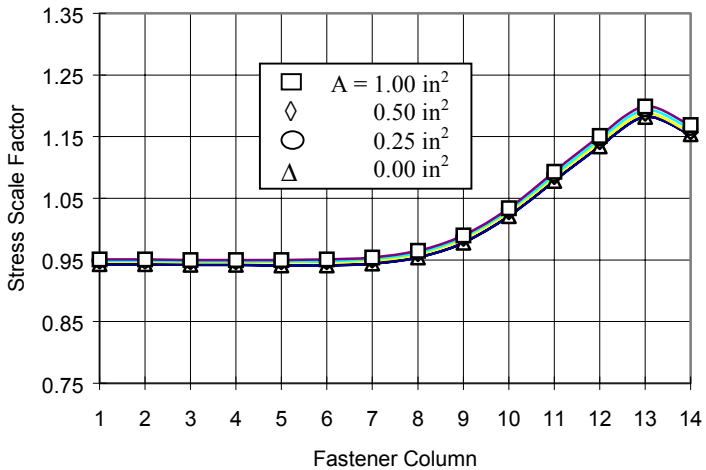

(d) Stress Scale Factors

Figure F15. Stiffener Located at the Corner Fastener Column, Skin Thickness = 0.090″, Doubler Thickness = 0.100″

F3. Geometry Factors

The stiffening effect on geometry factors compiled from reference 1 is provided below for the crack growth analysis of repairs at stiffeners. In the following presentation, the geometry factor is the ratio of the stress-intensity factor of a crack in the stiffened sheet divided by that of the Griffith crack in a unstiffened sheet. The following nomenclatures are used.

a = Half crack length
t = Sheet thickness
h = Fastener pitch
b = Center of crack to stiffener (figure 18)
or Stiffener spacing (figure 19)
A = Stiffener cross-sectional area
E_1 = Young's modulus of sheet
E_2 = Young's modulus of stiffener
$\lambda = 2E_1 at / (AE_2)$
$s = E_2 A / (E_1 bt)$

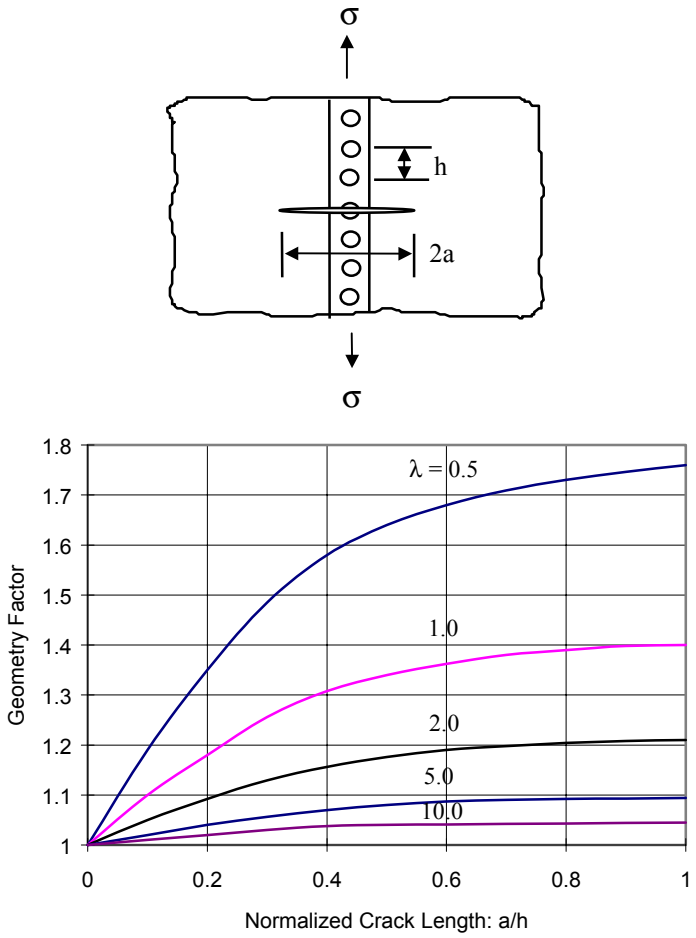

Figure F16. Crack Symmetrical About a Stiffener (Stiffener Broken at Crack Line)

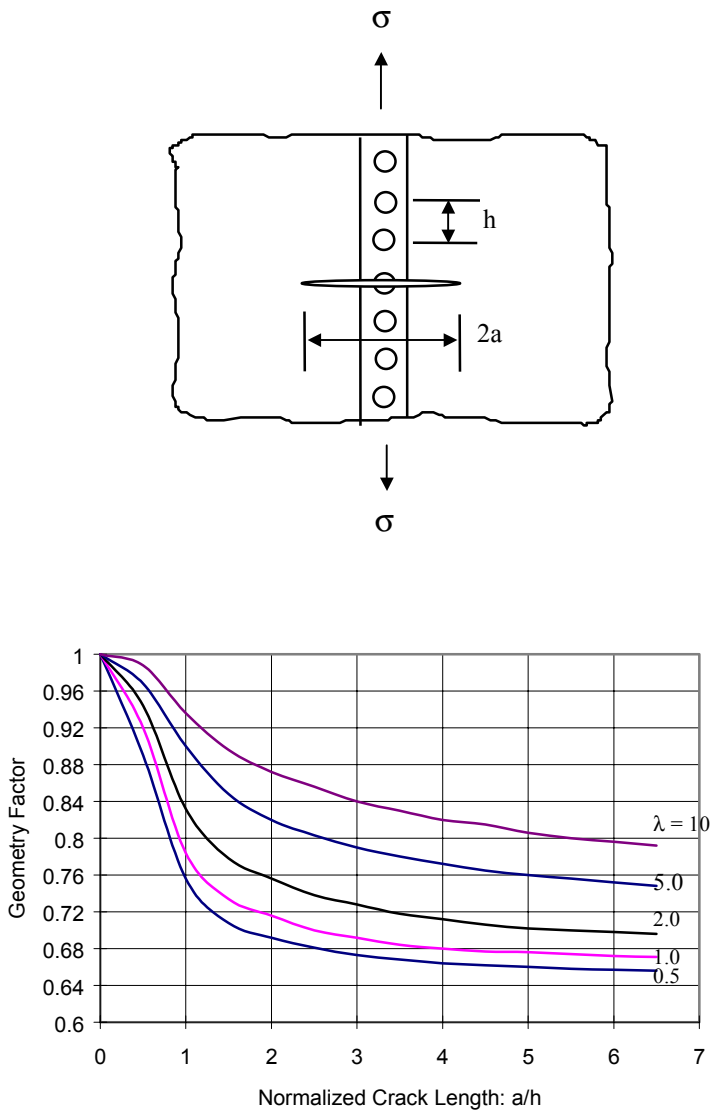

Figure F17. Crack Symmetrical About a Stiffener (Stiffener Intact at Crack Line)

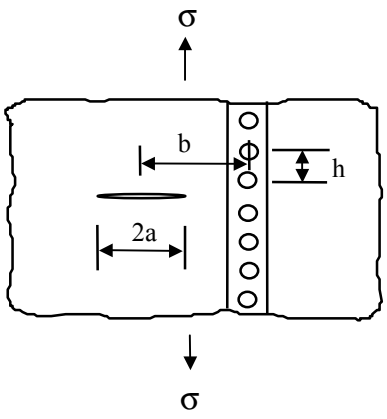

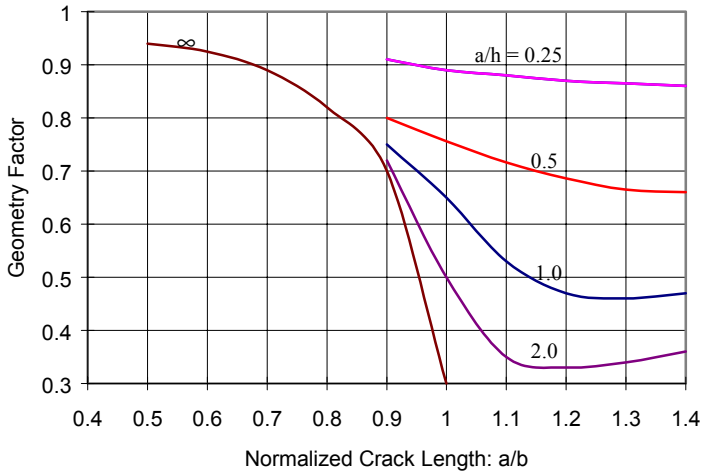

λ = 0.5

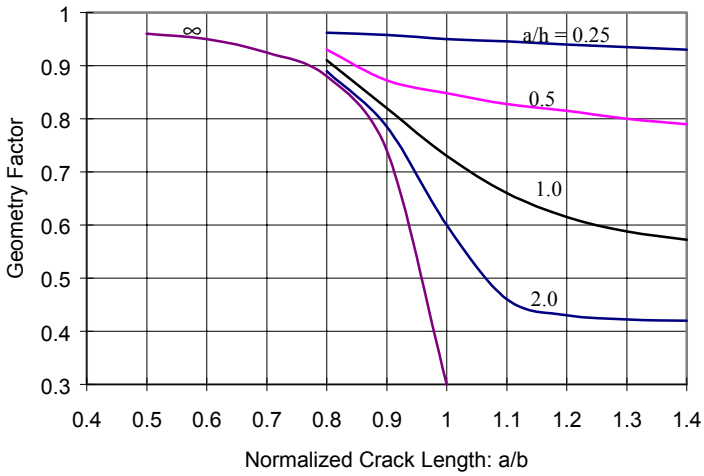

λ = 2.0

Figure F18. Crack Near a Stiffener in a Sheet

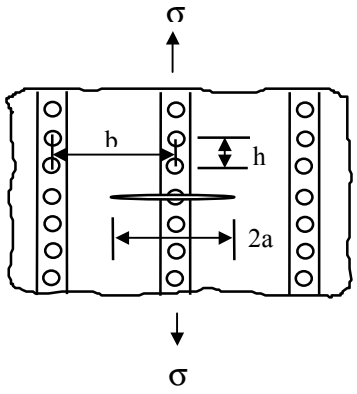

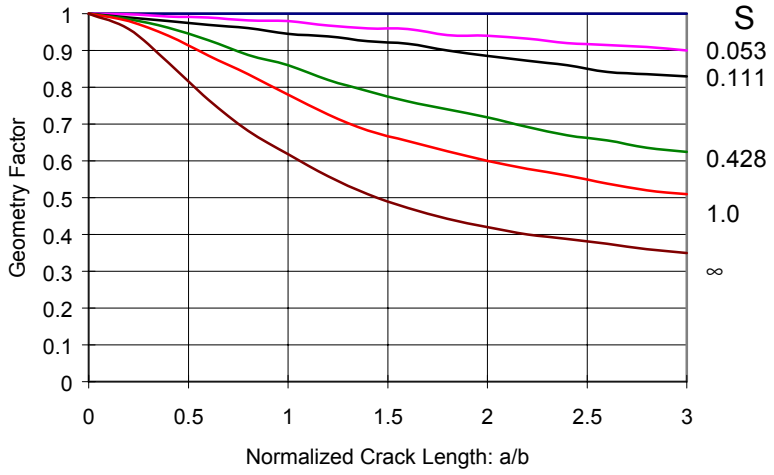

h/b = 1.0

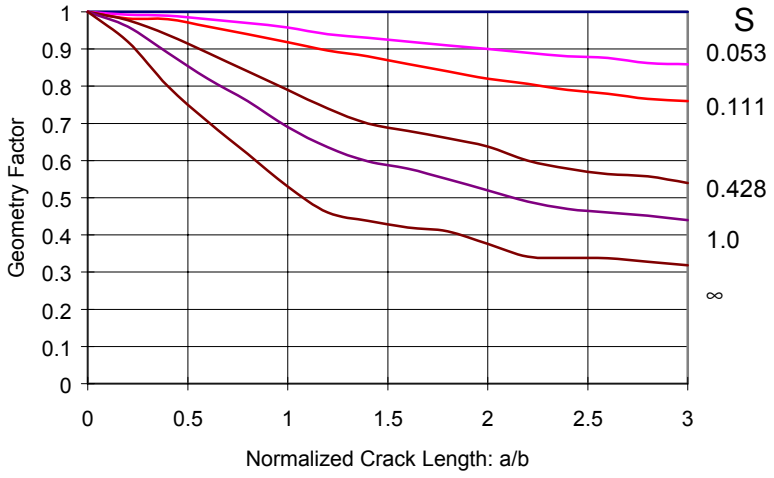

h/b = 2/3

Figure F19. Crack in a Sheet With Periodically Spaced Stiffeners, Crack at Stiffener

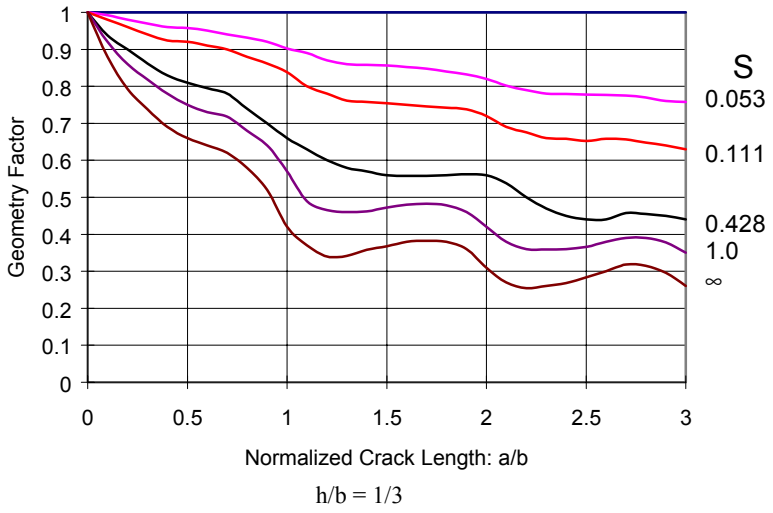

h/b = 1/3

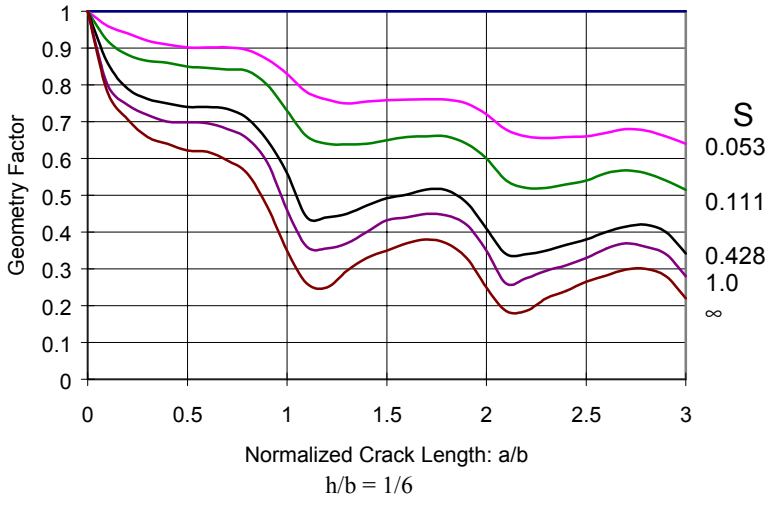

h/b = 1/6

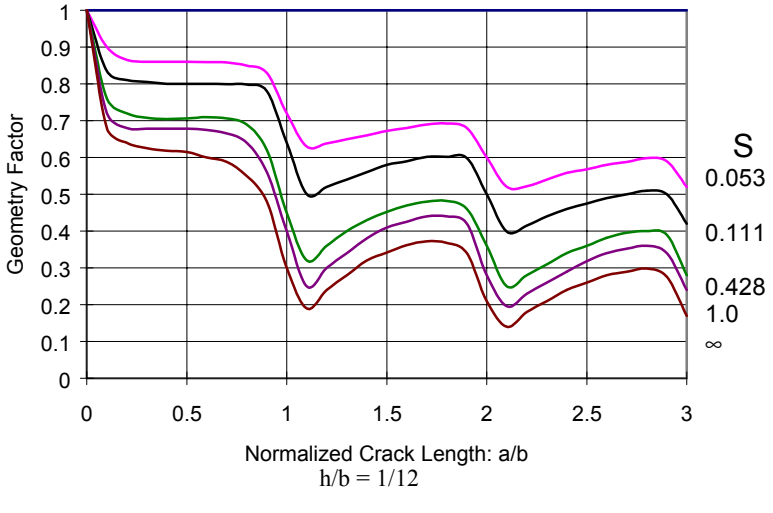

h/b = 1/12

Figure F19. Crack in a Sheet With Periodically Spaced Stiffeners, Crack at Stiffener (Continued)

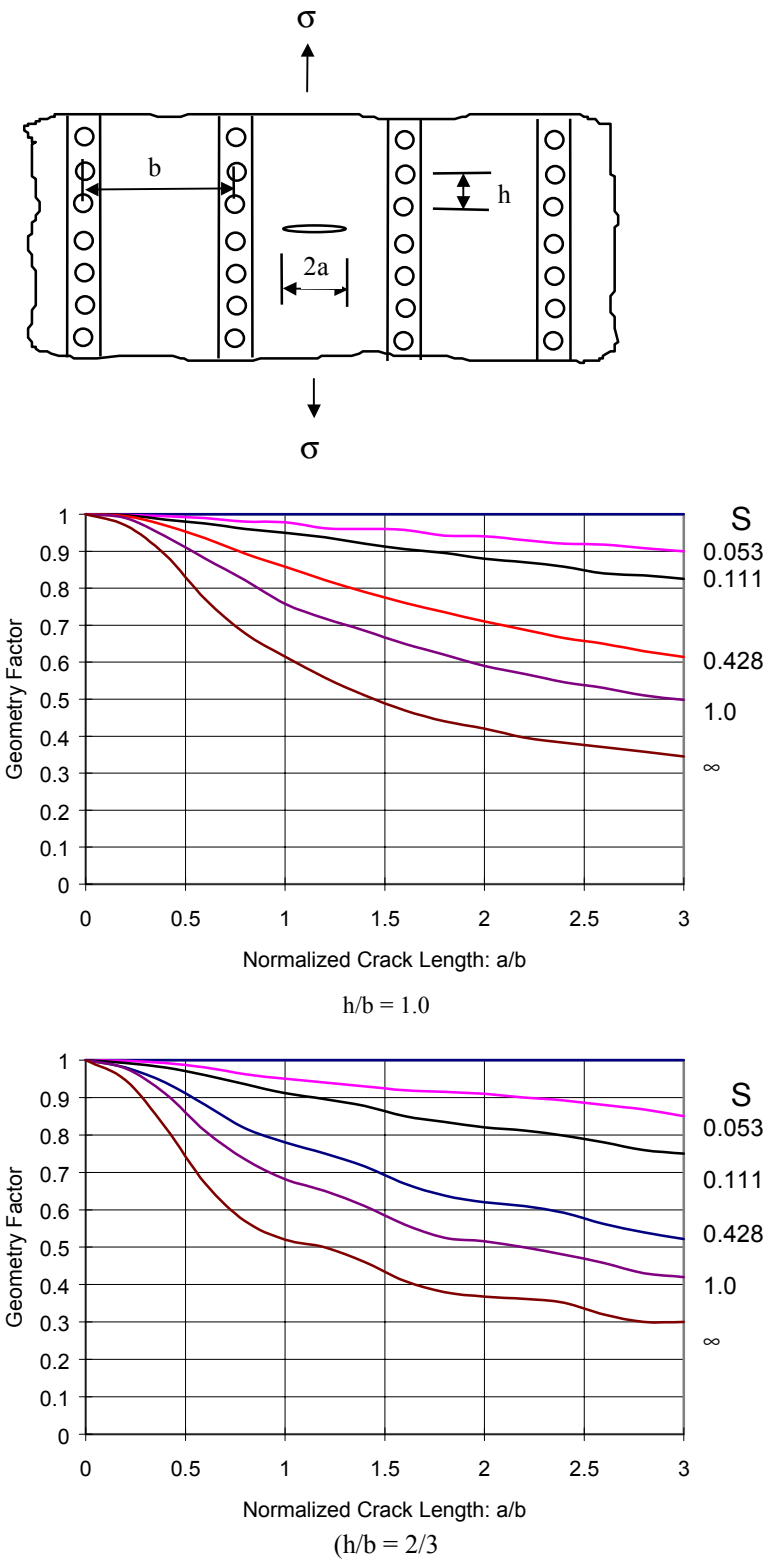

Figure F20. Crack in a Sheet With Periodically Spaced Stiffeners (Crack Midway Between Two Stiffeners)

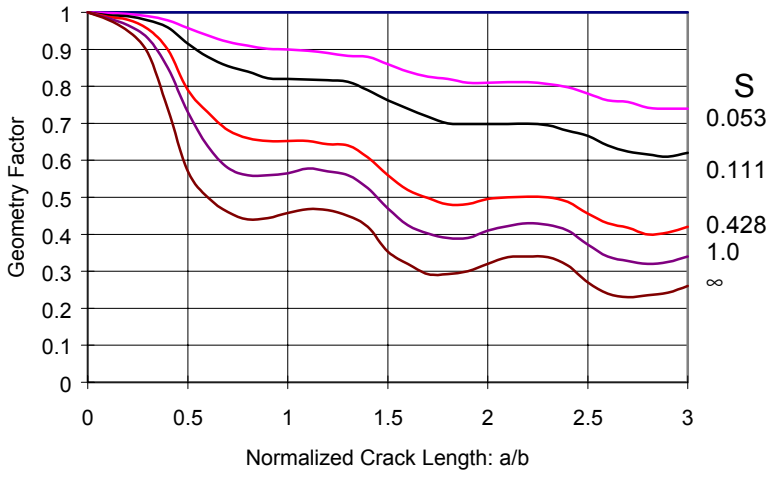

h/b = 1/3

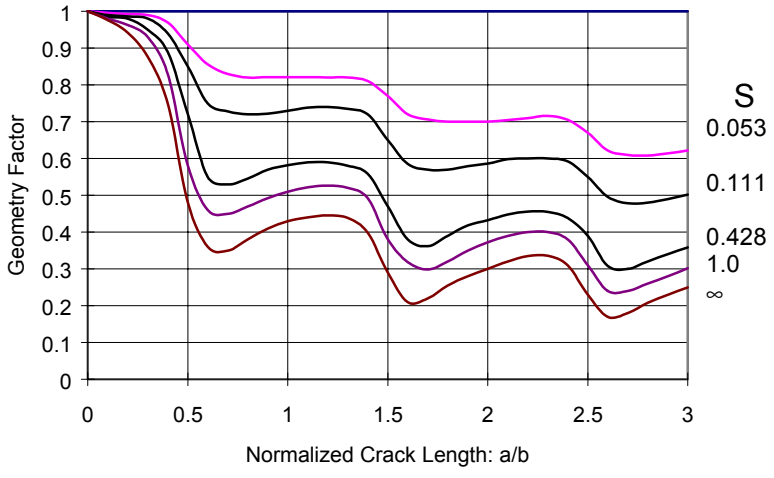

h/b = 1/6

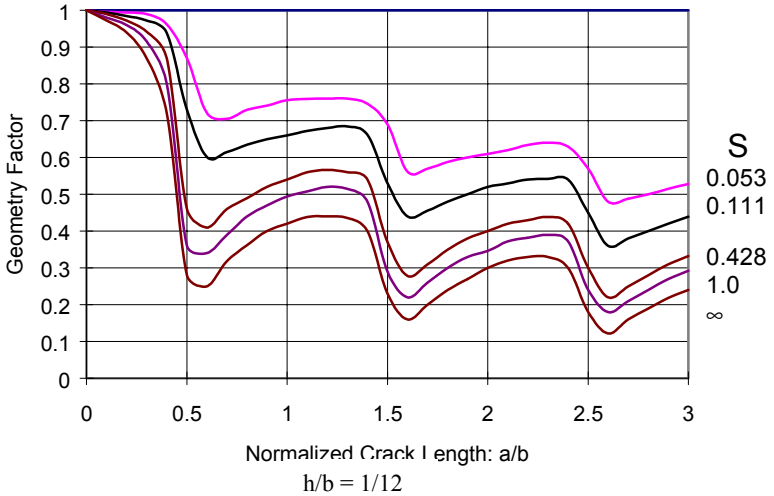

h/b = 1/12

Figure F20. Crack in a Sheet With Periodically Spaced Stiffeners, Crack Midway Between Two Stiffeners (Continued)

Reference

1. "Compendium of Stress Intensity Factors," D. P. Rooke and D. J. Cartwright, London, Her Majesty's Stationery Office, 1976.

Appendix G - Circular Repairs

G1. Introduction

This appendix describes the analysis of circular skin repairs to determine the load transfer at the critical fastener location.

G2. Approach

The analysis is performed using the finite element code FRANC2D/L [1]. Generally, a circular skin repair consists of a circular cutout replaced with a circular repair doubler. The doubler is mechanically fastened to the skin with fasteners arranged in a circular pattern. Figure G1 shows a typical circular skin repair.

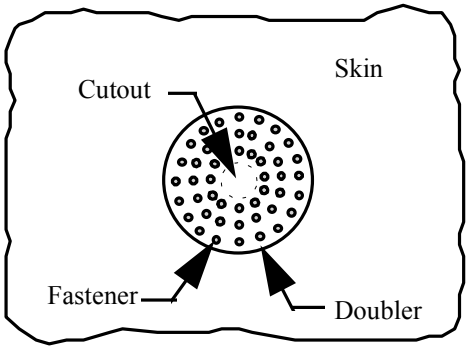

Figure G1. A Circular Skin Repair

Parameters considered in the analysis of circular skin repairs include

- Skin cutout size: 1″, 3″, and 5″ in diameter
- Skin thickness: 0.032″, 0.040″, 0.050″, 0.063″, and 0.071″
- Repair doubler thickness: 0.050″, 0.063″, 0.071″, and 0.080″
- Fastener size: 1/8″ and 1/4″
- Fastener materials: aluminum and steel
- Number of fastener rings: 3

Due to double symmetry of the geometry and the stress applied to the skin, the analysis is performed on one quarter of the repaired skin. A typical finite element model for FRANC2D/L analysis is shown below in figure G2.

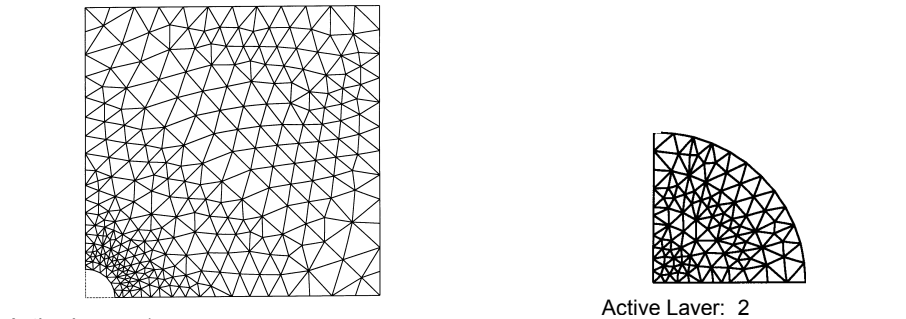

(a) Skin (b) Repair Doubler

Figure G2. FRANC2D/L Model of a Circular Repair

In the analysis, the skin and the repair doubler are modeled using the six-node triangular membrane element. The shear rigidity of fasteners is calculated based on the Swift's equation:

$$K = \frac{Ed}{A + B\left(\frac{d}{t_{Skin}} + \frac{d}{t_{Doubler}}\right)}$$

where E is the average modulus of skin and doubler materials, d is the fastener hole diameter, t_{Skin} and $t_{Doubler}$ are the thicknesses of the skin and doubler, respectively, and A and B are empirical constants taking the values of 5.0 and 0.8 for aluminum rivets, and 1.66 and 0.86 for steel rivets. The calculated value is input directly to the FRANC2D/L program. In the analysis, the repaired skin is subjected to a reference uniaxial far field stress of 1000 psi.

To perform the damage tolerance analysis of circular skin repairs, the stress field near the critical fastener hole needs to be known. Let the skin stress prior to the load transfer be referred as the gross stress, the bearing stress be the average hole bearing stress in the skin exerted by the fastener load, and the bypass stress be the skin stress after the load transfer. These skin stresses are shown in figure G3.

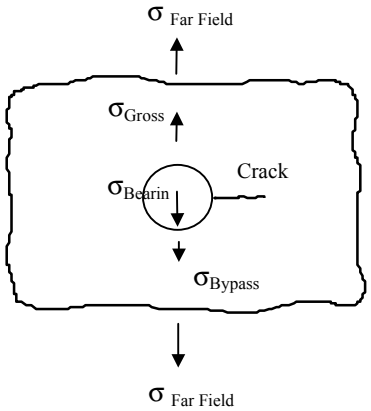

Figure G3. Skin Stresses Near a Fastener Hole

G3. Fastener Load Results

Analysis results are presented in terms of bearing factors, bypass factors, and stress scale factors in the database. The bearing, bypass, and stress scale factors are the ratios of the bearing, bypass, and gross stresses in the skin divided by the applied reference far field stress, respectively. These factors are calculated as follows.

$$\text{Bearing Factor (BRF)} = \sigma_{Bearing}/\sigma_{Far\ Field}$$
$$\text{Bypass Factor (BPF)} = \sigma_{Bypass}/\sigma_{Far\ Field}$$
$$\text{Stress Scale Factor (SSF)} = \sigma_{Gross}/\sigma_{Far\ Field}$$

A review of the FRANC2D/L analysis shows that the critical fastener is located at the top of the outer fastener ring as shown in figure G4. Also shown in the figure is the stress field pattern in the neighborhood of critical fastener hole. The skin stress prior to the load transfer decreases from the maximum gross stress σ_{Gross} to the far field stress $\sigma_{Far\ Field}$ in about ten fastener diameters. The bypass stress increases to the far field stress in the same distance as that of the gross stress.

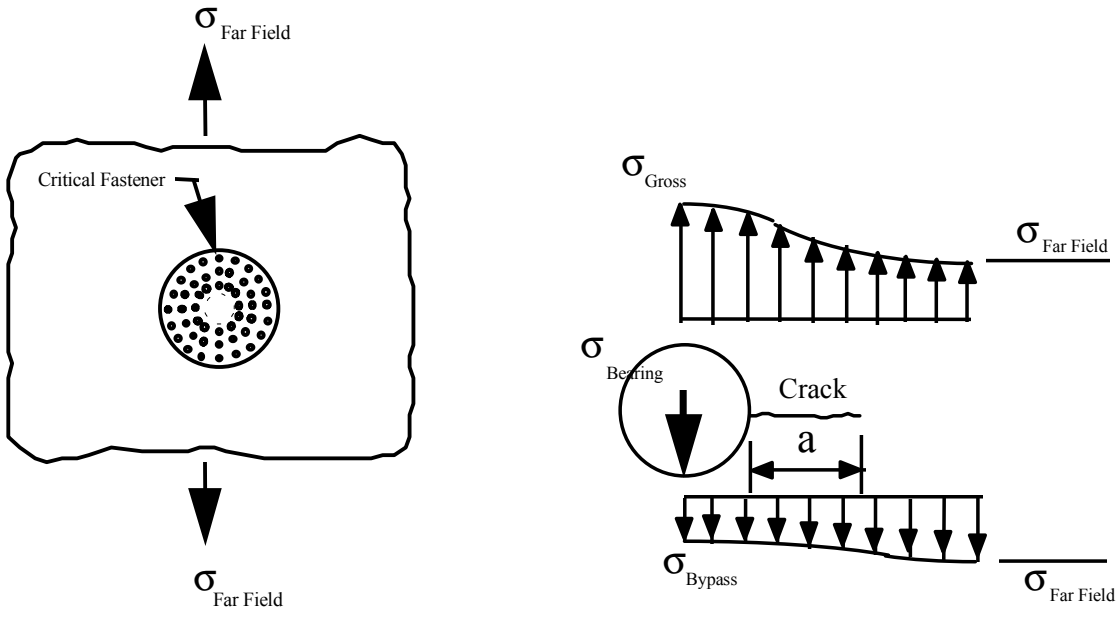

(a) Critical Fastener (b) Skin Stresses

Figure G4. Critical Fastener and Skin Stress

Analysis results of (a) bearing factors, (b) bypass factors, and (c) stress scale factors at the critical fastener location are presented in graphical form in figures G 5 through G8.

(a)

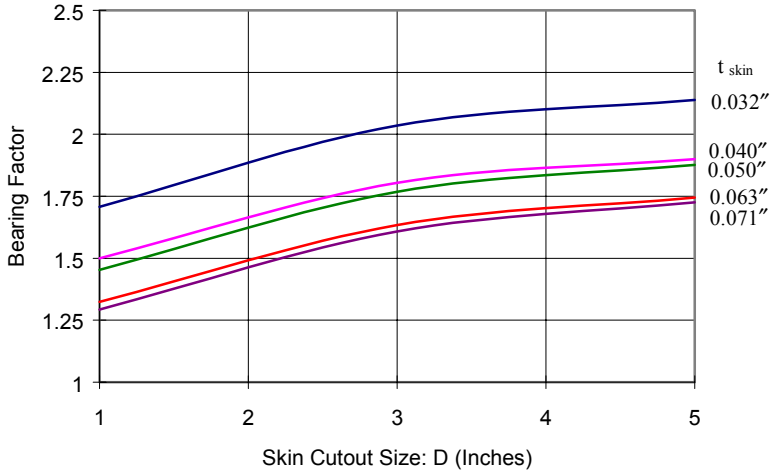

(b)

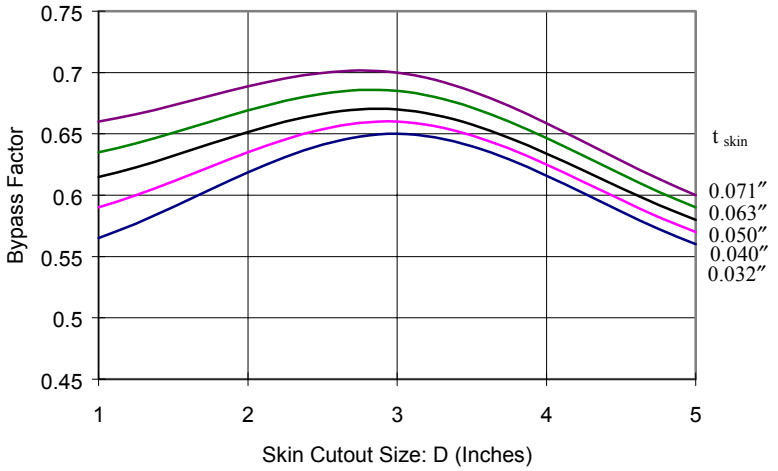

(c)

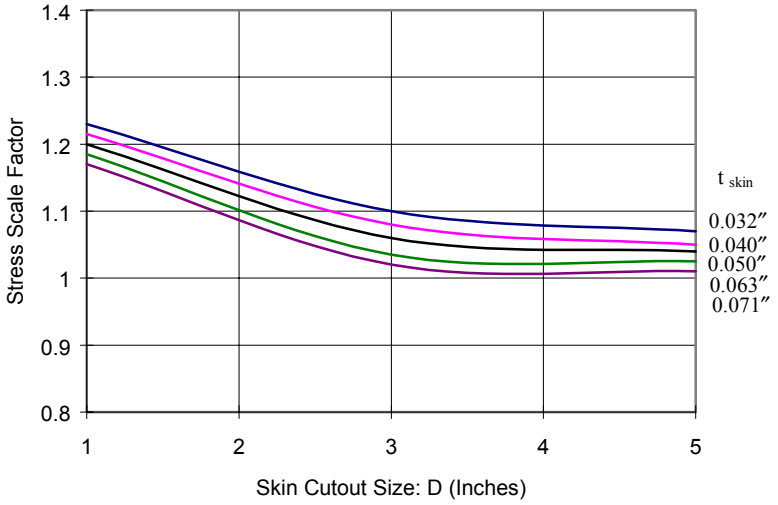

Figure G5. Analysis of Results of Repairs Using 1/8″ Aluminum Fasteners (a) Bearing Factors (b) Bypass Factors (c) Stress Scale Factors

(a)

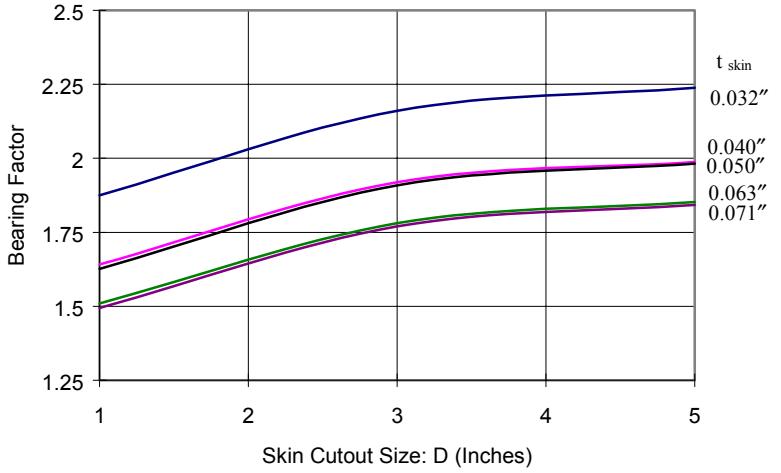

(b)

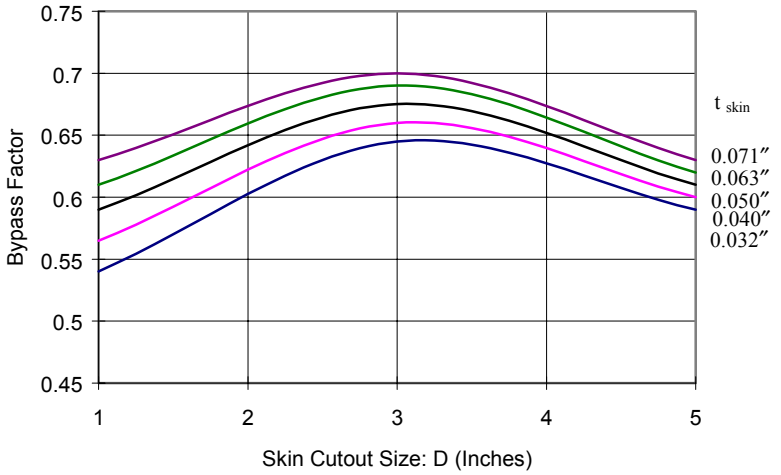

(c)

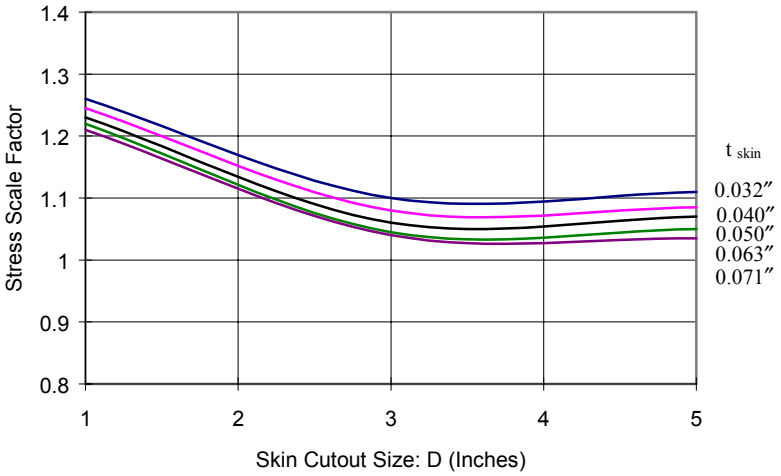

Figure G6. Analysis of Results of Repairs Using 1/8″ Steel Fasteners (a) Bearing Factors (b) Bypass Factors (c) Stress Scale Factors

(a)

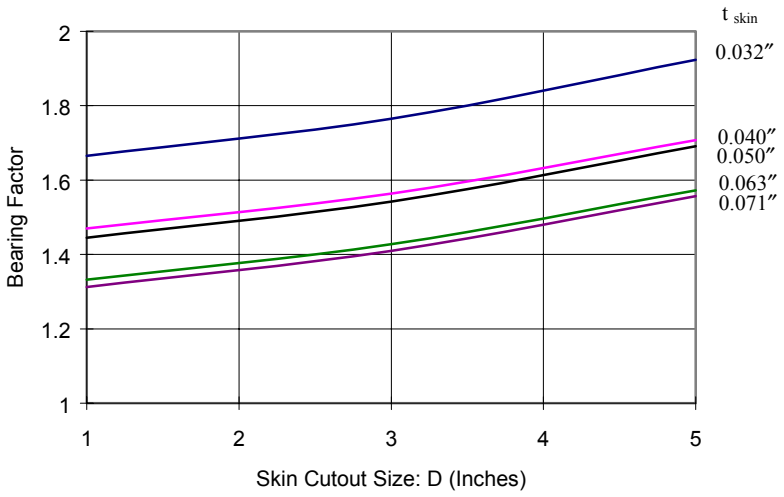

(b)

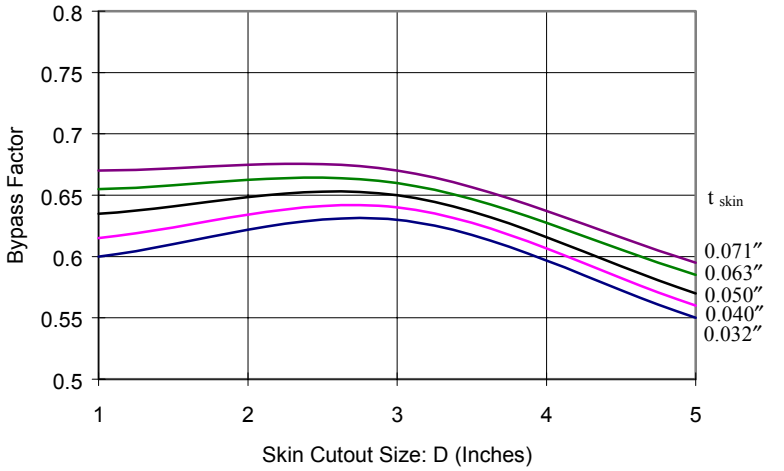

(c)

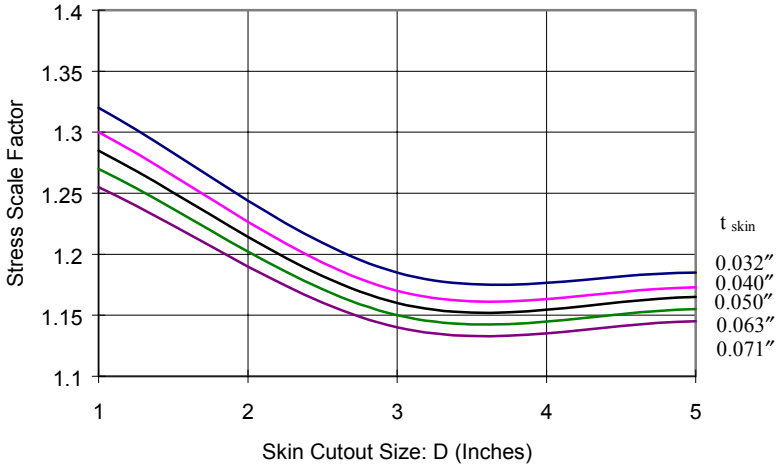

Figure G7. Analysis of Results of Repairs Using 1/4″ Aluminum Fasteners (a) Bearing Factors (b) Bypass Factors (c) Stress Scale Factors

(a)

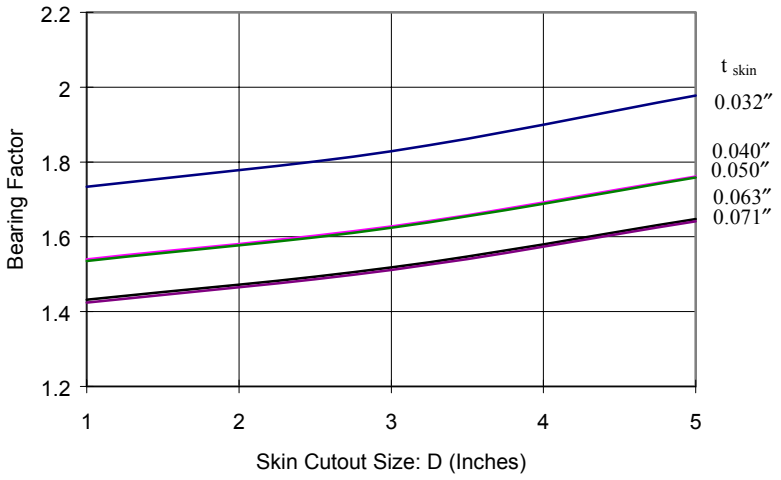

(b)

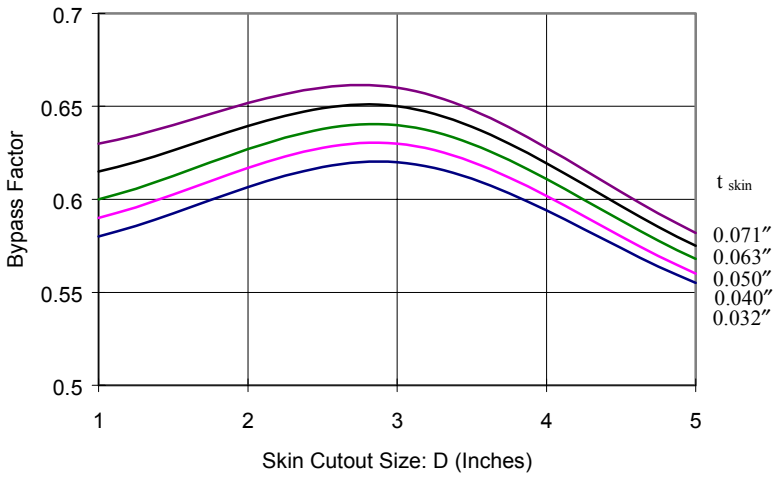

(c)

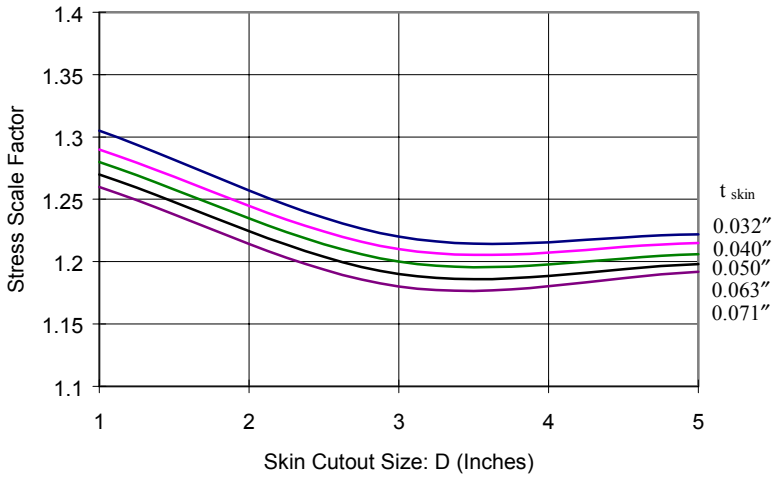

Figure G8. Analysis of Results of Repairs Using 1/4″ Steel Fasteners (a) Bearing Factors (b) Bypass Factors (c) Stress Scale Factors

To perform the damage tolerance analysis of a circular repair, the stress-intensity factor is calculated by the equation

$$K = \sigma_{\text{Far Field}} \sqrt{\pi a}\, \beta$$

where the geometry factor β is calculated as

$$\beta = \frac{1}{2}\left[(\text{SSF} + \text{BPF})\beta_{\text{Far Field}} + \text{BRF}\,\beta_{\text{Pin Loads}} \right]$$

The factors $\beta_{\text{Far Field}}$ and $\beta_{\text{Pin Loads}}$ are the geometry factors of a crack emanating from a hole in a wide plate subjected to far field stress and a pair of pin loads in the hole, respectively. Once the stress-intensity factor has been calculated, RAPIDC performs the residual strength and crack growth analysis of the circular repairs described in section 3.0.

Reference

1. FRANC2D/L: A Crack Propagation Simulator for Plane Layered Structures, Version 1.0 User's Guide, Kansas State University, Manhattan, Kansas.

Appendix H: RAPID-FEM Program

This appendix documents the use and validation, when feasible, of the RAPID-FEM program developed by Cornell University for RAPID under the FAA contract. RAPID-FEM is a two-dimensional finite element plane stress analysis program for multiple-layer sheet structures. The stack-up layers of the structure are connected at discrete joints via mechanical fasteners. Although RAPID-FEM is a general-purpose 2-D finite element program, it is intended for RAPID to perform the stress analysis of common repairs and antenna installations on fuselage skin.

Specifications for the inputs to and outputs from RAPID-FEM were initially defined by Cornell University and were finalized after several iterations of discussion with Boeing. Boeing manually prepared ASCII input files of five examples serving as benchmark problems to help Cornell develop the program. These examples include

- a circular antenna installation
- an elliptical antenna installation
- a rectangular antenna installation
- a 2-layer rectangular repair
- a 2-layer door opening repair

During the development cycle of the RAPID-FEM code, Boeing conducted beta testing of the program. Boeing then incorporated the stress intensity factor solution routines for arbitrary stress distribution along the potential crack paths.

RAPID-FEM consists of two modules, the mesher and the analysis modules. The mesher module reads ASCII input file describing the geometry and material properties of the layered structure and automatically creates finite element meshes of each layer. The analysis module assembles the stiffness of each layer and performs stress analysis of the layered structure subject to two separate reference stresses in the circumferential and longitudinal directions as prescribed in the input file.

Outputs from RAPID-FEM include load transfers at selected fasteners and stress gradients along potential crack paths in the skin layer.

Each of the five example problems representing a unique repair or a typical antenna installation was analyzed and documented in this Appendix. Validation of the RAPID-FEM program was conducted on antenna installation problems by removing all fasteners and the mounting plate in the analysis. Analysis results were then compared with known analytical solutions to determine the degree of accuracy of RAPID-FEM.

The following are analyses of the five example problems of RAPID-FEM.

Example 1: A Circular Antenna Installation

A circular antenna installation on a 0.040" thick skin is shown in Figure H1. The mounting plate is 0.050" thick and is mechanically fastened to the skin with two rows of 3/16" fasteners around a 1.0" diameter antenna connector hole in the skin and mounting plate. The skin is subject to a remote reference circumferential stress of 1,000 psi.

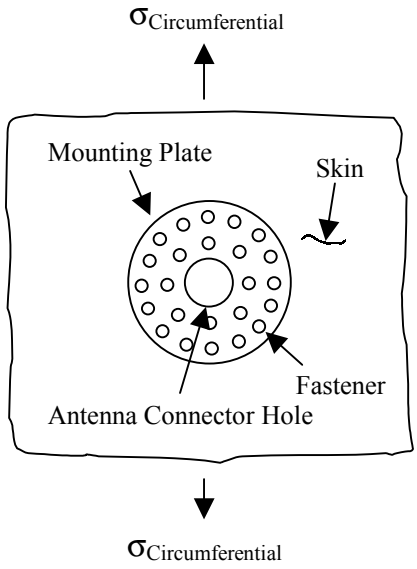

Skin thickness: 0.04"
Mounting plate thickness: 0.05"
Antenna connector hole: 1.0"
Mounting plate radius: 2.5"
Fastener diameter: 3/16"

Figure H1. A Circular Antenna Installation

Finite element meshes of one quarter of the mounting plate and skin created by RAPID-FEM are shown in Figure H2.

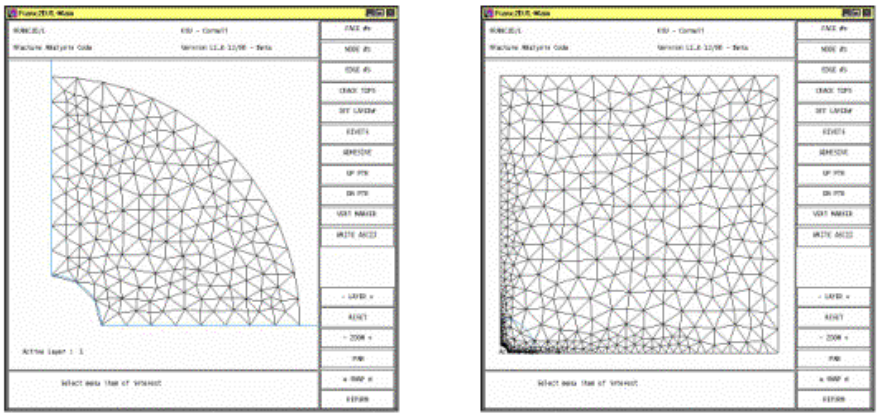

Mounting Plate Skin

Figure H2. Finite Element Meshes of one Quarter of the Mounting Plate and Skin

As a validation of RAPID-FEM, the analysis was first performed for the skin without the mounting plate. The stress concentration gradient along the path normal to the loading direction, as a function of the distance measured from the center of the hole, is obtained and compared with a known analytical solution. As shown in Figure H3, RAPID-FEM result agrees with the analytical solution.

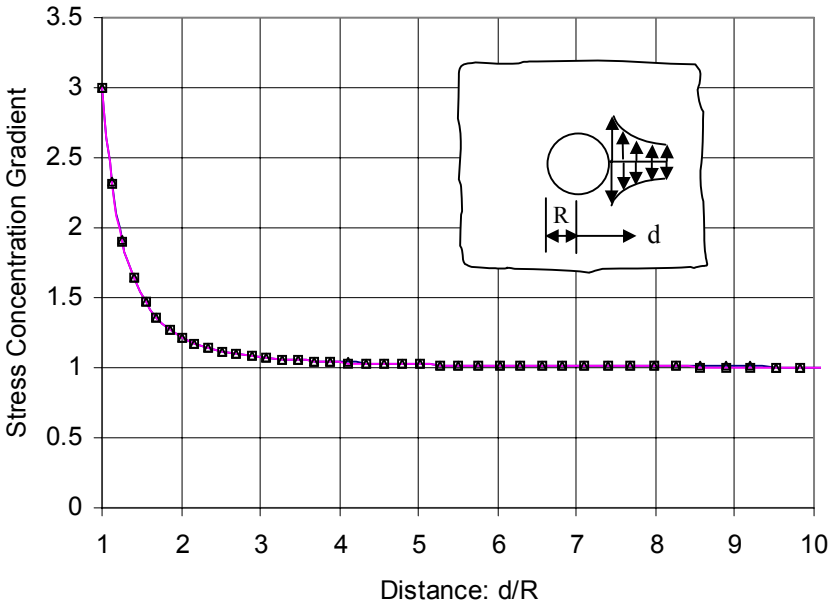

Figure H3. Comparison of RAPID-FEM Result with Known Analytical Solution

When the mounting plate is considered in the analysis, the load transfer at each fastener takes place and the skin concentration gradient near the hole reduces. The amount of reduction in stress concentration gradient depends on how effective the fasteners transferring loads from the skin to the mounting plate. Shown in Figure H4 is the comparison of stress concentration gradient between the two cases. The solid line represents the stress concentration gradient for the case without mounting plate. The dot line is for the case when the mounting plate is considered.

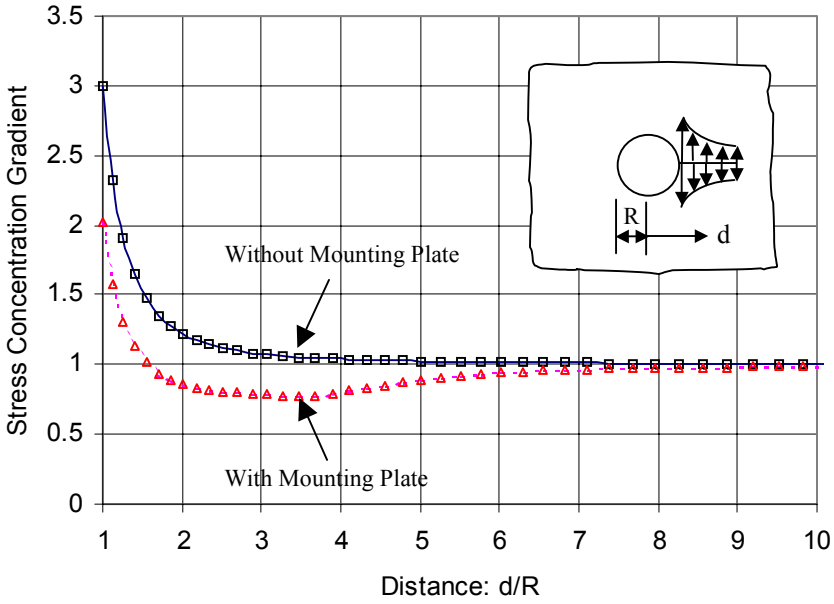

Figure H4. Comparison of Stress Concentration Gradient between Cases with and without Mounting Plate

To perform damage tolerance analysis, crack tip stress intensity factor solutions along the crack path are needed. One of the crack growth scenarios in antenna installations is the growth of a crack initiating at the antenna connector hole in the skin. The crack is assumed to grow along a path normal to the loading direction as shown in Figure H5.

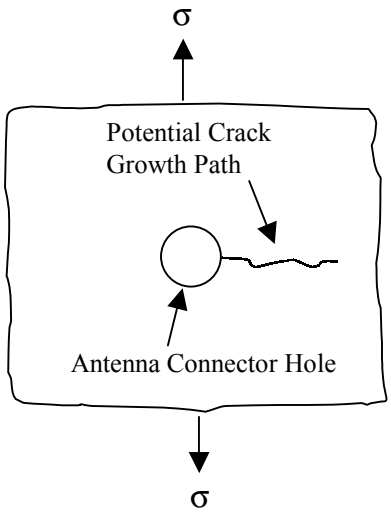

Figure H5. Potential Crack Growth Path

To predict crack growth along the potential path, stress intensity factors are calculated for stress gradient on crack faces along the path. When the calculation is carried out using the stress *concentration* gradient, the stress intensity factor is normalized to one unit of the applied stress. Generally, the stress intensity factor is also normalized with respect to a characteristic crack length and is denoted as the beta factor. Therefore, the beta factor is calculated as

$$\text{BetaFactor } \beta = \frac{K_I}{\sigma \sqrt{\pi a}}$$

where K_I is the first mode crack tip stress intensity factor, σ is the applied stress, and a is the characteristic length. In the following, K_I is the stress intensity factor of the right crack tip due to stress concentration gradient, i.e., $\sigma = 1.0$, and the characteristic crack length a is the crack length a_R.

Beta factors for two unequal-length cracks at a hole under stress concentration gradients in skin (Figure H3) are calculated and shown in Figure H6 for the case without mounting plate. It is noted that the line representing $a_L/R = 0.0$ is the beta factor for a single crack a_R/R growing out of the hole, which is essentially the well-known Bowie's beta factor solution. The curves for a_L/R between 0.0 and 10.0 represent the beta factors for the crack length a_L/R equal to 0.05, 0.10, 0.25, 0.50, 1.0, 2.0, 3.0, 4.0, 5.0, 6.0, 7.0, 8.0, and 9.0, respectively.

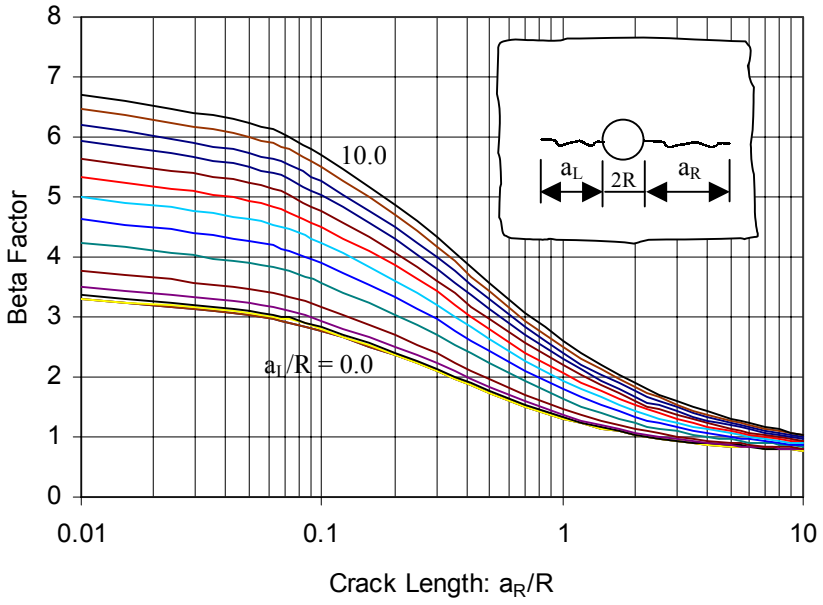

Figure H6. Beta Factors of Two Unequal Length Cracks at a Hole Subject to Stress Concentration Gradient (without Mounting Plate)

Using the stress concentration gradient for the case when the mounting plate is considered (Figure H4), beta factors are calculated and shown in Figure H7. Again, the line representing $a_L/R = 0.0$ is the beta factor for a single crack a_R/R growing out of the hole.

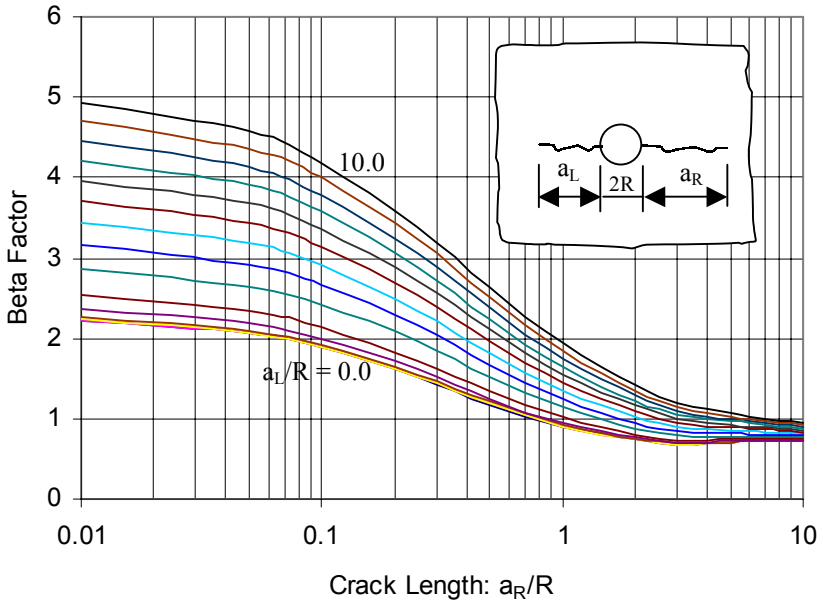

Figure H7. Beta Factors of Two Unequal Length Cracks at a Hole Subject to Stress Concentration Gradient (with Mounting Plate)

Example 2: An Elliptical Antenna Installation

An elliptical antenna installation on a 0.040" thick skin is shown in Figure H8. The mounting plate is 0.050" thick and is mechanically fastened to the skin using 3/16" fasteners around a 1.0" diameter antenna connector hole. The skin is subject to two separate remote reference stresses of 1,000 psi in the longitudinal and circumferential directions, respectively.

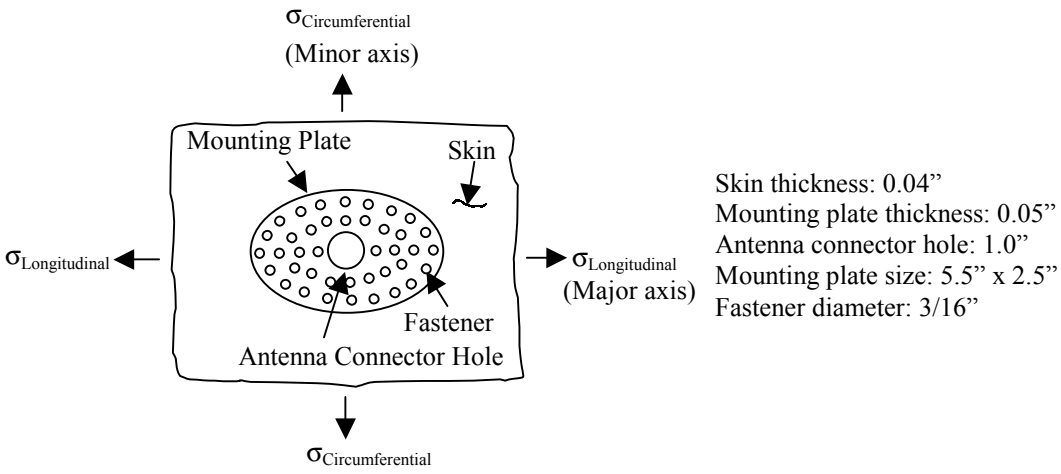

Figure H8. An Elliptical Antenna Installation

Finite element meshes of one quarter of the mounting plate and skin created by RAPID-FEM are shown in Figure H9.

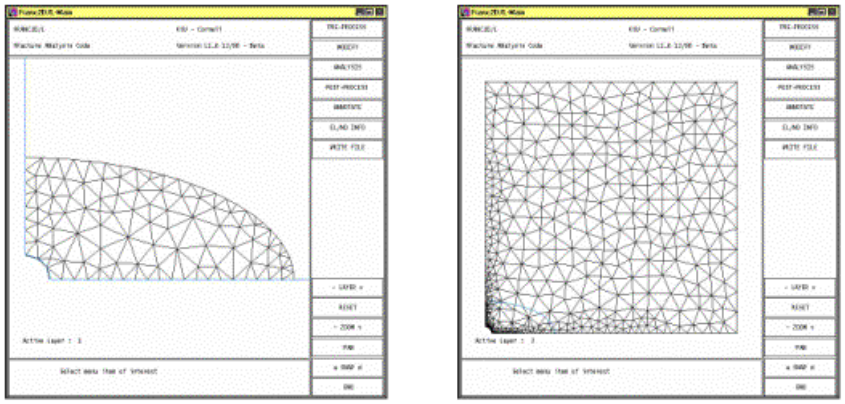

Mounting Plate Skin

Figure H9. Finite Element Meshes of one Quarter of the Mounting Plate and Skin

Shown in Figure H10 are stress concentration gradients along the potential crack paths when the stress is applied in the longitudinal direction for cases with and without the mounting plate.

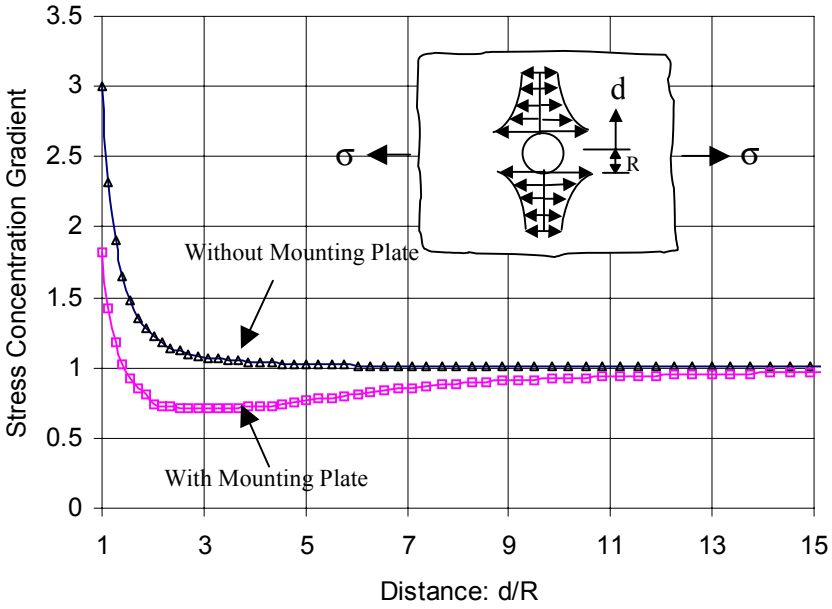

Figure H10. Stress Concentration Gradients

Stress concentration gradients along the potential crack paths for the case when the stress is applied in the circumferential direction are shown in Figure H11.

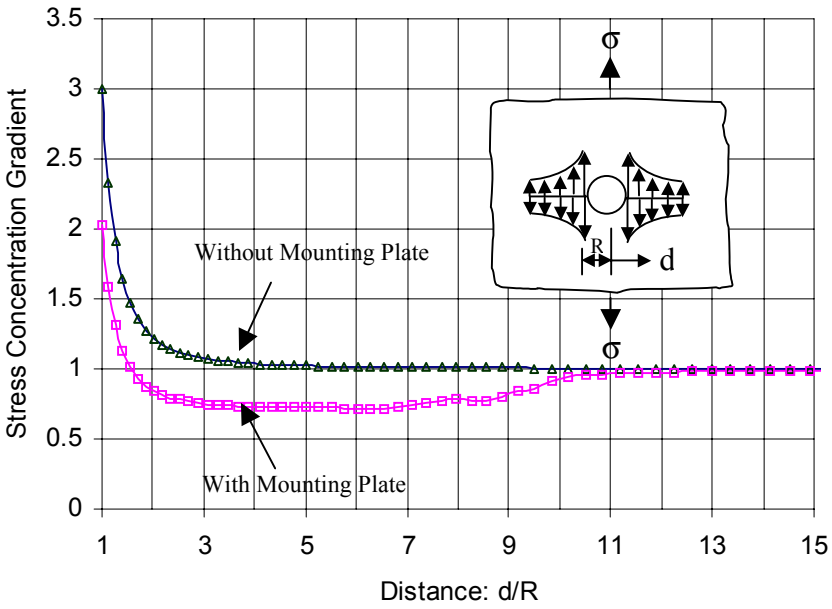

Figure H11. Stress Concentration Gradients

Beta factors for two unequal length cracks at a hole under stress concentration gradients in skin (Figure H10) are calculated and shown in Figures H12 and H13, respectively, for cases without and with the mounting plate. The line representing $a_L/R = 0.0$ in Figure H12 is the beta factor for a single crack a_R/R growing out of the hole, which is essentially the well-known Bowie's beta factor solution.

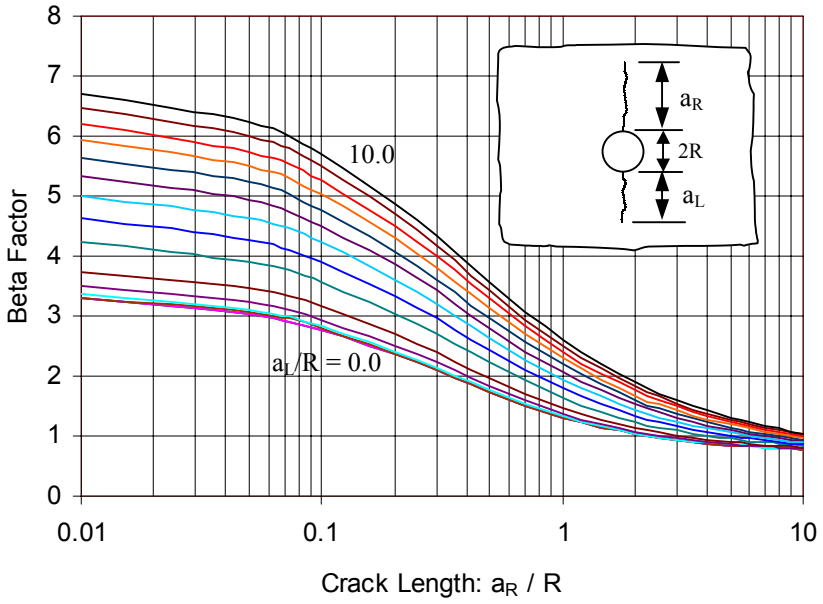

Figure H12. Beta Factors of Two Unequal Length Cracks at a Hole Subject to Stress Concentration Gradient (without Mounting Plate)

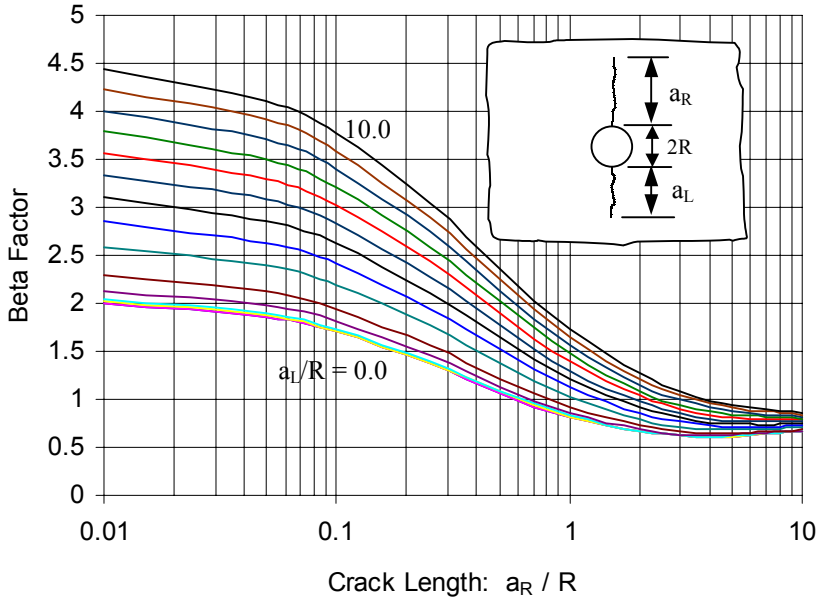

Figure H13. Beta Factors of Two Unequal Length Cracks at a Hole Subject to Stress Concentration Gradient (with Mounting Plate)

Beta factors for two unequal length cracks at a hole under stress concentration gradients in skin (Figure H11) are shown in Figures H14 and H15 for cases without and with the mounting plate, respectively.

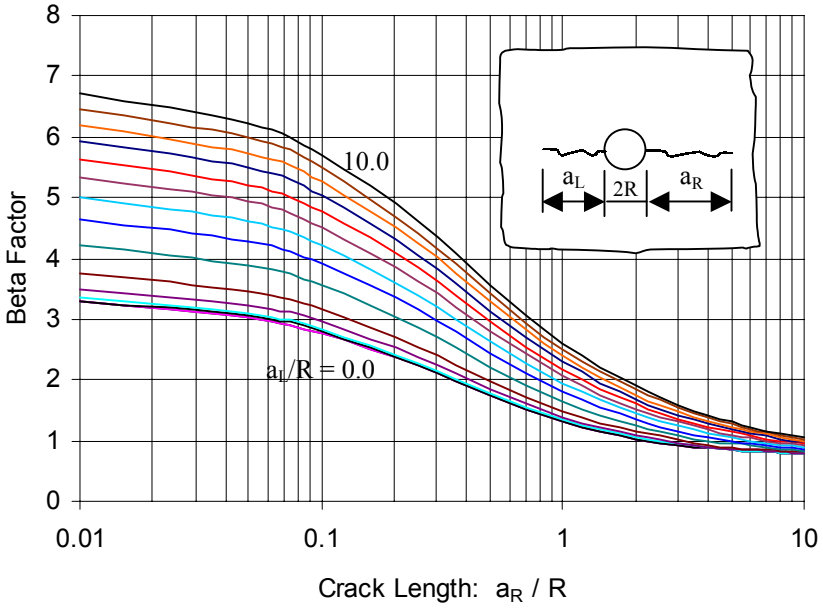

Figure H14. Beta Factors of Two Unequal Length Cracks at a Hole Subject to Stress Concentration Gradient (without Mounting Plate)

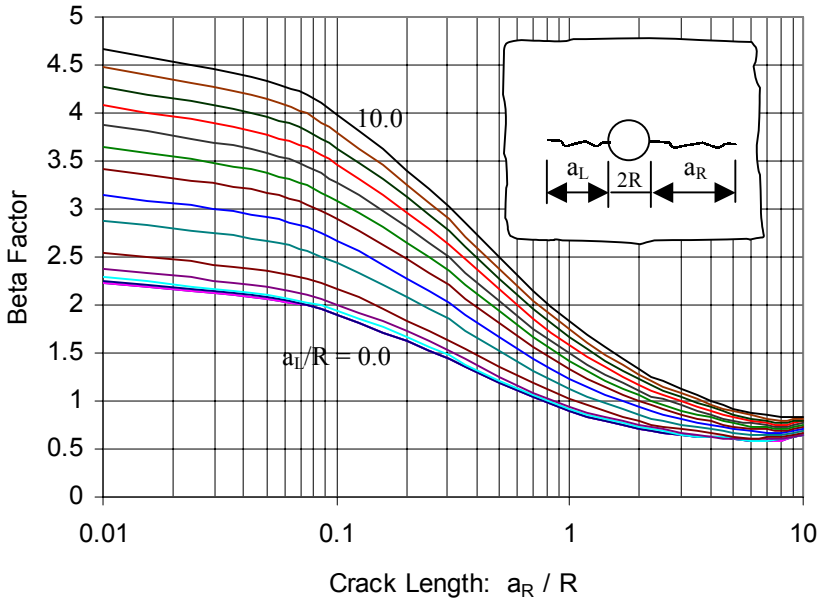

Figure H15. Beta Factors of Two Unequal Length Cracks at a Hole Subject to Stress Concentration Gradient (with Mounting Plate)

Example 3: A Rectangular Antenna Installation

A rectangular antenna installation on a 0.050" thick skin is shown in Figure H16. The mounting plate is 0.063" thick and is mechanically fastened to the skin using 3/16" fasteners around a 1.0" diameter antenna connector hole. The skin is subject to two separate remote reference stresses of 1,000 psi in the longitudinal and circumferential directions, respectively.

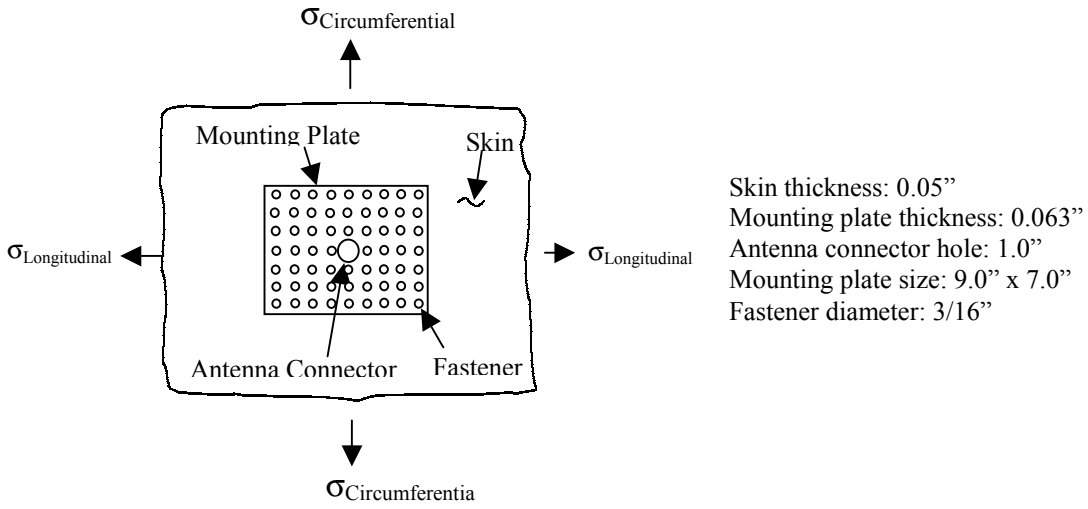

Figure H16. A Rectangular Antenna Installation

Finite element meshes of one quarter of the mounting plate and skin created by RAPID-FEM are shown in Figure H17.

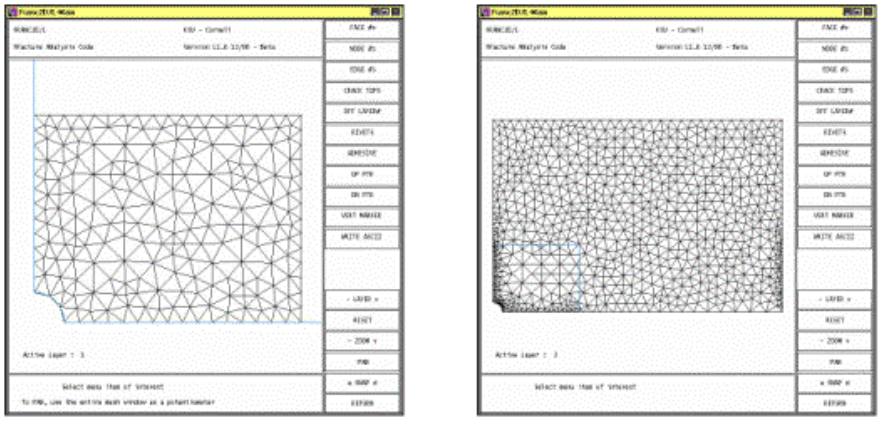

Figure H17. Finite Element Meshes of one Quarter of the Mounting Plate and Skin

Shown in Figure H18 are stress concentration gradients along the potential crack paths when the stress is applied in the longitudinal direction for cases with and without the mounting plate.

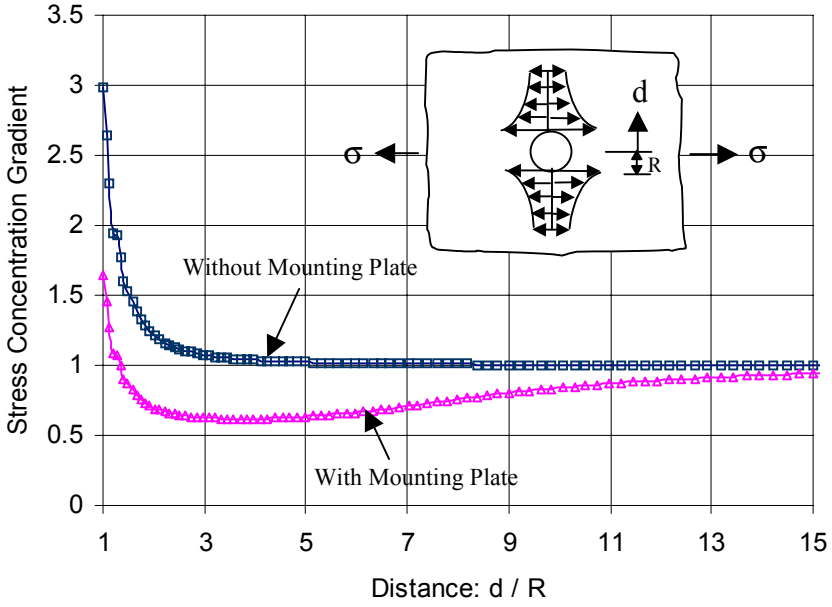

Figure H18. Stress Concentration Gradients

Stress concentration gradients along the potential crack paths when stress application is in the circumferential direction are shown in Figure H19.

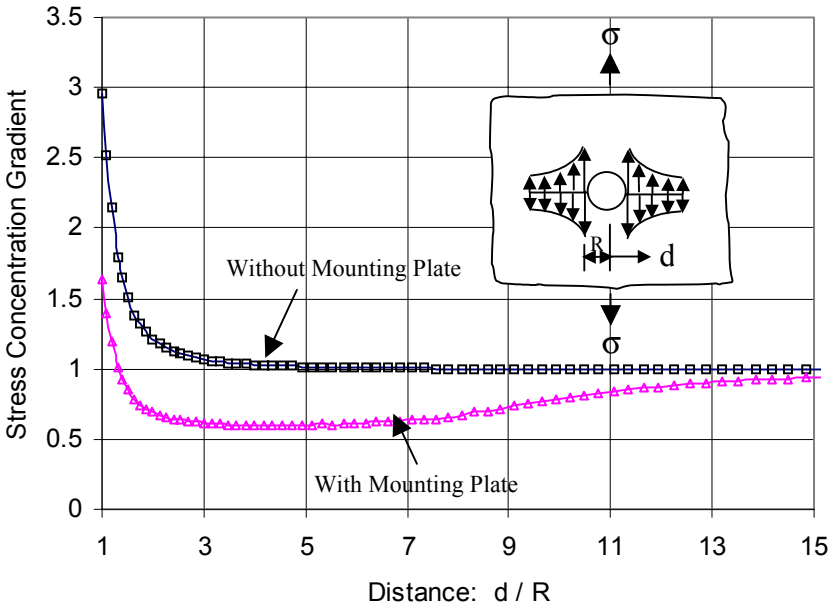

Figure H19. Stress Concentration Gradients

Beta factors for two unequal length cracks at a hole under stress concentration gradients in skin (Figure H18) are calculated and shown in Figures H20 and H21, respectively, for cases without and with the mounting plate. The line representing $a_L/R = 0.0$ in Figure H20 is the beta factor for a single crack a_R/R growing out of the hole, which is essentially the well-known Bowie's beta factor solution.

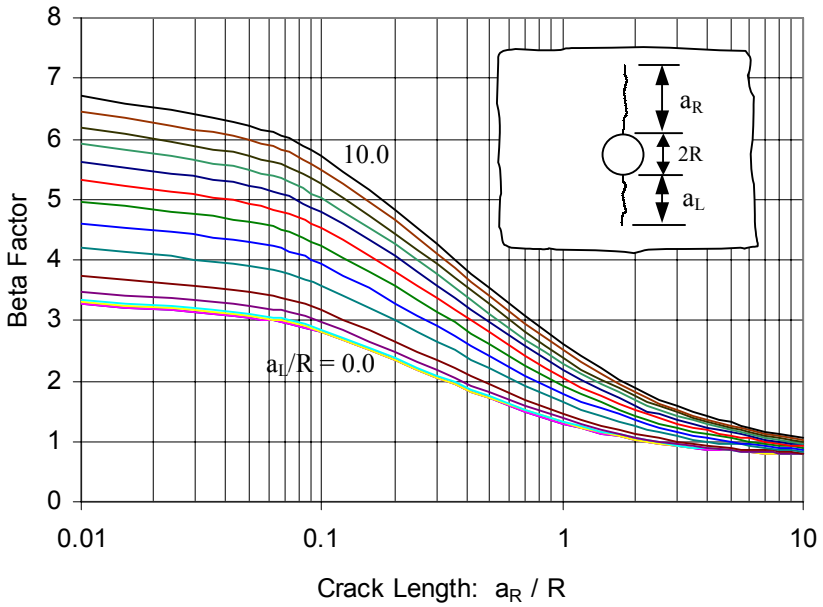

Figure H20. Beta Factors of Two Unequal Length Cracks at a Hole Subject to Stress Concentration Gradient (without Mounting Plate)

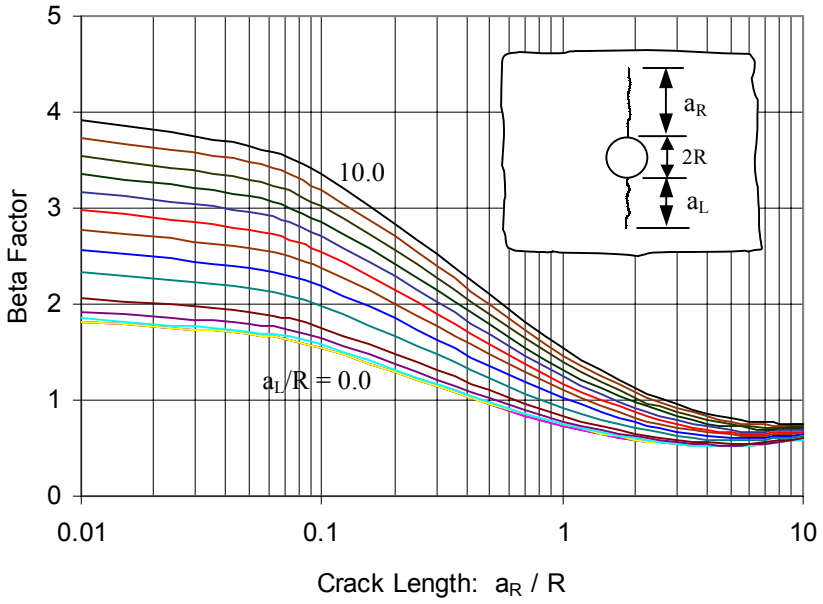

Figure H21. Beta Factors of Two Unequal Length Cracks at a Hole Subject to Stress Concentration Gradient (with Mounting Plate)

Beta factors for two unequal length cracks at a hole under stress concentration gradients in skin (Figure H19) are shown in Figures H22 and H23 for cases without and with the mounting plate, respectively.

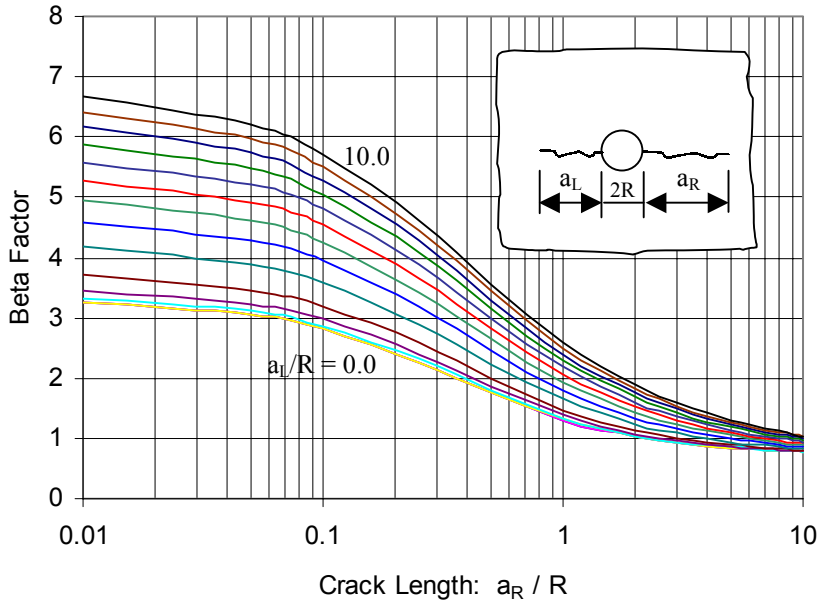

Figure H22. Beta Factors of Two Unequal Length Cracks at a Hole Subject to Stress Concentration Gradient (without Mounting Plate)

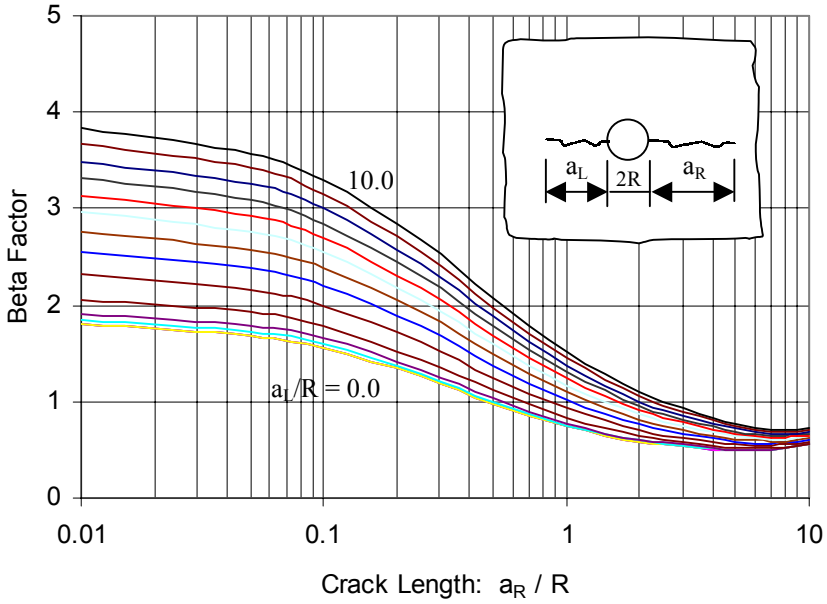

Figure H23. Beta Factors of Two Unequal Length Cracks at a Hole Subject to Stress Concentration Gradient (with Mounting Plate)

Example 4: A 2-Layer Rectangular Repair

A rectangular repair with two external doublers on a 0.063” thick skin is shown in Figure H24. The doublers are 0.040” and 0.050” thick, respectively, and are mechanically fastened to the skin using 3/16” fasteners around a 21.0” x 10.0” skin cutout. The skin is subject to two separate remote reference stress of 1,000 psi in the longitudinal and circumferential directions, respectively.

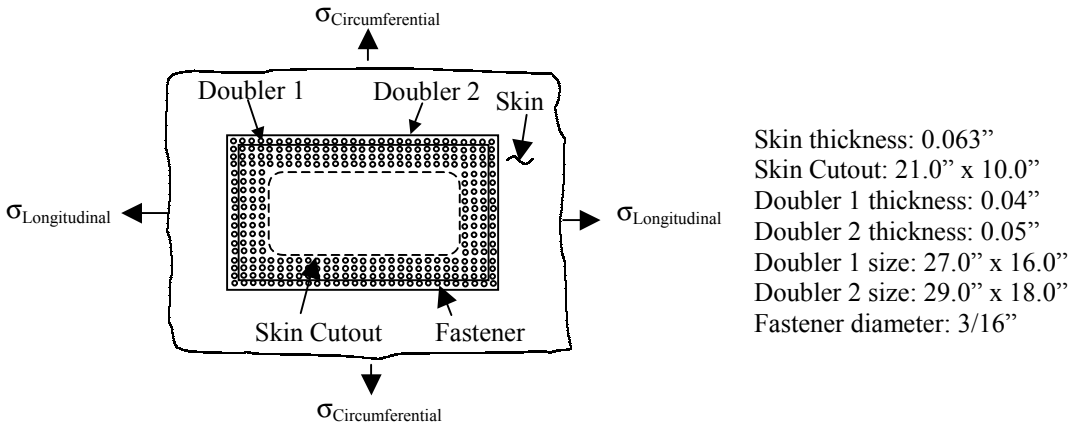

Figure H24. A 2-Layer Rectangular Repair

Finite element meshes of one quarter of the doublers and skin created by RAPID-FEM are shown in Figure H25.

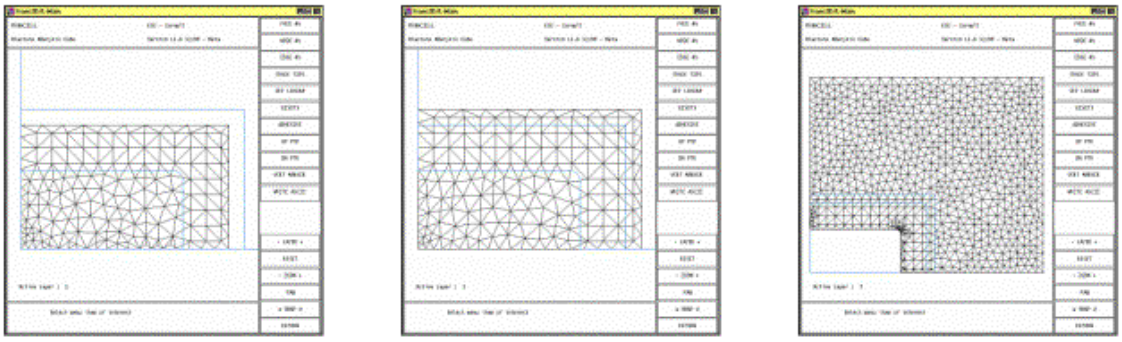

Doubler 1 Doubler 2 Skin

Figure H25. Finite Element Meshes of ¼ of the Doublers and Skin

Load transfers at fasteners along the rightmost fastener row in the skin subject to a reference longitudinal stress of 1,000 psi are shown in Figure H26. The fastener number 1 designates the center fastener, and the number 9 the corner fastener.

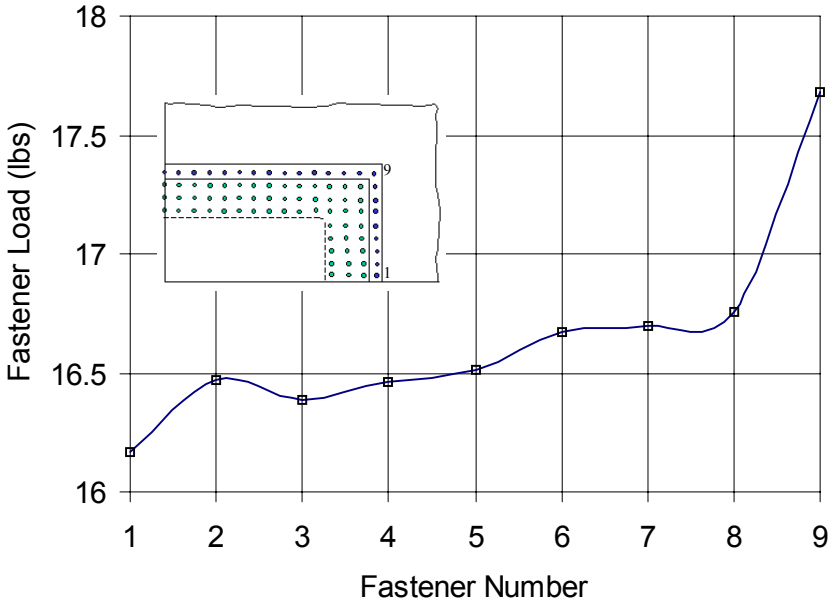

Figure H26. Fastener Loads along the Rightmost Fastener Row

Load transfers at fasteners along the uppermost fastener row in the skin subject to a reference circumferential stress of 1,000 psi are shown in Figure H27. The fastener number 1 designates the center fastener, and the number 15 the corner fastener.

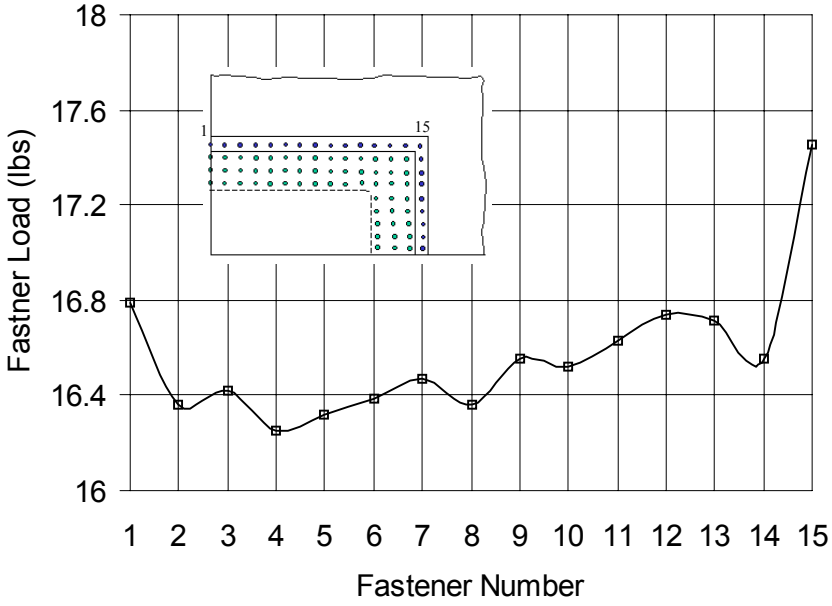

Figure H27. Fastener Loads along the Rightmost Fastener Row

Example 5: A Door Opening Repair

A sketch of a repair at the corner of a door opening with two external doublers on a 0.063" thick skin is shown in Figure H28. The doublers are 0.040" and 0.050" thick, respectively, and are mechanically fastened to the skin using 3/16" fasteners around an approximate 2.0" x 7.0" skin cutout. The skin is subject to two separate remote reference stresses of 1,000 psi in the longitudinal and circumferential directions, respectively.

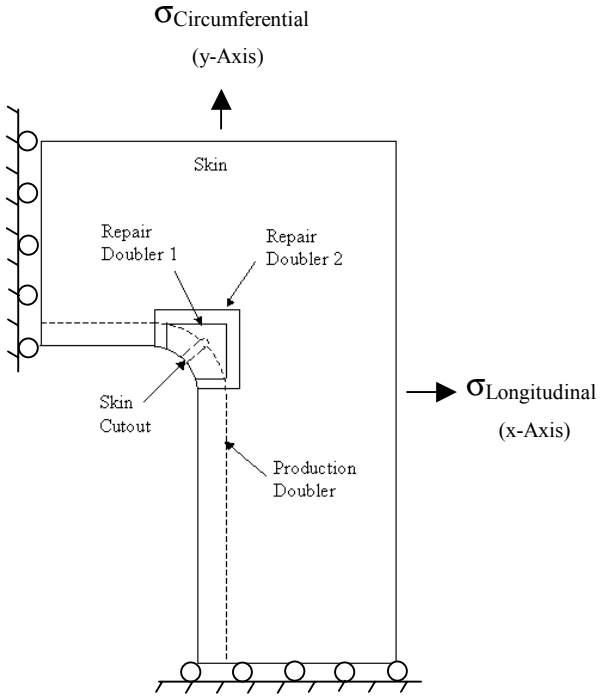

Figure 28. A Repair at Corner of a Door Opening

Fastener patterns between doublers, doubler and skin, and skin and production doubler are shown in Figure H29.

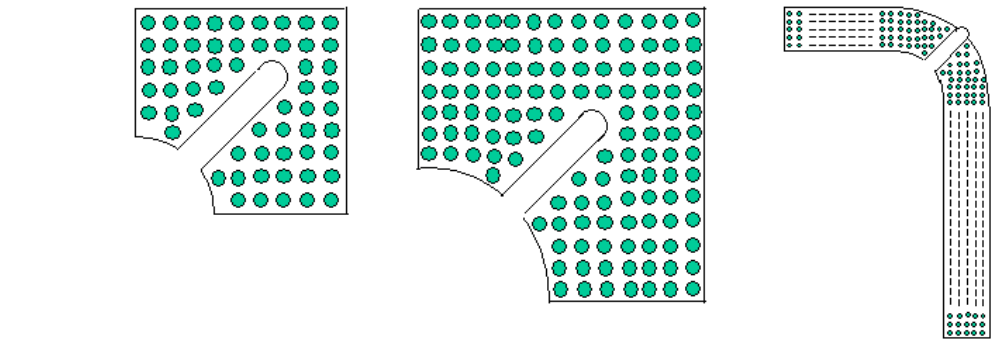

Between Doublers | Between Doubler and Skin | Between Skin and Production Doubler

Figure H29. Fastener Patterns

Finite element meshes of the doublers, skin, and production doubler created by RAPID-FEM are shown in Figure H30.

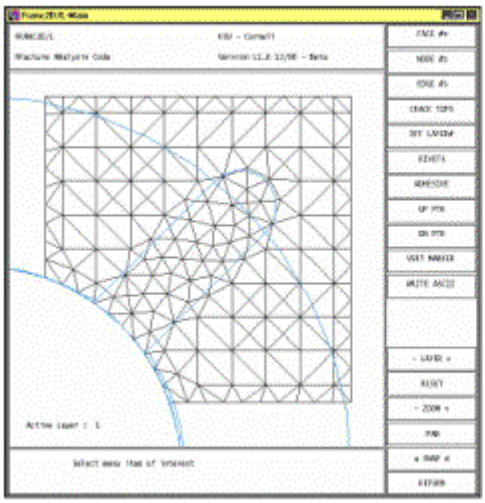

Doubler 1

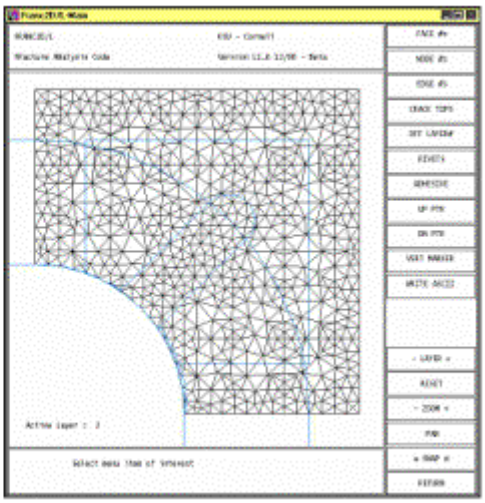

Doubler 2

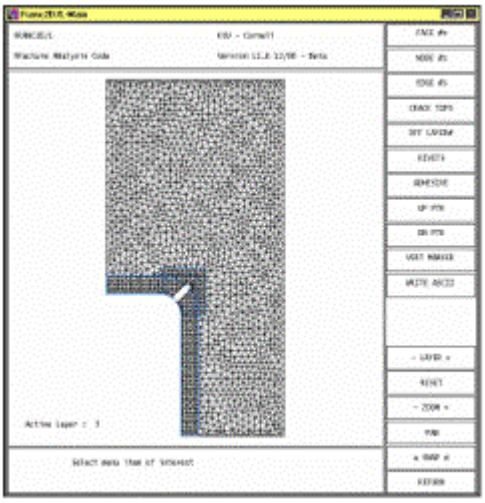

Skin

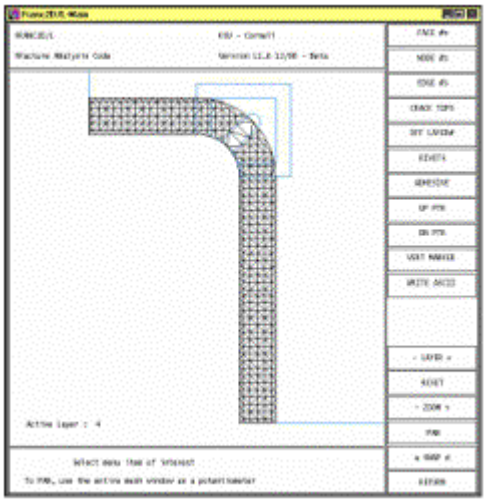

Production Doubler

Figure H30. Finite Element Meshes of the Doublers, Skin, and Production Doubler

Load transfers at fasteners along the leftmost fastener row in the skin subject to a reference longitudinal stress of 1,000 psi are shown in Figure H31. The fastener number 1 designates the bottom fastener, and the number 7 the top fastener.

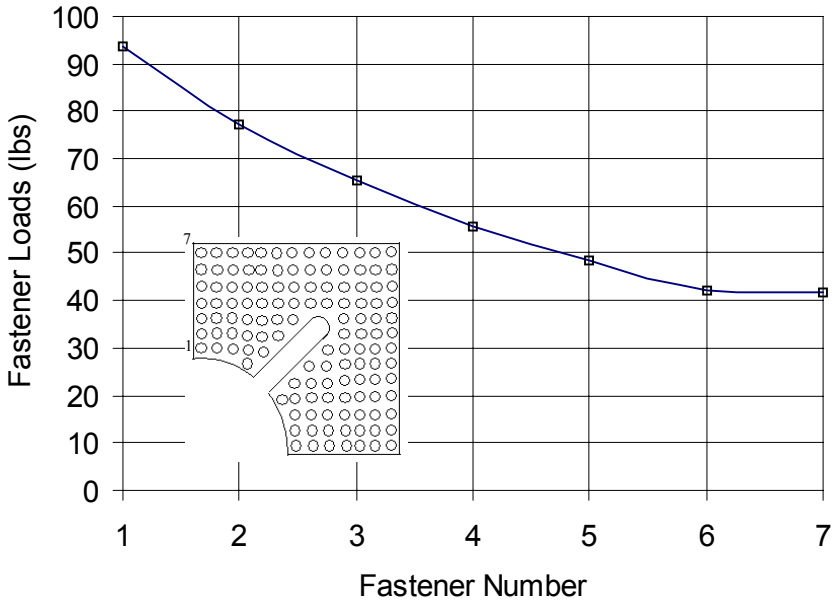

Figure H31. Fastener Loads along the Leftmost Fastener Row

Fastener loads along the rightmost fastener row in the skin subject to a reference longitudinal stress of 1,000 psi are shown in Figure H32. The fastener number 1 designates the bottom fastener, and the number 13 the top fastener.

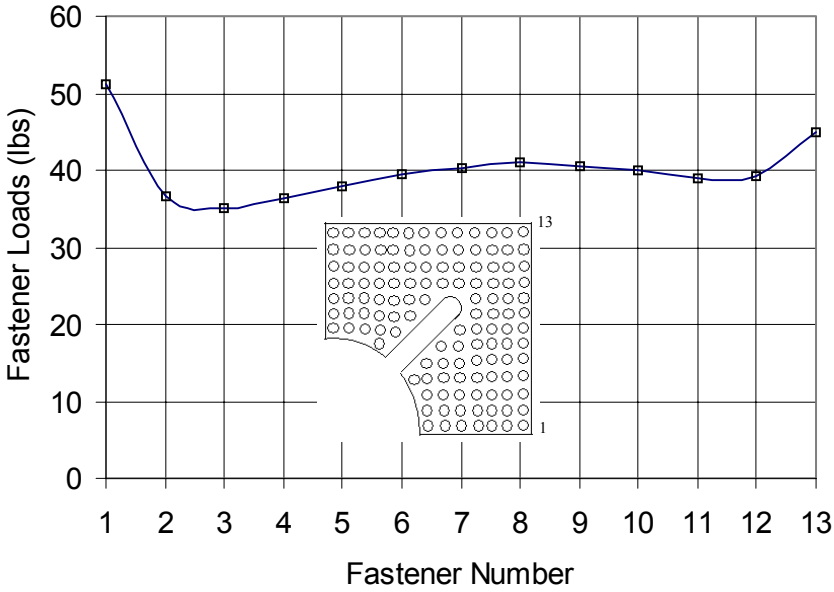

Figure H32. Fastener Loads along the Leftmost Fastener Row

Load transfers at fasteners along the lowermost fastener row in the skin subject to a reference circumferential stress of 1,000 psi are shown in Figure H33. The fastener number 1 designates the left fastener, and the number 7 the right fastener.

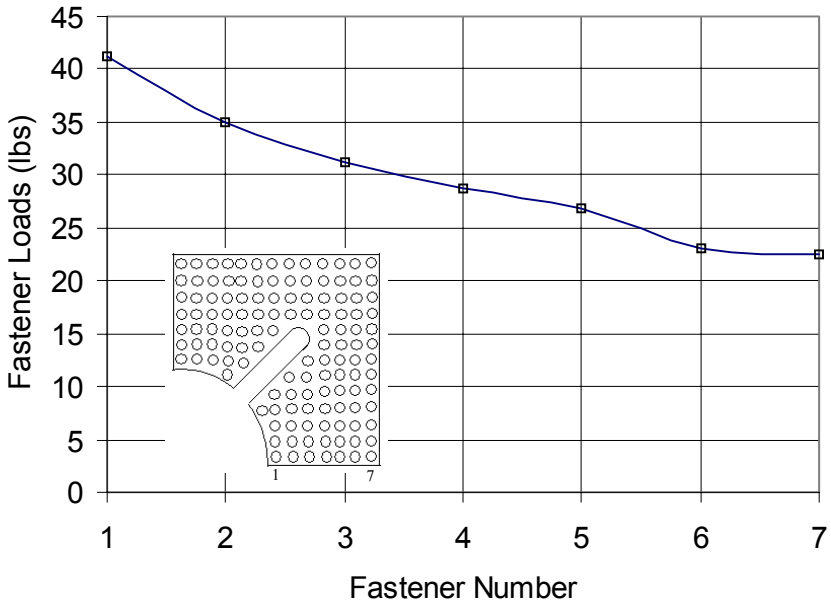

Figure H33. Fastener Loads along the Lowermost Fastener Row

Load transfers at fasteners along the uppermost fastener row in the skin subject to a reference circumferential stress of 1,000 psi are shown in Figure H34. The fastener number 1 designates the left fastener, and the number 7 the right fastener.

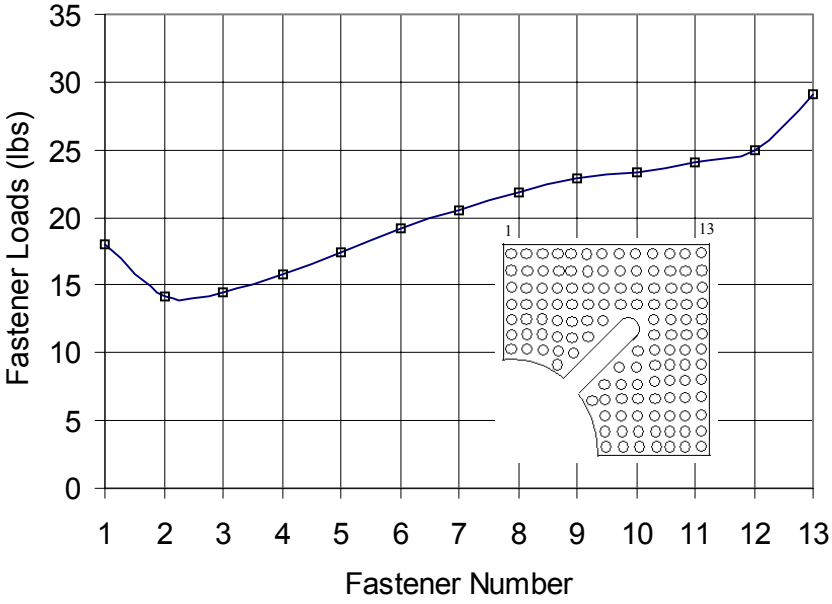

Figure H34. Fastener Loads along the Uppermost Fastener Row

Skin stresses σ_{xx}, σ_{yy}, and τ_{xy} along the 45-degree line for a 1,000 psi reference stress applied separately in the longitudinal and circumferential directions are obtained from RAPID-FEM. These stresses are used to calculate the stress concentration gradients normal to the 45-degree line as shown in Figures H35 and H36, respectively.

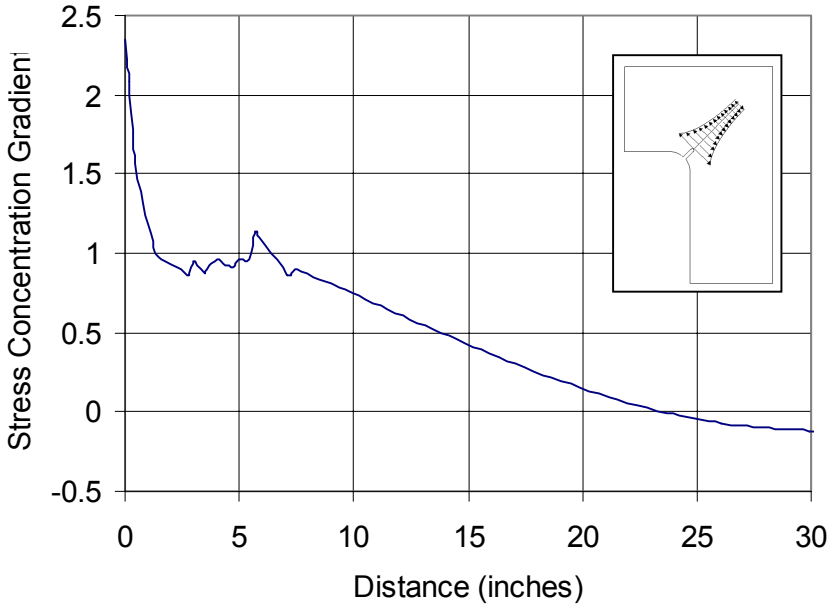

Figure H35. Stress Concentration Gradient due to 1,000 psi Longitudinal Stress

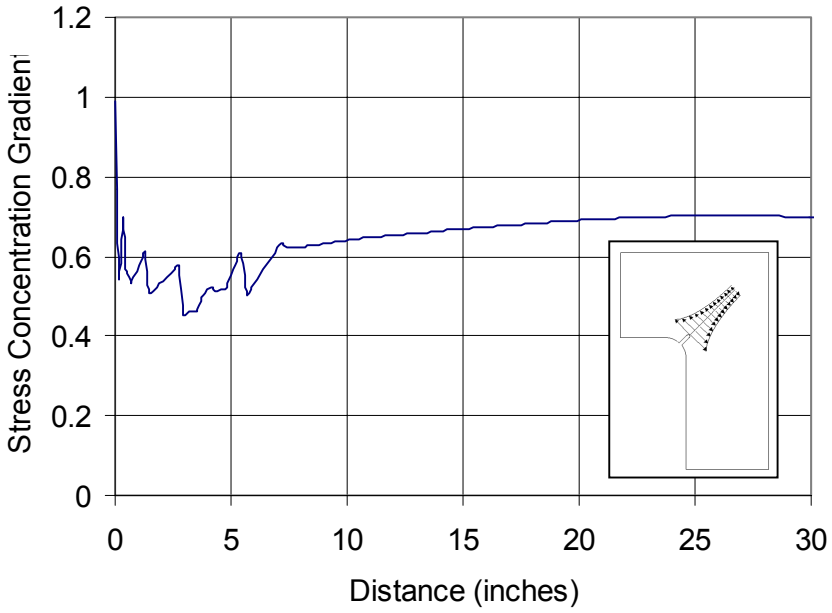

Figure H36. Stress Concentration Gradient due to 1,000 psi Circumferential Stress

Beta factors for a crack growing along the potential 45-degree-line path under stress concentration gradients due to longitudinal stress (Figure H35) and circumferential stress (Figure H36) are calculated and shown in Figures H37 and H38, respectively.

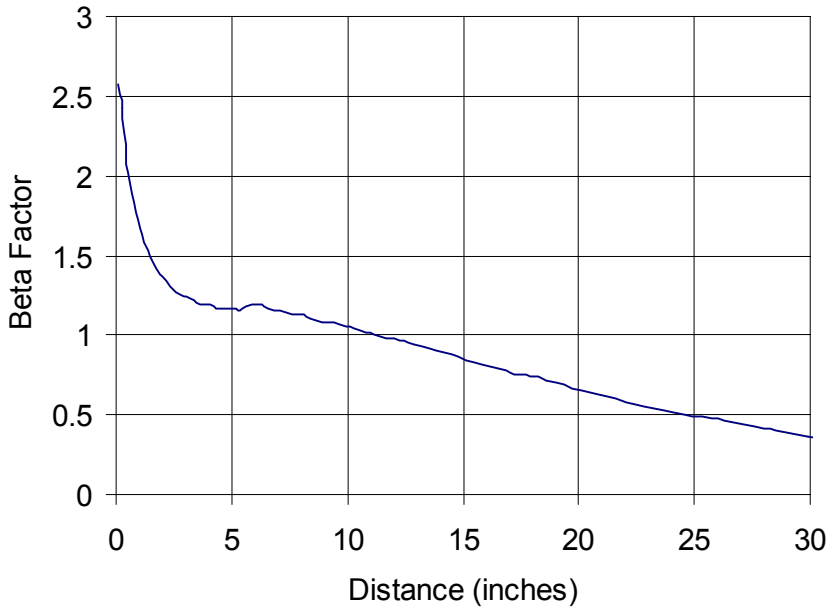

Figure H37. Beta Factors for a Crack Growing along the 45-Degree-Line Path under Stress Concentration Gradients due to Longitudinal Stress

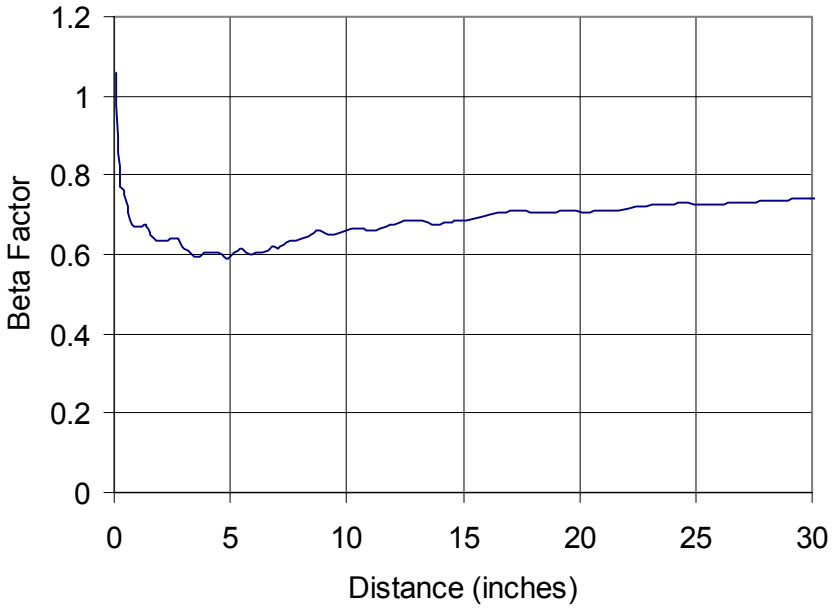

Figure H38. Beta Factors for a Crack Growing along the 45-Degree-Line Path under Stress Concentration Gradients due to Circumferential Stress

Appendix I: RAPID-FEM Development and 3-D Analysis of Fuselage Structures with a Door Opening

This appendix describes the development of RAPID-FEM code for 2-D analysis of layered structures. It also provides 3-D analysis of fuselage structures with a door opening and comparison of stresses around the opening corner with 2-D analysis. This appendix is prepared by Cornell University.

DOT/FAA/AR-xx/xx

Office of Aviation Research
Washington, D.C. 20591

Finite Element Stress Analysis Subroutines for RAPID

U.S. Department of Transportation
Federal Aviation Administration

technical note technical note

Finite Element Stress Analysis Subroutines for RAPID

U.S. Department of Transportation
Federal Aviation Administration

NOTICE

This document is disseminated under the sponsorship of the U.S. Department of Transportation in the interest of information exchange. The United States Government assumes no liability for the contents or use thereof. The United States Government does not endorse products or manufacturers. Trade or manufacturer's names appear herein solely because they are considered essential to the objective of this report.

Technical Report Documentation Page

1. Report No.	2. Government Accession No.	3. Recipient's Catalog No.
DOT/FAA/(AR or CT)-xx/xx		

4. Title and Subtitle	5. Report Date
FINITE ELEMENT STRESS ANALYSIS SUBROUTINES FOR RAPID	August, 2000
	6. Performing Organization Code

7. Author(s)	8. Performing Organization Report No.
Chuin-Shan "David" Chen, Paul A. "Wash" Wawrzynek, Anthony R. Ingraffea	

9. Performing Organization Name and Address	10. Work Unit No. (TRAIS)
Cornell Fracture Group 641 Rhodes Hall, Cornell University Ithaca, NY 14853	11. Contract or Grant No.

12. Sponsoring Agency Name and Address	13. Type of Report and Period Covered
	14. Sponsoring Agency Code

15. Supplementary Notes

.

16. Abstract

17. Key Words	18. Distribution Statement
	Reference paragraph 13b for the applicable availability statement.

19. Security Classif. (of this report)	20. Security Classif. (of this page)	21. No. of Pages	22. Price
Unclassified	Unclassified		

Form DOT F 1700.7 (8-72) Reproduction of completed page authorized

TABLE OF CONTENTS

LIST OF FIGURES

LIST OF TABLES

(M) EXECUTIVE SUMMARY

This is the final report of a six-month project undertaken by the Cornell Fracture Group in support of the RAPID (Repair Assessment Procedure and Integrated Design) program currently being developed by the FAA and the US Air Force. The objectives of the project are to:

- Develop two-dimensional (2D) finite element stress analysis codes that can be incorporated directly into the RAPID program.
- Perform three-dimensional (3D) thin-shell finite element analyses of fuselage structures with a door cutout configuration and compare stresses around the door corner with 2D finite element results.

Both objectives have been achieved and the results are detailed herein. For the first, before the inception of this project, assessment of repairs through RAPID was restricted to the regions in an airplane where the stress distributions are known through handbooks or empirical solutions. We successfully enhance the analysis tools by developing a built-in 2D finite element analysis engine for RAPID. The cores of the engine include a meshing capability for an arbitrary domain in a 2D layered structure and a solver with an efficient nodal renumbering algorithm.

For the second, the main concern was the fidelity of 2D stress analyses in a complex 3D structure under various loading conditions. The scenario we consider is an airplane fuselage with a door cutout. We analyze a wide-body model with a passenger door and a narrow-body with a cargo door, considering both pressure loading and vertical shear loading. Our results indicate that both geometries and boundary conditions play a key role in correlating 3D thin shell and 2D results.

(M) 1. INTRODUCTION.

RAPID (Repair Assessment Procedure and Integrated Design), is a repair analysis software tool for designing repairs of airplanes. Before the inception of this project, assessment of repairs through RAPID was restricted to the regions in an airplane where the stress distributions are known through handbooks or empirical solutions. This includes, for example, the repaired regions located between fwd and aft pressure bulkheads, but away from door and window cutouts. The main goal of the project is to develop and extend the analysis tools for RAPID so that the repair assessment can be conducted for a broader range of the problems.

The analysis methodology in RAPID can be greatly supplemented by a built-in two-dimensional (2D) finite element analysis engine. The capability allows users to perform rigorous static stress analyses for problems with complex geometries and boundary conditions using layered 2D assumptions. The first objective of the project was:

- [Objective 1] develop a 2D layered, linear elastic finite element stress analysis capability that can be incorporated directly into the RAPID program.

For some repair scenarios, for example, repairs around the door, because of the complexity of geometries and loading conditions, stress fields around a cutout are three-dimensional (3D) in nature. It is necessary to perform more detailed 3D stress analyses and to compare them with 2D approximations used in the RAPID program. The second objective of the project was:

- [Objective 2] perform 3D thin-shell finite element analyses of fuselage structures with a door cutout configuration and compare stresses around the door corner with the 2D finite element results.

In this report, we will discuss key aspects of the 2D finite element stress analysis code, including meshing for arbitrary layered structures, fast solver with nodal renumbering and input/output interfaces to the RAPID program. The source code for this capability has been delivered to Boeing for incorporation into RAPID. We will also discuss our key findings from 3D thin-shell finite element analysis, including the stress distributions at the door corners where most door repairs are likely taken place.

(M) 2. TWO-DIMENSIONAL FINITE ELEMENT STRESS ANALYSIS CODES FOR RAPID.

To develop a standalone finite element engine for RAPID, we consider the following critical issues when we design our codes:

- The interfaces between our codes and RAPID need to be as simple as possible, yet without sacrificing the flexibility for possible future enhancements. This consideration leads us to write our codes in the C++ programming language [1], which is well known for its built-in language capability to separate interfaces from implementations. The object-oriented concept also makes it much easier for future enhancements of the codes.
- The codes need to be tested separately from RAPID. Also the analysis results need to be verified independently by users. The first consideration leads us to design our codes so they can be either directly incorporated into the RAPID program or compiled as a simple standalone command-driven program. For the second consideration, we incorporate an optional feature to generate FRANC2DL [2] input records so users can perform independent verification studies using both the new program and a well-tested FRANC2DL program simultaneously. This not only allows users to gain more confidence while comparing their results with a well-tested program, but also gives users an opportunity to perform consequent crack growth simulations in FRANC2DL.
- The algorithms implemented in the codes need to be proven their robustness for the real life application. The key algorithms are meshing, finite element formulation and solution of the resulting set of linear equations. The Cornell Fracture Group (CFG) has substantial experience developing such software. This includes, for example, the FRANC2D [3], FRANC2DL [2], FRANC3D/STAGS [3] and FRANC3D/BES [3] codes.

In the following, we will discuss our key implementation strategy of developing the 2D finite element codes for the RAPID program. We first use a hypothetical door-corner configuration to illustrate a typical repaired problem and identify the crucial finite element capabilities needed to handle this class of the problems. We then discuss the key software modules and results of the 2D finite element codes. We shall emphasize that the codes have not only been tested by the authors during the development phase, but also tested by engineers at the Boeing company during the technology transfer phase [4].

(1st) 2.1 ILLUSTRATION PROBLEM.

Figure 1 shows a hypothetical door-corner configuration with a repair-patch in an aircraft fuselage. The door-corner contains a repair-patch mechanically fastened to the skin and frame. With the RAPID methodology, it is assumed that all structural components (patch, skin, and frames) can be idealized as 2D members. Separate 2D plane stress finite element meshes will be created for each of the components. The 2D meshes are tied at the fastener points, which are idealized as shear springs. Each individual mesh is referred to as a “layer”. All layers are assumed to be linear elastic and isotropic.

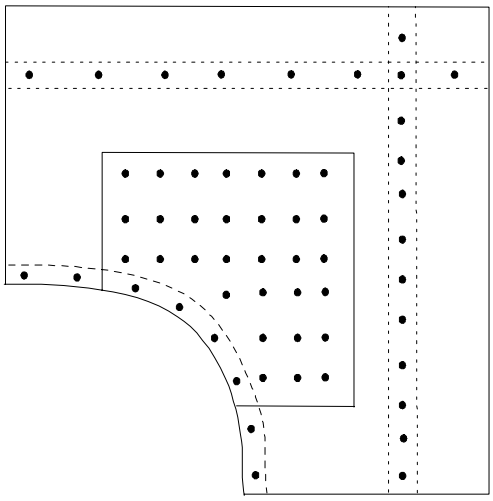

FIGURE 1. A HYPOTHETICAL DOOR-CORNER CONFIGURATION WITH A REPAIR-PATCH IN AIRCRAFT FUSELAGES

(1st) 2.2 SOFTWARE MODULES.

Based on our past experience, it is convenient to divide the necessary code implementations into four independent, yet related, software modules. These software modules are denoted the "Input Wrapper", the "Mesher", the "Finite Element Analysis" and the "Output Wrapper", as illustrated in Figure 2. We will discuss the key details of each module below.

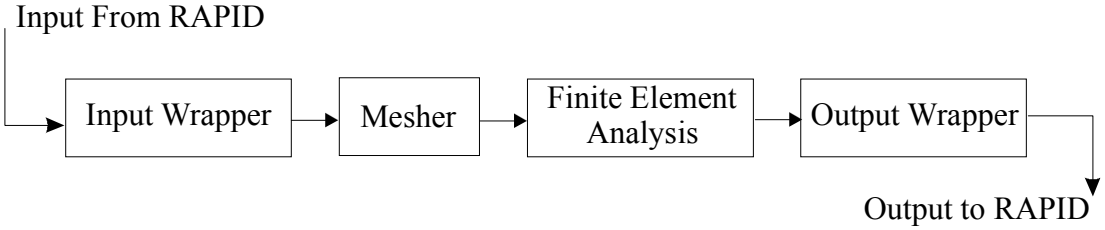

FIGURE 2. SOFTWARE MODULES AND THEIR INTERACTION WITH RAPID

(2nd) 2.2.1 Input Wrapper.

The Input Wrapper is responsible for reading the input specifications prescribed by RAPID and organizing the data for meshing and finite element analysis. The input is comprised primarily of geometry and boundary conditions, along with some control parameters for output. The current input specifications are described in Appendix A. The specifications are also distributed with the source codes.

(2nd) 2.2.2 Mesher.

The Mesher takes the data generated by Input Wrapper and creates all-triangular element meshes for the finite element analysis. We have implemented an advancing front mesher [5]. The technique is one of the most general automatic meshing technologies for the discretization of an arbitrary planar domain into high-quality triangular elements [6]. The process of generating front during triangulation is illustrated in figure 3. In figure 3a, the initial front is the entire boundary. In figure 3b, the triangle ABC is being constructed. In figure 3c, the updated front now includes triangle ABC. The process continues until there are no more line segments left in the front. In addition to the standard features found in the advancing front technique, the mesher also respects the specified boundary discretizations and rivet locations while generating the meshes for different layers.

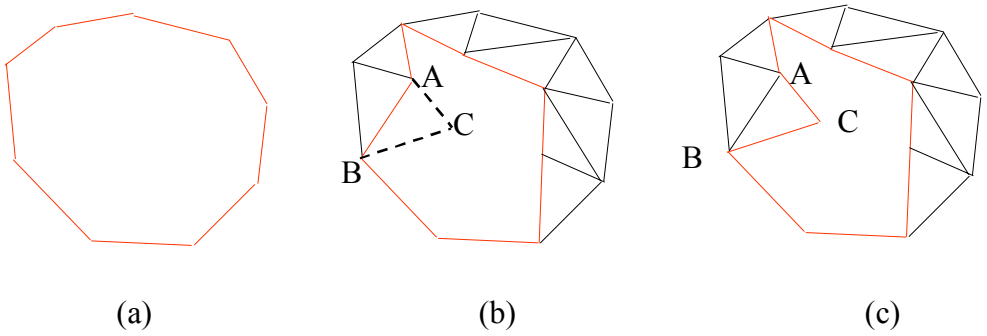

FIGURE 3. ILLUSTRATION OF ADVANCING FRONT GENERATION DURING TRIANGULATION. THE FRONT IS INDICATED BY THE RED LINES.

(2nd) 2.2.3 Finite Element Analysis.

In the Finite Element Analysis module, 2D layered, plane stress, linear-elastic finite element analysis is performed. Six-noded quadratic triangular elements and two-noded linear shear springs are used in the finite element analysis. We implement a fast direct solver using LD decomposition [7]. It is worth noting that for the layered meshes, it is crucial to renumber the finite element nodes before we solve the system of linear equations. Doing so allows us reduces the bandwidth of the problems to a minimum. The Sloan's nodal renumbering algorithm [8] based on the graph theory has been implemented.

(2nd) 2.2.4 Output Wrapper.

The Output Wrapper provides important analysis results for further repaired analysis and design. Most features of interests of the analysis results are controlled directly from users through input specifications. This includes:

- stresses along a prescribed line with subdivision number and ratio specified by users,
- element stresses, and
- rivet forces.

(1st) 2.3 ANALYSIS RESULTS.

We demonstrate the capability of the program with two examples: an antenna-installation and a door opening repaired problem. The examples were prepared using the input specifications given in Appendix A. We execute the program with the FRANC2DL option on, which allow us to perform independent verification studies. The input records were prepared manually by Boeing [4] during the developing phase of the project and are included in the Appendix B.

(2nd) 2.3.1 A Circular Antenna Installation Example.

[Problem Description] We consider a quarter model of a circular antenna installation example illustrated in figure 4. In this example, we model the problem as a two-layered plane stress problem connected with shear springs. The mounting plate is modeled as layer 0 and the skin as layer 1. Both are made of 2024-T3 aluminum alloy where the Young's modulus E = 10,500,000 psi and Poisson ratio $\upsilon = 0.3$. The thickness is 0.05 in. for the mounting plate and 0.04 in. for skin. Shear stiffness of the rivet is 167,550 lb/in., but only half of the value is assigned on the four rivets along the symmetry boundaries. The rivet positions based on the labels given in figure 4 are summarized in table 1. In addition to the symmetry boundary conditions, a uniform traction equal to 1000 lb is applied on the top edge of the model.

[Analysis Results] Figure 5 shows the meshes generated automatically by the program. We note that while in the overlapped area the meshes for layer 0 and layer 1 are different, the program automatically generates the necessary finite element nodes at the rivet positions to tie two layers. Table 2 lists the rivet forces computed from the analysis. The computed values agree with FRANC2DL results up to the machine accuracy. As expect, most of the load transfer action takes place at the first row of the rivets closest to the applied load. In this example, the critical rivets are rivet 3, 4, 5, 6 and 7.

Figure 6 plots the stress component σ_{yy} along a line path from (0.50001, 0.0) to (19.999, 0.0) at skin (layer 1). It is of interest to observe that without the mounting plate, the theoretical concentration factor for skin with a hole is 3.0. With load transfer taking effect between skin and mounting plate, we see a concentration factor about 1.6 near the circular hole for our example.

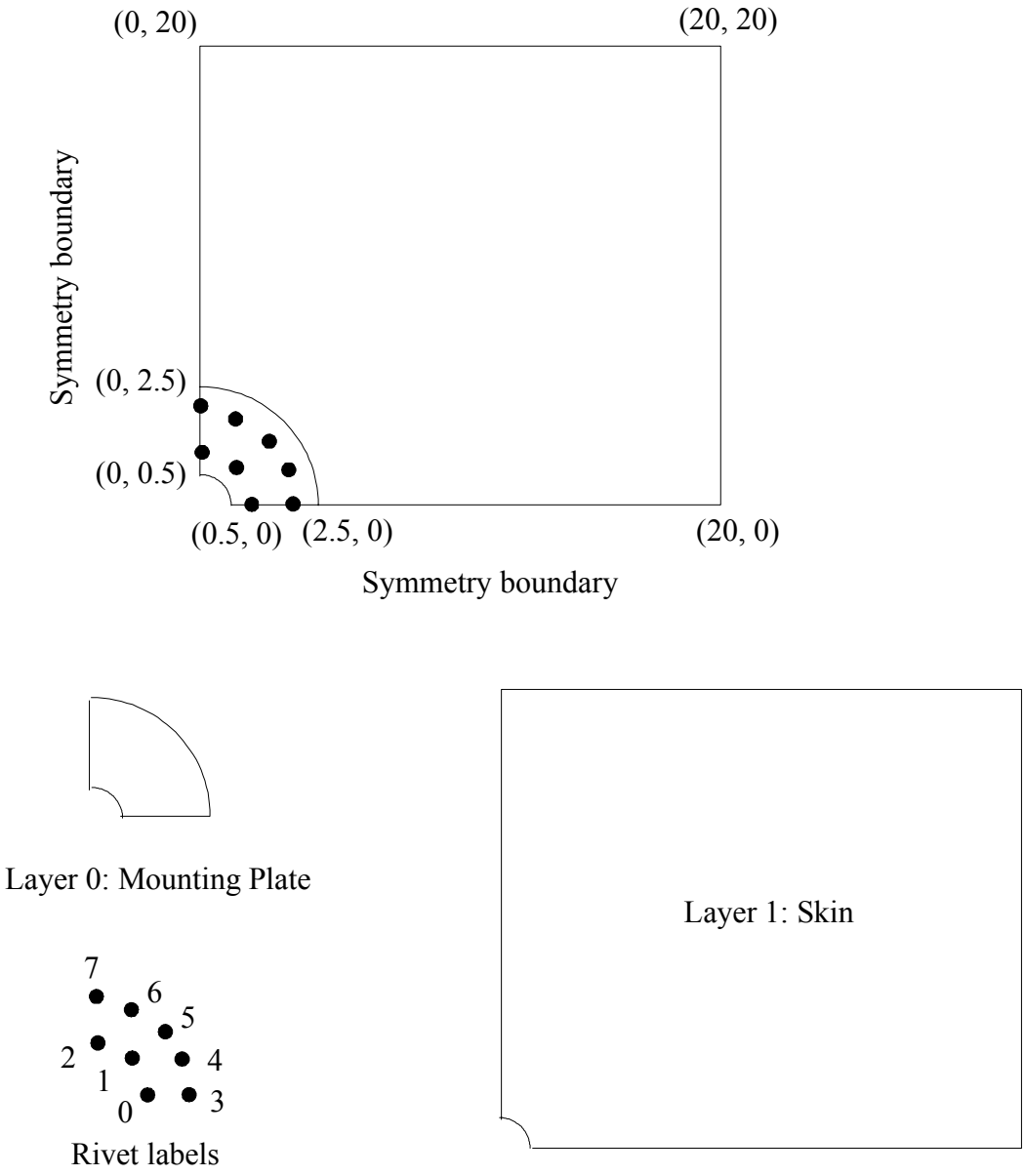

FIGURE 4. ILLUSTRATION OF THE CIRCULAR ANTENNA INSTALLATION.

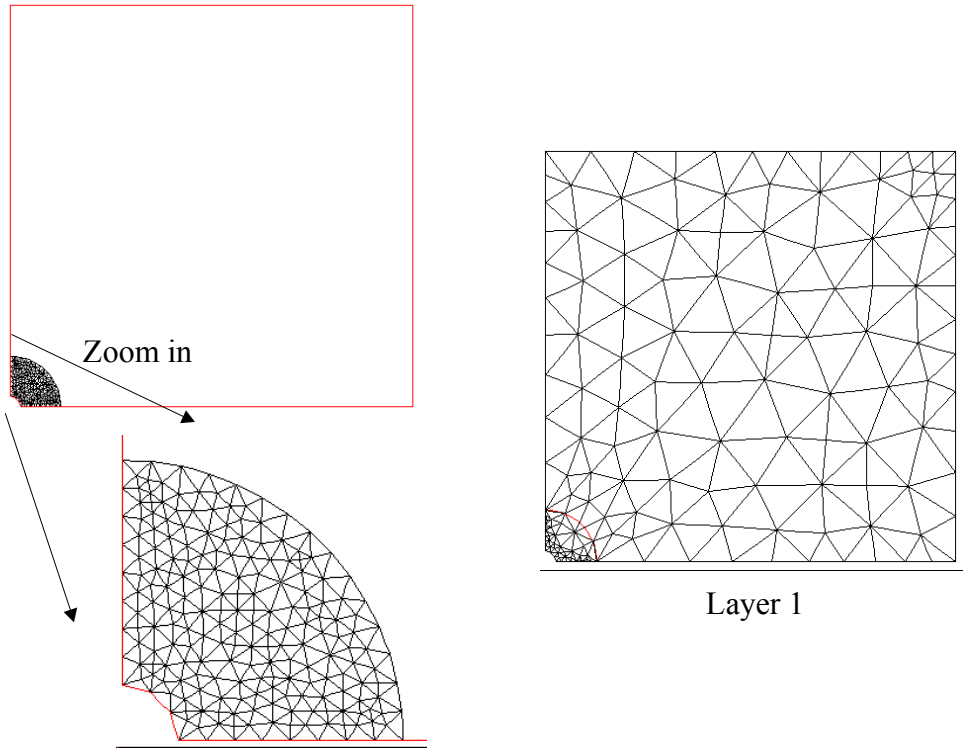

FIGURE 5. FINITE ELEMENT MESHES OF THE CIRCULAR ANTENNA INSTALLATION.

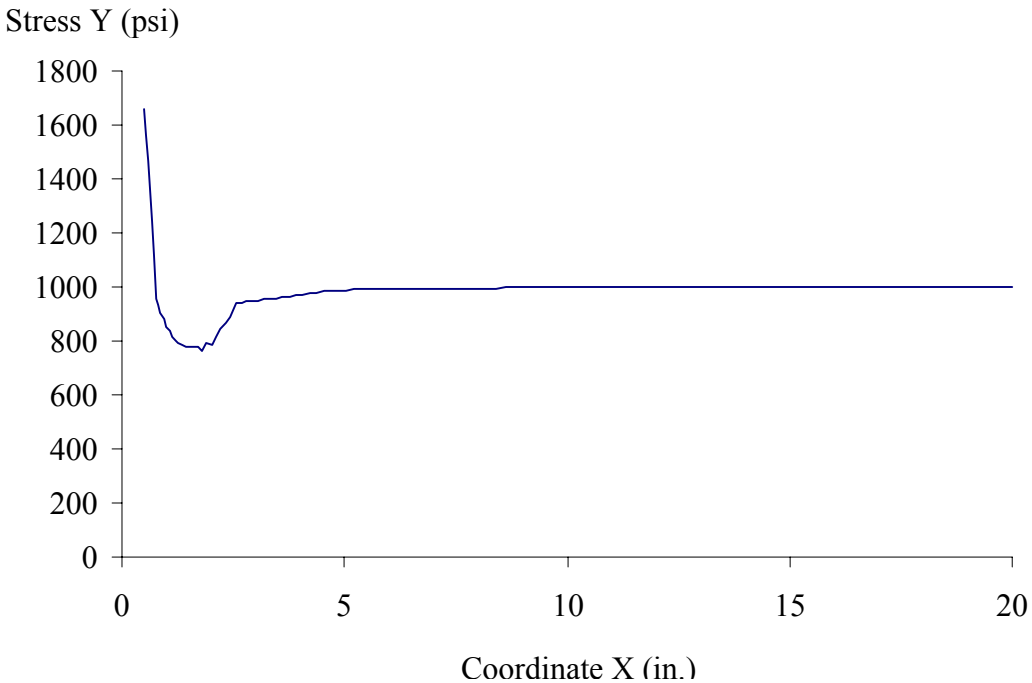

FIGURE 6. STRESS Y ALONG A LINE PATH FROM (0.5001,0.0) TO (19.999, 0.0) FOR THE CIRCULAR ANTENNA INSTALLATION

TABLE 1. RIVET POSITIONS OF THE CIRCULAR ANTENNA INSTALLATION

Rivet Label	X	Y
0	1.000	0.000
1	0.707	0.707
2	0.000	1.000
3	2.000	0.000
4	1.848	0.765
5	1.414	1.414
6	0.765	1.848
7	0.000	2.000

TABLE 2. RIVET FORCES OF THE CIRCULAR ANTENNA INSTALLATION

Rivet Label	Force X	Force Y
0	0.0064	0.0000
1	0.1446	3.1531
2	0.0000	2.2234
3	-0.2214	0.0000
4	-0.8887	4.8448
5	-1.5559	8.3741
6	-1.2162	9.6441
7	0.0000	4.6257

(2nd) 2.3.2 A Door Opening Repair

[Problem Description] In the second example, we consider a more complex layered model that is likely to be used for the repair scenario around the door cutout region in the airplane. Figure 7 shows the geometry of model, which consists of "repair doubler 1", "repair doubler 2", "skin" and "production doubler". We model them as layer 0, 1, 2, 3, respectively. The key points defining the geometry of each layer are labeled in Figure 8 where the detailed positions can be found in the input records in Appendix B. Figure 9 plots the rivet locations. The detailed positions of each rivet can be found in the input records in Appendix B. We note that a rectangular skin cutout is rarely used in practice. Instead a more rounded cutout is likely to be used. Nevertheless, the problem is sufficed to demonstrate the capability of the program.

[Analysis Results] For this example, we only show the meshes generated by the problem. However, the analysis results of any regions of interest can be easily produced using the program with the input records in Appendix B. Finite element meshes for layer 0 and layer 1 are shown in Figure 10. Again in the overlapped area, two layers have their own distinct mesh characteristics with finite element nodes automatically generated at the rivet locations. Finite element meshes for layer 2 and layer 3 are plotted in Figure 11.

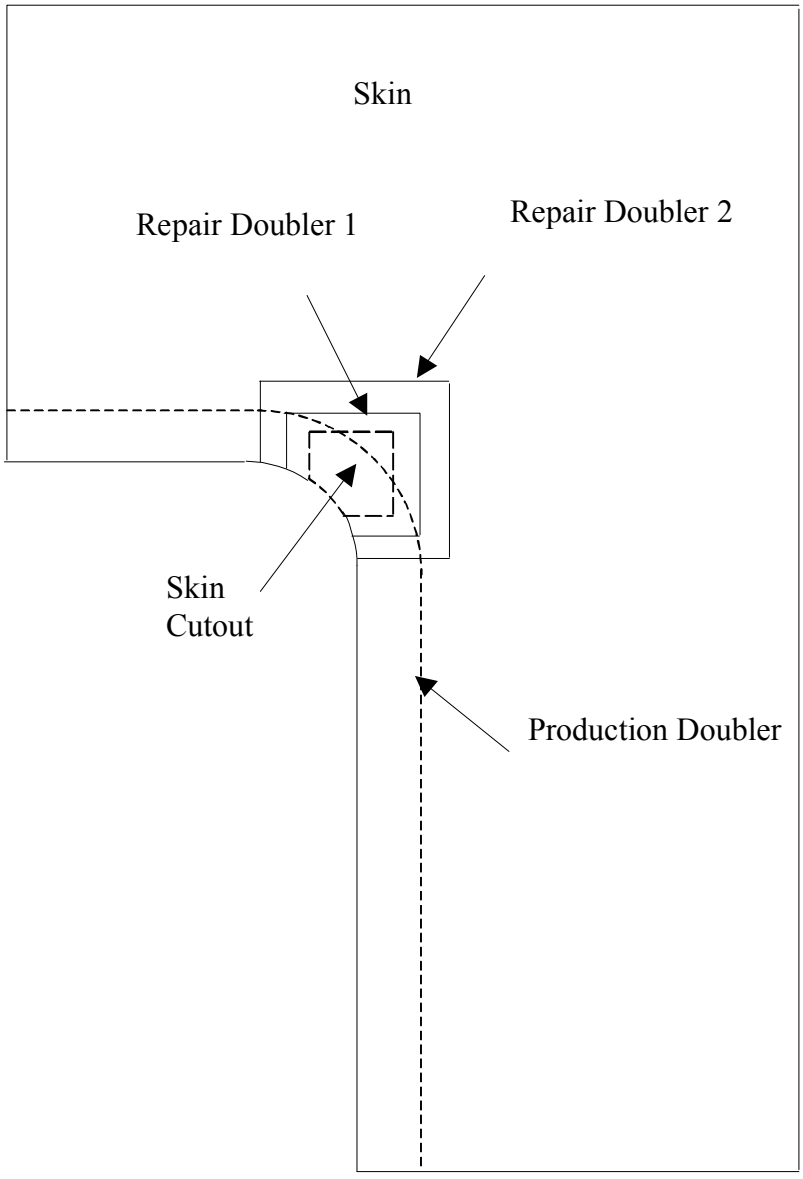

FIGURE 7. ILLUSTRATION OF THE DOOR OPENING REPAIR.

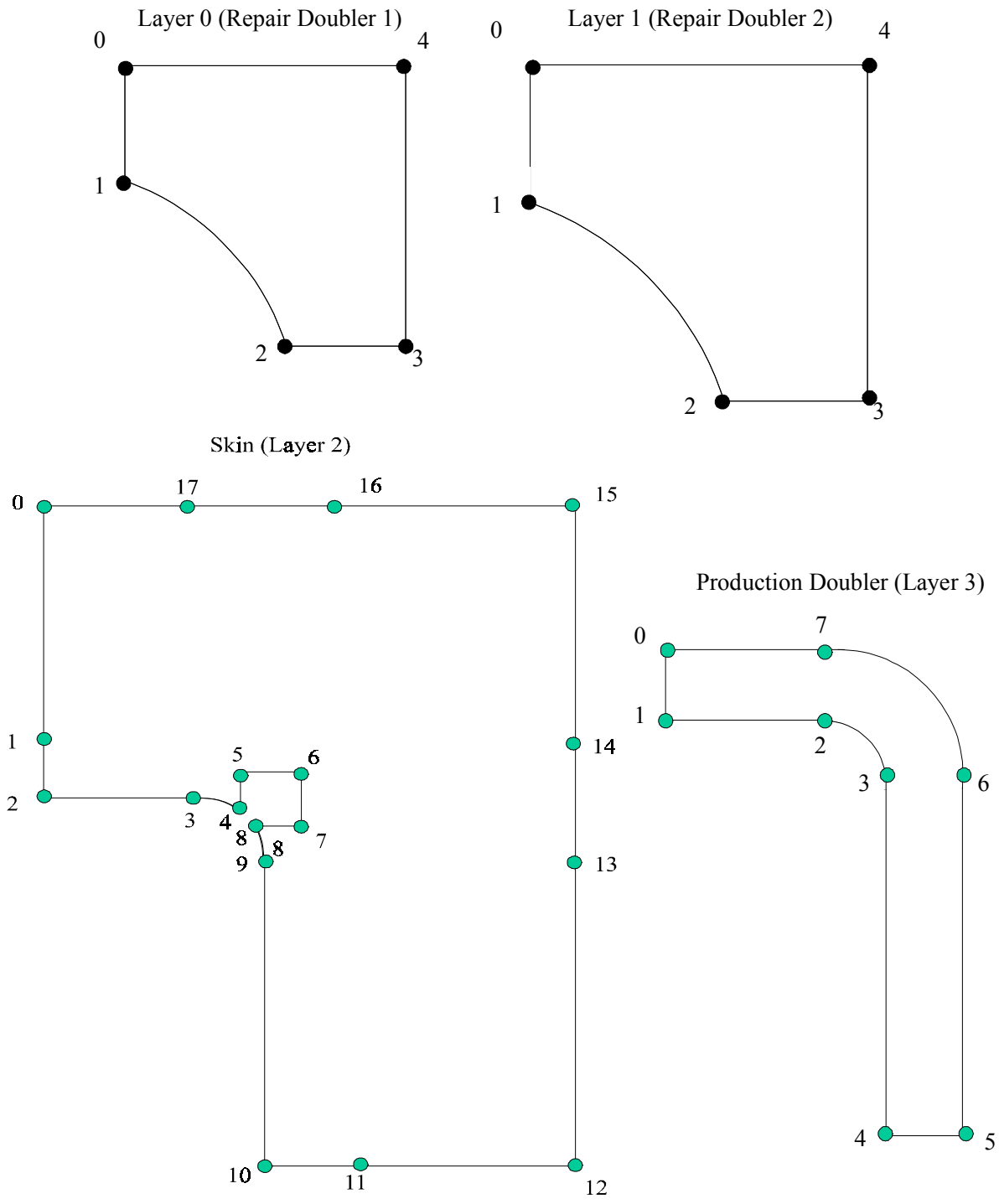

FIGURE 8. KEY POINT LABELS OF EACH LAYER OF THE DOOR OPENING REPAIR.

Rivets between Layer 0 and Layer 1

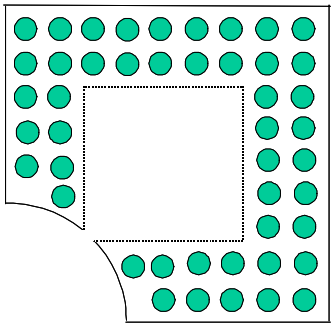

Number of rivets = 46

Rivets between Layer 1 and Layer 2

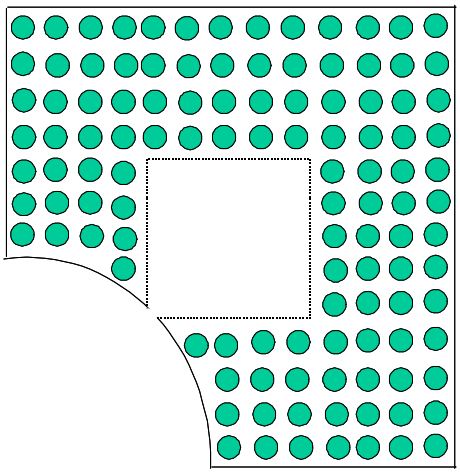

Number of rivets = 114

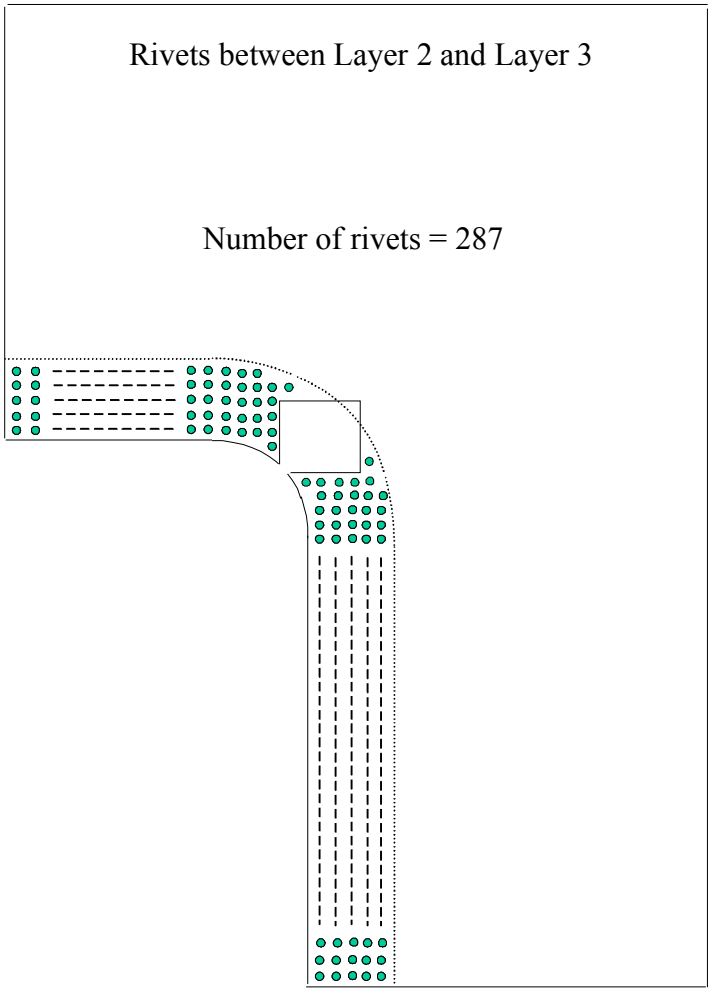

FIGURE 9. ILLUSTRSTATION OF RIVET LOCATIONS BETWEEN THE LAYERS FOR THE DOOR OPENING REPAIR.

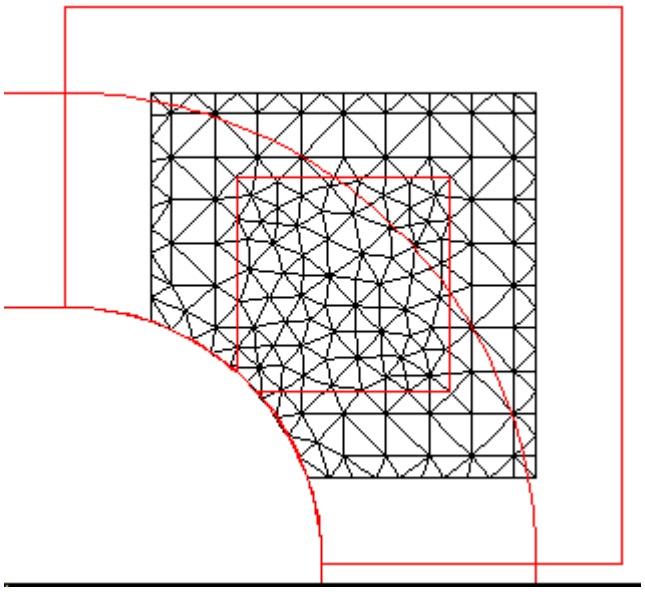

(Layer 0)

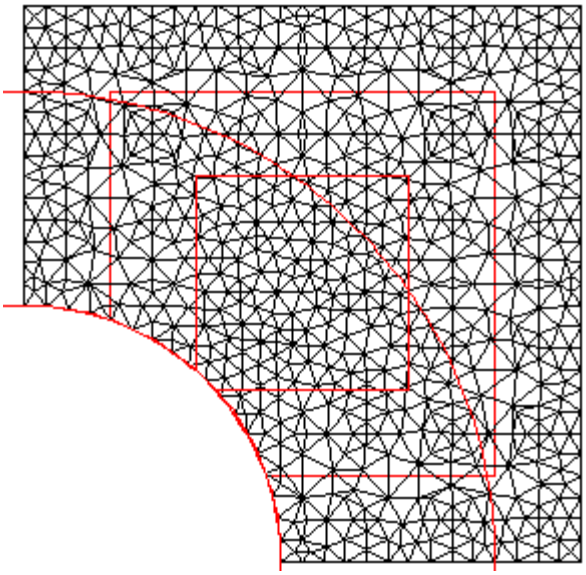

(Layer 1)

FIGURE 10. MESHES FOR LAYER 0 AND 1 OF DOOR OPENING REPAIR.

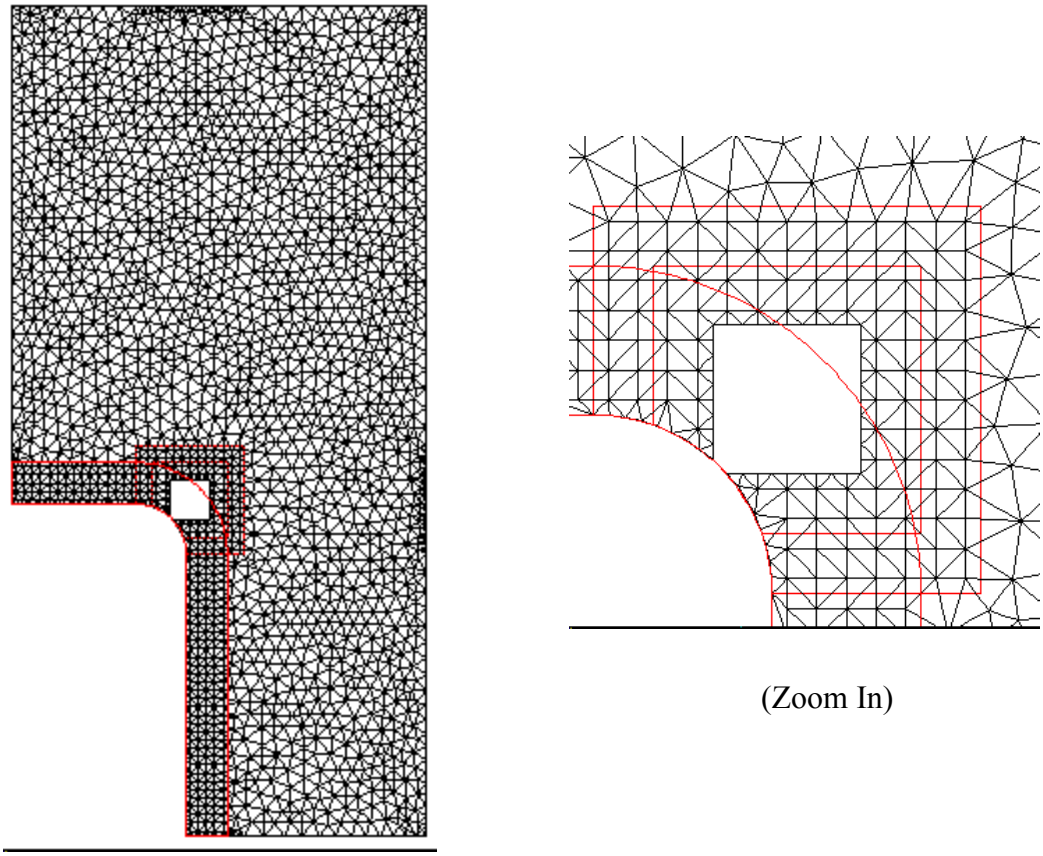

FIGURE 11. MESHES FOR LAYER 2 (SKIN) OF DOOR OPENING REPAIR.

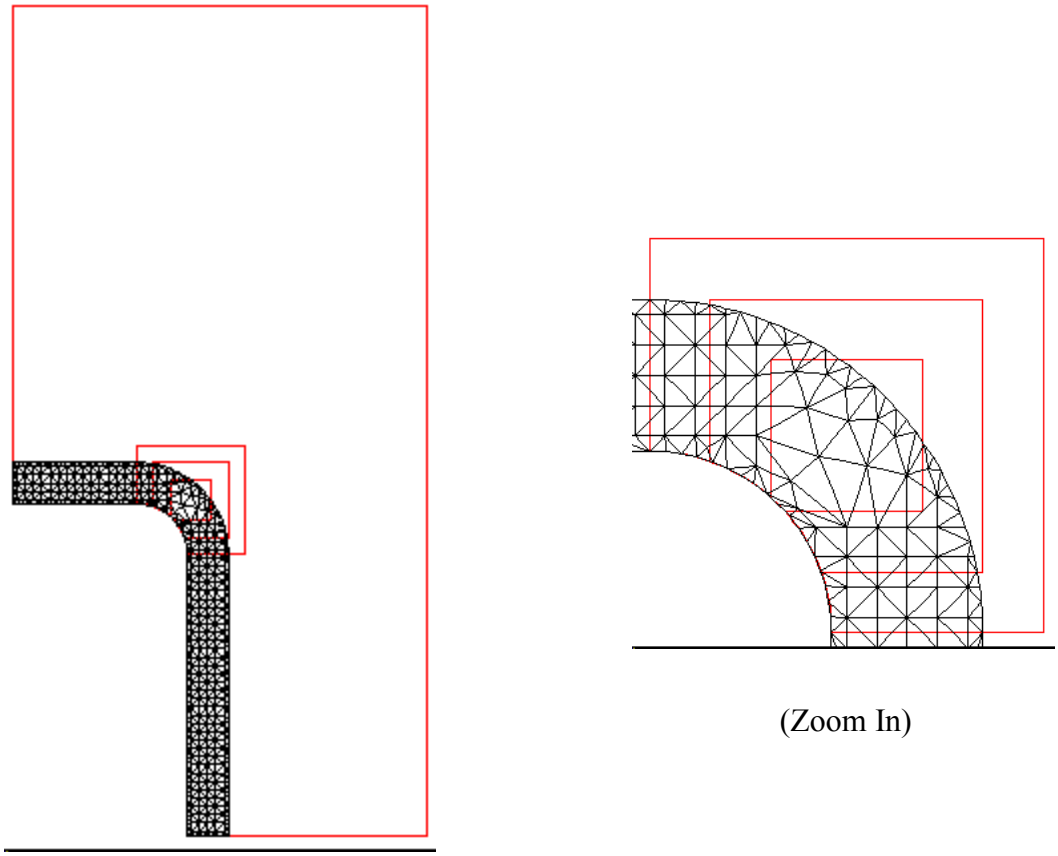

FIGURE 12. MESHES FOR LAYER 3 (PRODUCTION DOUBLER) OF DOOR OPENING REPAIR.

(M) 3. THREE-DIMENSIONAL THIN-SHELL FINITE ELEMENT ANALYSES OF FUSELAGE STRUCTURES WITH A DOOR CUTOUT

The second objective of the project is to perform 3D thin-shell finite element analyses of fuselage structures with a door cutout configuration and compare stresses around the door corner with the 2D finite element results. Due to the inherent complexity of thin shell finite element formulations, it is best to use existing robust finite element packages to accomplish the task. In this work, we use a general finite element package, ANSYS [9] to analyze the problems.

Our main purpose is to evaluate and correlate the predicted results between 3D thin shell and 2D plane stress analyses for a set of geometries and boundary conditions. Doing this successfully will allow us to provide a handbook of "correction factors" in the RAPID program to correlate 2D computed results for the real life 3D structures.

(1st) 3.1 Numerical Models

We consider both wide-body and narrow-body airplane fuselages. The wide-body model consists of a cylinder with a door cutout. The cylinder has a single radius and the door is above the floor line to model the passenger door. The narrow-body model also consists of a cylinder with a door cutout, but the cylinder has double radius and the door is below the floor line to model a cargo door. The sketches of the geometries and material properties are provided by Boeing [10] and are included in Appendix C.

(2nd) 3.1.1 Model Idealization

The major structural components consist of skin, longerons, frames, and floor beams. In the vicinity of the door cutout, we have several layers of doublers and a torque box around the door. We model skin and doublers with shell and layered shell elements. The shell finite element is an 8-noded quadratic shell. We model frames, longerons and floor beams with 3D beam elements with offset. For the torque box around the door, we model the geometry explicitly with shell elements. Both pressure loading and vertical shear loading are considered in our analysis. Figures 13 and 14 show the finite element meshes used for the wide-body and narrow-body fuselage models, respectively. These meshes are used for the case with pressure loading. For vertical shear loading, we add a set of rigid bars at the forward end of the fuselage and a rigid bar from the centroid of the forward end to the center of the fuselage (see figure 15). This allows us to apply the shear loading at the center of the fuselage.

For 2D models, we flatten out the structures in a local region around the door cutout and model all the structural components with quadratic plane stress elements.

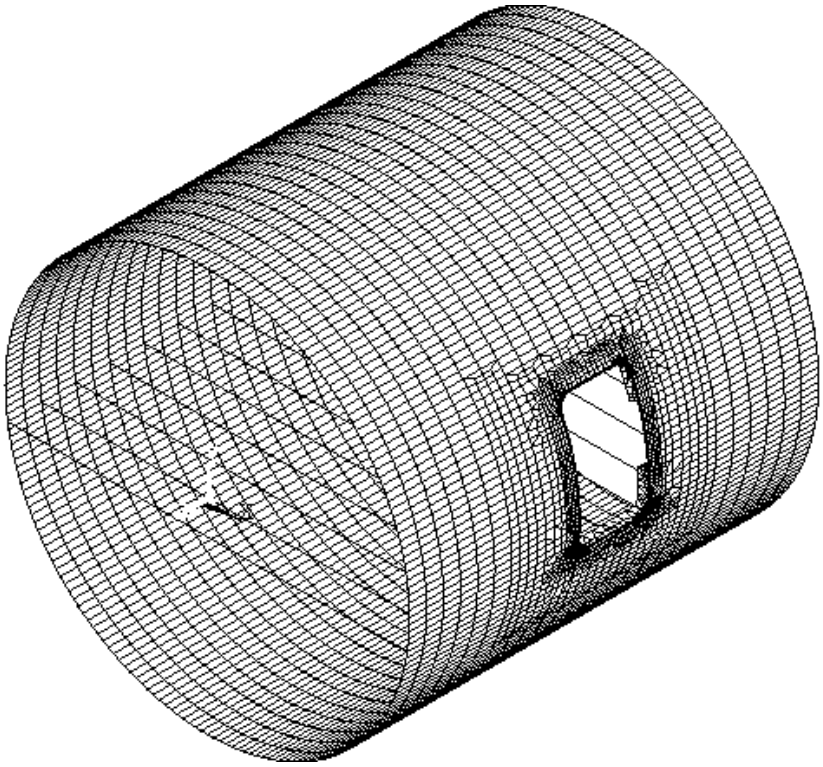

(a)

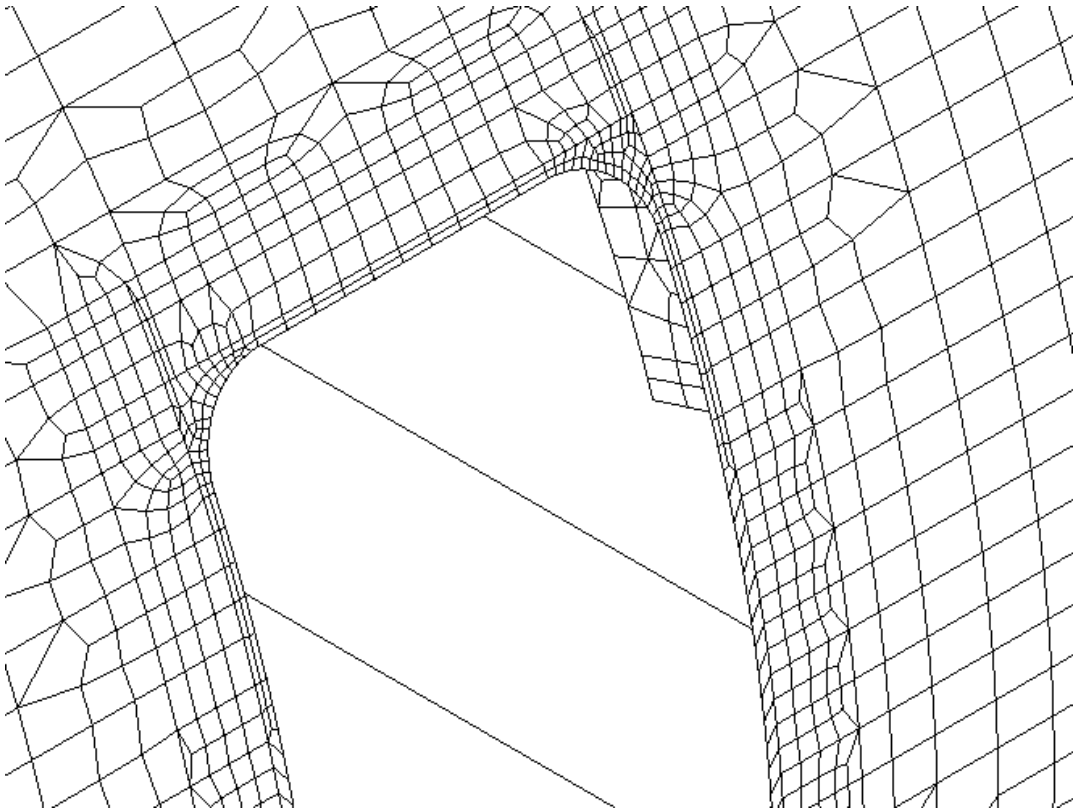

(b)

FIGURE 13. (A) FINITE ELEMENT MESHES FOR THE WIDE-BODY FUSELAGE MODEL AND (B) DETAIL AT THE DOOR CUTOUT REGION.

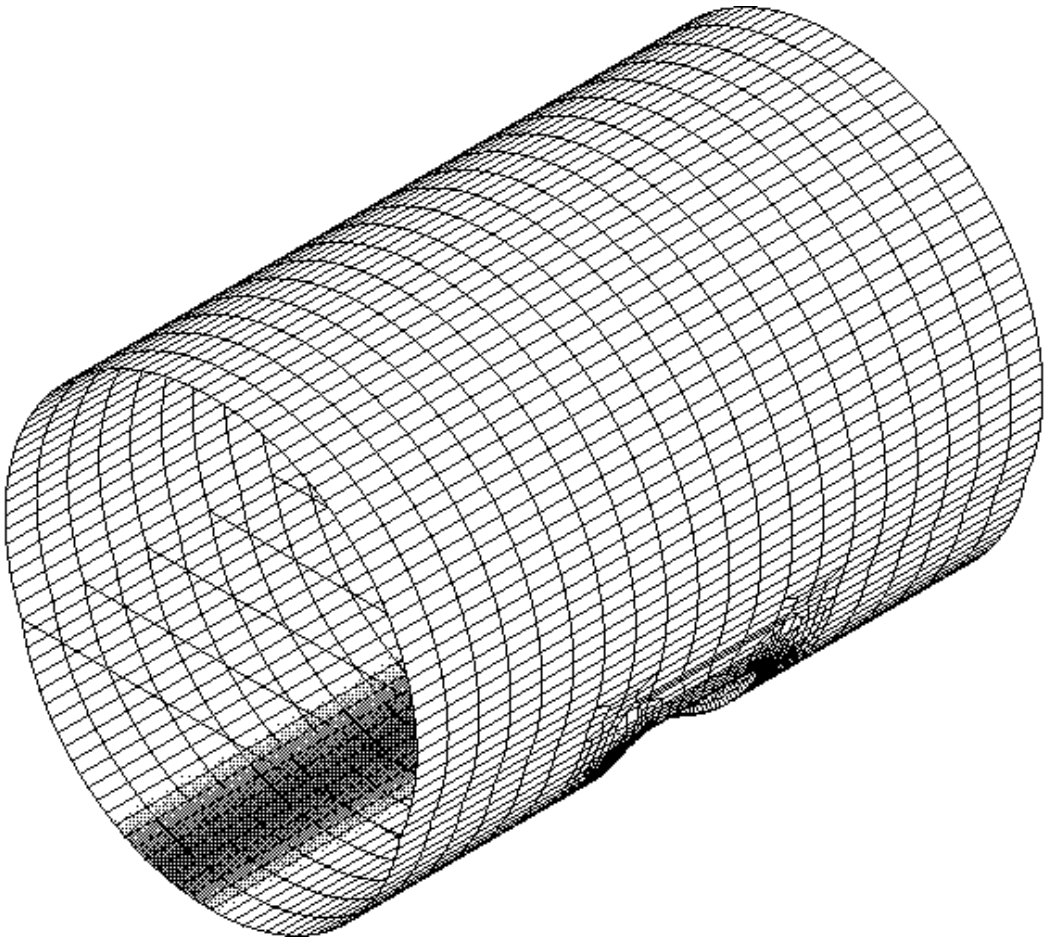

(a)

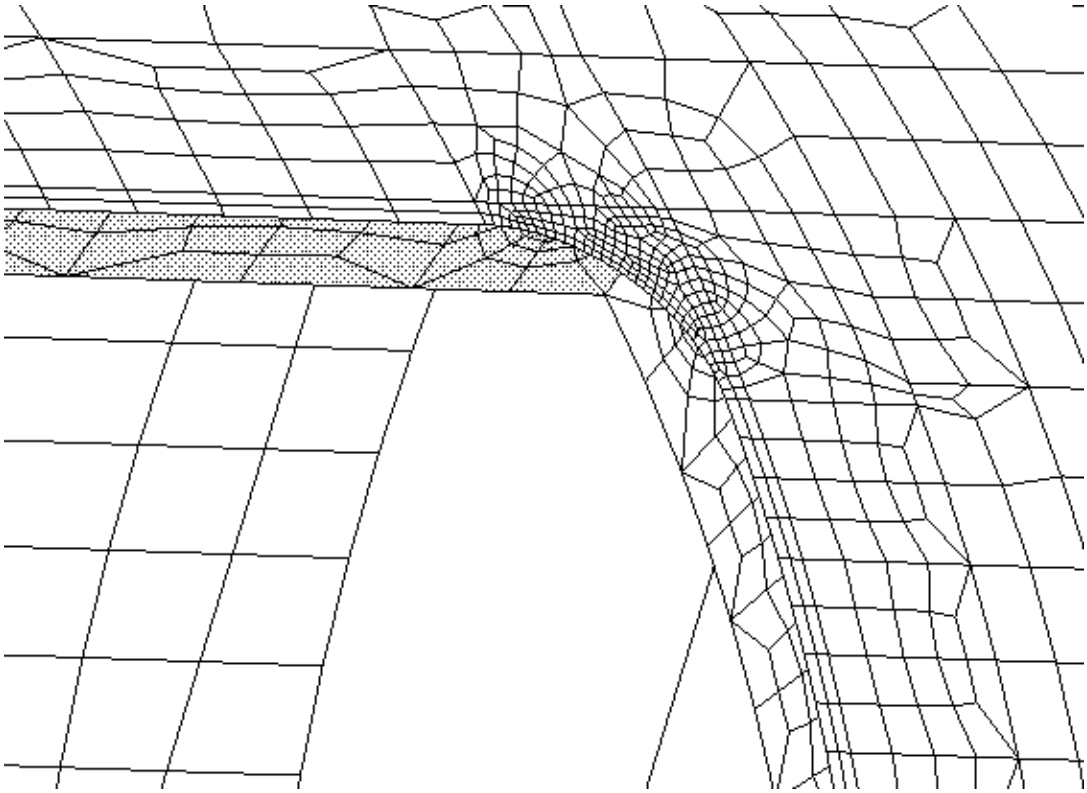

(b)

FIGURE 14. (A) FINITE ELEMENT MESHES FOR THE NARROW-BODY FUSELAGE MODEL AND (B) DETAIL AT THE DOOR CUTOUT REGION.

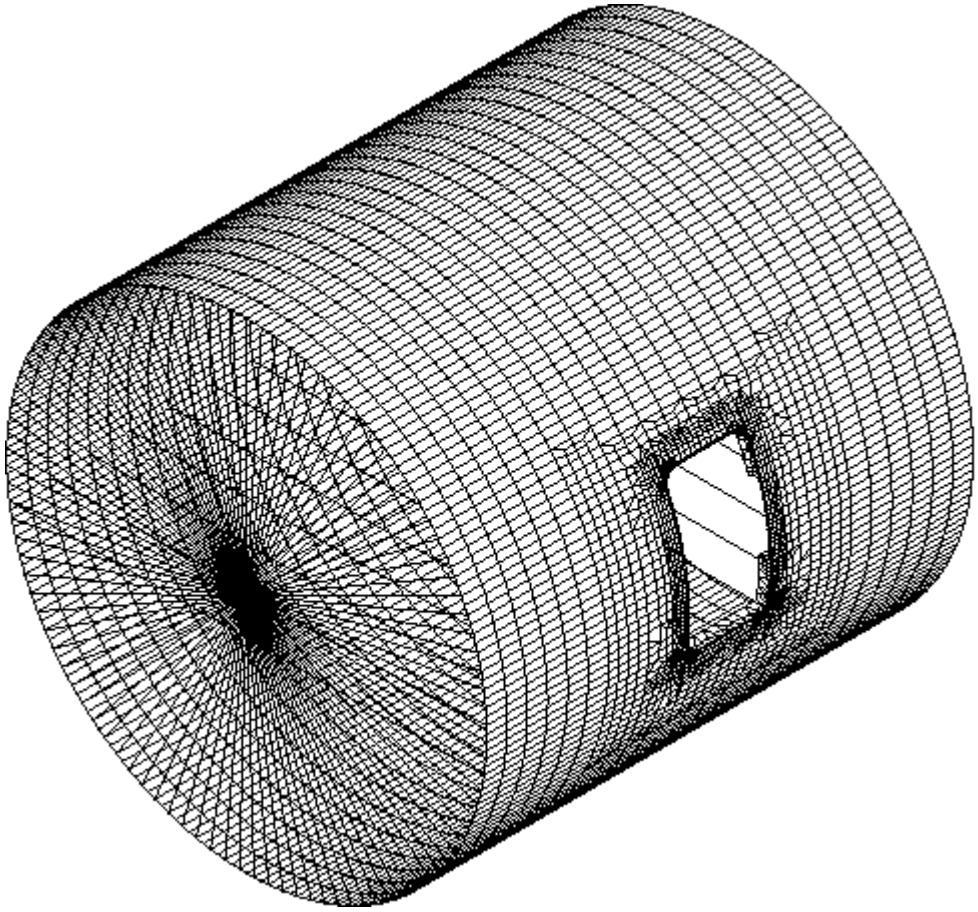

FIGURE 15. FINITE ELEMENT MESHES FOR CASE WITH THE VERTICAL SHEAR LOADING (WIDE-BODY FUSELAGE MODEL).

(2nd) 3.1.2 Boundary Conditions

We consider both pressure loading and vertical shear loading in our analysis. For the pressure loading, a nominal pressure equal to 8.0 psi is applied uniformly on the skin except at the door cutout region. At this region, we consider two extreme scenarios: one with nominal pressure 8.0 psi and the other with an effective pressure due to door jamb. The effective pressure is computed by lumping the pressure loading from the cutout to the door ring. In our cases, the effective pressure due to door jamb is equal to 93.2 psi for the wide-body model and 78.5 psi for the narrow-body model. In addition to the applied pressure, a longitudinal force equal to $\frac{pR}{2} \cdot 2\pi R$ together with a set of longitudinal constraint for uniform longitudinal expansion is applied at the aft end to simulate a closed cylinder. The longitudinal and circumferential boundary conditions at the forward end and the circumferential boundary conditions at the aft end are restrained.

For the vertical shear loading, a clamped end is applied at the aft end and a vertical shear load equal to 100,000 lb is applied at one end of a rigid bar located at the centroid of the fuselage where the other end of the rigid bar is located at centroid of the forward end.

For 2D models, we extract the traction boundary conditions from the thin-shell model and apply minimum constraints far away from the door cutout to prevent models from rigid body motions.

(1st) 3.2 Numerical Results

All the numerical results reported herein are obtained using linear elastic analysis. We conducted three different boundary conditions for both wide-body and narrow-body models; these are pressure loading, pressure loading with door jamb pressure and vertical shear loading. With their corresponding 2D counterparts, this leads to total 12 sets of analysis results. We show the predicted deformed shape and predicted maximum membrane principal stress distributions in the following order:

1) Wide Body Model With Pressure Loading, Thin Shell Analysis
2) Wide Body Model With Pressure Loading and Door Jamb Pressure, Thin Shell Analysis
3) Wide Body Model With Vertical Shear Loading, Thin Shell Analysis
4) Wide Body Model With Pressure Loading, 2D Analysis
5) Wide Body Model With Pressure Loading and Door Jamb Pressure, 2D Analysis
6) Wide Body Model With Vertical Shear Loading, 2D Analysis
7) Narrow Body Model With Pressure Loading, Thin Shell Analysis
8) Narrow Body Model With Pressure Loading and Door Jamb Pressure, Thin Shell Analysis
9) Narrow Body Model With Vertical Shear Loading, Thin Shell Analysis
10) Narrow Body Model With Pressure Loading, 2D Analysis
11) Narrow Body Model With Pressure Loading and Door Jamb Pressure, 2D Analysis
12) Narrow Body Model With Vertical Shear Loading, 2D Analysis

For the stress distributions in thin shell analysis, we denote membrane results as the computed average of the outer surface of the outer layer (skin) plus the inner surface of the inner layer (doubler 2 for the wide body configuration and double 1 for the narrow body configuration). Bending results are computed from the average of the outer surface of the outer layer minus the inner surface of the inner layer. For 2D analysis, only membrane results are available by its nature.

At the end of the section, we summarize a quantitative comparison of the computed stresses evaluated at the aft/upper end of the door corner from 3D thin shell analysis and 2D plane stress analysis.

(2nd) 3.2.1 Predicted Deformed Shape

We show a sequence of snapshots of predicted deformed shape in figures 16-27, following the order listed previously. Several observations are made from these predictions:

- For the cases with nominal pressure, the stiffening elements including doublers and torque box prevent the skin around the door cutout from bulging. This can be observed clearly by comparing figures 16 and 17 where the structure in the former shows a concave inward deformation around the door cutout, contrast to a typical bulging deformation one would expect from pressure loading.
- For cases with vertical shear loading, we observe an anticipated shearing deformation where the upper/aft and lower/forward corners of the door form an obtuse angle and the other two corners form a sharp angle in their deformed shapes. The shear loading also flattens out the curvature at the door corners, and we will see its effect on predicting bending stress in section 3.2.3.
- The location of the door cutout affects the deformation. The double radius in the narrow-body also increases the complexity, for example, more bulging is observed at the junction where the radius alters from one to the other.

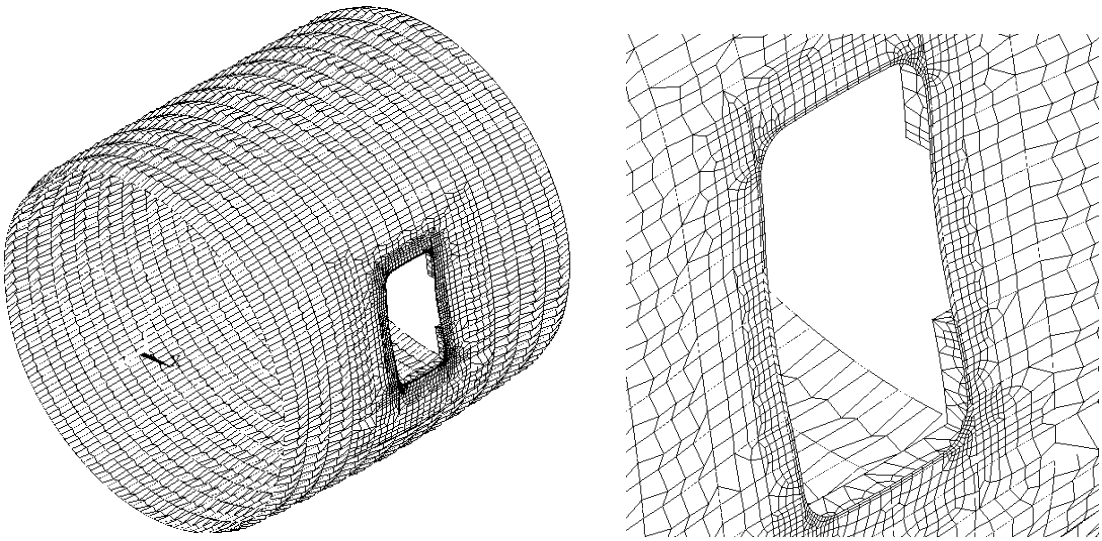

FIGURE 16. DEFORMED SHAPE FOR THE WIDE-BODY MODEL SUBJECTED TO PRESSURE LOADING; THIN SHELL ANALYSIS (1) (MAGNIFICATION FACTOR = 30).

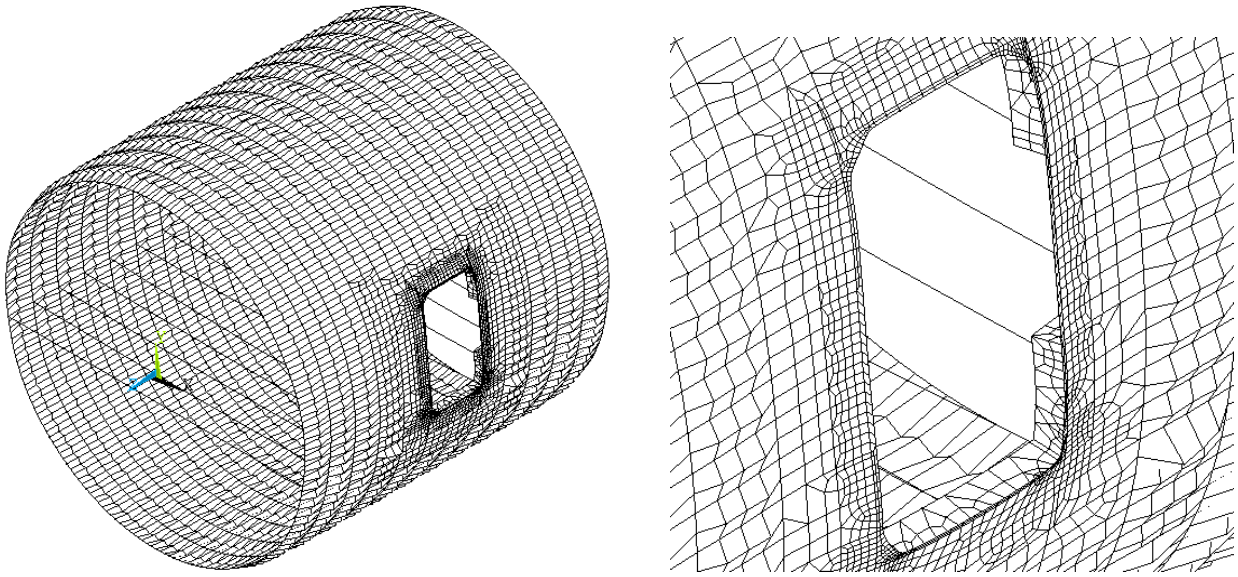

FIGURE 17. DEFORMED SHAPE FOR THE WIDE-BODY MODEL SUBJECTED TO PRESSURE LOADING AND DOOR JAMB PRESSURE; THIN SHELL ANALYSIS (2) (MAGNIFICATION FACTOR = 30).

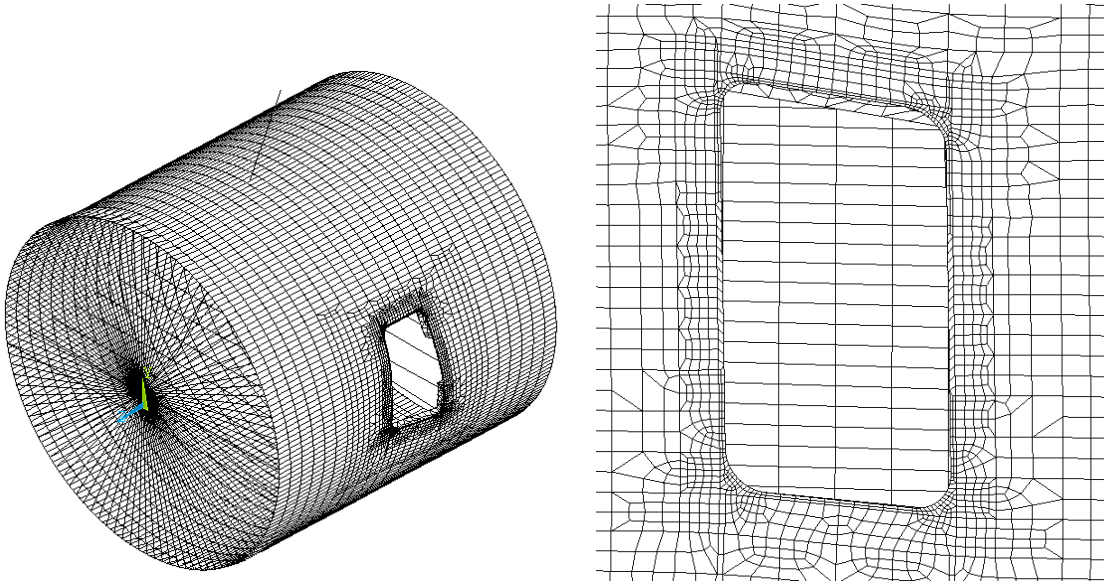

FIGURE 18. DEFORMED SHAPE FOR THE WIDE-BODY MODEL SUBJECTED TO VERTICAL SHEAR LOADING; THIN SHELL ANALYSIS (3) (MAGNIFICATION FACTOR = 30).

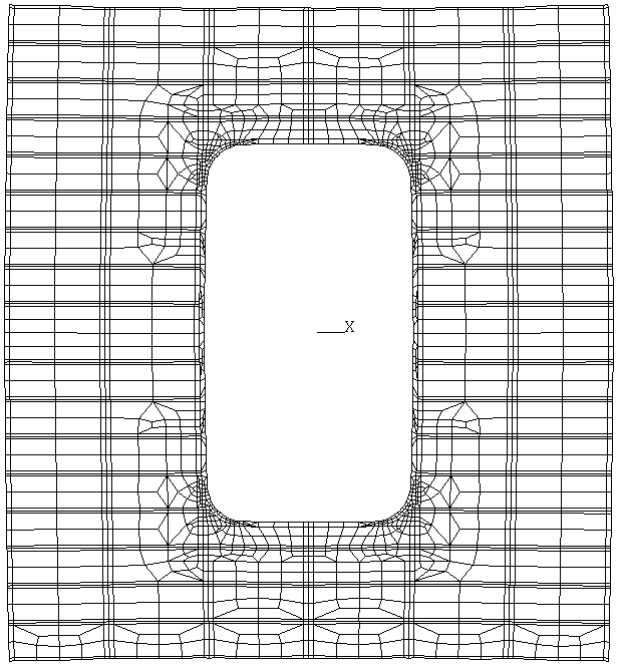

FIGURE 19. DEFORMED SHAPE FOR THE WIDE-BODY MODEL SUBJECTED TO PRESSURE LOADING; 2D ANALYSIS (4) (MAGNIFICATION FACTOR = 30).

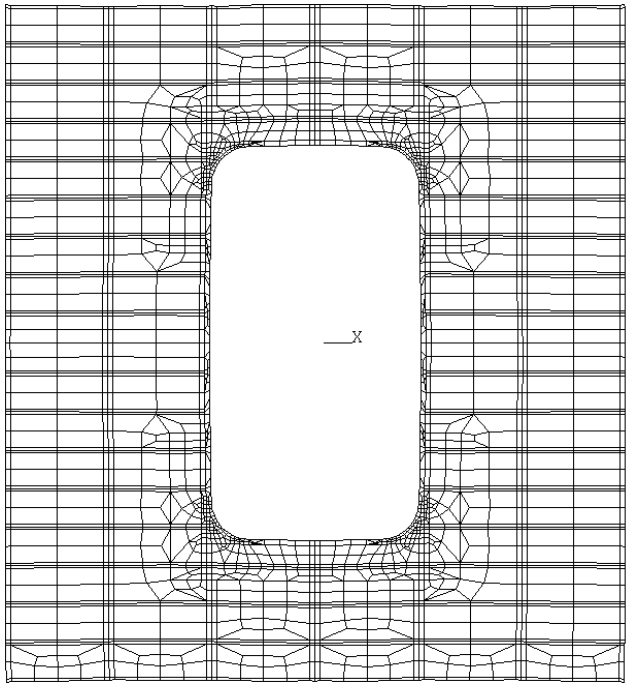

FIGURE 20. DEFORMED SHAPE FOR THE WIDE-BODY MODEL SUBJECTED TO PRESSURE LOADING AND DOOR JAMB PRESSURE; 2D ANALYSIS (5) (MAGNIFICATION FACTOR = 30).

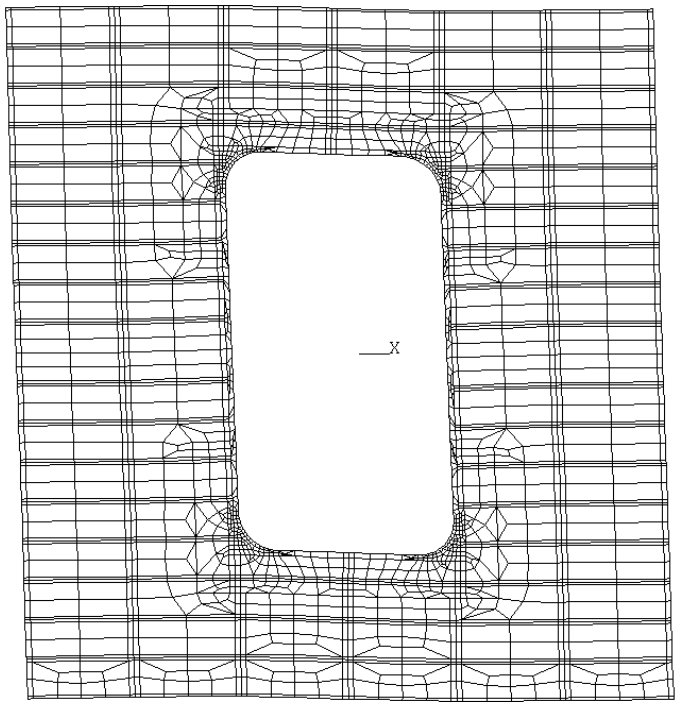

FIGURE 21. DEFORMED SHAPE FOR THE WIDE-BODY MODEL SUBJECTED TO VERTICAL SHEAR LOADING; 2D ANALYSIS (6) (MAGNIFICATION FACTOR = 30).

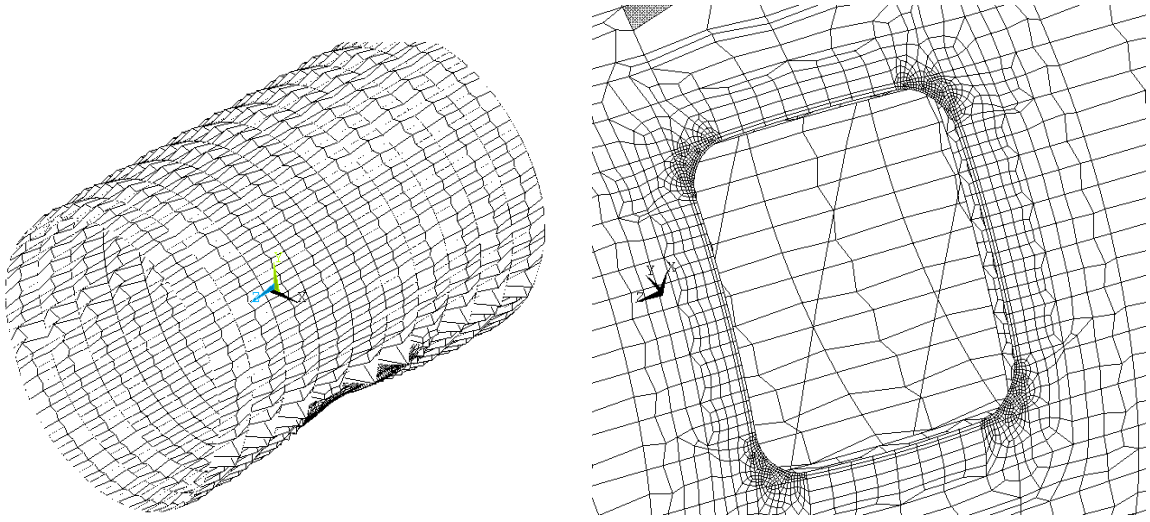

FIGURE 22. DEFORMED SHAPE FOR THE NARROW-BODY MODEL SUBJECTED TO PRESSURE LOADING; THIN SHELL ANALYSIS (7) (MAGNIFICATION FACTOR = 30).

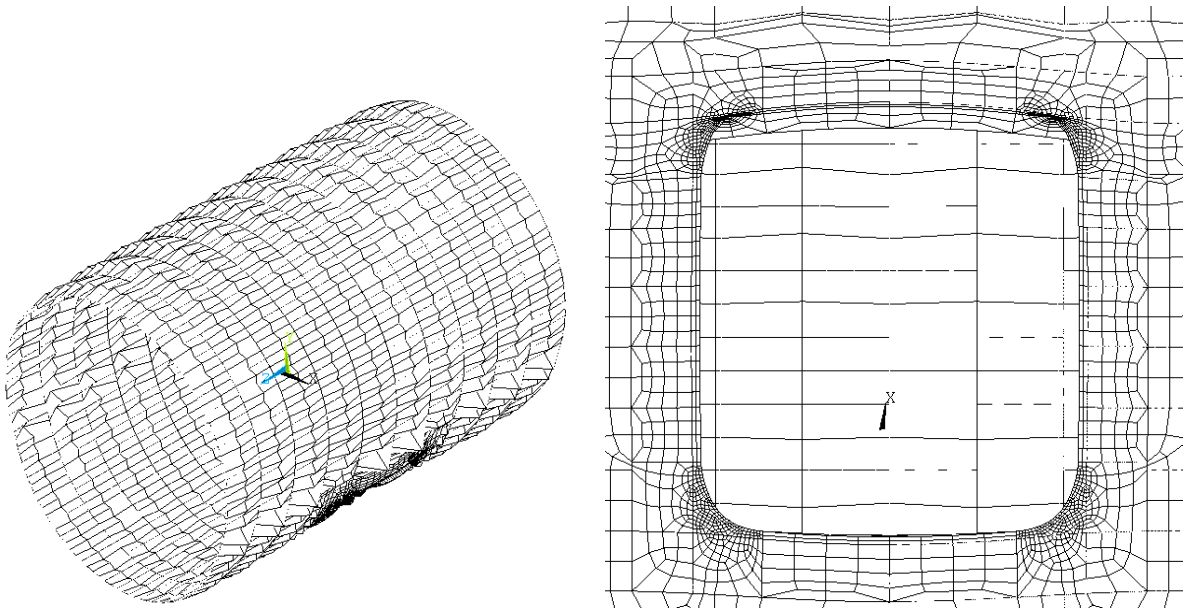

FIGURE 23. DEFORMED SHAPE FOR THE NARROW-BODY MODEL SUBJECTED TO PRESSURE LOADING AND DOOR JAMB PRESSURE; THIN SHELL ANALYSIS (8) (MAGNIFICATION FACTOR = 30).

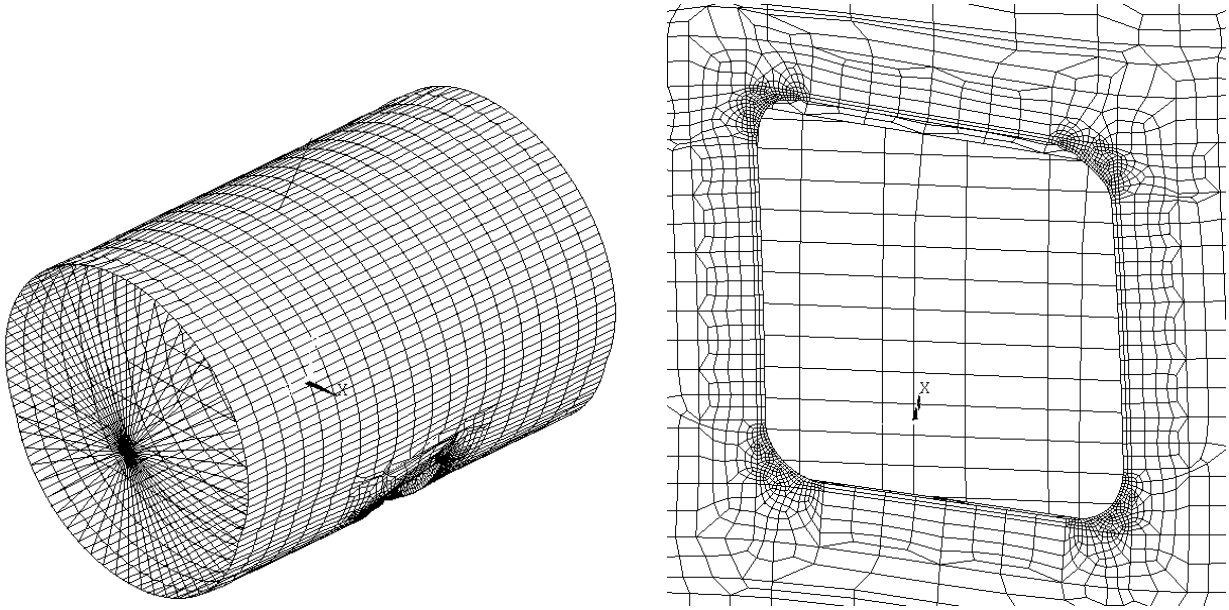

FIGURE 24. DEFORMED SHAPE FOR THE NARROW-BODY MODEL SUBJECTED TO VERTICAL SHEAR LOADING; THIN SHELL ANALYSIS (9) (MAGNIFICATION FACTOR = 30).

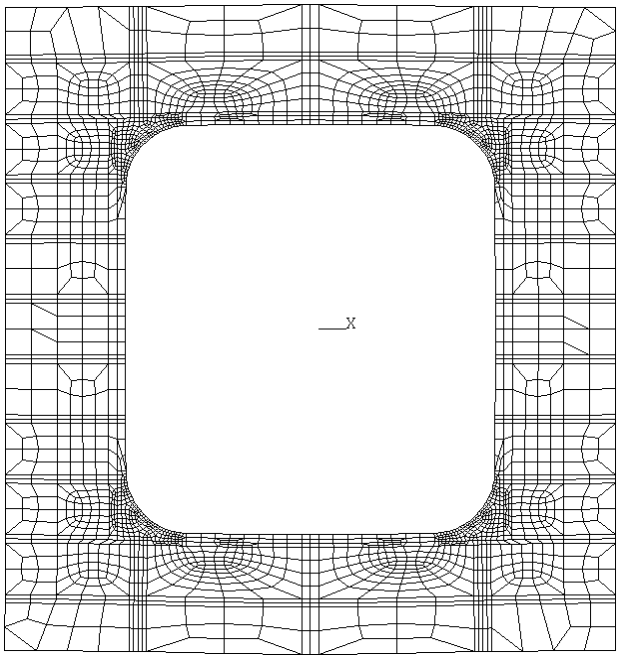

FIGURE 25. DEFORMED SHAPE FOR THE NARROW-BODY MODEL SUBJECTED TO PRESSURE LOADING; 2D ANALYSIS (10) (MAGNIFICATION FACTOR = 30).

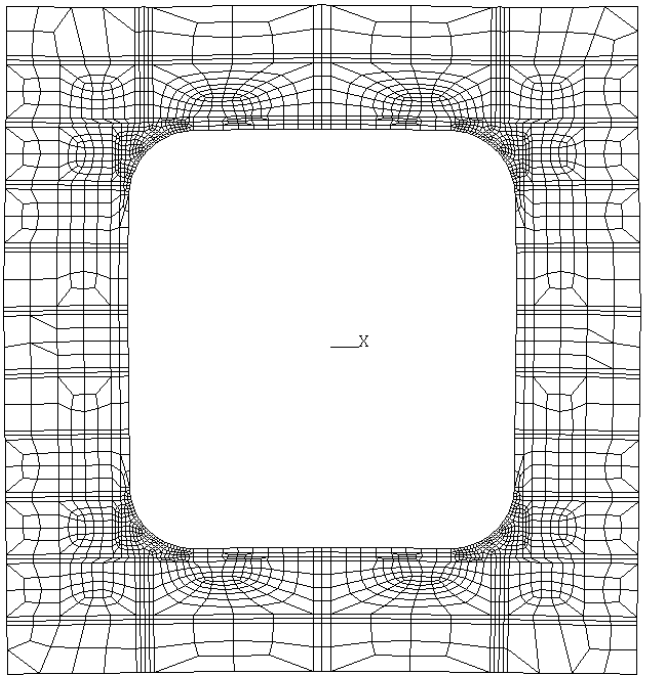

FIGURE 26. DEFORMED SHAPE FOR THE NARROW-BODY MODEL SUBJECTED TO PRESSURE LOADING AND DOOR JAMB PRESSURE; 2D ANALYSIS (11) (MAGNIFICATION FACTOR = 30).

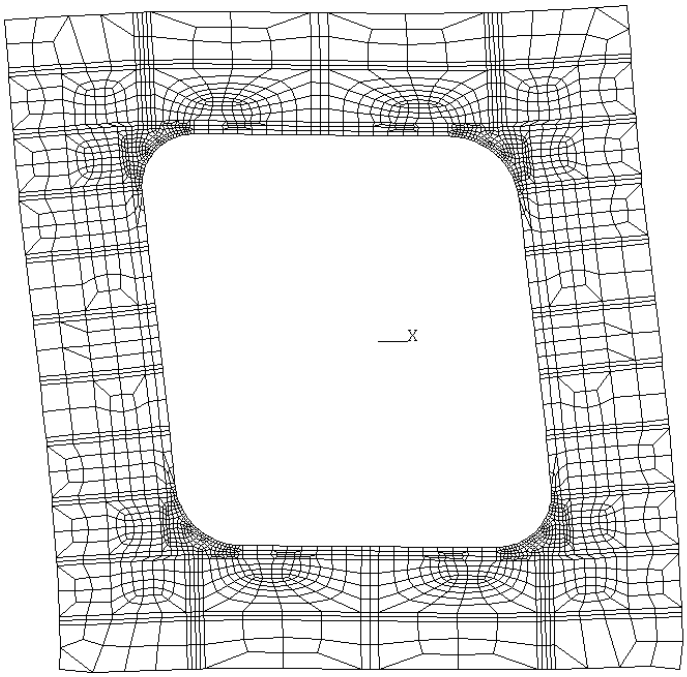

FIGURE 27. DEFORMED SHAPE FOR THE NARROW-BODY MODEL SUBJECTED TO VERTICAL SHEAR LOADING; 2D ANALYSIS (12) (MAGNIFICATION FACTOR = 30).

(2nd) 3.2.2 Predicted Maximum Membrane Principal Stress Distribution

We again show a sequence of snapshots of the predicted maximum membrane principal stress distribution in figures 28-39, following the order listed previously. Several observations are made:

- In 3D thin shell analysis, we observe the severe stress concentration occurring at the locations of the door corners for most of the cases. In 2D analysis, we occasionally observe some high stress concentrations at the boundaries. Nevertheless, these artifacts should not pollute the accuracy of our 2D estimates.
- The stiffening elements (doublers and the torque box) around the door cutout inevitably alter the stress distributions where we observe less severe stresses except in the vicinity of the corners.
- As expected, for pressure loading, we observe approximately equal stress concentrations at the four door corners, while for shear loading, we observe most severe stresses occurred at the upper/aft and lower/forward corners.

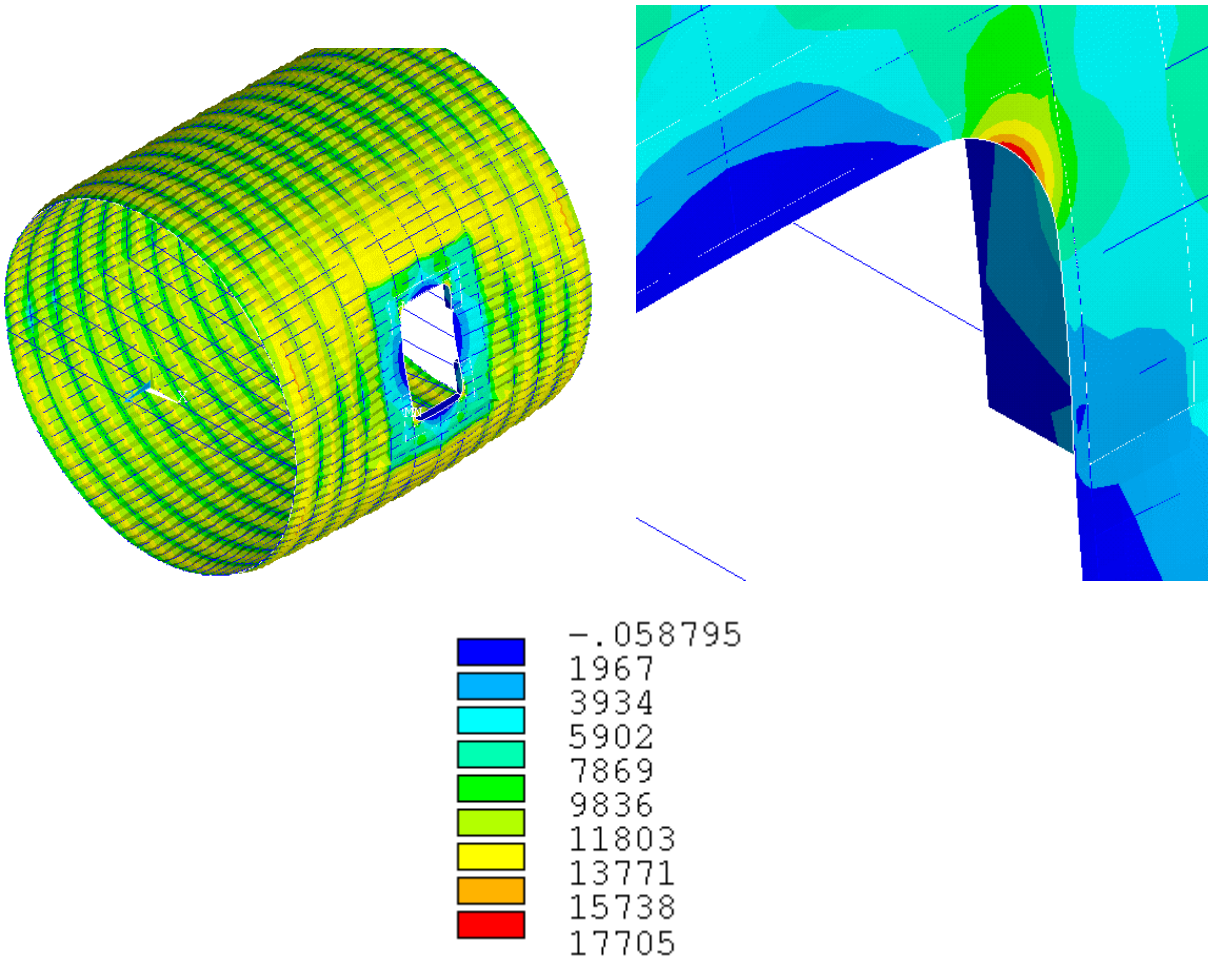

FIGURE 28. PREDICTED MAXIMUM PRINCIPAL MEMBRANE STRESS DISTRIBUTION FOR THE WIDE-BODY MODEL SUBJECTED TO PRESSURE LOADING; THIN SHELL ANALYSIS (1) (UNIT: PSI).

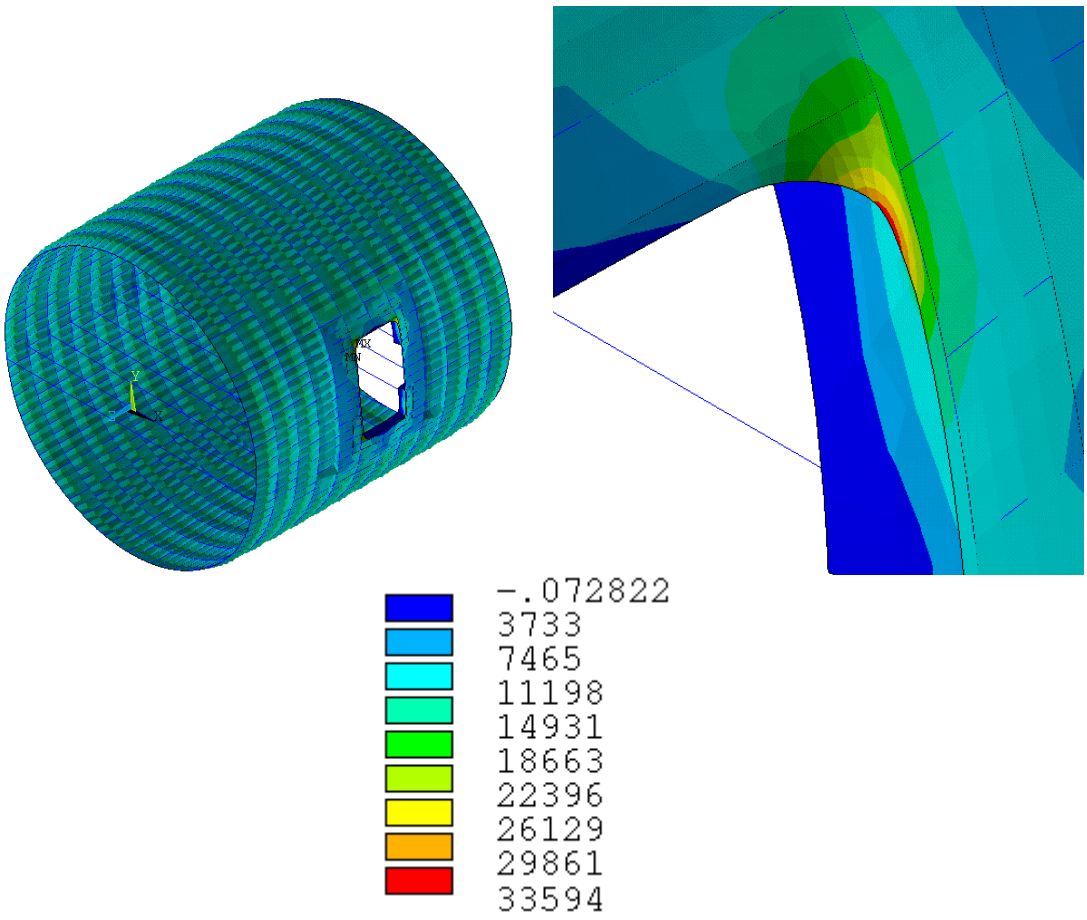

FIGURE 29. PREDICTED MAXIMUM PRINCIPAL MEMBRANE STRESS DISTRIBUTION FOR THE WIDE-BODY MODEL SUBJECTED TO PRESSURE LOADING AND DOOR JAMB PRESSURE; THIN SHELL ANALYSIS (2) (UNIT: PSI).

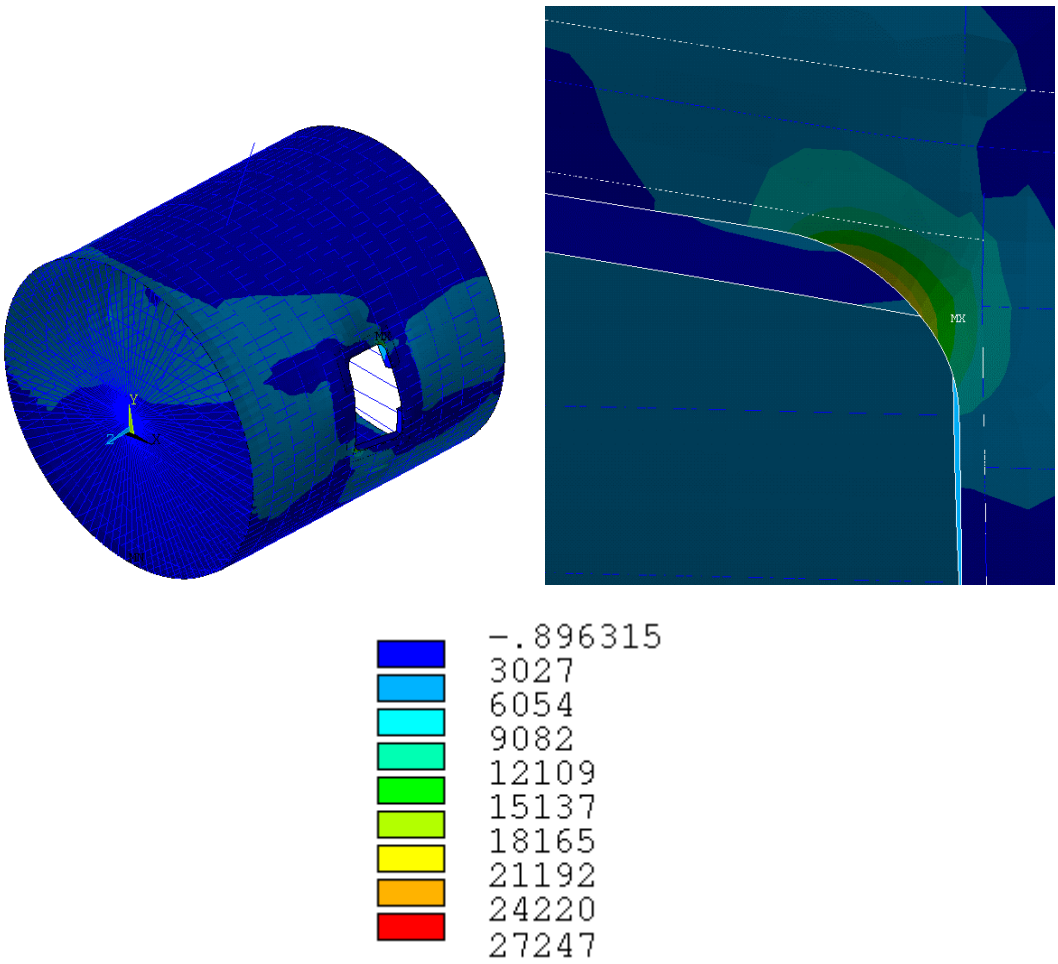

FIGURE 30. PREDICTED MAXIMUM PRINCIPAL MEMBRANE STRESS DISTRIBUTION FOR THE WIDE-BODY MODEL SUBJECTED TO VERTICAL SHEAR LOADING; THIN SHELL ANALYSIS (3) (UNIT: PSI).

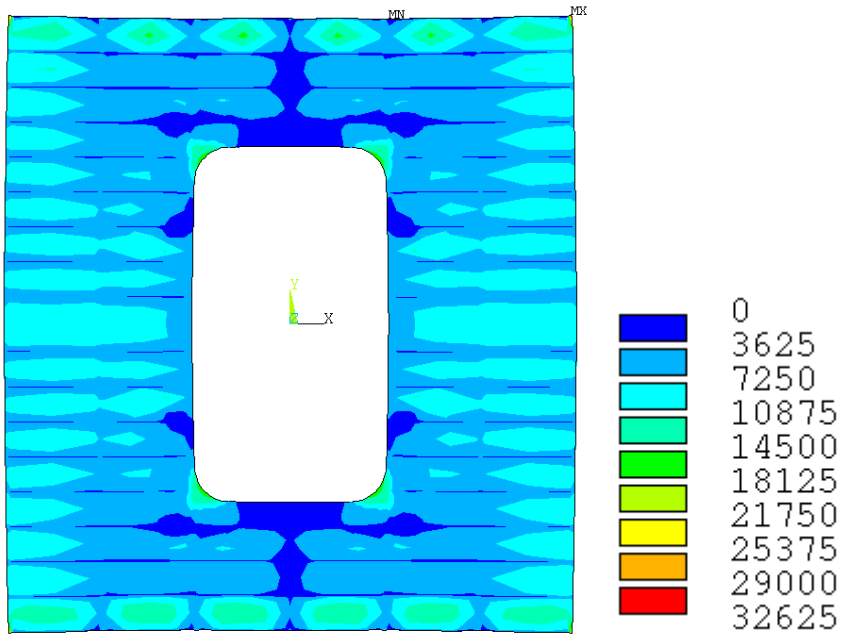

FIGURE 31. PREDICTED MAXIMUM PRINCIPAL MEMBRANE STRESS DISTRIBUTION FOR THE WIDE-BODY MODEL SUBJECTED TO PRESSURE LOADING; 2D ANALYSIS (4) (UNIT: PSI).

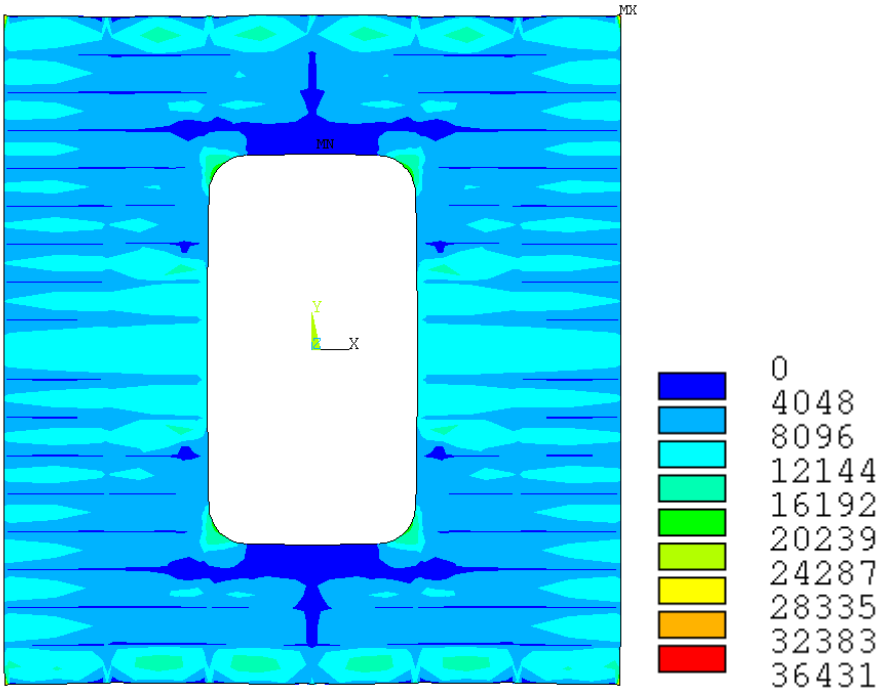

FIGURE 32. PREDICTED MAXIMUM PRINCIPAL MEMBRANE STRESS DISTRIBUTION FOR THE WIDE-BODY MODEL SUBJECTED TO PRESSURE LOADING AND DOOR JAMB PRESSURE; 2D ANALYSIS (5) (UNIT: PSI).

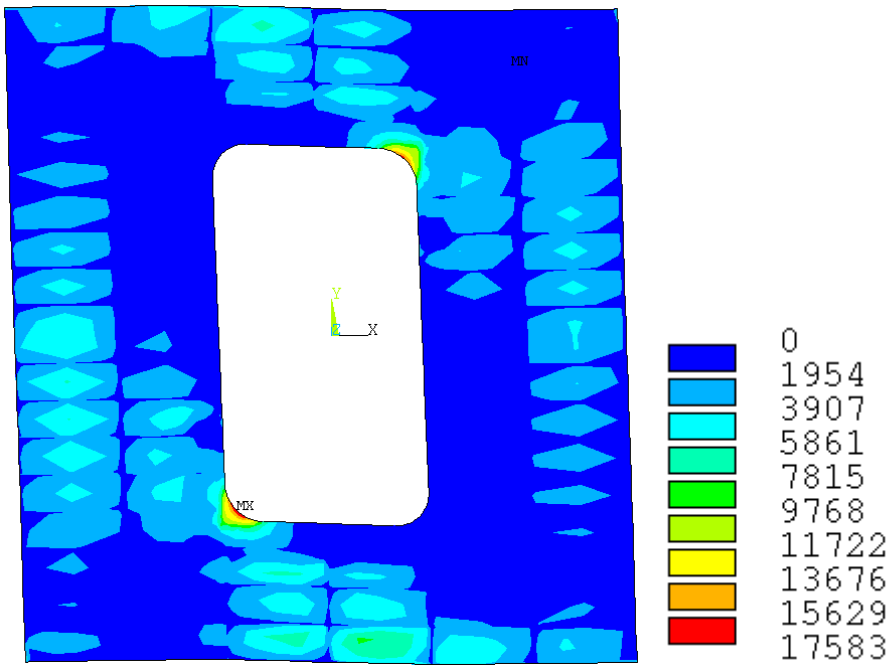

FIGURE 33. PREDICTED MAXIMUM PRINCIPAL MEMBRANE STRESS DISTRIBUTION FOR THE WIDE-BODY MODEL SUBJECTED TO VERTICAL SHEAR LOADING; 2D ANALYSIS (6) (UNIT: PSI).

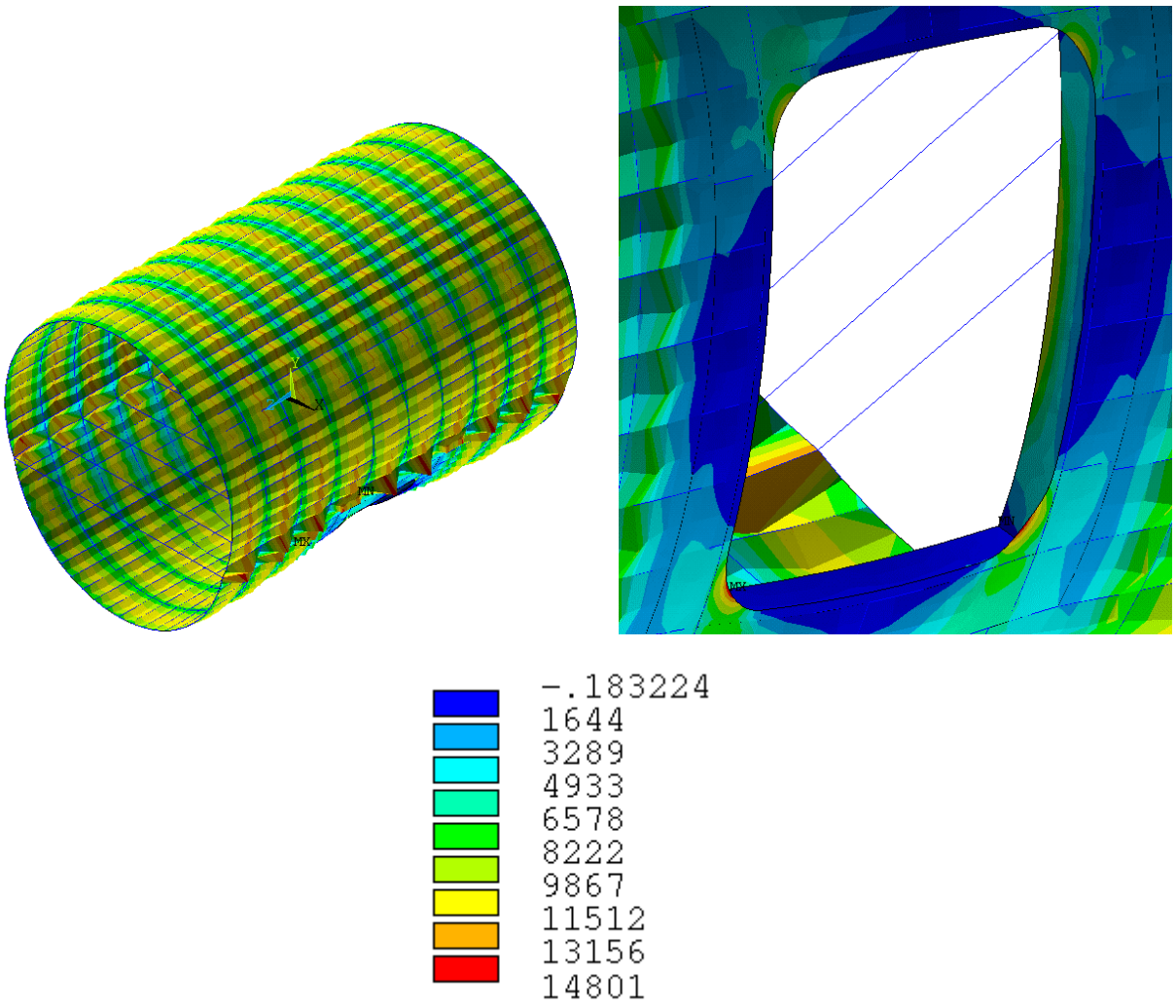

FIGURE 34. PREDICTED MAXIMUM PRINCIPAL MEMBRANE STRESS DISTRIBUTION FOR THE NARROW-BODY MODEL SUBJECTED TO PRESSURE LOADING; THIN SHELL ANALYSIS (7) (UNIT: PSI).

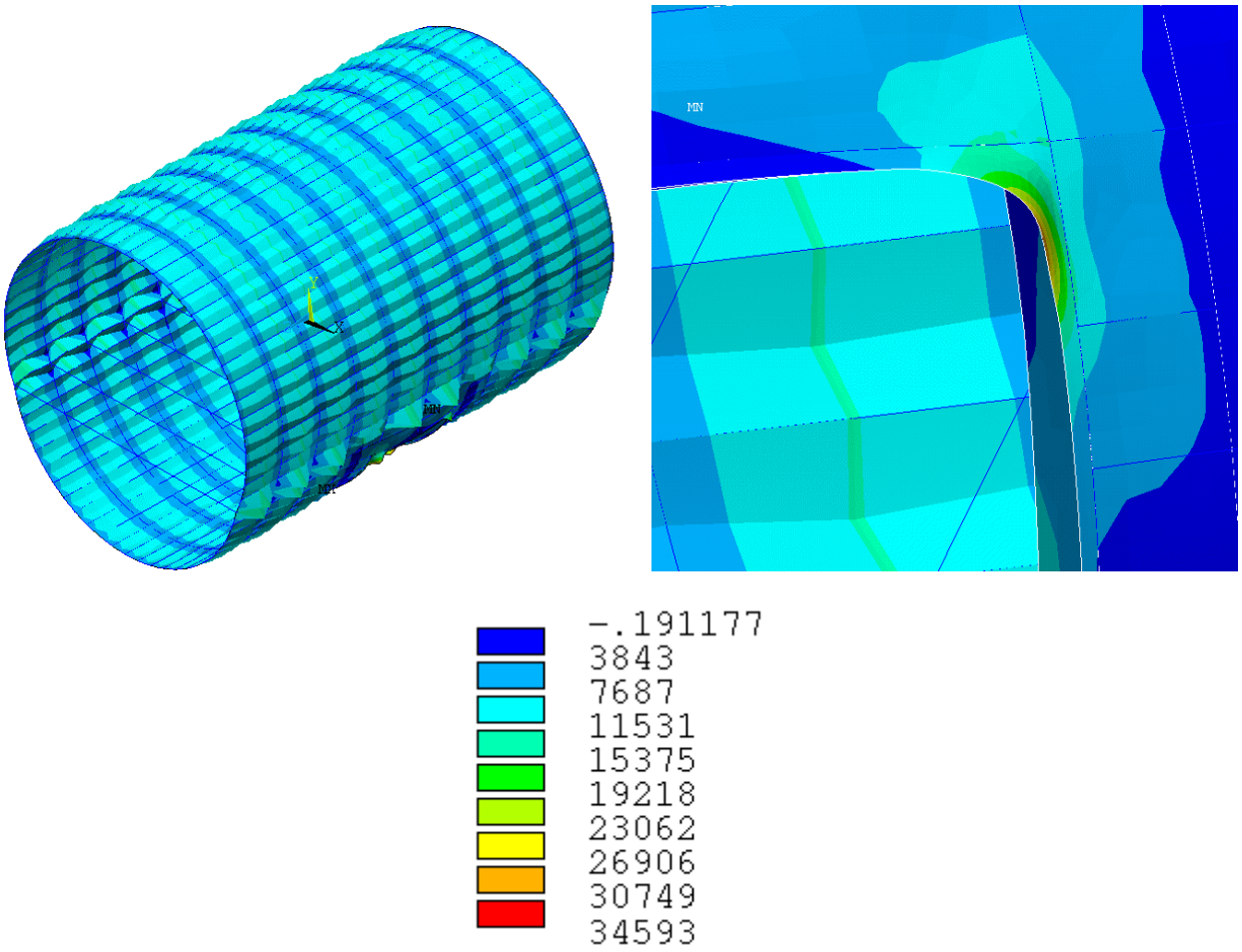

FIGURE 35. PREDICTED MAXIMUM PRINCIPAL MEMBRANE STRESS DISTRIBUTION FOR THE NARROW-BODY MODEL SUBJECTED TO PRESSURE LOADING AND DOOR JAMB PRESSURE; THIN SHELL ANALYSIS (8) (UNIT: PSI).

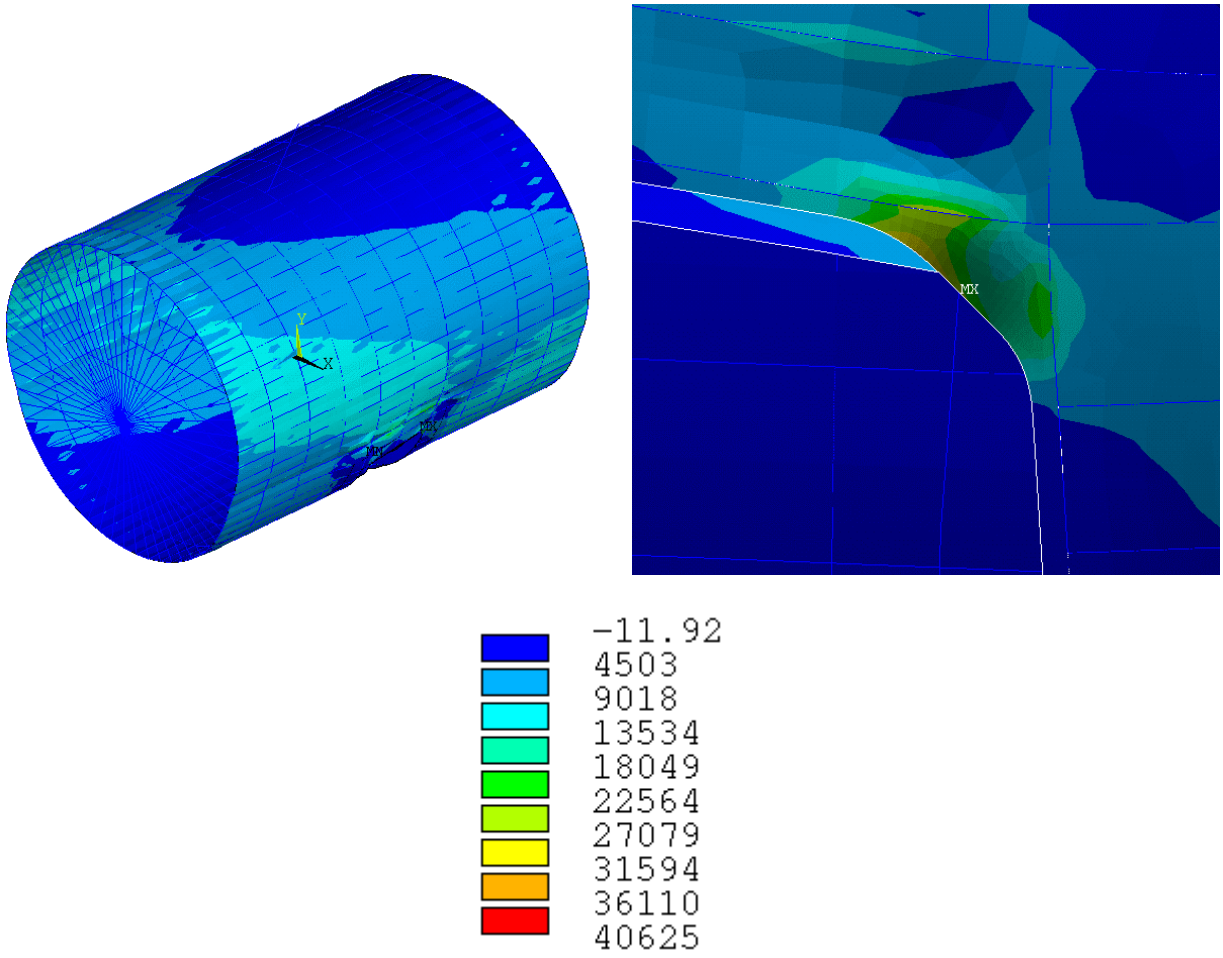

FIGURE 36. PREDICTED MAXIMUM PRINCIPAL MEMBRANE STRESS DISTRIBUTION FOR THE NARROW-BODY MODEL SUBJECTED TO VERTICAL SHEAR LOADING; THIN SHELL ANALYSIS (9) (UNIT: PSI).

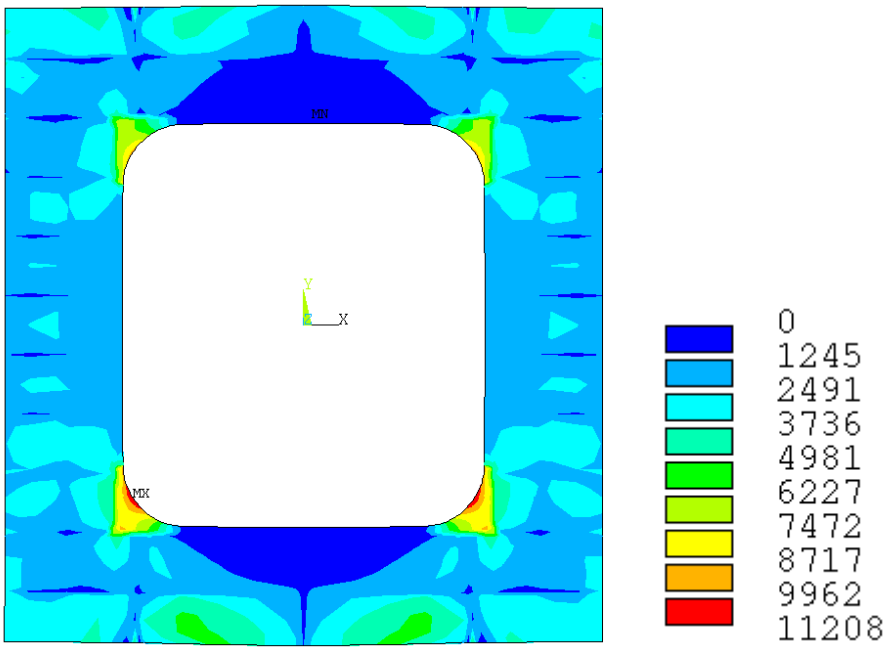

FIGURE 37. PREDICTED MAXIMUM PRINCIPAL MEMBRANE STRESS DISTRIBUTION FOR THE NARROW-BODY MODEL SUBJECTED TO PRESSURE LOADING; 2D ANALYSIS (10) (UNIT: PSI).

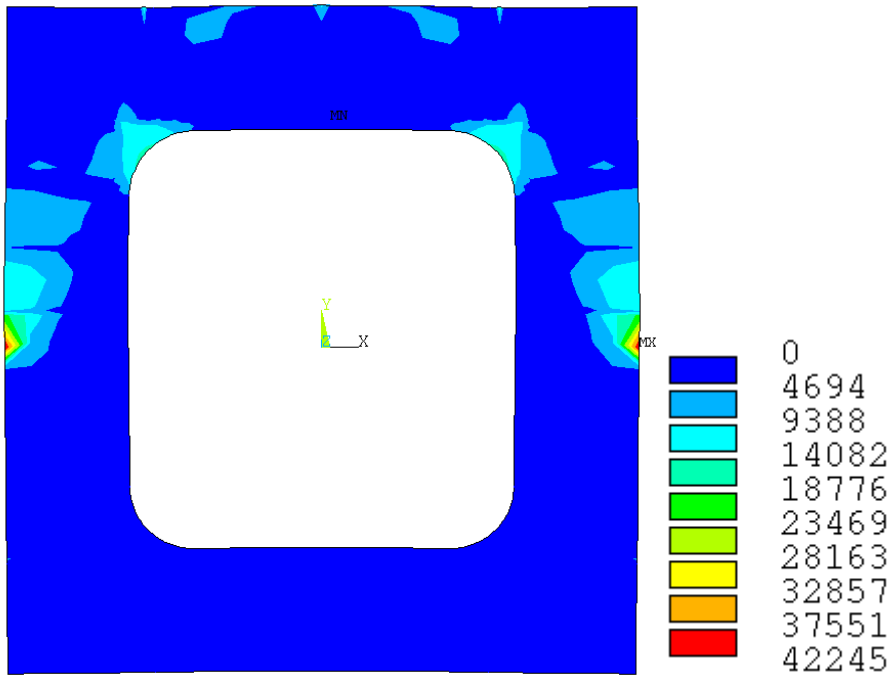

FIGURE 38. PREDICTED MAXIMUM PRINCIPAL MEMBRANE STRESS DISTRIBUTION FOR THE NARROW-BODY MODEL SUBJECTED TO PRESSURE LOADING AND DOOR JAMB PRESSURE; 2D ANALYSIS (11) (UNIT: PSI).

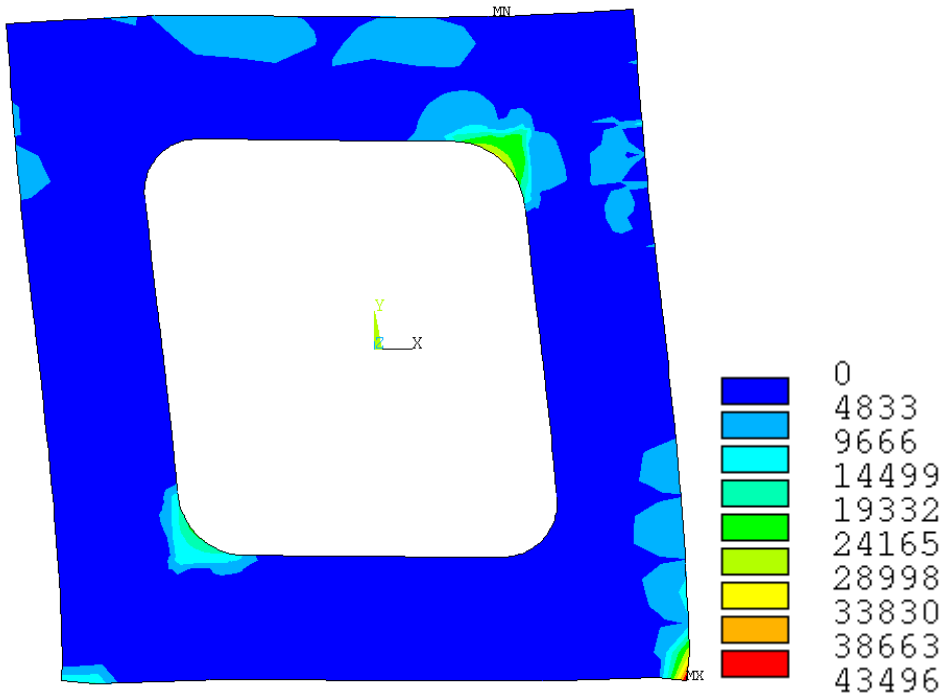

FIGURE 39. PREDICTED MAXIMUM PRINCIPAL MEMBRANE STRESS DISTRIBUTION FOR THE NARROW-BODY MODEL SUBJECTED TO VERTICAL SHEAR LOADING; 2D ANALYSIS (12) (UNIT: PSI).

(2nd) 3.2.3 3D and 2D Stress Comparison

In this section, we compare the predicted stresses evaluated at the aft/upper end of the door corner from 3D thin shell and 2D plane stress analyses. The point of interest is a stress concentration location where most of the door repairs are taken place in the field. We first tabulate our membrane results for 3D thin shell and 2D analyses (tables 3-8) and then tabulate the bending results for 3D thin shell analysis (tables 9-14). We use $\sigma_{\theta\theta}$, σ_{zz}, $\tau_{\theta z}$, σ_{11}, and σ_{mises}, to denote the computed hoop stress, shear stress, maximum principal stress, and von Mises stress, respectively. All the stress units are in psi.

TABLE 3 PREDICTED MEMBRANE STRESSES AT THE DOOR CORNER FOR THE WIDE-BODY MODEL SUBJECTED TO PRESSURE LOADING (1 AND 4)

	3D Thin Shell Analysis	2D Plane Stress Analysis	Difference (2D-3D)/3D
$\sigma_{\theta\theta}$	8,730	8,460	-3.09 %
σ_{zz}	8,870	8,430	-4.96 %
$\tau_{\theta z}$	8,740	8,410	-3.77 %
σ_{11}	17,550	16,860	-3.93 %
σ_{mises}	17,520	16,860	-3.77 %

TABLE 4 PREDICTED MEMBRANE STRESS AT THE DOOR CORNER FOR THE WIDE-BODY MODEL SUBJECTED TO PRESSURE LOADING AND DOOR JAMB PRESSURE (2 AND 5)

	3D Thin Shell Analysis	2D Plane Stress Analysis	Difference (2D-3D)/3D
$\sigma_{\theta\theta}$	14,630	9,180	-37.2 %
σ_{zz}	14,660	9,120	-37.8 %
$\tau_{\theta z}$	14,600	9,140	-37.4 %
σ_{11}	29,290	18,300	-37.5 %
σ_{mises}	29,270	18,290	-37.5 %

TABLE 5 PREDICTED MEMBRANE STRESS AT THE DOOR CORNER FOR THE WIDE-BODY MODEL SUBJECTED TO VERTICAL SHEAR LOADING (3 AND 6)

	3D Thin Shell Analysis	2D Plane Stress Analysis	Difference (2D-3D)/3D
$\sigma_{\theta\theta}$	10,430	7,970	-23.6 %
σ_{zz}	10,690	7,930	-25.8 %
$\tau_{\theta z}$	10,510	7,940	-24.4 %
σ_{11}	21,080	15,900	-24.6 %
σ_{mises}	21,060	15,890	-24.5 %

TABLE 6 PREDICTED MEMBRANE STRESS AT THE DOOR CORNER FOR THE NARROW-BODY MODEL SUBJECTED TO PRESSURE LOADING (7 AND 10)

	3D Thin Shell Analysis	2D Plane Stress Analysis	Difference (2D-3D)/3D
$\sigma_{\theta\theta}$	5,930	4,060	-31.5 %
σ_{zz}	5,930	4,030	-32.0 %
$\tau_{\theta z}$	5,920	4,040	-31.8 %
σ_{11}	11,860	8,090	-31.8 %
σ_{mises}	11,850	8,090	-31.7 %

TABLE 7 PREDICTED MEMBRANE STRESS AT THE DOOR CORNER FOR THE NARROW-BODY MODEL SUBJECTED TO PRESSURE LOADING AND DOOR JAMB PRESSURE (8 AND 11)

	3D Thin Shell Analysis	2D Plane Stress Analysis	Difference (2D-3D)/3D
$\sigma_{\theta\theta}$	12,650	7,800	-38.3 %
σ_{zz}	12,570	7,770	-38.1 %
$\tau_{\theta z}$	12,610	7,780	-38.3 %

σ_{11}	25,310	15,570	-38.5 %
σ_{mises}	25,340	15,560	-38.6 %

TABLE 8 PREDICTED MEMBRANE STRESS AT THE DOOR CORNER FOR THE NARROW-BODY MODEL SUBJECTED TO VERTICAL SHEAR LOADING (9 AND 12)

	3D Thin Shell Analysis	2D Plane Stress Analysis	Difference (2D-3D)/3D
$\sigma_{\theta\theta}$	15,720	15,010	-4.52 %
σ_{zz}	15,760	14,970	-5.01 %
$\tau_{\theta z}$	15,710	14,970	-4.71 %
σ_{11}	31,460	29,960	-4.77 %
σ_{mises}	31,450	29,950	-4.77 %

TABLE 9 PREDICTED BENDING STRESSES AT THE DOOR CORNER FOR THE WIDE-BODY MODEL SUBJECTED TO PRESSURE LOADING (1)

	3D Thin Shell Analysis (psi)
$\sigma_{\theta\theta}$	-500
σ_{zz}	-790
$\tau_{\theta z}$	-620
σ_{11}	-1,270
σ_{mises}	-1,260

TABLE 10 PREDICTED BENDING STRESS AT THE DOOR CORNER FOR THE WIDE-BODY MODEL SUBJECTED TO PRESSURE LOADING AND DOOR JAMB PRESSURE (2)

	3D Thin Shell Analysis (psi)
$\sigma_{\theta\theta}$	8,080
σ_{zz}	5,810
$\tau_{\theta z}$	6,870
σ_{11}	13,790
σ_{mises}	13,710

TABLE 11 PREDICTED BENDING STRESS AT THE DOOR CORNER FOR THE WIDE-BODY MODEL SUBJECTED TO VERTICAL SHEAR LOADING (3)

	3D Thin Shell Analysis (psi)
$\sigma_{\theta\theta}$	-1,260
σ_{zz}	-1,920
$\tau_{\theta z}$	-1,550
σ_{11}	-3,140
σ_{mises}	-3,120

TABLE 12 PREDICTED BENDING STRESS AT THE DOOR CORNER FOR THE NARROW-BODY MODEL SUBJECTED TO PRESSURE LOADING (7)

	3D Thin Shell Analysis (psi)
$\sigma_{\theta\theta}$	-300
σ_{zz}	-790
$\tau_{\theta z}$	-550
σ_{11}	-1,100
σ_{mises}	-1,100

TABLE 13 PREDICTED BENDING STRESS AT THE DOOR CORNER FOR THE NARROW-BODY MODEL SUBJECTED TO PRESSURE LOADING AND DOOR JAMB PRESSURE (8)

	3D Thin Shell Analysis (psi)
$\sigma_{\theta\theta}$	10,750
σ_{zz}	8,730
$\tau_{\theta z}$	9,780
σ_{11}	19,450
σ_{mises}	19,410

TABLE 14 PREDICTED BENDING STRESS AT THE DOOR CORNER FOR THE NARROW-BODY MODEL SUBJECTED TO VERTICAL SHEAR LOADING (9)

	3D Thin Shell Analysis (psi)
$\sigma_{\theta\theta}$	-3,920
σ_{zz}	-4,730
$\tau_{\theta z}$	-4,330
σ_{11}	-8,650
σ_{mises}	-8,650

Several observations are made from the tables:

- For the cases we have studied, 2D results evaluated at the aft/upper end of the door corner are always smaller than their 3D counterparts. Although it is premature to apply this observation to other geometries and boundary conditions, this raises the concerns that design based on 2D analyses may be unconservative.
- For pressure loading, 2D estimates are close to 3D results for the wide-body model. However, a reverse is observed in the case with vertical shear loading. This somewhat counter-intuitive result is believed due to the coupling between geometries and loading

conditions. More systematic evaluation, for example, using a single radius narrow-body model with a passenger door, is needed in the future to clarify this.

- It is of interest to observe that the sign of the bending stresses for the fuselage subjected to pressure loading and vertical shear loading is negative. The negative sign indicates a concave inward deformation at the door corners as we have observed in the deformed shape. The behavior is expected for the vertical shear loading since it tends to flatten the curved structure. For the pressure loading, it is the stiffening effect due to the torque box that causes the curvature altering its direction. For the pressure loading with door jamb pressure, we observe positive sign of bending stresses and a typical bulging outward deformation.

(M) 4. CONCLUSIONS AND RECOMMENDATIONS FOR FUTURE WORK.

We conclude this work with the following remarks:

For the task 1: development of 2D finite element stress analysis capability for RAPID

- We have successfully delivered a suite of C++ source codes for meshing and finite element analysis that can either be directly incorporated into the RAPID program or run separately as a standalone program. The program also provides an option to generate the FRANC2DL input file so users can verify their results independently.
- Based on the feedback of the engineers at the Boeing company [4], we consider our development of the finite element codes for the RAPID program to be a success. Our lightweight design pays off when others start to extend our codes to incorporate other sophisticated (and sometimes proprietary) analysis and design methodologies.

For the task 2: 2- and 3D finite element analyses of fuselage structures with a door cutout configuration

- We have analyzed three different loading conditions for both wide-body and narrow-body models. The loading conditions are nominal pressure loading, nominal pressure loading with effective door jamb pressure, and pure vertical shear loading. Our results show that both geometries and boundary conditions play a key role in correlating 3D thin shell and 2D results, as we should expect. In general, 2D analyses underpredict stresses in the door region.
- The 3D thin shell analysis, though expensive in terms of human and computational resources, gives us valuable insights in understanding the behaviors around the innately complex geometry parts. We consider our predicted results as the first step to systematically understand the behavior and correlate 2D results for door repaired problems.

For future work, we suggest the following should be considered:

- A crack growth module in 2D that will give advanced users of RAPID more powerful capability to evaluate the damage tolerance of the repaired parts.

- A graphic user interface (GUI) module to provide an independent interface for users to use the meshing and finite element functionalities developed herein.
- More systematically parametric studies to provide guidelines to correlate 2D results with 3D thin shell prediction. This should consider additional airframe configurations such as commuter fuselages.

(M) 5. REFERENCES.

1. Stroustrup, B. "The C++ Programming Language," 3rd edition, Addison Wesley Longman, Reading, MA. 1997.

2. James, Mark, and Swenson, Daniel, "FRANC2D/L: A Crack Propagation Simulator for Plane Layered Structures," available online from http://www.mne.ksu.edu/~franc2d.

3. FRANC2D, FRANC3D/STAGS, FRANC3D/BES, available on line from CFG website at http://www.cfg.cornell.edu.

4. Chen, C.-C., personal communication, 1999-2000.

5. Potyondy, D. O., Wawrzynek, P. A., and Ingraffea, A. R., "An Algorithm to Generate Quadrilateral or Triangular Element Surface Meshes in Arbitrary Domains with Applications to Crack Propagation," Int. J. Num. Meth. Eng., 38, 2677-2701, 1995.

6. Cheung, Y. K., Lo, S. H., and Leung, A. Y. T., "Finite Element Implementation," Blackwell Science Ltd, 1996.

7. Press, William H., Teukolsky, Saul A., Vetterling, William T. and Flannery, Brian P, "Numerical Recipes in C, the Art of Scientific Computing," 2nd edition, Cambridge University Press, 1992.

8. Sloan, S. W. "An algorithm for profile and wavefront reduction of sparse matrices," Int. J. Num. Meth. Eng., 23, 239-251, 1986.

9. ANSYS 5.6 from ANSYS Inc., product information available at http://www.ansys.com, 2000.

10. Nomura, Miles C., personal communication, 1999-2000.

11. Python, an *interpreted, interactive, object-oriented* programming language, available online at http://www.python.org.

(M) APPENDIX A: INPUT FILE FORMAT FOR INPUT WRAPPER.

number of layers
number of sets of material properties
number of sets of rivet properties
number of rivets
number of load cases
characteristic element size
line plot option flag (0 => do not produce line plot, 1 => produce line plot)
stress option flag (0 => do not compute nodal stresses, 1 => compute nodal stresses)
rivet force option flag (0=> do not compute rivet forces, 1=> compute all the rivet forces,
2=> compute some rivet foces)

for each set of material properties:
Young's modulus
Poisson ratio
thickness

for each set of rivet properties:
shear stiffness

for each rivet:
rivet property set number
x and y coordinates
first layer index
second layer index
type flag (0=>inside the domain, 1=>on keypoint, 2=>on boundary segment)
keypoint indices in the first layer and second layer (ignored if type flag == 0 or 2)
boundary segment indices in the first layer and second layer (ignored if
type flag == 0 or 1)
scaling factor

for each layer:
material property set
number of keypoints
number of boundary segments
number of displacement boundary condition descriptions
number of traction boundary condition descriptions for each load case
attribute output number

for each keypoint:
x and y coordinate

for each boundary segment:
starting keypoint index (location in the list of keypoints for this layer)

ending keypoint index
type flag (0 => line segment, 1 => circular arc segment, 2=>quarter elliptical arc)
x and y coordinate of circular/elliptical arc center (ignored for line segments)
subdivision flag (0=> use characteristic element size, 1=>user specified)
subdivision number and subdivision ratio (ignored if subdivision flag == 0)

for each displacement boundary condition description:
type flag (0 => apply to keypoint, 1 => apply to full boundary segment)
keypoint or boundary segment index for the BC
BC displacement type (0=>specified in x, 1=>in y, 2:=>in x and y)
BC displacement x value (ignored if BC displacement type == 1)
BC displacement y value (ignored if BC displacement type == 0)

for each load case
for each traction boundary condition description:
type flag (0 => apply to keypoint, 1 => apply to full boundary segment)
keypoint or boundary segment index for the BC
BC traction type (0=>specified in x, 1=>in y, 2:=>in x and y)
BC traction x value (ignored if BC traction type == 1)
BC traction y value (ignored if BC traction type == 0)

note: locations with unspecified boundary conditions are assumed to have zero tractions.

note: each layer has one outside boundary, and can have zero or more inside boundaries, which represent voids (cutouts). All outside and inside boundaries must be closed loops. No boundaries are allowed to cross each other. The boundary segments are oriented from the starting to ending keypoints. Outside boundaries should be specified in counter-clockwise order. Inside boundaries are specified in clockwise order. (If one moves from the starting keypoint to the ending keypoint, the region to be meshed should be on one's left).

if line plot option
number of line plot sets
for each set of line plot:
x and y coordinates of the starting point
x and y coordinates of the ending point
number of subdivision
subdivision ratio

if rivet force option flag == 2
number of rivet sets
for each rivet set
number of rivets
rivet index

(M) APPENDIX B: INPUT RECORDS FOR ANTENNA INSTALLATION AND DOOR OPENING REPAIRED EXAMPLES.

(1st) B.1 INPUT RECORDS FOR A CIRCULAR ANTENNA INSTALLATION EXAMPLE

```
#
#  Circular Antenna Installation
#
#  Count Data:
#
#  +---------------------------------- Number of layers
#  |   +------------------------------ Number of sets of material properties
#  |   |   +--------------------------- Number of sets of rivet properties
#  |   |   |   +----------------------- Number of rivets
#  |   |   |   |   +------------------- Number of load cases
#  |   |   |   |   |   +--------------- Characteristic element size
#  |   |   |   |   |   |    +---------- Line plot option flag
#  |   |   |   |   |   |    |   +------ Stress option flag
#  |   |   |   |   |   |    |   |   +-- Rivet force option flag
#  |   |   |   |   |   |    |   |   |
#  |   |   |   |   |   |    |   |   |
#--+---+---+---+---+---+----+---+---+
   2   2   2   8   1   0.25 1   0   2
#--+---+---+---+---+---+----+---+---+
#
#  Material Data:
#  Material property set
#
#  +----------------------------- Young's modulus
#  |            +---------------- Poisson ratio
#  |            |      +--------- Thickness
#  |            |      |
#--+------------+------+------
   10500000.0   0.3    0.050
   10500000.0   0.3    0.040
#--+------------+------+------
#
#  Rivet Data:
#  Rivet property set
#
#  +----------------------- Shear stiffness
#  |
#--+--------
   167550.0
    83775.0
#--+--------
#
#  Rivet data
#
#  +------------------------------------------------ Rivet property set
number
#  |     +------------------------------------------ X coordinate
#  |     |      +------------------------------------ Y coordinate
```

```
#  |      |       |      +------------------------------- First layer index
#  |      |       |      |    +---------------------------- Second layer index
#  |      |       |      |    |    +----------------------- Type flag (domain=0,
keypoint=1, Boundary=2)
#  |      |       |      |    |    |    +------------------ Keypoint index in the
1st layer
#  |      |       |      |    |    |    |    +------------- Keypoint index in the
2nd layer
#  |      |       |      |    |    |    |    |    +-------- Boundary segment
index in the 1st layer
#  |      |       |      |    |    |    |    |    |    +--- Boundary segment
index in the 2nd layer
#  |      |       |      |    |    |    |    |    |    |    |
#--+------+-------+------+----+----+----+----+----+----+----+
   1    1.000   0.000   0    1    2    2    3    2.0
   0    0.707   0.707   0    1    0         2.0
   1    0.000   1.000   0    1    2    0    1    2.0
   1    2.000   0.000   0    1    2    2    3    2.0
   0    1.848   0.765   0    1    0         2.0
   0    1.414   1.414   0    1    0         2.0
   0    0.765   1.848   0    1    0         2.0
   1    0.000   2.000   0    1    2    0    1    2.0
#--+------+-------+---
#
#  Layer 0: (mounting plate)
#
#  +----------------------- Material property set
#  |   +------------------- Number of keypoints
#  |   |   +--------------- Number of boundary segments
#  |   |   |   +----------- Number of displacement boundary condition
descriptions
#  |   |   |   |   +------ Number of traction boundary condition descriptions
for each load case
#  |   |   |   |   |
#--+---+---+---+---+
   0   4   4   2   0    1
#--+---+---+---+---+
#
#  Kepoints
#
#      +--------- X coordinate
#      |      +-- Y coordinate
#      |      |
#------+------+--
       0.0    2.5
       0.0    0.5
       0.5    0.0
       2.5    0.0
#------+------+--
#
# Boundary segments
#
#      +------------------------------------- Starting keypoint index
#      |   +---------------------------------- End keypoint index
```

```
#      |   |   +------------------------------ Type flag (line=0, circular=1,
elliptical=2)
#      |   |   |    +-------------------------- x coordinate (ignored for line
segment)
#      |   |   |    |    +--------------------- y coordinate (ignored for line
segment)
#      |   |   |    |    |    +---------------- Subdivision flag
#      |   |   |    |    |    |    +----------- Subdivision number
#      |   |   |    |    |    |    |    +------ Subdivision ratio
#      |   |   |    |    |    |    |    |
#------+---+---+----+----+----+----+----+----+
       0   1   0              0
       1   2   1    0.0  0.0  0
       2   3   0              0
       3   0   1    0.0  0.0  0
#------+---+---+----+----+----+----+----+----+
#
# Displacement boundary condition description
#
#      +--------------------- Type flag
#      |   +----------------- Index
#      |   |   +------------- BC displacement type
#      |   |   |    +-------- BC displacement x value
#      |   |   |    |    +--- BC displacement y value
#      |   |   |    |    |
#------+---+---+----+----+--
       1   0   0    0.0
       1   2   1         0.0
#------+---+---+----+----+--
#
#  Layer 1: (skin)
#
#  +---------------------- Material property set
#  |   +------------------ Number of keypoints
#  |   |   +-------------- Number of boundary segments
#  |   |   |   +---------- Number of displacement boundary condition
descriptions
#  |   |   |   |   +------ Number of traction boundary condition descriptions
for each load case
#  |   |   |   |   |
#--+---+---+---+---+
   1   7   7   4   1    0
#--+---+---+---+---+
#
#      Kepoints
#
#      +--------- X coordinate
#      |      +-- Y coordinate
#      |      |
#------+------+----
       0.0    20.0
       0.0     2.5
       0.0     0.5
       0.5     0.0
```

```
       2.5     0.0
      20.0     0.0
      20.0    20.0
#------+------+----
#
#      Boundary segments
#
#      +------------------------------------ Starting keypoint index
#      |   +-------------------------------- End keypoint index
#      |   |   +---------------------------- Type flag (line=0, circular=1,
elliptical=2)
#      |   |   |    +------------------------ x coordinate (ignored for line
segment)
#      |   |   |    |    +-------------------- y coordinate (ignored for line
segment)
#      |   |   |    |    |    +--------------- Subdivision flag
#      |   |   |    |    |    |    +---------- Subdivision number
#      |   |   |    |    |    |    |    +------ Subdivision ratio
#      |   |   |    |    |    |    |    |
#------+---+---+----+----+----+----+----+----+
       0   1   0                   1   10    0.5
       1   2   0                    0
       2   3   1   0.0  0.0  0
       3   4   0                    0
       4   5   0                   1   10    2.0
       5   6   0                   1   12    2.0
       6   0   0                   1   12    0.5
#------+---+---+----+----+----+----+----+----+
#
# Displacement boundary condition description
#
#      +--------------------- Type flag
#      |   +----------------- Index
#      |   |   +------------- BC displacement type
#      |   |   |    +-------- BC displacement x value (ignore if bc type == 1)
#      |   |   |    |    +--- BC displacement y value (ignore if bc type == 0)
#      |   |   |    |    |
#------+---+---+----+----+--
       1   0   0    0.0
       1   1   0    0.0
       1   3   1         0.0
       1   4   1         0.0
#------+---+---+----+----+--
#
# Load case 0
#
#      +---------------------- Type flag
#      |   +------------------ Index
#      |   |   +-------------- BC traction type
#      |   |   |   +---------- BC traction x value (ignore if type == 1)
#      |   |   |   |       +--- BC traction y value
#      |   |   |   |       |
#      |   |   |   |       |
#      |   |   |   |       |
```

```
#------+---+---+---+-------+-----
       1   6   1           1000.0
#------+---+---+---+-------+-----
#
# Line plot
#
#      +---------------------------------------- Number of line plot sets
#      |
#      |
#------+
       1
#------+
#
# Line plot description
#
#      +---------------------------------- x coordinate of the starting point
#      |     +---------------------------- y coordinate of the starting point
#      |     |     +---------------------- x coordinate of the ending point
#      |     |     |     +---------------- y coordinate of the ending point
#      |     |     |     |     +---------- Number of subdivision
#      |     |     |     |     |     +---- Subdivision ratio
#      |     |     |     |     |     |
#      |     |     |     |     |     |
#------+-----+-----+-----+-----+-----+
      0.50001 0.0  19.999 0.0    101   1
#------+-----+-----+-----+-----+-----+
#
# Rivet forces
#
#      +------------ Number of rivet sets
#       |
#       |
#------+
       1
#------+-----+-----+-----+-----+-----+
#
#      +------------ Number of rivet in rivet set 0
#      |
#      |
#------+
       1
#------+
#------+-----+-----+-----+-----+-----+
#
# Rivet index
#
#      +------------- Rivet index
#      |
#      |
#------+
       7
#------+
#
# End of Circular Antenna Installation input file
```

```
      #
```

(1st) B.2 INPUT RECORDS FOR A DOOR OPENING REPAIRED EXAMPLE

```
      #
      #  Door Opening Repair (Stiffeners ignored)
      #
      #  Case No. Door001
      #
      #  Count Data:
      #
      #  +----------------------------------- Number of layers
      #  |   +--------------------------------- Number of sets of material properties
      #  |   |   +----------------------------- Number of sets of rivet properties
      #  |   |   |   +------------------------- Number of rivets
      #  |   |   |   |    +-------------------- Number of load cases
      #  |   |   |   |    |   +---------------- Characteristic element size
      #  |   |   |   |    |   |    +----------- Line plot option flag
      #  |   |   |   |    |   |    |   +------ Stress option flag
      #  |   |   |   |    |   |    |   |   +-- Rivet force option flag
      #  |   |   |   |    |   |    |   |   |
      #  |   |   |   |    |   |    |   |   |
      #  V   V   V   V    V   V    V   V   V
      #--+---+---+---+----+---+----+---+---+
         4   4   3   447  2   0.5  1   0   2
      #--+---+---+---+----+---+----+---+---+
      #
      #  Material Data:
      #  Material property set
      #
      #  +----------------------------- Young's modulus
      #  |            +----------------- Poisson ratio
      #  |            |      +--------- Thickness
      #  |            |      |
      #  V            V      V
      #--+------------+------+------
         10500000.0   0.3    0.040
         10500000.0   0.3    0.050
         10500000.0   0.3    0.063
         10500000.0   0.3    0.071
      #--+------------+------+------
      #
      #  Rivet Data:
      #  Rivet property set
      #
      #  +----------------------- Shear stiffness
      #  |
      #  V
      #--+--------
         167550.0
         189650.0
         207400.0
      #--+--------
      #
```

```
#  Rivet data
#
#  +------------------------------------------------- Rivet property set
number
#  |     +------------------------------------------- X coordinate
#  |     |     +--------------------------------------- Y coordinate
#  |     |     |     +----------------------------------- First layer index
#  |     |     |     |    +------------------------------ Second layer index
#  |     |     |     |    |    +------------------------- Type flag (domain=0,
keypoint=1, Boundary=2)
#  |     |     |     |    |    |    +-------------------- Keypoint index in the
1st layer
#  |     |     |     |    |    |    |    +--------------- Keypoint index in the
2nd layer
#  |     |     |     |    |    |    |    |    +--------- Boundary segment index
in the 1st layer
#  |     |     |     |    |    |    |    |    |    +---- Boundary segment index
in the 2nd layer
#  |     |     |     |    |    |    |    |    |    |
#  V     V     V     V    V    V    V    V    V    V
#--+-----+-----+-----+----+----+----+----+----+----+
   0    2.5   6.5    0    1    0    1.0
   0    2.5   7.5    0    1    0    1.0
   0    2.5   8.5    0    1    0    1.0
   0    2.5   9.5    0    1    0    1.0
   0    2.5  10.5    0    1    0    1.0
   0    3.5   5.5    0    1    0    1.0
   0    3.5   6.5    0    1    0    1.0
   0    3.5   7.5    0    1    0    1.0
   0    3.5   8.5    0    1    0    1.0
   0    3.5   9.5    0    1    0    1.0
   0    3.5  10.5    0    1    0    1.0
   0    4.5   9.5    0    1    0    1.0
   0    4.5  10.5    0    1    0    1.0
   0    5.5   3.5    0    1    0    1.0
   0    5.5   9.5    0    1    0    1.0
   0    5.5  10.5    0    1    0    1.0
   0    6.5   2.5    0    1    0    1.0
   0    6.5   3.5    0    1    0    1.0
   0    6.5   9.5    0    1    0    1.0
   0    6.5  10.5    0    1    0    1.0
   0    7.5   2.5    0    1    0    1.0
   0    7.5   3.5    0    1    0    1.0
   0    7.5   9.5    0    1    0    1.0
   0    7.5  10.5    0    1    0    1.0
   0    8.5   2.5    0    1    0    1.0
   0    8.5   3.5    0    1    0    1.0
   0    8.5   9.5    0    1    0    1.0
   0    8.5  10.5    0    1    0    1.0
   0    9.5   2.5    0    1    0    1.0
   0    9.5   3.5    0    1    0    1.0
   0    9.5   4.5    0    1    0    1.0
   0    9.5   5.5    0    1    0    1.0
   0    9.5   6.5    0    1    0    1.0
```

```
0    9.5   7.5    0    1    0    1.0
0    9.5   8.5    0    1    0    1.0
0    9.5   9.5    0    1    0    1.0
0    9.5  10.5    0    1    0    1.0
0   10.5   2.5    0    1    0    1.0
0   10.5   3.5    0    1    0    1.0
0   10.5   4.5    0    1    0    1.0
0   10.5   5.5    0    1    0    1.0
0   10.5   6.5    0    1    0    1.0
0   10.5   7.5    0    1    0    1.0
0   10.5   8.5    0    1    0    1.0
0   10.5   9.5    0    1    0    1.0
0   10.5  10.5    0    1    0    1.0
1    0.5   6.5    1    2    0    1.0
1    0.5   7.5    1    2    0    1.0
1    0.5   8.5    1    2    0    1.0
1    0.5   9.5    1    2    0    1.0
1    0.5  10.5    1    2    0    1.0
1    0.5  11.5    1    2    0    1.0
1    0.5  12.5    1    2    0    1.0
1    1.5   6.5    1    2    0    1.0
1    1.5   7.5    1    2    0    1.0
1    1.5   8.5    1    2    0    1.0
1    1.5   9.5    1    2    0    1.0
1    1.5  10.5    1    2    0    1.0
1    1.5  11.5    1    2    0    1.0
1    1.5  12.5    1    2    0    1.0
1    2.5   6.5    1    2    0    1.0
1    2.5   7.5    1    2    0    1.0
1    2.5   8.5    1    2    0    1.0
1    2.5   9.5    1    2    0    1.0
1    2.5  10.5    1    2    0    1.0
1    2.5  11.5    1    2    0    1.0
1    2.5  12.5    1    2    0    1.0
1    3.5   5.5    1    2    0    1.0
1    3.5   6.5    1    2    0    1.0
1    3.5   7.5    1    2    0    1.0
1    3.5   8.5    1    2    0    1.0
1    3.5   9.5    1    2    0    1.0
1    3.5  10.5    1    2    0    1.0
1    3.5  11.5    1    2    0    1.0
1    3.5  12.5    1    2    0    1.0
1    4.5   9.5    1    2    0    1.0
1    4.5  10.5    1    2    0    1.0
1    4.5  11.5    1    2    0    1.0
1    4.5  12.5    1    2    0    1.0
1    5.5   3.5    1    2    0    1.0
1    5.5   9.5    1    2    0    1.0
1    5.5  10.5    1    2    0    1.0
1    5.5  11.5    1    2    0    1.0
1    5.5  12.5    1    2    0    1.0
1    6.5   0.5    1    2    0    1.0
1    6.5   1.5    1    2    0    1.0
1    6.5   2.5    1    2    0    1.0
```

```
1    6.5   3.5    1    2    0    1.0
1    6.5   9.5    1    2    0    1.0
1    6.5  10.5    1    2    0    1.0
1    6.5  11.5    1    2    0    1.0
1    6.5  12.5    1    2    0    1.0
1    7.5   0.5    1    2    0    1.0
1    7.5   1.5    1    2    0    1.0
1    7.5   2.5    1    2    0    1.0
1    7.5   3.5    1    2    0    1.0
1    7.5   9.5    1    2    0    1.0
1    7.5  10.5    1    2    0    1.0
1    7.5  11.5    1    2    0    1.0
1    7.5  12.5    1    2    0    1.0
1    8.5   0.5    1    2    0    1.0
1    8.5   1.5    1    2    0    1.0
1    8.5   2.5    1    2    0    1.0
1    8.5   3.5    1    2    0    1.0
1    8.5   9.5    1    2    0    1.0
1    8.5  10.5    1    2    0    1.0
1    8.5  11.5    1    2    0    1.0
1    8.5  12.5    1    2    0    1.0
1    9.5   0.5    1    2    0    1.0
1    9.5   1.5    1    2    0    1.0
1    9.5   2.5    1    2    0    1.0
1    9.5   3.5    1    2    0    1.0
1    9.5   4.5    1    2    0    1.0
1    9.5   5.5    1    2    0    1.0
1    9.5   6.5    1    2    0    1.0
1    9.5   7.5    1    2    0    1.0
1    9.5   8.5    1    2    0    1.0
1    9.5   9.5    1    2    0    1.0
1    9.5  10.5    1    2    0    1.0
1    9.5  11.5    1    2    0    1.0
1    9.5  12.5    1    2    0    1.0
1   10.5   0.5    1    2    0    1.0
1   10.5   1.5    1    2    0    1.0
1   10.5   2.5    1    2    0    1.0
1   10.5   3.5    1    2    0    1.0
1   10.5   4.5    1    2    0    1.0
1   10.5   5.5    1    2    0    1.0
1   10.5   6.5    1    2    0    1.0
1   10.5   7.5    1    2    0    1.0
1   10.5   8.5    1    2    0    1.0
1   10.5   9.5    1    2    0    1.0
1   10.5  10.5    1    2    0    1.0
1   10.5  11.5    1    2    0    1.0
1   10.5  12.5    1    2    0    1.0
1   11.5   0.5    1    2    0    1.0
1   11.5   1.5    1    2    0    1.0
1   11.5   2.5    1    2    0    1.0
1   11.5   3.5    1    2    0    1.0
1   11.5   4.5    1    2    0    1.0
1   11.5   5.5    1    2    0    1.0
1   11.5   6.5    1    2    0    1.0
```

```
1   11.5   7.5    1    2    0    1.0
1   11.5   8.5    1    2    0    1.0
1   11.5   9.5    1    2    0    1.0
1   11.5  10.5    1    2    0    1.0
1   11.5  11.5    1    2    0    1.0
1   11.5  12.5    1    2    0    1.0
1   12.5   0.5    1    2    0    1.0
1   12.5   1.5    1    2    0    1.0
1   12.5   2.5    1    2    0    1.0
1   12.5   3.5    1    2    0    1.0
1   12.5   4.5    1    2    0    1.0
1   12.5   5.5    1    2    0    1.0
1   12.5   6.5    1    2    0    1.0
1   12.5   7.5    1    2    0    1.0
1   12.5   8.5    1    2    0    1.0
1   12.5   9.5    1    2    0    1.0
1   12.5  10.5    1    2    0    1.0
1   12.5  11.5    1    2    0    1.0
1   12.5  12.5    1    2    0    1.0
2  -14.5   6.5    2    3    0    1.0
2  -14.5   7.5    2    3    0    1.0
2  -14.5   8.5    2    3    0    1.0
2  -14.5   9.5    2    3    0    1.0
2  -14.5  10.5    2    3    0    1.0
2  -13.5   6.5    2    3    0    1.0
2  -13.5   7.5    2    3    0    1.0
2  -13.5   8.5    2    3    0    1.0
2  -13.5   9.5    2    3    0    1.0
2  -13.5  10.5    2    3    0    1.0
2  -12.5   6.5    2    3    0    1.0
2  -12.5   7.5    2    3    0    1.0
2  -12.5   8.5    2    3    0    1.0
2  -12.5   9.5    2    3    0    1.0
2  -12.5  10.5    2    3    0    1.0
2  -11.5   6.5    2    3    0    1.0
2  -11.5   7.5    2    3    0    1.0
2  -11.5   8.5    2    3    0    1.0
2  -11.5   9.5    2    3    0    1.0
2  -11.5  10.5    2    3    0    1.0
2  -10.5   6.5    2    3    0    1.0
2  -10.5   7.5    2    3    0    1.0
2  -10.5   8.5    2    3    0    1.0
2  -10.5   9.5    2    3    0    1.0
2  -10.5  10.5    2    3    0    1.0
2   -9.5   6.5    2    3    0    1.0
2   -9.5   7.5    2    3    0    1.0
2   -9.5   8.5    2    3    0    1.0
2   -9.5   9.5    2    3    0    1.0
2   -9.5  10.5    2    3    0    1.0
2   -8.5   6.5    2    3    0    1.0
2   -8.5   7.5    2    3    0    1.0
2   -8.5   8.5    2    3    0    1.0
2   -8.5   9.5    2    3    0    1.0
2   -8.5  10.5    2    3    0    1.0
```

```
2   -7.5   6.5    2    3    0    1.0
2   -7.5   7.5    2    3    0    1.0
2   -7.5   8.5    2    3    0    1.0
2   -7.5   9.5    2    3    0    1.0
2   -7.5  10.5    2    3    0    1.0
2   -6.5   6.5    2    3    0    1.0
2   -6.5   7.5    2    3    0    1.0
2   -6.5   8.5    2    3    0    1.0
2   -6.5   9.5    2    3    0    1.0
2   -6.5  10.5    2    3    0    1.0
2   -5.5   6.5    2    3    0    1.0
2   -5.5   7.5    2    3    0    1.0
2   -5.5   8.5    2    3    0    1.0
2   -5.5   9.5    2    3    0    1.0
2   -5.5  10.5    2    3    0    1.0
2   -4.5   6.5    2    3    0    1.0
2   -4.5   7.5    2    3    0    1.0
2   -4.5   8.5    2    3    0    1.0
2   -4.5   9.5    2    3    0    1.0
2   -4.5  10.5    2    3    0    1.0
2   -3.5   6.5    2    3    0    1.0
2   -3.5   7.5    2    3    0    1.0
2   -3.5   8.5    2    3    0    1.0
2   -3.5   9.5    2    3    0    1.0
2   -3.5  10.5    2    3    0    1.0
2   -2.5   6.5    2    3    0    1.0
2   -2.5   7.5    2    3    0    1.0
2   -2.5   8.5    2    3    0    1.0
2   -2.5   9.5    2    3    0    1.0
2   -2.5  10.5    2    3    0    1.0
2   -1.5   6.5    2    3    0    1.0
2   -1.5   7.5    2    3    0    1.0
2   -1.5   8.5    2    3    0    1.0
2   -1.5   9.5    2    3    0    1.0
2   -1.5  10.5    2    3    0    1.0
2   -0.5   6.5    2    3    0    1.0
2   -0.5   7.5    2    3    0    1.0
2   -0.5   8.5    2    3    0    1.0
2   -0.5   9.5    2    3    0    1.0
2   -0.5  10.5    2    3    0    1.0
2    0.5   6.5    2    3    0    1.0
2    0.5   7.5    2    3    0    1.0
2    0.5   8.5    2    3    0    1.0
2    0.5   9.5    2    3    0    1.0
2    0.5  10.5    2    3    0    1.0
2    1.5   6.5    2    3    0    1.0
2    1.5   7.5    2    3    0    1.0
2    1.5   8.5    2    3    0    1.0
2    1.5   9.5    2    3    0    1.0
2    1.5  10.5    2    3    0    1.0
2    2.5   6.5    2    3    0    1.0
2    2.5   7.5    2    3    0    1.0
2    2.5   8.5    2    3    0    1.0
2    2.5   9.5    2    3    0    1.0
```

```
2    2.5  10.5    2    3    0    1.0
2    3.5   5.5    2    3    0    1.0
2    3.5   6.5    2    3    0    1.0
2    3.5   7.5    2    3    0    1.0
2    3.5   8.5    2    3    0    1.0
2    3.5   9.5    2    3    0    1.0
2    4.5   9.5    2    3    0    1.0
2    5.5   3.5    2    3    0    1.0
2    6.5 -33.5    2    3    0    1.0
2    6.5 -32.5    2    3    0    1.0
2    6.5 -31.5    2    3    0    1.0
2    6.5 -30.5    2    3    0    1.0
2    6.5 -29.5    2    3    0    1.0
2    6.5 -28.5    2    3    0    1.0
2    6.5 -27.5    2    3    0    1.0
2    6.5 -26.5    2    3    0    1.0
2    6.5 -25.5    2    3    0    1.0
2    6.5 -24.5    2    3    0    1.0
2    6.5 -23.5    2    3    0    1.0
2    6.5 -22.5    2    3    0    1.0
2    6.5 -21.5    2    3    0    1.0
2    6.5 -20.5    2    3    0    1.0
2    6.5 -19.5    2    3    0    1.0
2    6.5 -18.5    2    3    0    1.0
2    6.5 -17.5    2    3    0    1.0
2    6.5 -16.5    2    3    0    1.0
2    6.5 -15.5    2    3    0    1.0
2    6.5 -14.5    2    3    0    1.0
2    6.5 -13.5    2    3    0    1.0
2    6.5 -12.5    2    3    0    1.0
2    6.5 -11.5    2    3    0    1.0
2    6.5 -10.5    2    3    0    1.0
2    6.5  -9.5    2    3    0    1.0
2    6.5  -8.5    2    3    0    1.0
2    6.5  -7.5    2    3    0    1.0
2    6.5  -6.5    2    3    0    1.0
2    6.5  -5.5    2    3    0    1.0
2    6.5  -4.5    2    3    0    1.0
2    6.5  -3.5    2    3    0    1.0
2    6.5  -2.5    2    3    0    1.0
2    6.5  -1.5    2    3    0    1.0
2    6.5  -0.5    2    3    0    1.0
2    6.5   0.5    2    3    0    1.0
2    6.5   1.5    2    3    0    1.0
2    6.5   2.5    2    3    0    1.0
2    6.5   3.5    2    3    0    1.0
2    7.5 -33.5    2    3    0    1.0
2    7.5 -32.5    2    3    0    1.0
2    7.5 -31.5    2    3    0    1.0
2    7.5 -30.5    2    3    0    1.0
2    7.5 -29.5    2    3    0    1.0
2    7.5 -28.5    2    3    0    1.0
2    7.5 -27.5    2    3    0    1.0
2    7.5 -26.5    2    3    0    1.0
```

```
2    7.5 -25.5    2    3    0    1.0
2    7.5 -24.5    2    3    0    1.0
2    7.5 -23.5    2    3    0    1.0
2    7.5 -22.5    2    3    0    1.0
2    7.5 -21.5    2    3    0    1.0
2    7.5 -20.5    2    3    0    1.0
2    7.5 -19.5    2    3    0    1.0
2    7.5 -18.5    2    3    0    1.0
2    7.5 -17.5    2    3    0    1.0
2    7.5 -16.5    2    3    0    1.0
2    7.5 -15.5    2    3    0    1.0
2    7.5 -14.5    2    3    0    1.0
2    7.5 -13.5    2    3    0    1.0
2    7.5 -12.5    2    3    0    1.0
2    7.5 -11.5    2    3    0    1.0
2    7.5 -10.5    2    3    0    1.0
2    7.5  -9.5    2    3    0    1.0
2    7.5  -8.5    2    3    0    1.0
2    7.5  -7.5    2    3    0    1.0
2    7.5  -6.5    2    3    0    1.0
2    7.5  -5.5    2    3    0    1.0
2    7.5  -4.5    2    3    0    1.0
2    7.5  -3.5    2    3    0    1.0
2    7.5  -2.5    2    3    0    1.0
2    7.5  -1.5    2    3    0    1.0
2    7.5  -0.5    2    3    0    1.0
2    7.5   0.5    2    3    0    1.0
2    7.5   1.5    2    3    0    1.0
2    7.5   2.5    2    3    0    1.0
2    7.5   3.5    2    3    0    1.0
2    8.5 -33.5    2    3    0    1.0
2    8.5 -32.5    2    3    0    1.0
2    8.5 -31.5    2    3    0    1.0
2    8.5 -30.5    2    3    0    1.0
2    8.5 -29.5    2    3    0    1.0
2    8.5 -28.5    2    3    0    1.0
2    8.5 -27.5    2    3    0    1.0
2    8.5 -26.5    2    3    0    1.0
2    8.5 -25.5    2    3    0    1.0
2    8.5 -24.5    2    3    0    1.0
2    8.5 -23.5    2    3    0    1.0
2    8.5 -22.5    2    3    0    1.0
2    8.5 -21.5    2    3    0    1.0
2    8.5 -20.5    2    3    0    1.0
2    8.5 -19.5    2    3    0    1.0
2    8.5 -18.5    2    3    0    1.0
2    8.5 -17.5    2    3    0    1.0
2    8.5 -16.5    2    3    0    1.0
2    8.5 -15.5    2    3    0    1.0
2    8.5 -14.5    2    3    0    1.0
2    8.5 -13.5    2    3    0    1.0
2    8.5 -12.5    2    3    0    1.0
2    8.5 -11.5    2    3    0    1.0
2    8.5 -10.5    2    3    0    1.0
```

```
2    8.5  -9.5    2    3    0    1.0
2    8.5  -8.5    2    3    0    1.0
2    8.5  -7.5    2    3    0    1.0
2    8.5  -6.5    2    3    0    1.0
2    8.5  -5.5    2    3    0    1.0
2    8.5  -4.5    2    3    0    1.0
2    8.5  -3.5    2    3    0    1.0
2    8.5  -2.5    2    3    0    1.0
2    8.5  -1.5    2    3    0    1.0
2    8.5  -0.5    2    3    0    1.0
2    8.5   0.5    2    3    0    1.0
2    8.5   1.5    2    3    0    1.0
2    8.5   2.5    2    3    0    1.0
2    8.5   3.5    2    3    0    1.0
2    9.5 -33.5    2    3    0    1.0
2    9.5 -32.5    2    3    0    1.0
2    9.5 -31.5    2    3    0    1.0
2    9.5 -30.5    2    3    0    1.0
2    9.5 -29.5    2    3    0    1.0
2    9.5 -28.5    2    3    0    1.0
2    9.5 -27.5    2    3    0    1.0
2    9.5 -26.5    2    3    0    1.0
2    9.5 -25.5    2    3    0    1.0
2    9.5 -24.5    2    3    0    1.0
2    9.5 -23.5    2    3    0    1.0
2    9.5 -22.5    2    3    0    1.0
2    9.5 -21.5    2    3    0    1.0
2    9.5 -20.5    2    3    0    1.0
2    9.5 -19.5    2    3    0    1.0
2    9.5 -18.5    2    3    0    1.0
2    9.5 -17.5    2    3    0    1.0
2    9.5 -16.5    2    3    0    1.0
2    9.5 -15.5    2    3    0    1.0
2    9.5 -14.5    2    3    0    1.0
2    9.5 -13.5    2    3    0    1.0
2    9.5 -12.5    2    3    0    1.0
2    9.5 -11.5    2    3    0    1.0
2    9.5 -10.5    2    3    0    1.0
2    9.5  -9.5    2    3    0    1.0
2    9.5  -8.5    2    3    0    1.0
2    9.5  -7.5    2    3    0    1.0
2    9.5  -6.5    2    3    0    1.0
2    9.5  -5.5    2    3    0    1.0
2    9.5  -4.5    2    3    0    1.0
2    9.5  -3.5    2    3    0    1.0
2    9.5  -2.5    2    3    0    1.0
2    9.5  -1.5    2    3    0    1.0
2    9.5  -0.5    2    3    0    1.0
2    9.5   0.5    2    3    0    1.0
2    9.5   1.5    2    3    0    1.0
2    9.5   2.5    2    3    0    1.0
2    9.5   3.5    2    3    0    1.0
2    9.5   4.5    2    3    0    1.0
2   10.5 -33.5    2    3    0    1.0
```

```
   2   10.5 -32.5    2    3    0    1.0
   2   10.5 -31.5    2    3    0    1.0
   2   10.5 -30.5    2    3    0    1.0
   2   10.5 -29.5    2    3    0    1.0
   2   10.5 -28.5    2    3    0    1.0
   2   10.5 -27.5    2    3    0    1.0
   2   10.5 -26.5    2    3    0    1.0
   2   10.5 -25.5    2    3    0    1.0
   2   10.5 -24.5    2    3    0    1.0
   2   10.5 -23.5    2    3    0    1.0
   2   10.5 -22.5    2    3    0    1.0
   2   10.5 -21.5    2    3    0    1.0
   2   10.5 -20.5    2    3    0    1.0
   2   10.5 -19.5    2    3    0    1.0
   2   10.5 -18.5    2    3    0    1.0
   2   10.5 -17.5    2    3    0    1.0
   2   10.5 -16.5    2    3    0    1.0
   2   10.5 -15.5    2    3    0    1.0
   2   10.5 -14.5    2    3    0    1.0
   2   10.5 -13.5    2    3    0    1.0
   2   10.5 -12.5    2    3    0    1.0
   2   10.5 -11.5    2    3    0    1.0
   2   10.5 -10.5    2    3    0    1.0
   2   10.5  -9.5    2    3    0    1.0
   2   10.5  -8.5    2    3    0    1.0
   2   10.5  -7.5    2    3    0    1.0
   2   10.5  -6.5    2    3    0    1.0
   2   10.5  -5.5    2    3    0    1.0
   2   10.5  -4.5    2    3    0    1.0
   2   10.5  -3.5    2    3    0    1.0
   2   10.5  -2.5    2    3    0    1.0
   2   10.5  -1.5    2    3    0    1.0
   2   10.5  -0.5    2    3    0    1.0
   2   10.5   0.5    2    3    0    1.0
   2   10.5   1.5    2    3    0    1.0
   2   10.5   2.5    2    3    0    1.0
#--+-----+-----+-----+----+----+----+----+----+----+
#
#  Layer 0: (repair doubler 1)
#
#  +---------------------- Material property set
#  |   +------------------ Number of keypoints
#  |   |   +-------------- Number of boundary segments
#  |   |   |   +---------- Number of displacement boundary condition
descriptions
#  |   |   |   |   +------ Number of traction boundary condition descriptions
for each load case
#  |   |   |   |   |
#  V   V   V   V   V
#--+---+---+---+---+
   0   5   5   0   0    1
#--+---+---+---+---+
#
#  Kepoints
```

```
#
#      +--------- X coordinate
#      |      +-- Y coordinate
#      |      |
#      V      V
#------+------+--
      2.000 11.000
      2.000  5.657
      5.657  2.000
     11.000  2.000
     11.000 11.000
#------+------+--
#
# Boundary segments
#
#      +------------------------------------ Starting keypoint index
#      |   +-------------------------------- End keypoint index
#      |   |   +---------------------------- Type flag (line=0, circular=1,
elliptical=2)
#      |   |   |    +------------------------- x coordinate (ignored for line
segment)
#      |   |   |    |    +-------------------- y coordinate (ignored for line
segment)
#      |   |   |    |    |    +----------------- Subdivision flag
#      |   |   |    |    |    |    +------------ Subdivision number
#      |   |   |    |    |    |    |    +------ Subdivision ratio
#      |   |   |    |    |    |    |    |
#      V   V   V    V    V    V    V    V
#------+---+---+----+----+----+----+----+
       0   1   0                   0
       1   2   1    0.0  0.0  0
       2   3   0                   0
       3   4   0                   0
       4   0   0                   0
#------+---+---+----+----+----+----+----+----+
#
#  Layer 1: (repair doubler 2)
#
#  +---------------------- Material property set
#  |   +------------------ Number of keypoints
#  |   |   +-------------- Number of boundary segments
#  |   |   |   +---------- Number of displacement boundary condition
descriptions
#  |   |   |   |   +------ Number of traction boundary condition descriptions
for each load case
#  |   |   |   |   |
#  |   |   |   |   |
#  V   V   V   V   V
#--+---+---+---+---+
   1   5   5   0   0    1
#--+---+---+---+---+
#
#      Kepoints
#
```

```
#      +--------- X coordinate
#      |      +-- Y coordinate
#      |      |
#      V      V
#------+------+--
      0.000 13.000
      0.000  6.000
      6.000  0.000
     13.000  0.000
     13.000 13.000
#------+------+--
#
#      Boundary segments
#
#      +------------------------------------ Starting keypoint index
#      |   +-------------------------------- End keypoint index
#      |   |   +---------------------------- Type flag (line=0, circular=1,
elliptical=2)
#      |   |   |    +------------------------- x coordinate (ignored for line
segment)
#      |   |   |    |    +--------------------- y coordinate (ignored for line
segment)
#      |   |   |    |    |    +---------------- Subdivision flag
#      |   |   |    |    |    |    +----------- Subdivision number
#      |   |   |    |    |    |    |    +------ Subdivision ratio
#      |   |   |    |    |    |    |    |
#      V   V   V    V    V    V    V    V
#------+---+---+----+----+----+----+----+
       0   1   0               0
       1   2   1    0.0  0.0   0
       2   3   0               0
       3   4   0               0
       4   0   0               0
#------+---+---+----+----+----+----+----+
#
#  Layer 2: (skin)
#
#  +---------------------- Material property set
#  |   +------------------ Number of keypoints
#  |   |   +-------------- Number of boundary segments
#  |   |   |   +---------- Number of displacement boundary condition
descriptions
#  |   |   |   |   +------ Number of traction boundary condition descriptions
for each load case
#  |   |   |   |   |
#  |   |   |   |   |
#  V   V   V   V   V
#--+---+---+---+---+
   2   18  18  4   3    0
#--+---+---+---+---+
#
#      Kepoints
#
#      +--------- X coordinate
```

```
#      |      +-- Y coordinate
#      |      |
#      V      V
#------+------+--
    -15.0   66.0
    -15.0   13.0
    -15.0    6.0
      0.0    6.0
      4.0    4.5
      4.0    9.0
      9.0    9.0
      9.0    4.0
      4.5    4.0
      6.0    0.0
      6.0  -34.0
     13.0  -34.0
     35.0  -34.0
     35.0    0.0
     35.0   13.0
     35.0   66.0
     13.0   66.0
      0.0   66.0
#------+------+--
#
#      Boundary segments
#
#      +------------------------------------- Starting keypoint index
#      |   +--------------------------------- End keypoint index
#      |   |   +----------------------------- Type flag (line=0, circular=1,
elliptical=2)
#      |   |   |    +------------------------- x coordinate (ignored for line
segment)
#      |   |   |    |    +--------------------- y coordinate (ignored for line
segment)
#      |   |   |    |    |    +---------------- Subdivision flag
#      |   |   |    |    |    |    +----------- Subdivision number
#      |   |   |    |    |    |    |    +------ Subdivision ratio
#      |   |   |    |    |    |    |    |
#      V   V   V    V    V    V    V    V
#------+---+---+----+----+----+----+----+--
       0   1   0                   1   30   0.5
       1   2   0                   0
       2   3   0                   1   10   0.5
       3   4   1   0.0   0.0   0
       4   5   0                   0
       5   6   0                   0
       6   7   0                   0
       7   8   0                   0
       8   9   1   0.0   0.0   0
       9  10   0                   1   20   2.0
      10  11   0                   0
      11  12   0                   1   12   2.0
      12  13   0                   1   20   0.5
      13  14   0                   0
```

```
      14  15   0                1   30   2.0
      15  16   0                1   12   0.5
      16  17   0                0
      17   0   0                1   10   2.0
#------+---+---+----+----+----+----+----+--
#
# Displacement boundary condition description
#
#      +--------------------- Type flag
#      |   +----------------- Index
#      |   |   +------------- BC displacement type
#      |   |   |    +-------- BC displacement x value
#      |   |   |    |    +--- BC displacement y value
#      |   |   |    |    |
#      V   V   V    V    V
#------+---+---+----+----+--
       1   0   0    0.0
       1   1   0    0.0
       1   10  1         0.0
       1   11  1         0.0
#------+---+---+----+----+--
#
# Load case 0
#
#      +----------------------- Type flag
#      |   +------------------- Index
#      |   |   +--------------- BC traction type
#      |   |   |   +----------- BC traction x value
#      |   |   |   |       +--- BC traction y value
#      |   |   |   |       |
#      |   |   |   |       |
#      |   |   |   |       |
#      V   V   V   V       V
#------+---+---+---+-------+-----
       1   12  0   1000.0
       1   13  0   1000.0
       1   14  0   1000.0
#------+---+---+---+-------+-----
#
# Load case 1
#
#      +----------------------- Type flag
#      |   +------------------- Index
#      |   |   +--------------- BC traction type
#      |   |   |   +----------- BC traction x value
#      |   |   |   |       +--- BC traction y value
#      |   |   |   |       |
#      |   |   |   |       |
#      |   |   |   |       |
#      V   V   V   V       V
#------+---+---+---+-------+-----
       1   15  1         1000.0
       1   16  1           1000.0
       1   17  1           1000.0
```

```
#------+---+---+---+-------+-----
#
#  Layer 3: (production doubler)
#
#  +---------------------- Material property set
#  |   +------------------ Number of keypoints
#  |   |   +-------------- Number of boundary segments
#  |   |   |   +---------- Number of displacement boundary condition
descriptions
#  |   |   |   |   +------ Number of traction boundary condition descriptions
for each load case
#  |   |   |   |   |
#  |   |   |   |   |
#  V   V   V   V   V
#--+---+---+---+---+
   3   8   8   2   0    1
#--+---+---+---+---+
#
#      Kepoints
#
#      +--------- X coordinate
#      |      +-- Y coordinate
#      |      |
#      V      V
#------+------+--
    -15.0   11.0
    -15.0    6.0
      0.0    6.0
      6.0    0.0
      6.0  -34.0
     11.0  -34.0
     11.0    0.0
      0.0   11.0
#------+------+--
#
#      Boundary segments
#
#      +------------------------------------- Starting keypoint index
#      |   +----------------------------------- End keypoint index
#      |   |   +------------------------------- Type flag (line=0, circular=1,
elliptical=2)
#      |   |   |    +-------------------------- x coordinate (ignored for line
segment)
#      |   |   |    |    +--------------------- y coordinate (ignored for line
segment)
#      |   |   |    |    |    +---------------- Subdivision flag
#      |   |   |    |    |    |    +----------- Subdivision number
#      |   |   |    |    |    |    |    +------ Subdivision ratio
#      |   |   |    |    |    |    |    |
#      V   V   V    V    V    V    V    V
#------+---+---+----+----+----+----+----+--
       0   1   0                 0
       1   2   0                 1   10    0.5
       2   3   1   0.0   0.0  0
```

```
       3   4   0                1   20    2.0
       4   5   0                0
       5   6   0                1   20    0.5
       6   7   1   0.0   0.0  0
       7   0   0                1   10    2.0
#------+---+---+----+----+----+----+----+--
#
# Displacement boundary condition description
#
#      +--------------------- Type flag
#      |   +----------------- Index
#      |   |   +------------- BC displacement type
#      |   |   |    +-------- BC displacement x value
#      |   |   |    |    +--- BC displacement y value
#      |   |   |    |    |
#      V   V   V    V    V
#------+---+---+----+----+--
       1   0   0    0.0
       1   4   1       0.0
#------+---+---+----+----+--
#
# Line plot
#
#      +---------------------------------------- Number of line plot sets
#      |
#      |
#      V
#------+
       1
#------+
#
# Line plot description
#
#      +---------------------------------- x coordinate of the starting point
#      |     +---------------------------- y coordinate of the starting point
#      |     |     +---------------------- x coordinate of the ending point
#      |     |     |     +---------------- y coordinate of the ending point
#      |     |     |     |     +---------- Number of subdivision
#      |     |     |     |     |     +---- Subdivision ratio
#      |     |     |     |     |     |
#      |     |     |     |     |     |
#      V     V     V     V     V     V
#------+-----+-----+-----+-----+-----+
      9.001 9.001 20.0  20.0   101   5
#------+-----+-----+-----+-----+-----+
#
# Rivet forces
#
#      +------------ Number of rivet sets
#      |
#      |
#      V
##### NOTE: It should be broken into 4 sets to fetch fastener loads
#####       along the outermost fastener rows between the repair
```

```
#####       doubler (layer 1) and the skin (layer 2)
#------+
       4
#------+
#
#      +------------ Number of rivets in set 0
#      |
#      |
#      V
#------+
       7
#------+
#
# Rivet index
#
#      +------------- Rivet index (left fastener row along x=0.5)
#      |
#      |
#      V
#------+
      46
      47
      48
      49
      50
      51
      52
#------+
#
#      +------------ Number of rivets in set 1
#      |
#      |
#      V
#------+
       13
#------+
#
# Rivet index
#
#      +------------- Rivet index (right fastener row along x=12.5)
#      |
#      |
#      V
#------+
     147
     148
     149
     150
     151
     152
     153
     154
     155
     156
```

```
     157
     158
     159
#------+
#
#      +------------ Number of rivets in set 2
#      |
#      |
#      V
#------+
       7
#------+
#
# Rivet index
#
#      +------------- Rivet index (bottom fastener row along y=0.5)
#      |
#      |
#      V
#------+
      84
      92
     100
     108
     121
     134
     147
#------+
#
#      +------------ Number of rivets in set 3
#      |
#      |
#      V
#------+
       13
#------+
#
# Rivet index
#
#      +------------- Rivet index (top fastener row along y=12.5)
#      |
#      |
#      V
#------+
      52
      59
      66
      74
      78
      83
      91
      99
     107
     120
```

```
     133
     146
     159
#------+
#
# End of door opening repair input file
#
```

(M) APPENDIX C. DOOR CONFIGURATIONS FROM BOEING.

In the following door, we reproduce the sketches of the wide-body and narrow-body configurations with a door cutout provided by personnel at the Boeing Company [??].

(1st) C.1 Wide Body Fuselage With A Passenger Door

All Longerons are as follows

ycg 0.5332 in
Area 0.2744 in^2
Ixx 0.0381 in^4
Iyy 0.0784 in^4
Material 7075 -T6 Clad Sheet
E 10.4E6 psi

Spacing of longerons is 7.22 inches
Total number of longerons is 103

All Frames are as follows

ycg 2.2668 in
Area 0.7280 in^2
Ixx 2.4723 in^4
Iyy 0.0656 in^4
Material 7075 -T6 Clad Sheet
E 10.4E6 psi

Frame Spacing is 20 inches

All floor beams are as follows

xcg 0.3575 in
ycg 3.7804 in
Area 1.0881 in^2
Ixx 7.5168 in^4
Iyy 0.1844 in^4
Material 7075 -T6 Clad Sheet
E 10.4E6 psi

Floor beams are connected to the frames (spaced every 20 inches when there isn't a frame)
Floor beams are 18 inches below the center axis of the cross section

Skin thickness is 0.068 inches
Skin material 2024-T3 Clad Al
Skin E = 10.5E6 psi

Ixx is tangent to the skin
Ycg is measured from the interface between the skin and the longeron or frame.

Radius of barrel is 118.5 inches

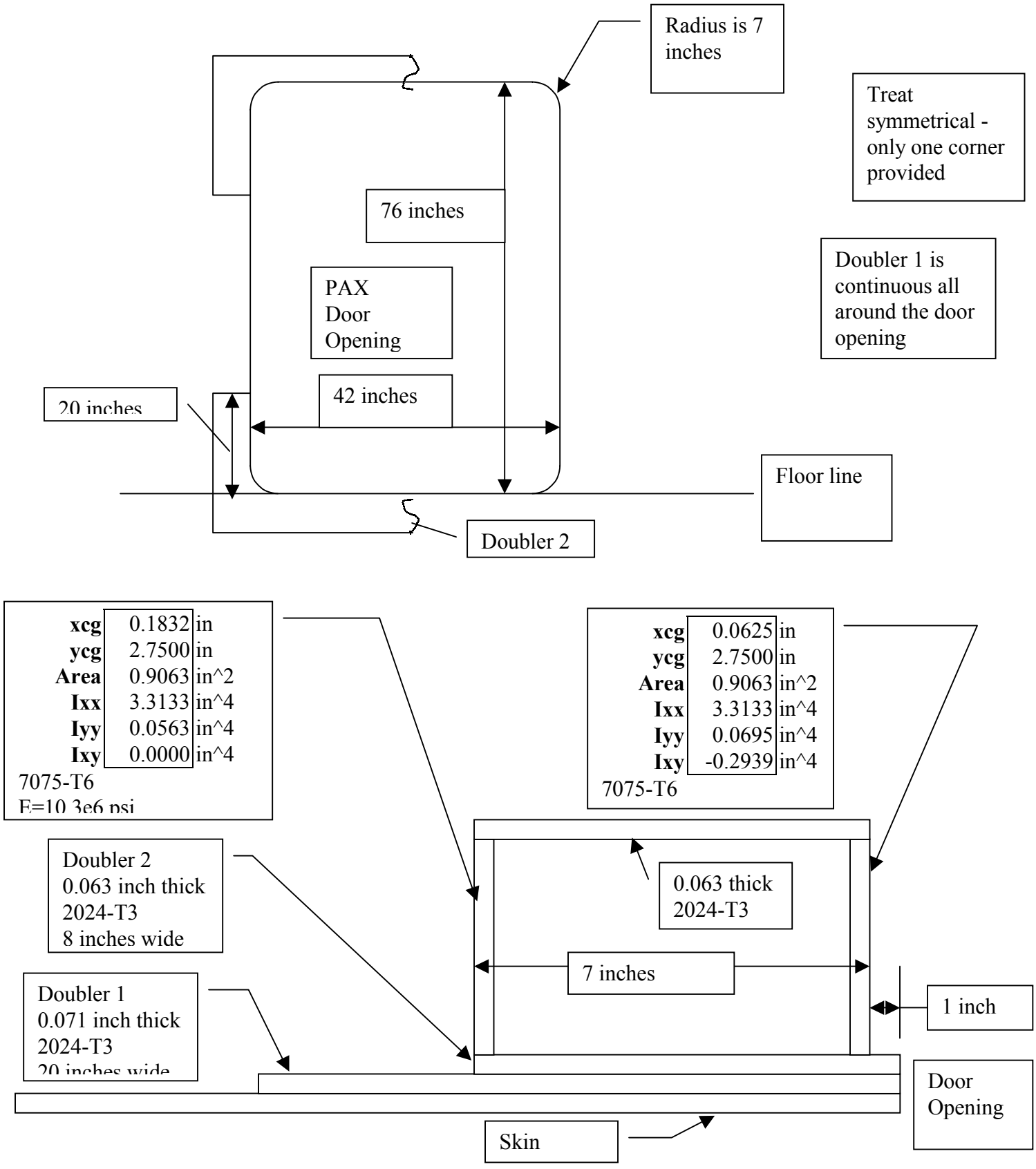
Radius is 7 inches
Treat symmetrical - only one corner provided
76 inches
Doubler 1 is continuous all around the door opening
PAX Door Opening
42 inches
20 inches
Floor line
Doubler 2
xcg 0.1832 in
ycg 2.7500 in
Area 0.9063 in^2
Ixx 3.3133 in^4
Iyy 0.0563 in^4
Ixy 0.0000 in^4
7075-T6
E=10.3e6 psi
xcg 0.0625 in
ycg 2.7500 in
Area 0.9063 in^2
Ixx 3.3133 in^4
Iyy 0.0695 in^4
Ixy -0.2939 in^4
7075-T6
Doubler 2
0.063 inch thick
2024-T3
8 inches wide
0.063 thick
2024-T3
7 inches
1 inch
Doubler 1
0.071 inch thick
2024-T3
20 inches wide
Door Opening
Skin

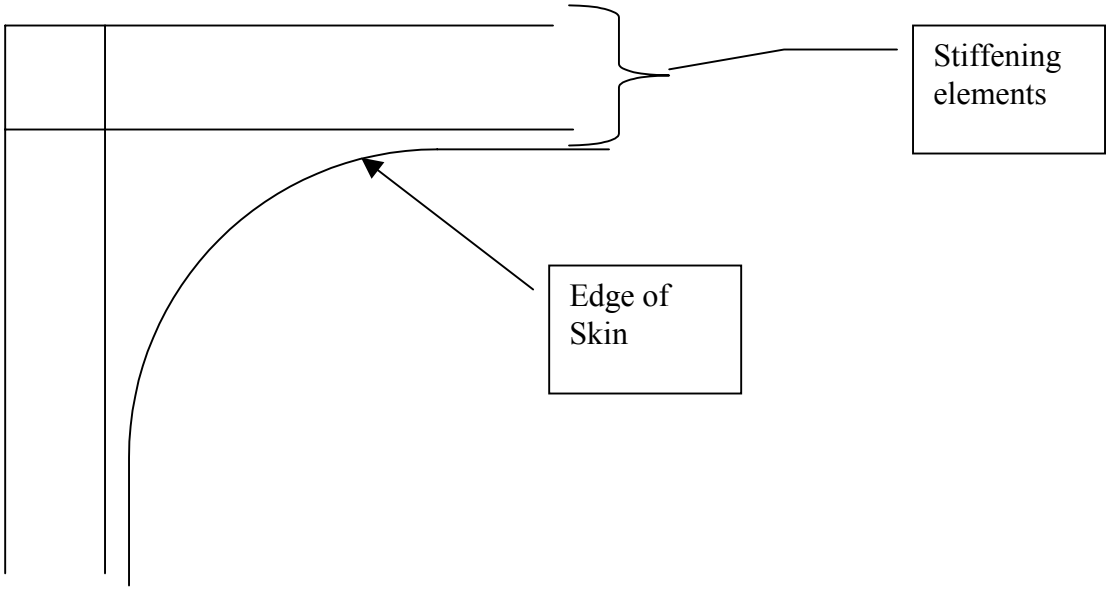

(1st) C.2 Narrow Body Fuselage With A Cargo Door

Narrow body geometry

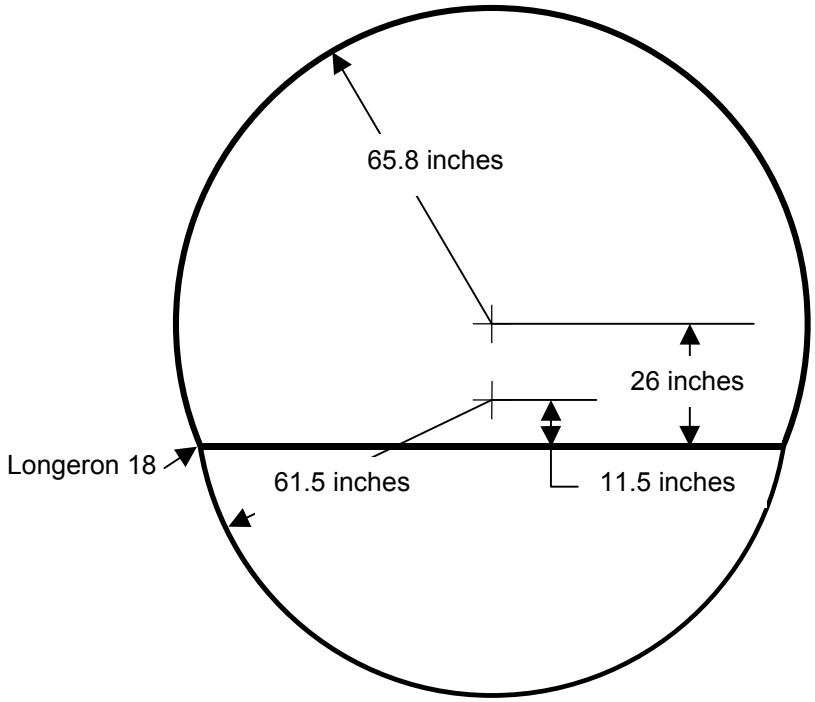

There are 58 longerons around the fuselage. Longeron 18 is the floor. There is 1 longeron 1 and it is at top center. There is a longeron 30 at the bottom center. Longerons are spaced equally around at approximately 7 inches.

The door in this case is below the floor. The opening starts at longeron 20 and ends at longeron 27. The width of the door opening is 43 inches.

All Longerons are as follows

ycg	0.5332 in
Area	0.2744 in^2
Ixx	0.0381 in^4
Iyy	0.0784 in^4
Material	7075 -T6 Clad Sheet
E	10.4E6 psi

All Frames are as follows

ycg	2.2668 in
Area	0.7280 in^2
Ixx	2.4723 in^4
Iyy	0.0656 in^4
Material	7075 -T6 Clad Sheet
E	10.4E6 psi

Frame Spacing is 20 inches

All floor beams are as follows

xcg	0.3575 in
ycg	3.7804 in
Area	1.0881 in^2
Ixx	7.5168 in^4
Iyy	0.1844 in^4
Material	7075 -T6 Clad Sheet
E	10.4E6 psi

Floor beams are connected to the frames (spaced every 20 inches when there isn't a frame)
Floor beams are 18 inches below the center axis of the cross section

Skin thickness is 0.050 inches
Skin material 2024-T3 Clad Al
Skin E = 10.5E6 psi

Ixx is tangent to the skin
Ycg is measured from the interface between the skin and the longeron or frame.

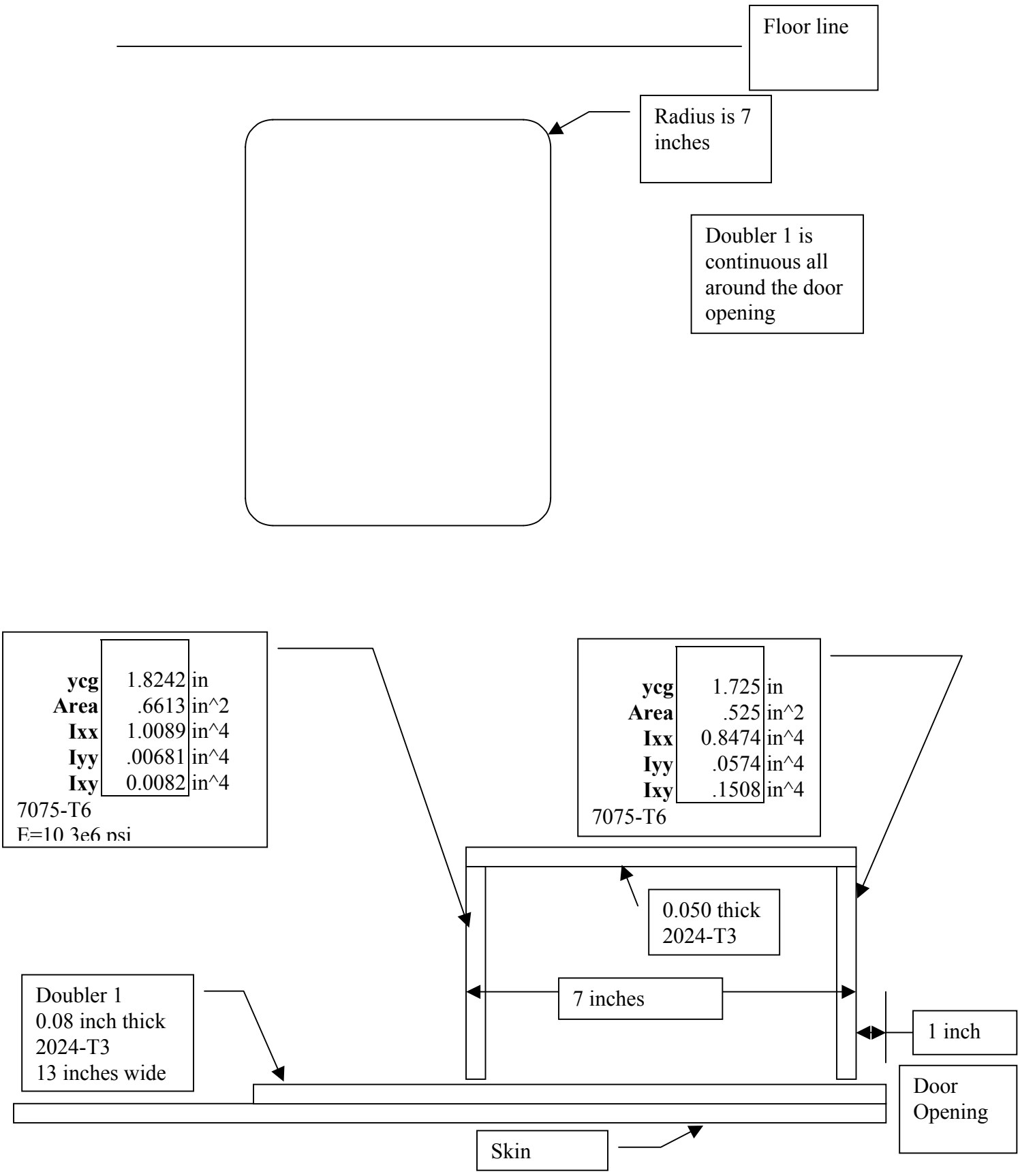
Floor line
Radius is 7 inches
Doubler 1 is continuous all around the door opening
ycg 1.8242 in
Area .6613 in^2
Ixx 1.0089 in^4
Iyy .00681 in^4
Ixy 0.0082 in^4
7075-T6
E=10.3e6 psi
ycg 1.725 in
Area .525 in^2
Ixx 0.8474 in^4
Iyy .0574 in^4
Ixy .1508 in^4
7075-T6
0.050 thick
2024-T3
7 inches
1 inch
Doubler 1
0.08 inch thick
2024-T3
13 inches wide
Door Opening
Skin

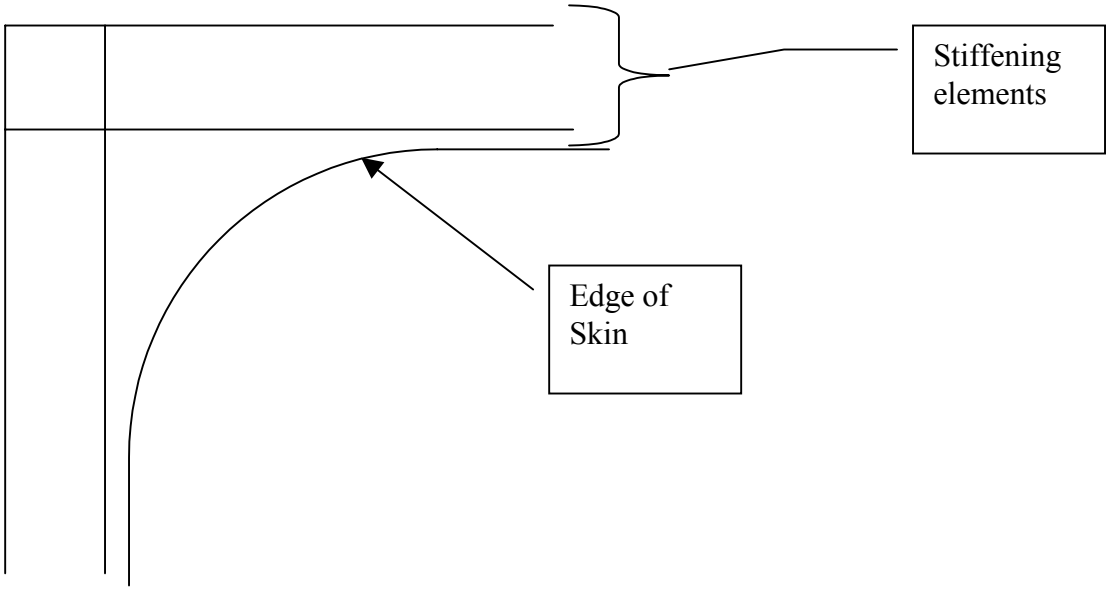
Stiffening elements
Edge of Skin

Appendix J: Stress Analysis of Three Fuselage Sections with a Door Opening

Introduction

A rectangular door opening will deform under inertia loads into a parallelogram, inducing local skin bending at the corners. The effects can only be properly determined by analyzing the three-dimensional fuselage structure. However, analysis of any three-dimensional structure of this nature would be impractical in most cases. This Section documents the approach taken to investigate the feasibility of establishing a correlation between the two-dimensional results and three-dimensional results.
Three-dimensional stress analysis of three fuselage sections with a door opening in large transport aircraft is documented in this Appendix. The purposes of the analysis are to

- Investigate the 3-D bending versus 2-D membrane effect on skin stresses near the door opening corner, and
- Determine an enveloped stress amplification factor to be applied in stress spectrum for the damage tolerance analysis of door opening corner repairs.

Boeing chose three door configurations, each from a KC-10, a C-9, and a C-17 fuselage sections. Analyses of the KC-10 and the C-9 fuselage sections were performed by Cornell University under the FAA contract in support of the ongoing RAPID program. Boeing performed the C-17 fuselage section analysis.

Descriptions of each fuselage section including a simplified door configuration, finite element modeling, analysis results and their interpretations are provided as follows.

J.1 Descriptions of Fuselage Sections with Door Opening

The three fuselage sections investigated include a KC-10, a C-9 and a C-17 aircraft. The KC-10 door is a main deck crew entrance door. The C-9 door is a lower cargo door. The C-17 door is the crew entrance door.

The KC-10 fuselage cross section is circular shape with a radius of 118.5 inches. The longerons are spaced approximately 7 inches apart with a total of 103 longerons spaced around the circumference. The frames are spaced approximately 20 inches. The typical skin thickness ranges from 0.068 to 0.071 inches and is made from 2024-T3 clad aluminum. The structure around the door opening provides rigidity to reduce the amount deformation the door opening experiences when the airframe is loaded. The rigidity is provided by a built up structure that includes internal production doublers, intercostals, frames, longerons and webs. This built up structure creates a box like structure around the door. The finite element model accounts for a majority of this structure although in a much simplified manner. The skin in the model is 0.068 inches thick 2024-T3 clad aluminum. The longerons have the following properties:

ycg	0.5332 in
Area	0.2744 in^2
Ixx	0.0381 in^4
Iyy	0.0784 in^4
Material	7075 -T6 Clad Sheet
E	10.4E6 psi

The frames have the following properties:

ycg	2.2668 in
Area	0.7280 in^2
Ixx	2.4723 in^4
Iyy	0.0656 in^4
Material	7075 -T6 Clad Sheet
E	10.4E6 psi

The floor beams have the following properties:

xcg	0.3575 in
ycg	3.7804 in
Area	1.0881 in^2
Ixx	7.5168 in^4
Iyy	0.1844 in^4
Material	7075 -T6 Clad Sheet
E	10.4E6 psi

Floor beams are connected to the frames (spaced every 20 inches when there isn't a frame) and are 18 inches below the center axis of the cross section. The structure around the door and the geometry of the door is provided in Figure J1.

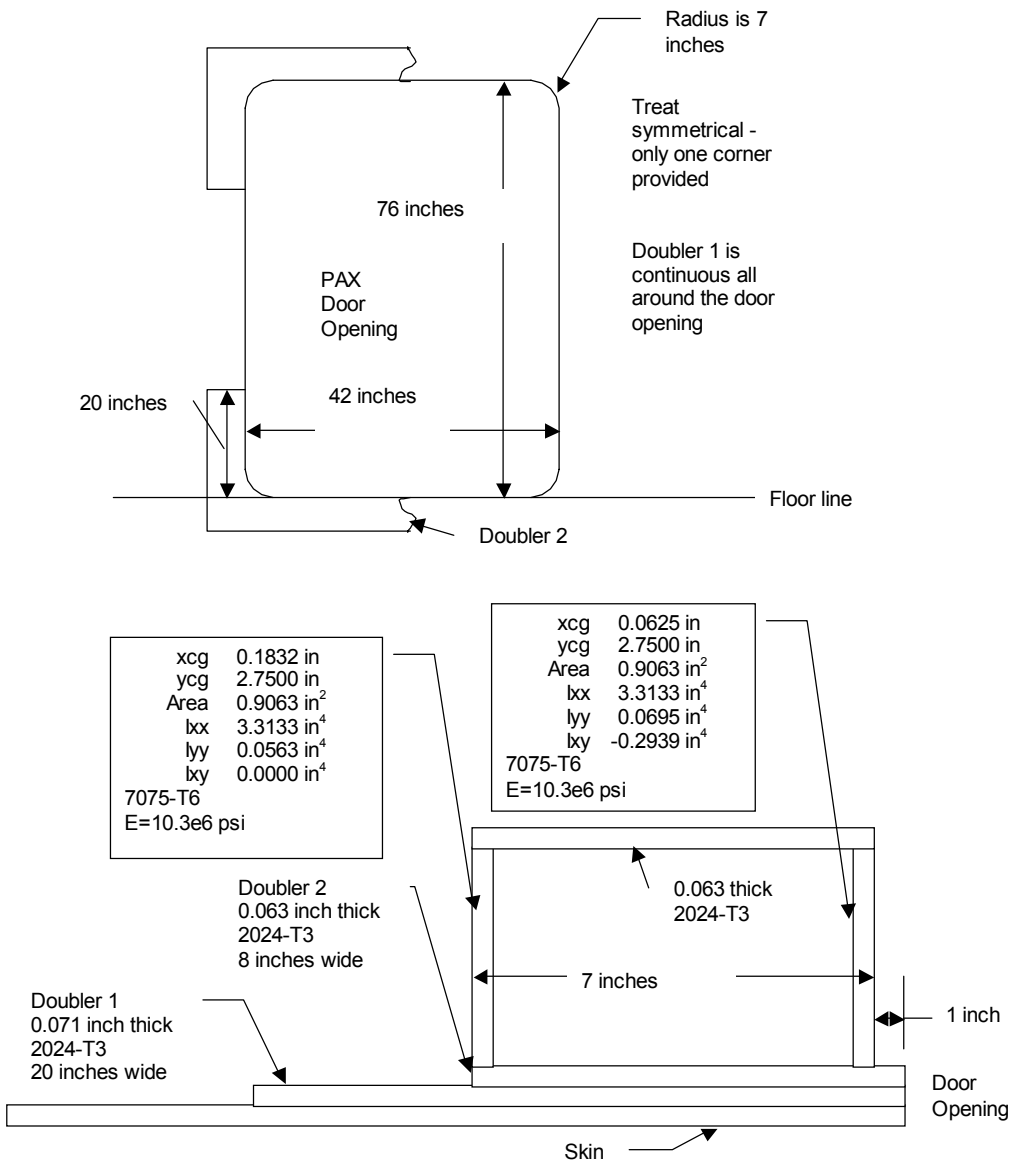

Figure J1. Door Geometry in the KC-10 Fuselage Section

The C-9 fuselage cross section is a double bubble with an upper radius of 65.8 inches and a lower radius of 61.5 inches. Figure J2 illustrates the cross section.

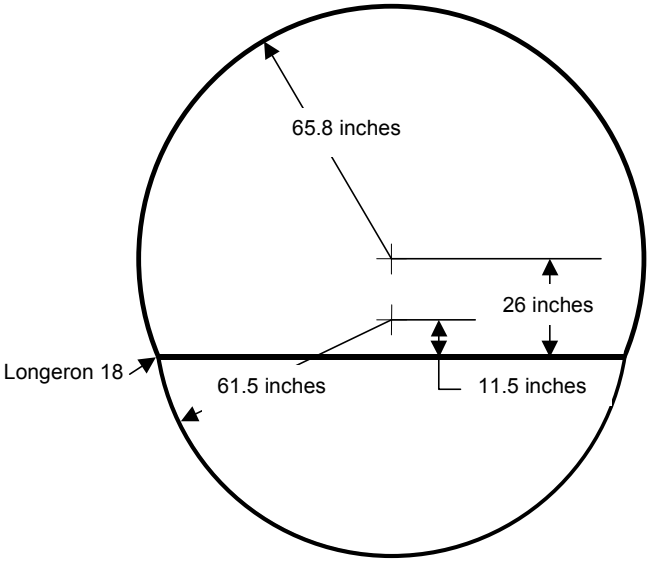

Figure J2. Cross Section of the C-9 Fuselage Section

The longerons are spaced approximately 7 inches apart with a total of 58 longerons spaced around the circumference. Longeron 18 is at the floor level. Longeron 1 is at top and Longeron 30 at the bottom. The frames are spaced approximately 20 inches. The typical skin thickness ranges from 0.050 to 0.063 inches and is made from 2024-T3 clad aluminum. The structure around the door opening provides rigidity to reduce the amount deformation the door opening experiences when the airframe is loaded. The rigidity is provided by a built up structure that includes internal production doublers, intercostals, frames, longerons and webs. This built up structure creates a box like structure around the door. The finite element model accounts for a majority of this structure although in a much simplified manner. The skin in the model is 0.050 inches thick 2024-T3 clad aluminum. The longerons have the following properties:

ycg	0.5332 in
Area	0.2744 in^2
Ixx	0.0381 in^4
Iyy	0.0784 in^4
Material	7075 -T6 Clad Sheet
E	10.4E6 psi

The frames have the following properties:

ycg	2.2668 in
Area	0.7280 in^2
Ixx	2.4723 in^4
Iyy	0.0656 in^4
Material	7075 -T6 Clad Sheet
E	10.4E6 psi

The floor beams have the following properties:

xcg	0.3575 in
ycg	3.7804 in
Area	1.0881 in^2
Ixx	7.5168 in^4
Iyy	0.1844 in^4
Material	7075 -T6 Clad Sheet
E	10.4E6 psi

Floor beams are connected to the frames (spaced every 20 inches when there isn't a frame) and are 18 inches below the center axis of the cross section. The structure around the door and the geometry of the door is provided in Figure J3.

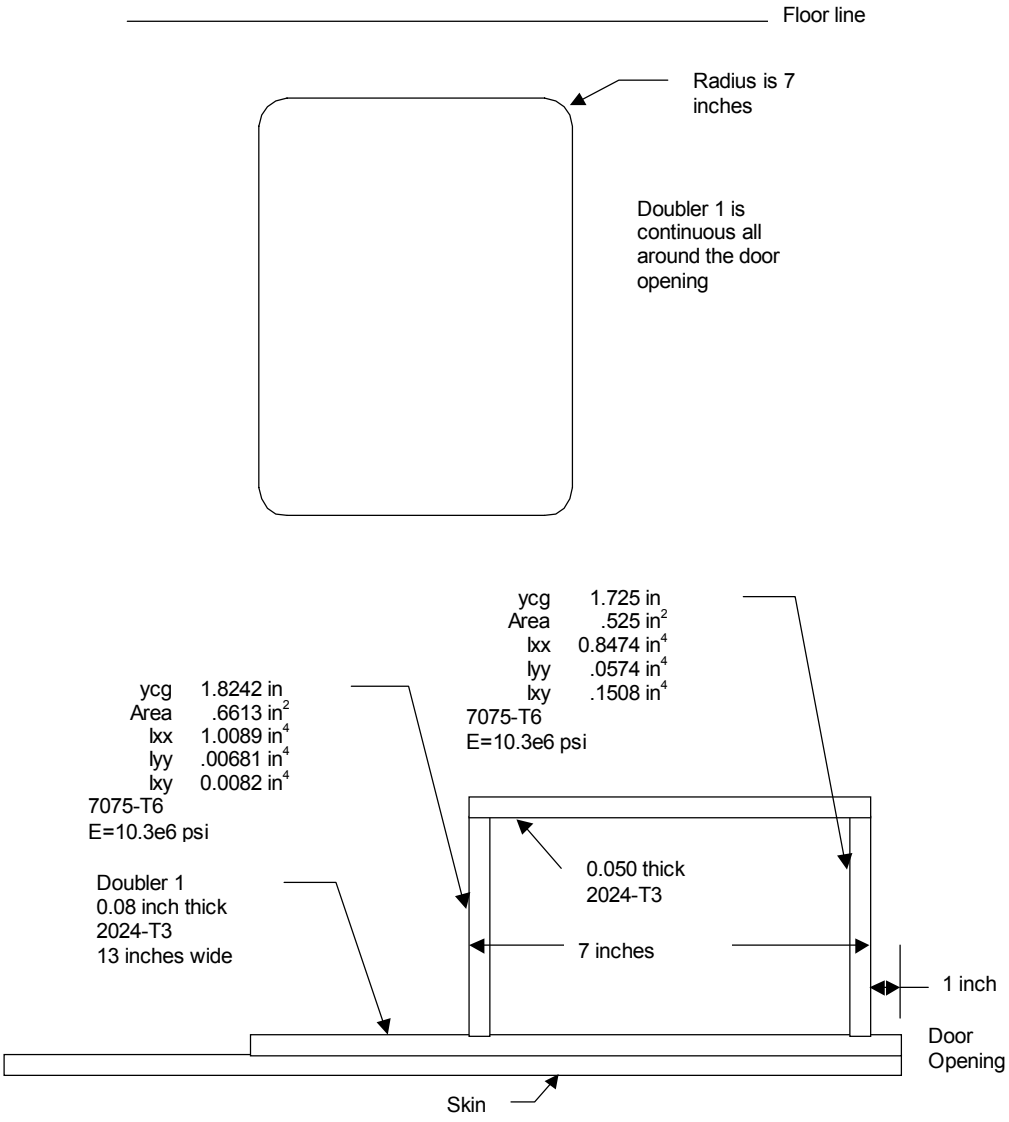

Figure J3. Door Geometry in the C-9 Fuselage Section

Figure J4 shows the fuselage section of the C-17 that was used in the analysis. The section includes the Crew Entry door cutout.

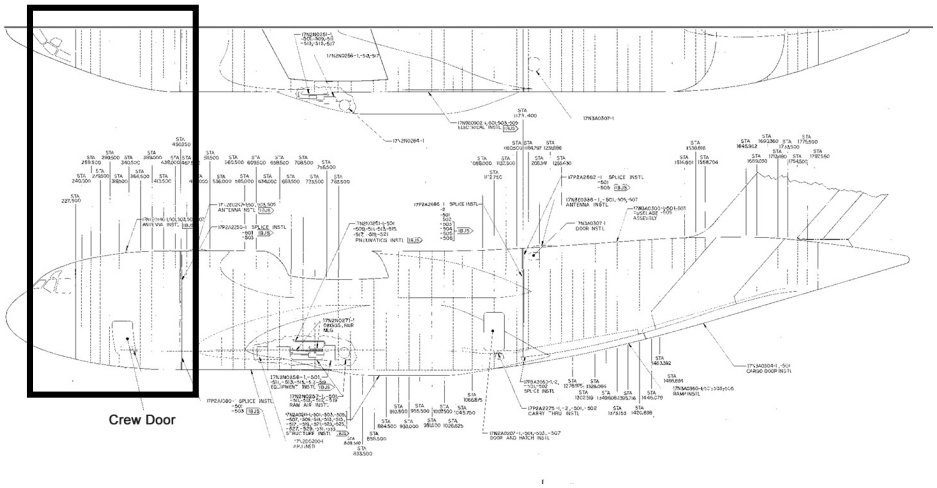

Figure J4. C-17 Fuselage Section Used in Analysis

J.2 Finite Element Models

Boeing provided Cornell with

- A fuselage section of a KC-10 aircraft including a simplified crew entrance door opening structural details and
- A fuselage section of a C-9 aircraft including a simplified cargo door opening structural details.

Cornell performed linear elastic analyses of the fuselage sections under two separate loading conditions, the internal pressure and the shear load, using the ANSYS code. Finite element model of each door is described as follows.

J.2.1 A KC-10 Fuselage Section with a Crew Entrance Door Opening

The forward fuselage section of the KC-10 aircraft was modeled using thin shell elements. Figure J5 shows the finite element meshes of the full barrel for the internal pressure. A close look of the door opening corner is shown in Figure J6.

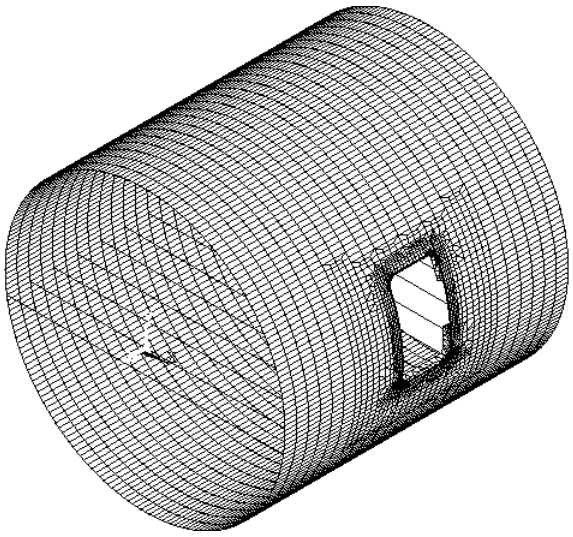

Figure J5. Finite Element Meshes of the KC-10 Fuselage Section

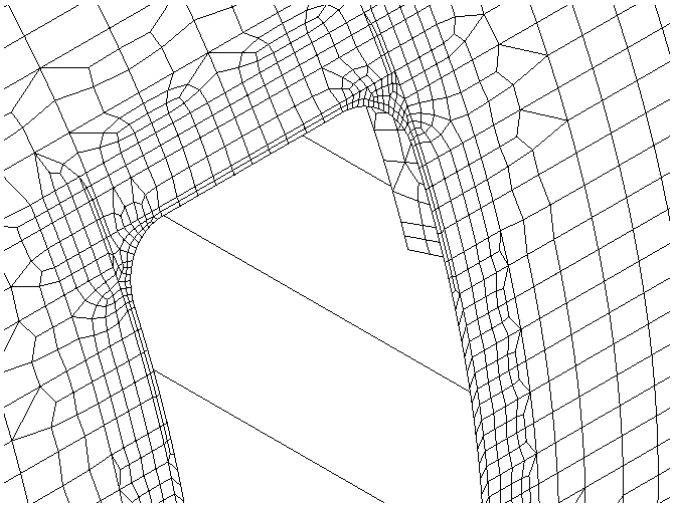

Figure J6. A Close Look of the Door Opening Corner

For internal pressure loading analysis, the forward end is constrained. A nominal pressure equal to 8.0 psi is applied uniformly on the skin except in the reinforced door opening region. An effective pressure of 93.2 psi due to door jam is applied in that region. The effective pressure is calculated as the load exerted on the door due to internal pressure divided by the area of the reinforced door opening region. In addition, a longitudinal force equal to πpR^2 together with a set of longitudinal constraints is enforced at the afterward end of the fuselage section to ensure it behaves like a closed cylinder.

For the shear load analysis, rigid bars are constructed as in a wagon wheel at the forward end of the barrel. The afterward end of the fuselage section is clamped. A rigid bar is added from the centroid of the forward end to the door cutout location. A concentrated vertical shear load equal to 100,000 lbs is applied at the end of the rigid bar. The finite element model is shown in Figure J7.

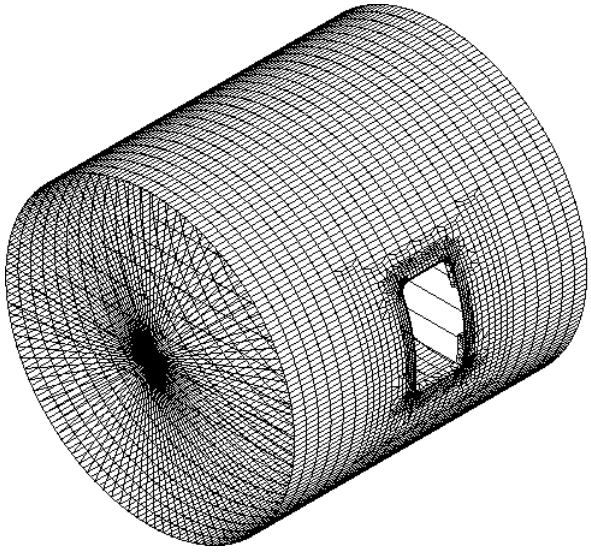

Figure J7. Finite Element Meshes of the KC-10 Fuselage Section for Shear Load Condition

J.2.2 A C-9 Fuselage Section with a Cargo Door Opening

Similar modeling technique is employed for the C-9 fuselage section with a cargo door opening. Figure J8 shows the finite element meshes of the full barrel. A close look of one of the door opening corners is shown in Figure J9.

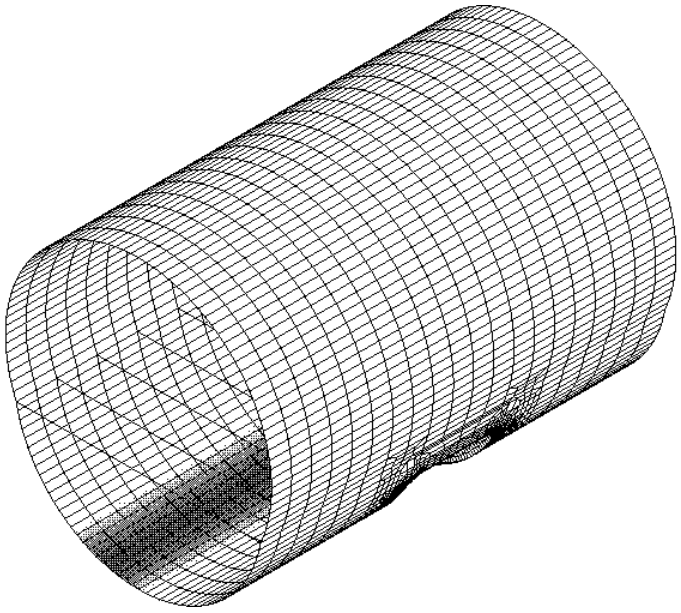

Figure J8. Finite Element Meshes of the C-9 Fuselage Section

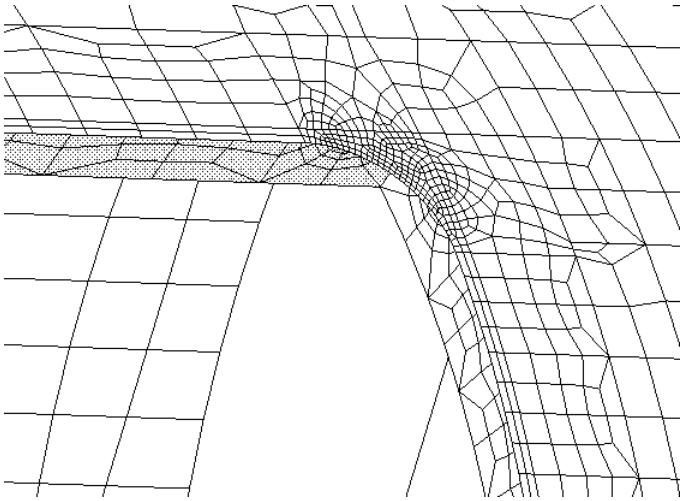

Figure J9. A Close Look of the Door Opening Corner

J.2.3 2-D Analysis

Cornell also performed 2-D membrane stress analysis of the KC-10 and C-9 fuselage sections. The analysis was accomplished by flattening an area of the 3-D model. Nodal loads of the 3-D model were then applied to the 2-D model at the same angles to the elements. In other words, the load vectors rotate with the nodal coordinates. In the 2-D model, deformations were constrained in the direction normal to the plane of the model. Free edges of the model were fixed to re-act the applied nodal loads. In the case of pressure loading, the lateral loads on the skin were ignored.

J.2.4 A C-17 Fuselage Section with a Crew Entrance Door Opening

The C-17 door cutout analysis used a finite element model of the left hand side of the forward fuselage, symmetric about the plane's centerline (X=0.0). The model extends from the forward pressure bulkhead at Sta. Y=123 (just aft of the radome) to Sta. Y=487, and from longeron L-1 through L-46. The finite element model is given in Figures K10.

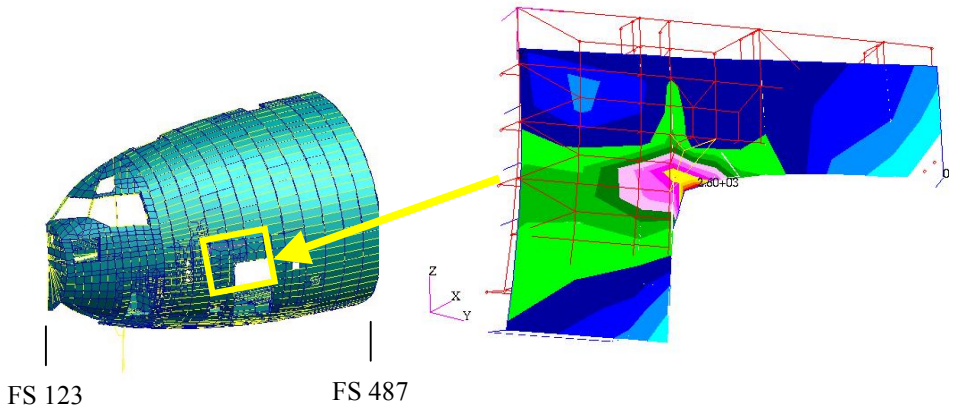

Figure J10. Finite Element Model of the C-17 Fuselage Section

Due to symmetry, only one half of the structure is modeled. Appropriate symmetric conditions are imposed on the model along the plane of symmetry (Y-Z). The afterward end of the model is constrained as a clamped end. The model was originally developed to determine the membrane stresses in the fuselage skin and axial forces and shear flow in the stiffening structural elements such as frame and longeron using the in-house F.E code CASD. This CASD model was translated into a NASTRAN model. The CASD model has coarse mesh near the door cutout corners. Hence, the mesh near the critical corner was refined. This refined mesh of the skin together with the attached frames and longerons are grouped together into a local model (see left picture of Figure J10). All membrane elements that represent the fuselage skin in the local model were changed into

plate bending elements. The final NASTRAN model contains about 5,076 nodes and 13,836 elements.

Only a vertical shear loading condition is considered in the analysis. A vertical shear load of 100,000 lb is applied at approximately station FS 325 (near the middle of the door cutout). This shear load was transmitted to the forward pressure bulkhead by a rigid bar and distributed to the skin structure through a number of rigid bars forming a wagon wheel.

J.3 Summary and Correction Factor for 2-D Analysis

Results for the shear loading case are summarized in Table J1. The values in column one and two from the left are the maximum stress at the critical door cut-out corner for the case of concentrated shear loading. It is seen the ratios of the maximum to minimum principle stress from the 3-D analysis range from 1.3 to 1.8. The ratios of the maximum stress to the two-dimensional results for KC-10 and C-9 are 1.5 and 1.3 respectively. No two-dimensional analysis was performed for C-17 as door is located in the cone shape fuselage region, difficult to create an equivalent two-dimensional finite element model.

Table J1. Stresses at the Critical Loading under Vertical Shear Load of 100,000 lbs

Aircraft	**In-Plane Stress σ_M (ksi)**	**Bending Stress σ_B (ksi)**	**σ_{max} / σ_{min}**	**2-D Membrane Stress σ_{2D} (ksi)**	**σ_{max} / σ_{2D}**
KC-10	21.0	3.0	1.3	16.0	1.5
C-9	31.0	9.0	1.8	30.0	1.3
C-17	29.0	3.0	1.3	-	-

Similar comparisons for the case of pressure loads are shown in Table J2. The 0.8 ratio of maximum stress to the 2-D stress for C-9 is not expected - reason for this is not known. But it is observed that the effects are not as significant as can be seen from the overall lower ratios of maximum to minimum stress. The case of global bending was not considered for the same reason. Hence, only the results from the shear loading study will be used to draw some conclusions here.

Table J2. Stresses at the Critical Loading under Pressure of 10 psi

Aircraft	**In-Plane Stress σ_M (ksi)**	**Bending Stress σ_B (ksi)**	**σ_{max} / σ_{min}**	**2-D Membrane Stress σ_{2D} (ksi)**	**σ_{max} / σ_{2D}**
KC-10	22.0	1.6	1.2	23.0	1.0
C-9	15.0	1.3	1.2	20.0	0.8
C-17	12.0	2.0	1.4	-	-

Based on the data shown in Table J1, it appears that if a factor of 2.0 is used to multiply the two-dimensional analysis results to account for the local bending effects, the repair assessment should be on the conservative side. While the data obtained appear to support the concept presented here, more studies on various door cutout configurations are needed to substantiate the validity of this approach and better define the range of correction factors.

Appendix K – Antenna Installations

Static strength and damage tolerance analysis methods for skin modifications to antenna installations on the fuselage of commuter airplanes are described in this appendix. The methods are implemented in the analysis program of RAPIDC Version 1.0 for commuters. Three types of antenna installation in terms of the shapes of mounting plate are first defined. The applicability of antenna systems within the analysis capability of RAPIDC is next addressed. Static strength and damage tolerance analysis procedures are then described. The damage tolerance analysis procedure is demonstrated using an illustrative example.

K1.0 RAPIDC Capabilities

The analysis of a modified fuselage skin to antenna installation in RAPIDC for commuter airplanes is an addition to the RAPID program originally developed for common repairs to large transport aircraft. The analysis capability of RAPIDC Version 1.0 for antenna installations is limited to the types and systems described below.

K1.1 Types of Antenna Installation

Three common types of antenna installation are considered. They differ only in the shapes of mounting plates: rectangular, circular, and elliptical shape as shown in Figure K1. The mounting plates are mechanically fastened to the skin around the cutout.

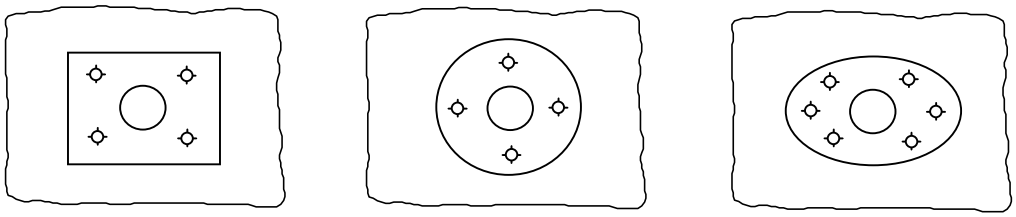

(a) Rectangular (b) Circular (c) Elliptical

Figure K1. Three types of antenna installation

In RAPIDC Version 1.0, only the circular and rectangular installations are considered. The elliptical installations will be included in the next version release.

K1.2 Antenna System Applicability

RAPIDC Version 1.0 excludes the case of skin bending that is induced by antenna vibrations subjected to aerodynamic loading. Therefore, communication antennas (typically 5” long by 3” wide by 10” tall) are excluded. However, antenna systems such as ADF (12” long by 6” wide by 1” tall), GPS (4” long by 4” wide by 0.5” tall), Transponder and DME (5” long by 2” wide by 4” tall), and TCAS are covered in the analysis.

K2.0 Static Strength Analysis

Typical antenna installations on the fuselage of commuter airplanes generally involve cutting a hole in the skin for the antenna connector. A mounting plate is then mechanically fastened to the skin around the skin cutout. To assess the static strength of the modified skin, three independent criteria are used to evaluate the margins of safety of the mounting plate and fasteners: the mounting plate allowable, the joint allowable, and the shear allowable.

K2.1 The Mounting Plate Allowable and Margin of Safety

To assess the loss of skin strength due to antenna connector hole cutout, the margin of safety of the mounting plate is calculated as

$$\text{Margin of Safety} = \frac{P_{pu}}{P_p} - 1$$

where P_{pu}, the mounting plate load allowable, is calculated using the equation

$$P_{pu} = F_{tu} (w_p - D) t_p$$

in which F_{tu}, w_p, D, and t_p are the ultimate tensile strength, width, cutout diameter, and thickness of the mounting plate, respectively.

The skin internal force, P_p , is calculated using the equation

$$P_p = \sigma_u D t_s$$

where σ_u and t_s are the design ultimate tensile stress and thickness of the skin, respectively.

K2.2 The Fastener Joint Allowable and Margin of Safety

In the vicinity of an antenna installation on the skin, skin stresses are transferred to the mounting plate through fasteners via fastener shear and hole bearing. The fastener together with the skin and mounting plate represents a fastener joint. A joint can only transfer a certain amount of load until it fails. The point at which this fastener joint fails is the joint allowable. The calculation of the joint allowable is based upon two loading conditions, fastener shear and hole bearing. Two hole types also have to be considered when determining the joint allowable, the straight shank and countersunk.

K2.2.1 Fastener Joint Allowable in Straight Shank Holes

Straight shank holes are used for protruding head fasteners and for the mounting plate that have a flush head fastener installed but are not countersunk. The joint allowable is

the lower of the shear allowable or the hole bearing allowable. An allowable is calculated for the skin and mounting plate that the fastener goes through.

The single shear allowable for straight shank holes is calculated using the following equation

$$P_{su} = F_{su} \times A_f \times S_{CF1}$$

The mounting plate shear allowable for straight shank holes is calculated using the following equation

$$P_{su} = 2 \times F_{su} \times A_f \times S_{CF2}$$

In both equations, F_{su} is the ultimate shear strength of the fastener material, A_f is the cross-sectional area of each fastener, S_{CF1} is the single shear correction factor and S_{CF2} is the double shear correction factor. S_{CF1} and S_{CF2} are used only for solid rivets and can be found in MIL-Handbook 5F Table 8.1.2.1(b).

The hole bearing allowable for the straight shank hole is calculated using the following equation

$$P_{bru} = F_{bru} \times d \times t$$

in which F_{bru} is the ultimate bearing stress of the plate (skin or mounting plate) material, d is the fastener hole diameter, and t is the thickness. Currently, the F_{bru} is for the case E/D (edge distance to hole diameter) equal to 2.0.

The joint allowable for a given joint is the lower of P_{su} or P_{bru}denoted by $P_{joint.}$

K2.2.2 Fastener Joint Allowable in Countersunk Holes

The fastener joint allowables for countersunk holes are different from the straight shank holes. They are determined by tests and can be found in MIL-Handbook 5F Section 8.

K2.2.3 Fastener Joint Margin of Safety

The fastener joint margin of safety is determined by summing each fastener joint allowable in the skin and mounting plate, and this is done for each side of the mounting plate.

$$P_{total} = \sum_{n=1}^{K} (P_{joint})_n$$

in which P_{total} is the total fastener joint load, $(P_{joint})_n$ is the fastener joint load for the nth fastener and K is the number of fasteners.

The P_{total} for the skin and mounting are then compared. The smaller of the two is the fastener joint allowable for that side of the mounting plate and is used in determining the margin of safety for the fastener joints.

An applied load is needed to determine a margin of safety. That load is the ultimate applied load to the structure, or if that is not known, then the tensile ultimate strength of the material F_{tu} is used. This applied load $P_{applied}$ is given by

$$P_{applied} = \sigma_u D t_s$$

where σ_u is either the design ultimate tensile stress or the tensile ultimate skin strength, t_s is the skin thickness, D is the diameter of antenna connector cutout hole. The margin of safety is given by

$$\text{Margin of Safety} = \frac{P_{total}}{P_{applied}} - 1$$

K2.3 The Shear Margin of Safety

The shear margin of safety of the antenna installation is calculated by

$$\text{Margin of Safety} = \frac{(F_{SU}\ t)_p}{(F_{SU}\ t)_s} - 1$$

where F_{SU} is the ultimate shear strength of the skin or mounting plate material. The equation is used for each side of the mounting plate.

K2.4 Margin of Safety as a Criterion

The margins of safety (MS) based on the mounting plate allowable and the fastener joint allowable were calculated to determine the adequacy of the antenna installation on fuselage skin.

- MS < 0 Antenna installation is statically inadequate
- MS = 0 Antenna installation is marginally adequate
- MS > 0 Antenna installation is statically adequate

For antenna installations that are not statically adequate, they must be redesigned to ensure the adequacy of the antenna installation.

K2.5 The Stiffness Check of the Antenna Installation

The stiffness ratio between the mounting plate and the skin is calculated using the following equation

$$\text{Stiffness Ratio} = \frac{(E\,t)_p}{(E\,t)_s}$$

The antenna installation is considered adequate if the ratio is between 1.0 and 1.5. The antenna installation is too stiff when the value is greater than 1.5 and not stiff enough when it is less than 1.0.

K2.6 The Fastener Bending Check of the Antenna Installation

The fastener bending is checked using the following equation

$$Q = \frac{t_s + t_p}{d}$$

Where d is the fastener diameter, t_s and t_p are the thickness of skin and mounting plate, respectively. The parameter Q is the fastener bending indicator. For aluminum fasteners, the bending is important. A Q value above 2 may indicate that the aluminum rivet will not fill the hole but instead may buckle in the hole. In such a case, RAPIDC recommends steel or titanium fasteners be used. For steel and titanium fasteners, there is no constraint for typical fuselage antenna installations.

K2.7 The Inter-Rivet Buckling Guideline

To avoid inter-rivet buckling in the modified skin, the fastener spacing should be four to six times the diameter of the fastener shank diameter. This guideline is enforced during user input phase of RAPIDC.

K3.0 Damage Tolerance Analysis

To perform the damage tolerance analysis of a modified skin for antenna installations, critical locations in the skin must first be determined. Assumptions of initial flaws at fracture critical locations and the continuing damage need to be made. The stress spectrum must also be prescribed. In addition, the following data are needed:

- Crack growth rate data of the skin material
- Fracture toughness of the skin material
- Stress intensity factors of relevant crack configurations

Damage tolerance analysis procedure is described in the flowchart shown in Figure K2. Each element in the analysis procedure is described as follows.

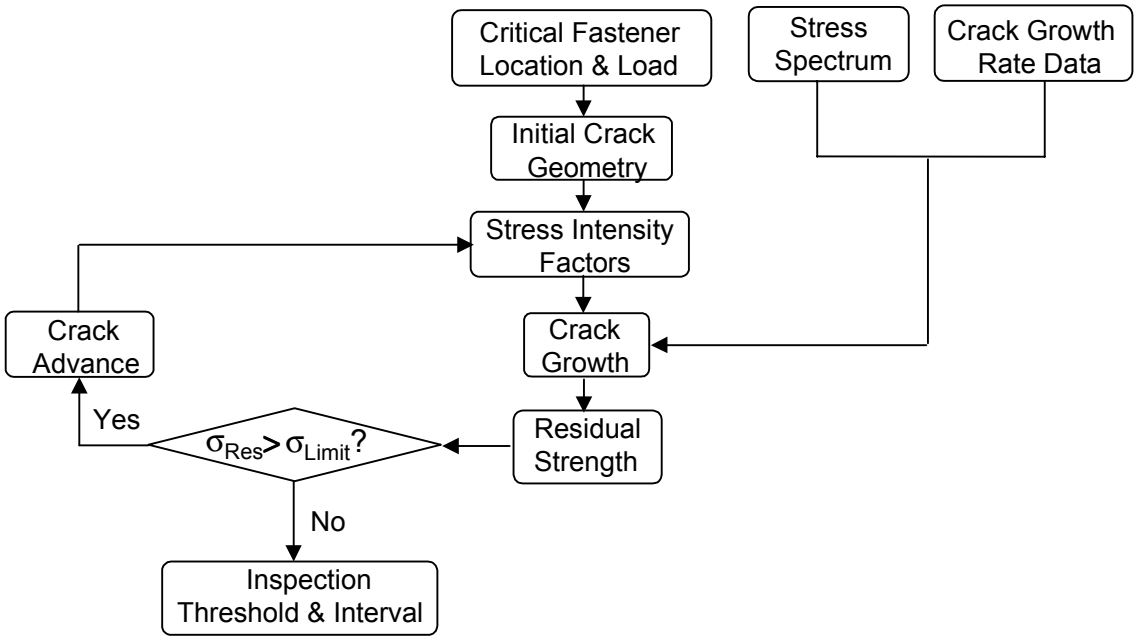

Figure K2. Flow Chart of Damage Tolerance Analysis Procedure

K3.1 Critical Fastener Locations

Damage tolerance analysis of the modified skin begins by postulating the initial flaws at the critical locations. For rectangular installations, two locations are identified at the center and corner fastener holes in the outermost fastener rows that have higher load transfer. A third location is identified at the edge of antenna connector hole cutout in the skin where stress concentration is the highest. For circular installations, the critical locations are identified at the top or bottom fastener in the outermost ring and at the antenna connector hole cutout as well. The critical fastener locations in circular and rectangular installations are indicated in Figure K3.

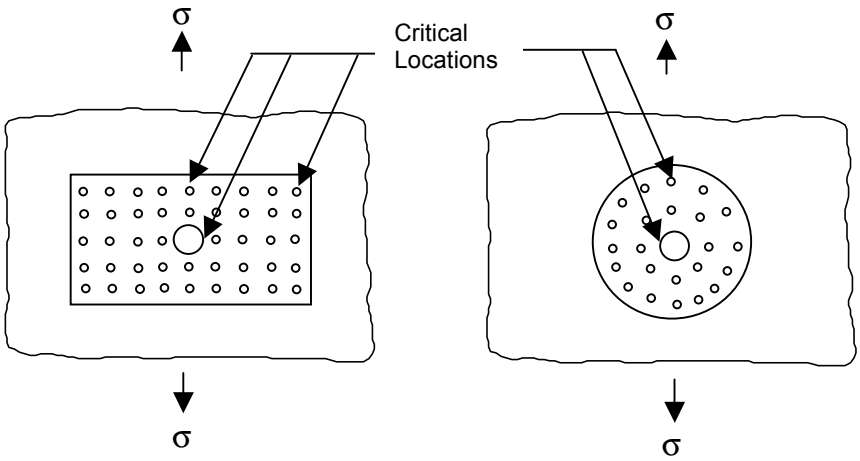

Figure K3. Critical Fastener Locations

K3.2 Fastener Loads and Skin Stress Gradients

The fastener loads or skin stress gradients along the potential crack growth path are needed for calculating crack tip stress intensity factors. The determination of fastener loads and skin stress gradients was accomplished using the FRANC2D/L program developed jointly at Cornell University and Kansas State University sponsored by NASA-Langley Research center. The finite element model was created using the FRANC2D/L preprocessor program called CASCA developed at Cornell University.

In FRANC2D/L analysis, the fastener shear rigidity needs to be calculated separately and input into the program. The FRANC2D/L program then assembles stiffnesses contributing from skin, mounting plate, and fasteners to form the overall stiffness matrix. The shear rigidity can be calculated using the Swift's empirical equation:

$$K = \frac{E\,d}{A + B\left(\frac{d}{t_{Skin}} + \frac{d}{t_{MountingPlate}}\right)}$$

where E is the weighted Young's modules of the skin and mounting plate, d is the fastener hole diameter, t_{Skin} and $t_{Mounting\ Plate}$ are the thickness of the skin and mounting plate, respectively, and A and B are material dependent empirical constants. The values of A and B, for aluminum fasteners, are 5.0 and 0.8, respectively.

In RAPIDC, databases of fastener loads and skin stress gradients along the potential crack growth path are developed for circular and rectangular installations. Parameters considered include:

Skin thickness: 0.032", 0.040", 0.050", and 0.063"
Mounting plate thickness: 1 gauge higher than skin thickness
Cutout diameter: 1.0", 2.0", and 3.0"
Fastener size: 1/8", 5/32", and 3/16"
Number of fastener rows: 1 ~ 5
Aspect ratio: 1:1 (square), 1:1.3 and 1:1.6
Materials: Aluminum skin and mounting plate
Aluminum fastener

K3.3 Initial Flaw Size and Subsequent Growth Scenarios

To simplify the damage tolerance analysis of the modified skin, initial flaws and their growth pattern were assumed. Three scenarios are considered in RAPIDC for rectangular antenna installations, according to the decision made in a technical review meeting (September 22, 1999 in Albuquerque, New Mexico), and are described below in Figure 4.

Scenario 1: Center fastener hole in the outermost fastener row

Initial Crack: Two diametric through cracks of lengths 0.05" and 0.005", respectively, emanating from the center fastener hole together with a 0.005" crack at one side of every other hole

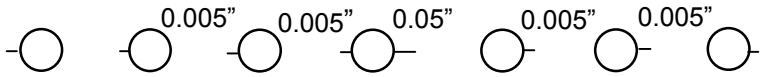

Subsequent Damage: All cracks grow concurrently but independently, interaction between cracks being ignored. The amount of growth δa_1 for the 0.005" crack is added to its original length when the 0.05" crack grows into the adjacent hole. The same process continues in successive growth.

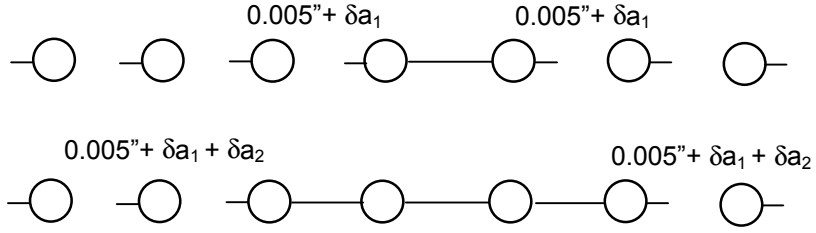

Scenario 2: Corner fastener hole in the outermost fastener row

Initial Crack: Two diametric through cracks of lengths 0.05", pointing toward the adjacent hole, and 0.005", respectively, emanating from the corner fastener hole together with a 0.005" crack at one side of every other hole

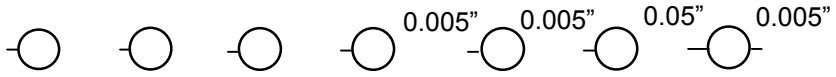

Subsequent Damage: All cracks grow concurrently but independently, without interaction between cracks being considered. The amount of growth δa for the 0.005" crack is added to its original length when the 0.05" crack grows into the adjacent hole. The same process continues in successive growth.

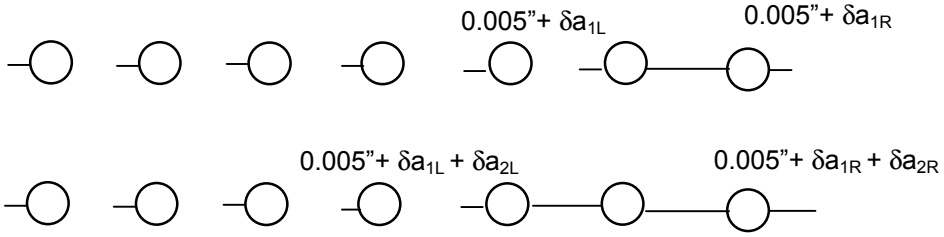

It is noted that successive growths of the 0.005" at corner fastener hole $\delta a_{1R,}$ $\delta a_{2R,}$ etc. are different from the growths at other holes $\delta a_{1L,}$ $\delta a_{2L,}$ etc. because the former does not grow toward an adjacent hole but others do.

Scenario 3: Antenna connector hole

Initial Crack: Two diametric through cracks of lengths 0.05" and 0.005", respectively, emanating from the antenna connector hole together with a 0.005" crack at one side of every other hole

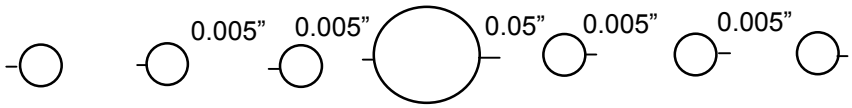

Subsequent Damage: All cracks grow concurrently but independently, ignoring interaction between cracks. The amount of growth δa for the 0.005" crack is added to its original length when the 0.05" crack grows into the adjacent hole. The same process continues in successive growth.

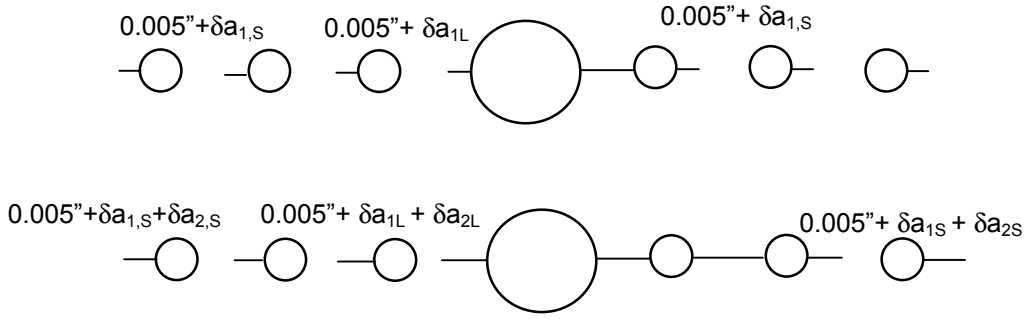

It is noted that successive growths of the 0.005" at antenna connector hole $\delta a_{1L,}$ $\delta a_{2L,}$ etc. are different from the growths of 0.005" crack at fastener holes $\delta a_{1S,}$ $\delta a_{2S,}$ etc. because the hole sizes and fastener pitches are different.

Figure K4. Initial Flaws and Subsequent Growths Assumptions

For circular antenna installations, two scenarios are considered. The first scenario postulates two initial diametric cracks with 0.05" and 0.005" at the top or bottom fastener in the outermost ring. The cracks grow concurrently but independently in the skin. The second scenario is the same as Scenario 3 for the rectangular antenna installation.

K3.4 Stress Intensity Factors

In RAPIDC, methods of stress intensity factor calculations for a crack emanating from a pin-loaded fastener hole in the skin are described in Appendix B. For a crack emanating from the antenna connector open hole in the skin, it is calculated from stress gradients using the weight function method. To account for the hole effect as a crack is growing toward the adjacent hole, the compounding method described in Appendix B is used. In the following, the weight function method is described.

The stress intensity factor of a crack emanating from a hole in a wide plate subjected to stress gradients on crack faces as shown in Figure K5(a) can be calculated using the weight function method. In this case, the stress intensity factor is obtained by summing up stress intensity factors for each pair of point loads acting on crack faces at a distance x from the edge of the hole as shown in Figure K5(b).

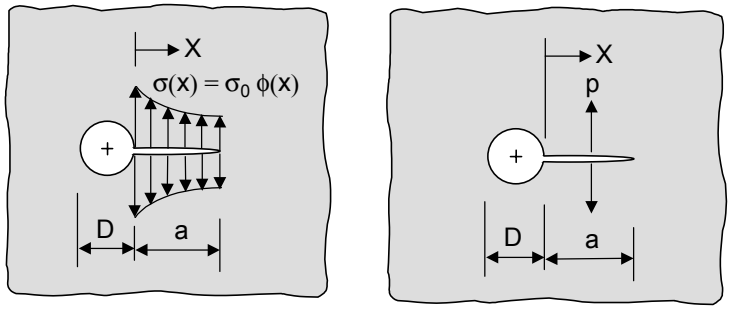

(a) Stress Gradients (b) A Pair of Point Loads

Figure K5. Illustration of the Weight Function Method

Suppose the stress intensity factor of the crack geometry subjected to the load condition described in Figure K5(b) is known as

$$\Delta K(p,a,x) = p\sqrt{\pi a}\; G(x)$$

where G(x) is the Green's function representing the geometry factor of the crack geometry under a unit of point loads on crack faces. The stress intensity factor solution for the problem in Figure K5(a) can be calculated as

$$K(p,a) = \int_0^a \Delta K(p,a,x)\,dx$$

For the stress gradient $\sigma(x) = \sigma_0\,\phi(x)$ as shown in Figure K5(a), the load per unit thickness at a distance x from the edge of the hole can be expressed by

$$p(x) = \sigma_0\,\phi(x)\,dx$$

Therefore, the stress intensity factor for the same geometry subjected to the stress gradient $\sigma(x) = \sigma_o\phi(x)$ on crack faces can be calculated as

$$K = \sigma_0\sqrt{\pi a}\int_0^a \phi(x)G(x)dx$$

The geometry factor βcan be obtained as

$$\beta = K / K_o$$

where K_o is the stress intensity factor, i.e., $K_0 = \sigma_0\sqrt{\pi a}$.

H4.0 Example Problem

The damage tolerance analysis of a modified skin to an antenna installation is performed below for three crack scenarios described in Section K3.3.

Description of the Example Problem

Figure K6 depicts an example problem of an antenna installation on the fuselage of a commuter airplane. Assume that the skin is subjected to an equivalent one cycle circumferential stress of 18 ksi with zero stress ratio. Damage tolerance analysis of the modified skin is carried out to demonstrate the analysis procedure.

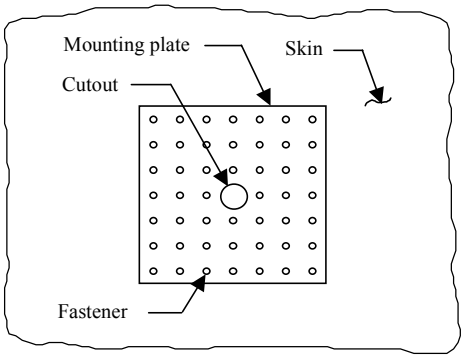

Fuselage radius: 60.0”
Skin thickness: 0.050”
Mounting plate thickness: 0.063”
Cutout diameter: 1.0”
Fastener diameter: 3/16”
Fastener rows: 3
Fastener pitch: 1.0”
Skin and mounting plate: Al2024T3
Fastener: NAS1097
Fracture toughness: 153 ksi sqrt(in)
Pressure differential: 8.6 psi

Figure K6. Description of the Example Problem

Fastener Loads and Stress Gradients

(1) Fastener Loads

Figure K7 shows load transfers at fasteners in pounds due to 1000 psi reference skin stress. These fastener loads were obtained using FRANC2DL as described in Appendix I. As expected, the outer row is the critical fastener row.

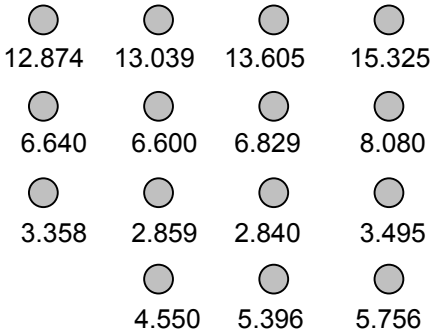

Figure K7. Fastener Loads

2. Stress Gradients

The crack growth scenario 3 described in Section K3.3 is depicted in Figure K8.

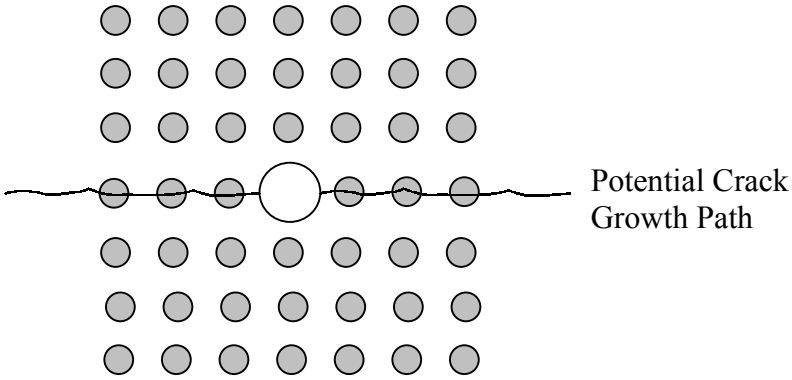

Figure K8. Potential Crack Growth Paths

The stress gradient along the potential crack path subjected to 1,000 psi reference skin stress is shown in Figure K9. The distance d is measured from the center of the hole.

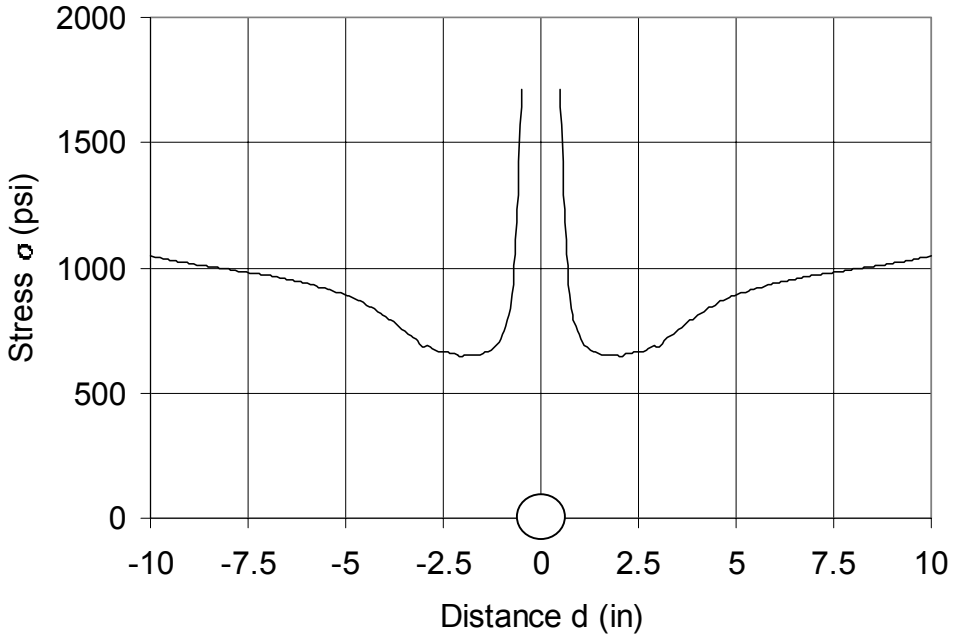

Figure K9. Stress Gradient along Potential Crack Growth Path

Residual Strength and Crack Growth

To demonstrate the residual strength and crack growth analysis of the example problem, analysis is performed for three Scenarios described in Section K3.3.

(1) Stress Intensity Factors

Stress intensity factors for a crack initiating from the center or the corner fastener hole due to gross, bearing, and bypass stresses are calculated using the superposition method. The effect of a crack growing toward an adjacent hole is accounted for using the compounding method.

For a crack initiating from the antenna connector hole, the weight function method is used. Using the stress gradients shown in Figure K9, the normalized stress intensity factor or geometry factor is obtained as shown in Figure K10.

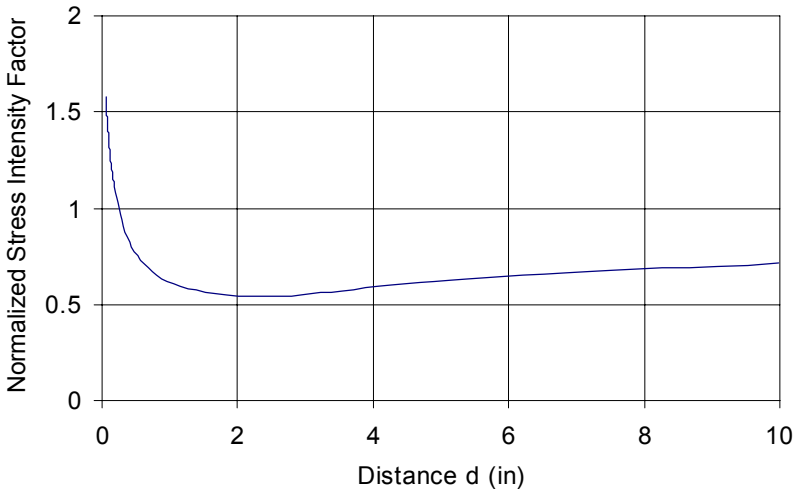

Figure K10. Normalized Stress Intensity Factors

The effect of a crack growing toward an adjacent hole is accounted for using the compounding method.

(2) Residual Strength

Residual strengths of the skin are calculated using the fracture toughness method and modified using Fedderson's criterion. The calculation terminates when the residual strength reaches the limit stress of 12,072 psi obtained using the circumferential limit stress equation in Section K3.5.2. Figure K11 shows the residual strength curve.

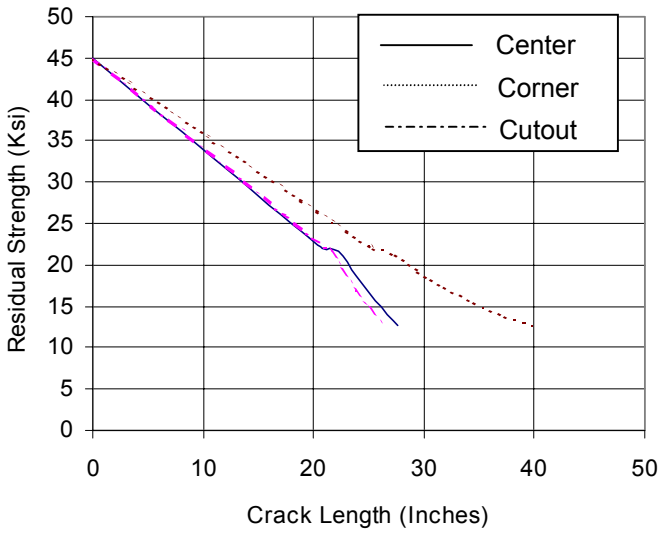

Figure K11. Residual Strength

(3) Crack Growth Lives

Figure K12 shows the crack growth lives obtained using the simplified crack growth analysis method.

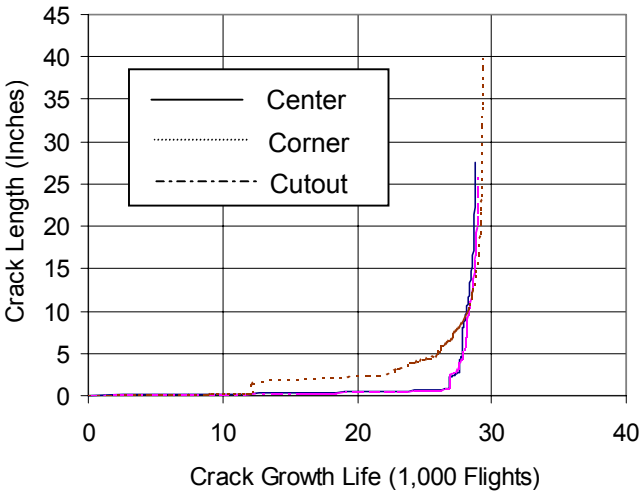

Figure K12. Crack Growth Life

Inspection Threshold and Interval

Once the residual strength and crack growth life have been obtained, the critical crack length can be determined from the residual strength at the limit stress. The crack growth life at the critical crack length can then be determined from the crack growth life curve.

With the crack growth history, the inspection threshold and interval can be determined from the crack growth life based on the detectable crack size of the inspection method.